

**DEVELOPMENT AND CHARACTERIZATION OF
GRAPHITE NANOCOMPOSITE GREEN
ELECTROCHEMICAL SENSORS FOR MULTIPLEX
DETECTION OF ANTIOXIDANTS AND DNA BASES**

NG KHAN LOON

**FACULTY OF SCIENCE
UNIVERSITY OF MALAYA
KUALA LUMPUR**

2017

**DEVELOPMENT AND CHARACTERIZATION OF
GRAPHITE NANOCOMPOSITE GREEN
ELECTROCHEMICAL SENSORS FOR MULTIPLEX
DETECTION OF ANTIOXIDANTS AND DNA BASES**

NG KHAN LOON

**THESIS SUBMITTED IN FULFILMENT OF THE
REQUIREMENTS FOR THE DEGREE OF DOCTOR OF
PHILOSOPHY**

**DEPARTMENT OF CHEMISTRY
FACULTY OF SCIENCE
UNIVERSITY OF MALAYA
KUALA LUMPUR**

2017

UNIVERSITY OF MALAYA
ORIGINAL LITERARY WORK DECLARATION

Name of Candidate: **NG KHAN LOON**

Matric No: **SHC140004**

Name of Degree: **Doctor of Philosophy**

Title of Project Paper/Research Report/Dissertation/Thesis (“this Work”):

Development and Characterization of Graphite Nanocomposite Green Electrochemical Sensors for Multiplex Detection of Antioxidants and DNA Bases

Field of Study: **Analytical Chemistry**

I do solemnly and sincerely declare that:

- (1) I am the sole author/writer of this Work;
- (2) This Work is original;
- (3) Any use of any work in which copyright exists was done by way of fair dealing and for permitted purposes and any excerpt or extract from, or reference to or reproduction of any copyright work has been disclosed expressly and sufficiently and the title of the Work and its authorship have been acknowledged in this Work;
- (4) I do not have any actual knowledge nor do I ought reasonably to know that the making of this work constitutes an infringement of any copyright work;
- (5) I hereby assign all and every rights in the copyright to this Work to the University of Malaya (“UM”), who henceforth shall be owner of the copyright in this Work and that any reproduction or use in any form or by any means whatsoever is prohibited without the written consent of UM having been first had and obtained;
- (6) I am fully aware that if in the course of making this Work I have infringed any copyright whether intentionally or otherwise, I may be subject to legal action or any other action as may be determined by UM.

Candidate’s Signature

Date:

Subscribed and solemnly declared before,

Witness’s Signature

Date:

Name:

Designation:

ABSTRACT

Graphite material is abundantly available from recyclable sources such as used alkaline dry batteries. It possesses unique polymorph with free valence sp^2 hybridize carbon that can potentially interact with various nanomaterials. Sensors that based upon glassy carbon (GCE) or silica have been widely studied, but limited to multiplex analysis because of lacking in overpotential, effective surface area (Eff A) and electrocatalytic properties. In this Ph.D. study, the potential use of graphite obtained from used battery was explored as electrochemical sensor; where electrode surface modification with different nanomaterials was conducted to overcome these limitations. The practicability use of the developed sensors was tested for multiplex detection of anti-oxidants and DNA bases in real samples. Au-NPs/graphite sensor was successfully developed from graphite that obtained from used battery. In comparison to bare graphite, the deposited gold nanoparticles have improved the Eff A and heterogeneous electron transfer rate (k_s) of the sensor by 3-folds. With larger electrode surface active sites (Eff A), more redox reaction could be accommodated by the sensor before the surfaces get saturated. The Au-NPs/graphite was successfully utilized for myricetin analysis using square wave voltammetry (SWV) technique; with sensitivity improvement by 2.5 folds, low limit of detection (LOD), and high accuracy that fit for beverages samples analyses. Besides, the developed graphite nanocomposite electrochemical sensor was also explored for the multiplex measurements of BHT, BHA, and TBHQ in various food samples using linear sweep voltammetry. Monitoring of these additives level in food is important especially since consumption of these substances above $3000 \mu\text{g g}^{-1}$ can promote cancer proliferation. The reliability of Au-NPs/graphite sensor was challenged by liquid chromatography (LC), where results correlation above 99.0% was achieved. Addition of sodium lauryl sulphate during sample extraction was found to amplify the sensor

detection signal. Sensors with low LOQ, high accuracy, wide linearity, good precision, spike recovery and selectivity allow it for potential use in regulatory control. The performance of graphite was further explored using different combination of nanomaterials, and used for multiplex analysis of adenine, guanine, thymine and cytosine. Au–ErGO/MWCNT/graphite was developed using electro-codeposition of gold nanoparticles and graphene (ErGO). Electrochemical characteristic studies showed significant improvement in the k_s , OP and electrocatalytic activity of the sensor. These have attributed to the remarkable applied potential range especially in cytosine detection that can be extended up to 1.4 V without being oxidized. Study of DNA composition has been an interesting research topic especially in DNA damage and genotoxicity study. The reliability of the sensor was confirmed with LC method, where a result correlation of 103.7% was achieved with the sensitivity, selectivity and accuracy that are comparable to LC. In conclusion, the objective of my Ph.D. study has been successfully achieved with the development of Au–NPs/graphite and Au–ErGO/MWCNT/graphite electrodes for multiplex detection of anti-oxidants and DNA bases, respectively. Future development on miniaturizing graphite sensor can be potential study for on-site analysis.

ABSTRAK

Kebanyakan bahan grafit boleh didapati dari sumber kitar semula seperti bateri alkali. Ia mempunyai polimorf unik dengan valensi sp^2 silang karbon yang berpotensi sebagai pengantara kepada pelbagai bahan nano. Penyelidikan penderia yang berasaskan karbon berkaca (GCE) atau platform silika telah banyak dijalankan; namun aplikasinya terhadap kepada pengukuran multipleks disebabkan oleh keterbatasan sifatnya dari segi tenaga keupayaan, permukaan tapak redoks (Eff A) dan sifat elektro-pemangkin. Dalam pengajian Ph.D. saya ini, potensi penggunaan platform grafit daripada bateri telah diterokai untuk pembangunan penderia elektrokimia, pengubahsuaian terhadap permukaan electrode telah dilakukan dengan pelbagai bahan nano dalam usaha mengatasi keterbatasan sifat grafit terutamanya dalam pengukuran multipleks. Keupayaan sebenar penderia ini seterusnya diuji dalam pengukuran multipleks antioksidan dan asid deoksiribosa nukleik (DNA). Penderia Au-NPs/grafit telah berjaya dibangunkan dalam penyelidikan ini, berasaskan grafit yang diperolehi dari bateri, dimana teknik elektropeendapan telah digunakan untuk mengubahsuaikan permukaan grafit dengan nanopartikel emas. Pembangunan ini telah menunjukkan penambahbaikan yang drastik kepada sifat heterogen kadar pemindahan elektron (k_s) dan Eff A yang terlebih, dimana ia mempunyai kemampuan untuk menampung pengesanan sebatian kimia yang lebih pekat sebelum mencapai takat tepu redoks. Penderia itu berjaya digunakan untuk pengukuran myricetin dalam sampel minuman dengan teknik gelombang voltametri persegi; dimana penderia itu telah menunjukkan peningkatan dalam takat rendah pengesanan (LOD), ketepatan, dan kepekaan sebanyak 2.5 kali ganda. Seterusnya, pretasi penderia Au-NPs/grafit itu diterokai dengan terperinci terutamanya dalam pengukuran multipleks BHA, BHT dan TBHQ di dalam sampel makanan; dimana teknik voltammetry sapuan linear telah digunakan untuk pengukuran antioksidan itu. Pemantauan antioksidan sintetik ini adalah penting apabila penggunaan melebihi $3000 \mu\text{g g}^{-1}$ dalam makanan

boleh menyebabkan percambahan kanser. Kejituan penderia Au-NPs/grafit ini seterusnya dibandingkan dengan kaedah kromatografi, di mana korelasi liner diantara dua kaedah itu mencapai kejituan yang melebihi 99.0%. Selain itu, tambahan sodium lauryl sulfat dalam langkah penyediaan sampel juga menunjukkan amplifikasi dalam takat pengesanan antioksidan itu. Penderia Au-NPs/grafit dengan takat rendah LOQ, ketepatan yang tinggi, kelinearan luas, ketepatan yang baik, peratusan perolehan yang sepuh dan selektif ini, telah menunjuk potensi penderia Au-NPs/graphit terutama dalam aplikasi pengawalan regulatori makanan. Pretasi penderia grafit ini seterusnya diuji dengan menggunakan kombinasi bahan nano untuk tujuan pengukuran multipleks adenina, guanina, timina, dan sitosina. Penderia Au-ErGO/MWCNT/grafit telah berjaya dihasilkan dengan menggunakan kaedah elektro-peendapan nanopartikel emas dan graphene oksida bersama. Dimana, Pencirian elektrokima terhadap penderia menunjukkan peningkatan dalam k_s , keupayaan lampau dan elektro-pemangkin. Hasilnya dapat dilihat dengan jelas terutamanya dalam pengesanan sitosin, dimana aplikasi voltan penderia boleh dilanjutkan sehingga 1.4 V tanpa melalui pengoksidaan. Kajian mengenai komposisi DNA telah menjadi topik yang menarik dalam penyelidikan terutamanya dalam bidang kerosakan DNA dan kajian genotoksik. Kejituan penderia Au-ErGO/MWCNT/grafit seterusnya dibandingkan dengan kaedah kromatografi, di mana korelasi linear diantara dua kaedah itu mencapai kejituan 103.7%. Selain itu kepekaan, takat rendah pengesanan, ketepatan dan selektif penderia juga setanding kaedah kromatografi dan memenuhi tujuan aplikasi. Secara kesimpulannya, pengajian Ph.D. saya ini telah berjaya menghasilkan penderia Au-NPS/grafit dan Au-ErGO/MWCNT/grafit bagi pengukuran multipleks dalam antioksidan dan DNA. Penyelidikan penderia grafit mikro berpotensi untuk diterokai pada masa hadapan, terutamanya dalam aplikasi kajian-analisis lapangan.

ACKNOWLEDGMENTS

I sincerely thank my supervisor Dr. Khor Sook Mei for all her constant guidance and supervision in providing valuable knowledge, information, and comments that spark solution, idea and encouragement in completing this thesis. Highly appreciate on her patience and effortless proofreading of my manuscripts and experiment reports. Besides, I would like to thank Prof. Dr. Tan Guan Huat, for his patience and supervision during my early Ph.D. candidature, before his retirement in Feb 2016. In monetary support, I would like to thank University of Malaya Post Graduate grant (PPP) for funding on the necessity chemical and apparatus, which is vital for my day to day experiments. I would like to thank my lab mates in sharing their technical insights, experiences, and support to the experiment work that undertaken during my Ph.D. study. To Dr. Ang Shu Hwang, Dr. Lee Bai Qin and Khoo Mai Mai, I thank them for their help and support when needed. I would like to thank the staff of Chemistry department especially Mr. Shukri for his help with FE–SEM analysis.

I'm grateful for all the emotional support and encouragements from my family, especially to my wife Ms. Pit York Kin and my son Ng Yon Shun for all the love and cares given to me; it would not be possible for me to complete my Ph.D. thesis without their minutes of support, which I sincerely thank them for this fortunate. To my mother Tsze Sow Lan and father Ng Kim Teng, I thank them on their their strong encouragement and faith on me to continue my Ph.D. study.

Last but not least, I would like to give a big thank to my company, Wipro Manufacturing services Sdn. Bhd. in supporting my Ph.D. scholarship. More importantly, to my superior Ms. Toh Mong Sah for her encouragement and support, also to my Wipro colleagues and friends on their encouragement, support and help that have been given to me.

TABLE OF CONTENTS

Abstract	iii
Abstrak	v
Acknowledgments	vii
Table of Contents.....	viii
List of Figures.....	xvi
List of Tables.....	xxiii
List of Symbols and Abbreviations	xxv
CHAPTER 1: GENERAL INTRODUCTION.....	1
1.1 Electrochemical sensor	1
1.2 Exploration of graphite as a new potential material for the working electrode/transducer in sensor development	4
1.3 Surface modification of graphite-based electrochemical sensor.....	8
1.4 Electrochemical analysis for multiplex detection of anti-oxidants and nucleic acid bases	11
1.4.1 Anti-oxidants	11
1.4.2 Deoxyribose nucleic acid bases (DNA)	14
1.5 Scope and objectives of the study.....	17
CHAPTER 2: A REVIEW ON THE GRAPHITE BASED COMPOSITE WORKING ELECTRODE AND THE ANALYTICAL METHODOLOGY USED IN ANTI-OXIDANTS AND DNA BASES ANALYSIS.....	21
2.1 Introduction	21
2.2 Fabrication of graphite based sensor	22
2.2.1 Graphite-epoxy sensor	22

2.2.2	Pencil graphite sensor	24
2.2.3	Industrial graphite sensor	27
2.3	Surface modification of electrochemical sensor.....	28
2.3.1	Noble metal nanoparticles	29
2.3.2	Carbon nanoparticles.....	34
2.3.3	Conducting polymer materials.....	39
2.3.4	Biomaterials.....	42
2.4	Analysis of anti-oxidants	46
2.4.1	Sample preparation of anti-oxidant.....	47
2.4.1.1	Liquid extraction	48
2.4.1.2	Soxhlet extraction.....	51
2.4.1.3	Reflux extraction.....	52
2.4.1.4	Freeze drying.....	53
2.4.1.5	Solid phase extraction.....	54
2.4.2	Qualitative and quantitative analysis of anti-oxidants	55
2.4.2.1	Qualitative analysis of anti-oxidants	56
2.4.2.2	Quantitative analysis of anti-oxidants	62
2.5	Analysis of DNA bases.....	68
2.5.1	Preparation of DNA samples.....	69
2.5.1.1	DNA Isolation	69
2.5.1.2	Hydrolysis or digestion of DNA	71
2.5.1.3	DNA enrichment	74
2.5.2	Quantitative analysis of DNA.....	76
2.5.2.1	Gel electrophoresis	76
2.5.2.2	Immunoassay	78
2.5.2.3	Liquid chromatography	80

2.5.2.4 Electrochemical sensor	82
--------------------------------------	----

CHAPTER 3: ELECTROCHEMICAL PREPARATION AND CHARACTERISATION OF A GOLD NANOPARTICLES MODIFIED GRAPHITE ELECTRODE..... 85

3.1 Introduction and scope of work.....	85
3.2 Experimental	87
3.2.1 Chemicals and apparatus.....	87
3.2.2 Fabrication of graphite electrode.....	88
3.2.3 Electro-deposition and activation of gold nanoparticles on the graphite electrode	89
3.2.4 Electrochemical characterisation of Au-NPs/graphite.....	90
3.2.5 Morphology analysis by field emission SEM	90
3.2.6 Electrochemical analysis of myricetin using the Au-NPs/graphite electrode	91
3.2.6.1 Electrochemical characteristic of myricetin.....	91
3.2.6.2 Analysis of myricetin by SWV	91
3.2.6.3 pH effect in myricetin analysis	91
3.3 Results and discussion	92
3.3.1 Electrodeposition of gold nanoparticles on graphite electrode	92
3.3.2 Activation of Au-NPs/graphite electrode.....	93
3.3.3 Morphology characterisation by field emission SEM.....	94
3.3.4 Electrochemical characterisation of Au-NPs/graphite electrode by CV .	96
3.3.4.1 Effective surface area	96
3.3.4.2 Surface coverage	99
3.3.4.3 Heterogeneous electron transfer rate (k_s).....	100

3.3.4.4	Electron transfer efficiency.....	103
3.3.4.5	Electrode overpotential.....	104
3.3.5	Electrochemical characterisation of Au-NPs/graphite electrode by electro impedance spectroscopy.....	105
3.3.6	Electrochemical analysis of myricetin using the Au–NPs/graphite electrode	109
3.3.6.1	Analysis of myricetin using CV	109
3.3.6.2	pH effect in myricetin analysis	112
3.3.6.3	Quantitative determination of myricetin by SWV	114
3.3.6.4	Limit of detection (LOD) for myricetin detection in Britton Robinson buffer.....	117
3.3.6.5	Analysis of myricetin in tap water samples	117
3.4	Conclusion.....	118

CHAPTER 4: ELECTROCHEMICAL MULTIPLEX ANALYSIS OF SYNTHETIC ANTI-OXIDANTS IN FOOD SAMPLES USING GOLD NANOPARTICLES MODIFIED GRAPHITE ELECTRODE 120

4.1	Introduction.....	120
4.2	Materials and methods	122
4.2.1	Chemicals and apparatus.....	122
4.2.2	Preparation of the Au-NP/graphite working electrode	123
4.2.3	Individual CV analysis of BHA, BHT, and TBHQ	123
4.2.4	Multiplex detection of TBHQ, BHA, and BHT using LSV analysis.....	123
4.2.5	Optimisation of sodium dodecyl sulphate solution.....	124
4.2.6	LSV analysis of food samples	124
4.2.7	Method validation using UPLC-PDA analysis.....	125

4.2.8	Selectivity and stability study of Au-NP/graphite sensor	125
4.3	Results and discussion	126
4.3.1	Enhancement of individual antioxidant electrochemical characteristics using the Au-NP/graphite electrode.....	126
4.3.2	Morphology of the Au-NP/graphite working electrode.....	131
4.3.3	Effect of pH on the electrochemical characteristics of individual BHA, BHT, and TBHQ investigated by CV	132
4.3.4	Simultaneous determination of BHA, BHT, and TBHQ using LSV	135
4.3.5	Impact of sodium dodecyl sulfate on the multiplex detection of TBHQ, BHA, and BHT	137
4.3.6	Analytical performance of the Au-NP/graphite electrode for multiplex detection of BHA, BHT, and TBHQ.....	139
4.3.7	Analytical performance of UPLC-PDA in multiplex detection of BHA, BHT, and TBHQ.....	143
4.3.8	Analysis of antioxidants in real food samples and method validation with UPLC-PDA.....	146
4.3.9	Interference and stability study of the Au-NP/graphite sensor.....	150
4.4	Conclusion.....	153

CHAPTER 5: DEVELOPMENT AND CHARACTERISATION OF AU-ERGO/MWCNT/GRAPHITE NANOCOMPOSITE SENSOR FOR THE DETERMINATION OF DNA BASES IN PLANT AND ANIMAL DNA..... 154

5.1	Introduction	154
5.2	Experimental	156
5.2.1	Chemicals and apparatus.....	156

5.2.2	Particle size analysis of MWCNT suspension using dynamic light scattering method (DLS).....	158
5.2.3	MWCNT/graphite preparation.....	158
5.2.4	Co-electrodeposition of gold nanoparticles and graphene oxide on MWCNT /graphite electrode.....	158
5.2.5	Electrochemical characterisation of Au-ErGO/MWCNT/graphite electrode	159
5.2.6	Morphology characterization of Au-ErGO/MWCNT/graphite sensor .	159
5.2.7	CV evaluation of DNA bases	160
5.2.8	SWV analysis of nucleotide bases using Au-ErGO/MWCNT/graphite electrode	160
5.2.9	pH response study of individual A, G ,T and C.....	160
5.2.10	Impact study of different supporting electrolyte in multiplex determination using SWV with Au-ErGO/MWCNT/graphite sensor.....	161
5.2.11	Analytical performance study for the multiplex determination of DNA bases using SWV with Au-ErGO/MWCNT/graphite sensor	161
5.2.12	Acid hydrolysis and DNA composition analysis in real sample	161
5.2.13	Validation of DNA nucleic acid bases analysis in real samples using ultra-performance liquid chromatography with photo diode array detector (UPLC-PDA)	162
5.2.14	Selectivity and stability evaluation of Au-ErGO/MWCNT/Graphite electrode	163
5.3	Results and discussion	164
5.3.1	Characterisation of MWCNT-COOH particles	164
5.3.2	Surface casting and electrochemical characterisation of MWCNT/graphite sensor.....	166

5.3.3	Co-electrodeposition of gold and graphene oxide on MWCNT-COOH/graphite surface.....	172
5.3.4	Optimization of Au–ErGO deposition cycle.....	175
5.3.5	Electrochemical impedance spectroscopy analysis of Au–ErGO/MWCNT/graphite.....	177
5.3.6	Morphology evaluation of the Au-ErGO/MWCNT/graphite.....	180
5.3.7	Electrochemical characteristic of Au–ErGO/MWCNT/graphite nanocomposite electrode in comparison to other surface modified graphite sensor.....	181
5.3.8	Electrochemical characteristic of A, G, C and T using Au–ErGO/MWCNT/Graphite.....	185
5.3.9	Impact of pH to DNA bases oxidation on Au–ErGO/MWCNT/graphite.....	187
5.3.10	Multiplexes oxidation of A, G, C and T using Au–ErGO/MWCNT/graphite nanocomposite electrode.....	191
5.3.11	Effect of supporting electrolyte in multiplexes analysis of A, G, T and C using Au–ErGO/MWCNT/graphite.....	192
5.3.12	Analytical performance of Au–ErGO/MWCNT/graphite electrode in multiplex analysis of DNA bases.....	194
5.3.13	Hydrolysis of DNA samples by acid digestion.....	197
5.3.14	Analysis of DNA bases in real samples.....	199
5.3.15	Accuracy and precision study of Au–ErGO/MWCNT/graphite sensor	201
5.3.16	Method validation with UPLC-PDA.....	201
5.3.17	Selectivity and stability study of Au–ErGO/MWCNT–COOH/Graphite in DNA bases analysis.....	206
5.4	Conclusion.....	209

CHAPTER 6: GENERAL CONCLUSION AND FUTURE WORK.....	211
References	213
List of Publications	231
List of Papers Presented	232
List of Publication (front page)	233
Oral presentation (certificate).....	236

University of Malaya

LIST OF FIGURES

Figure 1.1: Honeycomb-laminar structure of bi-layer graphite.....	6
Figure 1.2: Chemical structure of natural anti-oxidants.	12
Figure 1.3: Chemical structure of synthetic anti-oxidants.	12
Figure 1.4: Chemical structure of A, C, G and T.	15
Figure 3.1: Fabricated graphite electrode from used battery.	89
Figure 3.2: CV of gold nanoparticles deposition on graphite electrode.	92
Figure 3.3: SEM of bare graphite (image A) and gold nanoparticles graphite electrode prepared at 8 th (image B), 16 th (image C) and 24 th (image D) deposition cycles.	93
Figure 3.4: CV of Au-NPs/graphite during activation in 0.5 M sulfuric acid. The dotted and solid line corresponds to the first and 20 th CV scan respectively.	94
Figure 3.5: SEM of bare graphite (image A) and gold nanoparticles graphite electrode prepared at 8 th (image B), 16 th (image C) and 24 th (image D) deposition cycles.	95
Figure 3.6: EDX spectral of Au-NPs/graphite surface electrode prepared at 16 th deposition CV cycle.	96
Figure 3.7: CV of 1.0 mmol L ⁻¹ ferricyanide solution using bare graphite electrode at various scan rates.	97
Figure 3.8: Correlation graph of current versus square root of scan rate measured using bare graphite electrode.	97
Figure 3.9: Eff A versus deposition cycle of gold nanoparticle using CV, and comparison made between activated, inactivated and bare graphite electrode.	98
Figure 3.10: Linear correlation graph of peak potential versus logarithm of scan rate that performed using CV and bare graphite electrode in 1.0 mmol L ⁻¹ ferricyanide solution.	101
Figure 3.11: Heterogeneous electron transfer rate (k_s) versus deposition cycle of gold nanoparticles using CV and comparison between activated, inactivated and bare graphite.	103
Figure 3.12: CV of 1.0 mmol L ⁻¹ ferricyanide solution performed using bare graphite versus Au-NPs/graphite electrode prepared at 16 th deposition cycle.	104

Figure 3.13: Randles-circuit model that represents an electrochemical interface of a working electrode with bulk solution.	105
Figure 3.14: Nyquist plot of bare graphite (sphere marker), inactivated Au-NPs/graphite (square marker) and activated Au-NPs/graphite (triangle marker) which was prepared at 16 th CV deposition cycle.	106
Figure 3.15: Graph of double layer capacitance (C_{dl}) versus the number of CV gold nanoparticles deposition cycles.	107
Figure 3.16: (a) CV of myricetin at various scan rates (0.05, 0.10, 0.20, 0.40, 0.60 and 0.80 V s ⁻¹) (b) Graph of peak current versus square root of scan rate of myricetin that performed using Au-NPs/graphite (c) CV of myricetin performed using Au-NPs/graphite versus bare graphite in 0.1 mol L ⁻¹ Britton Robinson buffer.	110
Figure 3.17: SWV of 6.0 µg mL ⁻¹ myricetin measured at pH 2, pH 3, pH 4, pH 5, pH 6 and pH 7 in a 0.1 mol L ⁻¹ Britton Robinson buffer.	112
Figure 3.18: Correlation graph of myricetin anodic peak potential versus pH.	113
Figure 3.19: Schematic illustration of myricetin oxidation (deprotonation) and reduction (protonation) under different pH conditions, with pK _a referring to the dissociation constant of myricetin.	114
Figure 3.20: SWV of myricetin at blank, 2.0, 4.0, 6.0, 8.0 and 10.0 µg mL ⁻¹ of myricetin standard.	115
Figure 3.21: Calibration curve of peak response (current) versus concentration of myricetin.	116
Figure 3.22: SWV of 10 µg mL ⁻¹ myricetin analysis using Au-NPs graphite prepared at 16 th deposition cycle (dotted line) and bare graphite (solid line).	116
Figure 3.23: SWV of myricetin with concentration increment order correspond to 0.2, 0.4, 0.6, 0.8 and 1.0 µg mL ⁻¹ in Britton Robinson buffer.	117
Figure 4.1: CV of 40 µg mL ⁻¹ TBHQ obtained using Au-NP/graphite electrode (solid line) and bare graphite (dotted line).	127
Figure 4.2: CV of 40 µg mL ⁻¹ BHA obtained using Au-NP/graphite electrode (solid line) and bare graphite (dotted line).	127
Figure 4.3: CV of 40 µg mL ⁻¹ BHT obtained using Au-NP/graphite electrode (solid line) and bare graphite (dotted line).	128

Figure 4.4: CV of TBHQ, BHA and BHT that perform at various scan rates (0.05, 0.1, 0.2, 0.4, 0.8 and 1.2 V s ⁻¹) using bare graphite and Au-NP/graphite sensor.	130
Figure 4.5: Linear correlation plot of individual TBHQ, BHA, and BHT anodic peak current (I _{pa}) against the square root of scan rate that was performed using Au-NP/graphite sensor.	131
Figure 4.6: SEM images of (a) Au-NP/graphite electrode surface and (b) bare graphite at 35000 magnifications.	132
Figure 4.7: Linear correlation graph of individual BHA, BHT, and TBHQ anodic peak potential (mV) versus pH. The experiment was performed using Au-NP/graphite electrode.	133
Figure 4.8: Possible mechanism of BHA, BHT and TBHQ oxidation on the Au-NP/graphite electrode surface.	134
Figure 4.9: Comparison of the anodic peak current of TBHQ (striped), BHA (black), and BHT (grey) at pH values of 2–7.	135
Figure 4.10: LSV voltammograms obtained for simultaneous determination of TBHQ, BHA, and BHT performed using Au-NPs/graphite electrode and bare graphite electrode.	136
Figure 4.11: Multiplex LSV detection of TBHQ, BHA, and BHT using the Au-NP/graphite electrode at different scan rates. Note: for a clearer comparison, the LSV performed at 0.1 V s ⁻¹ is represented with a dotted line to prevent confusion from the LSV of 0.2 V s ⁻¹	137
Figure 4.12: LSV curves for a 40 µg mL ⁻¹ mixed TBHQ, BHA, and BHT standard at different SDS concentrations.	138
Figure 4.13: Multiplex detection of TBHQ, BHA, and BHT by LSV at concentrations between 5 and 80 µg mL ⁻¹ with addition of 0.2 mmol L ⁻¹ SDS.	139
Figure 4.14: Linear regression plot of antioxidant anodic peak current responses against concentration (5 to 140 µg mL ⁻¹) with the presence of 0.2 mmol L ⁻¹ SDS.	140
Figure 4.15: Multiplex detection of TBHQ, BHA, and BHT by LSV technique at concentrations ranged between 5 and 80 µg mL ⁻¹ without addition of SDS.	141
Figure 4.16: Linear regression plots of antioxidant anodic peak current responses against concentration (5 to 140 µg mL ⁻¹) without addition of SDS.	142

Figure 4.17: LSV for multiplex detection of BHA, BHT and TBHQ using Au-NPs/graphite. Analysis performed at concentration of 0.1, 0.4 and 0.6 $\mu\text{g mL}^{-1}$ for limit of detection (LOD) study.	143
Figure 4.18: UPLC-PDA chromatogram for multiplex detection of TBHQ, BHA, and BHT at concentrations ranging between 10 and 100 $\mu\text{g mL}^{-1}$	144
Figure 4.19: Linear regression plot of peak area (AU) versus concentration of TBHQ, BHA, and BHT standard performed using UPLC-PDA.	145
Figure 4.20: Correlation plot of samples and spike result that performed using LSV and UPLC methods.	148
Figure 4.21: Stability analysis of the Au-NP/graphite electrode performed over 21 days for multiplex detection of TBHQ (striped), BHA (black), and BHT (grey) under storage conditions at room temperature (25°C).....	151
Figure 4.22: Stability analysis of the Au-NP/graphite electrode performed over 21 days for multiplex detection of TBHQ (striped), BHA (black), and BHT (grey) under storage conditions at 45°C.....	152
Figure 5.1: Hydrodynamic particle size (solid line) and surface zeta potential (dashed line) of MWCNT-COOH particles suspended in Britton Robinson buffer across pH 2, 4, 7 and 9.....	165
Figure 5.2: Schematic flow of Au-ErGO/MWCNT/graphite sensor fabrication.	166
Figure 5.3: CV of MWCNT/graphite that prepared at different pH. The experiment was performed in a 1mmol L^{-1} ferricyanide solution at scan rate of (0.05, 0.10, 0.20, 0.40, 0.60, 0.80 and 1.00 V s^{-1}).....	167
Figure 5.4: Heterogeneous electron transfer rate of the bare graphite (dashed line), and MWCNT-COOH/graphite (solid line) that was prepared at different pH conditions...	168
Figure 5.5: (a) CV of ferricyanide that was performed using MWCNT-COOH/graphite electrode prepared at pH 9 (solid line) and pH 7 (dashed line) conditions. (b) CV of ferricyanide that was performed using MWCNT-COOH/graphite electrode prepared at pH 7 (solid line), pH 4 (dotted line) and pH 2 (dashed line) conditions.....	170
Figure 5.6: Eff A of bare graphite (dashed line) and MWCNT-COOH/graphite electrode (solid line) that was prepared at different pH condition.	170
Figure 5.7: CV of the co-electrodeposition of gold and graphene oxide on MWCNT-COOH/graphite surface at 1 st cycle (dashed line), 8 th cycle (dotted line) and 16 th cycle (solid line).....	172

Figure 5.8: CV of gold nanoparticles/MWCNT-COOH/graphite versus Au-ErGO/MWCNT-COOH/graphite tested in 0.1 mol L ⁻¹ sulfuric acid solution.....	174
Figure 5.9: CV of Au-ErGO/MWCNT/graphite prepared at (a) 8 th ; (b) 12 th ; (c) 16 th ; (d) 20 th ; (e) 24 th deposition cycles. The experiments were performed at 1.0 mmol L ⁻¹ ferricyanide solution at various scan rate from i to viii corresponds to 0.05, 0.1, 0.2, 0.4, 0.6, 0.8, 1.0 and 1.2 V s ⁻¹	175
Figure 5.10: Graph of heterogeneous electron transfer rate (solid line) and effective surface area (dotted line) versus the co-electrodeposition cycle number of gold and graphene oxide.....	176
Figure 5.11: Nyquist plots of Au-ErGO/MWCNT-COOH/graphite (solid) and bare graphite (dotted) electrode performed in ferricyanide solution (1 mmol L ⁻¹).	178
Figure 5.12: Modified Randles-circuit model that represents an electrochemical interface of Au-ErGO/MWCNT/graphite sensor.....	178
Figure 5.13: Nyquist plot fitting between the experimental data and the prediction model of Nyquist plot which was performed using Au-ErGO/MWCNT/graphite.....	179
Figure 5.14: SEM images of (a) bare graphite electrode. (b) MWCNT-COOH/ graphite electrode at 4500x magnification. (c) Au-ErGO/MWCNT-COOH/ graphite electrode at above 30,000x magnification. (d) MWCNT-COOH/graphite electrode at 30,000x magnification.....	180
Figure 5.15: EDX spectral of Au-ErGO/MWCNT/graphite surface sensor.	181
Figure 5.16: CV of 1 mmol L ⁻¹ ferri/ferrocyanide that was performed using MWCNT-COOH/graphite (blue), Au-NPs/graphite (brown), Au-ErGO/MWCNT/graphite (green) and bare graphite (black) at scan rate of 0.2 V s ⁻¹	183
Figure 5.17: CV of guanine (a) and adenine (b) performed using Au-ErGO/MWCNT/graphite. The solid line and dotted line correspond to the 20 µg mL ⁻¹ standard and blank solution CV scan respectively that was performed in phosphate buffer (0.1 mol L ⁻¹ , pH 7).	185
Figure 5.18: CV of T (a) and C (b) was performed using Au-ErGO/MWCNT/graphite. The insets illustrate the enlarged version of the T and C peaks, respectively. The solid line and dotted line correspond to 20 µg mL ⁻¹ standard and blank solution CV scan, respectively that was performed using phosphate buffer (0.1 mol L ⁻¹ , pH 7).	186
Figure 5.19: SWV of guanine (a) and adenine (b) performed using Au-ErGO/MWCNT/graphite at various pH conditions.	187

Figure 5.20: SWV of cytosine (a) and thymine (b) performed using Au–ErGO/MWCNT/graphite at various pH conditions.	188
Figure 5.21: Graph of anodic peak current response of G (lines), A (dotted), C (grey) and T (black) versus pH of the prepared standard solution (20 $\mu\text{g mL}^{-1}$) for effective pH selection study.	189
Figure 5.22: Linear correlation graph of anodic peak potential of C, T, A and G that was performed using Au–ErGO/MWCNT/graphite at various pH conditions. The slope of G, A, T and C were corresponding to $-55.31 \text{ mV pH}^{-1}$, $-62.18 \text{ mV pH}^{-1}$, $-56.00 \text{ mV pH}^{-1}$, and $-66.17 \text{ mV pH}^{-1}$, respectively.	189
Figure 5.23: Oxidation reaction of G, A, T and C on Au–ErGO/MWCNT/graphite surface.	190
Figure 5.24: SWV of simultaneous detection of G, A, T and C that was performed using different surface modified graphite electrode compared to the bare graphite electrode.	191
Figure 5.25: SWV of simultaneous detection of G, A, T and C using Au–ErGO/MWCNT/graphite in (a) 0.1 mol L^{-1} potassium chloride; (b) 0.1 mol L^{-1} phosphate buffer (c) 0.1 mol L^{-1} sodium nitrate; and (d) 0.1 mol L^{-1} Britton Robinson buffer. The standard A, G, T and C is represented by solid lines, and blank as dotted line.	193
Figure 5.26: SWV of simultaneous detection of G, A, T and C with a concentration ranging from 2 to $20 \mu\text{g mL}^{-1}$ for G, A; and 6 to $60 \mu\text{g mL}^{-1}$ for T and C analyte.	194
Figure 5.27: Correlation graph of peak current versus concentration for (a) G and A. (b) C and T.	195
Figure 5.28: SWV of G, A, C and T tested at concentration (I) $0.25 \mu\text{g mL}^{-1}$; (II) $0.5 \mu\text{g mL}^{-1}$; and (III) $1.0 \mu\text{g mL}^{-1}$	196
Figure 5.29: Percentage recovery of A, T, G and C in calf thymus DNA that was prepared at different hydrolysis time using 8 mol L^{-1} sulfuric acid (Note: actual content A = 28.0 %, T = 28.0 %, G = 22.0 % and C = 22.0 % in calf thymus DNA).....	198
Figure 5.30: SWV of calf thymus DNA composition of hydrolyse using 8 mol L^{-1} of sulfuric acid (H_2SO_4 , solid line) versus hydrochloric acid (HCl, dotted line).	199
Figure 5.31: Liquid chromatogram of C, G, T and A peaks that was performed using UPLC with concentration ranging from 1 to $50 \mu\text{g mL}^{-1}$	202
Figure 5.32: Calibration graph of A, G, T and C that was performed using UPLC.	203

Figure 5.33: Correlation graph of SWV result (Au–ErGO/MWCNT/graphite sensor) versus UPLC result. 205

Figure 5.34: Percentage response of Au–ErGO/MWCNT/graphite electrode to A (line), G(dot), C(black) and T(grey) under storage condition of (a) 25°C room temperature and (b) 45°C accelerated temperature condition; throughout 28 days. 208

University of Malaya

LIST OF TABLES

Table 1.1: Classification and type of electrochemical sensors (Stradiotto et al., 2003)... 2	2
Table 1.2: Type of electrochemical base materials with its advantages and disadvantages (Campbell & Compton, 2010; Wissler, 2006)..... 4	4
Table 1.3: Type and materials used for surface modification (Bélanger & Pinson, 2011). 9	9
Table 3.1: Electrochemical characterisation of bare graphite electrode by CV. 98	98
Table 3.2: Electrochemical characterisation of inactivated Au–NPs/graphite electrode by CV. 99	99
Table 3.3: Electrochemical characterisation of activated Au–NPs/graphite electrode by CV. 99	99
Table 3.4: Peak potential difference (ΔE_p) of Au–NPs/graphite (16 th deposition cycle) at various scan rates. 104	104
Table 3.5: Surface roughness factor (R) and constant phase fitting (CPE) of activated Au–NPs/graphite that prepared at different CV deposition cycles. 108	108
Table 3.6: Determination of myricetin in tap water samples using Au–NPs/graphite sensor. 118	118
Table 4.1: Electrochemical characterisation of individual BHA, BHT, and TBHQ that was performed using Au–NP/graphite and bare graphite electrodes. 129	129
Table 4.2: Comparison of the analytical performance made between UPLC–PDA and LSV Au–NP/graphite methods for the multiplex analysis of TBHQ, BHA, and BHT. 143	143
Table 4.3: Simultaneous determination of TBHQ, BHA, and BHT content in food and spiked food samples using LSV method (Au–NP/graphite electrode)..... 146	146
Table 4.4: Simultaneous determination of TBHQ, BHA, and BHT content in food and spiked food samples using UPLC-PDA method. 147	147
Table 4.5: Comparison of the analytical performance shown by different reported electrochemical sensor for the analysis of TBHQ, BHA and BHT. 149	149
Table 4.6: Recovery percentages of the 40 $\mu\text{g mL}^{-1}$ TBHQ, BHA, and BHT standard in the presence of individual interferent using the Au–NP/graphite electrode. 150	150
Table 5.1: Electrochemical characterisation of MWCNT/graphite electrode by CV... 169	169

Table 5.2: Electrochemical characterization of Au–ErGO/MWCNT/graphite electrode over the different deposition cycle by CV.	177
Table 5.3: Comparison of the analytical performance of UPLC–PDA and SWV Au–ErGO/ MWCNT /graphite methods for the simultaneous analysis of G, A, C and T.	197
Table 5.4: Simultaneous determination of G, A, Tand C contents in calf thymus and extracted onion DNA using SWV Au–ErGO/MWCNT/graphite and UPLC.....	200
Table 5.5: Simultaneous determination of G, A, T and C contents in calf thymus DNA that was spiked with a known standard using SWV Au–ErGO/MWCNT/graphite and UPLC.	204
Table 5.6: Comparison of the analytical performance shown by different reported electrochemical sensors used for multiplex DNA base analysis.	205
Table 5.7: Percentage recovery of 20 $\mu\text{g mL}^{-1}$ G, A, Tand C mix standard in the presence of individual interference compounds using SWV Au–ErGO/MWCNT/graphite.	207

LIST OF SYMBOLS AND ABBREVIATIONS

A	:	Adenine
Ag/AgCl	:	Silver-silver chloride reference electrode
BHA	:	Butylated hydroxylanisole
BHT	:	Butylated hydroxyltoluene
C	:	Cytosine
C_{dl}	:	Double layer capacitance
CNT	:	Carbon nanotubes
CWES	:	Coated wired electrode sensor
CV	:	Cyclic voltammetry
DNA	:	Deoxyribose nucleic acid
EDX	:	Energy dispersive X-ray Spectroscopy
EFF A	:	Effective surface area
EIS	:	Electrochemical impedance spectroscopy
E_{pa}	:	Anodic peak potential
E_{pc}	:	Cathodic peak potential
eq.	:	Equation
FETS	:	Field effect transistor sensor
G	:	Guanine
I_{pa}	:	Anodic peak current
I_{pc}	:	Cathodic peak current
ISE	:	Ion selective electrode
k_s	:	Heterogeneous electron transfer rate
MWCNT	:	Multi-walled carbon nanotubes
NPs	:	Nanoparticles

PDA	:	Photo–diode array detector
R_{ct}	:	Electron transfer resistant
ErGO	:	Electrochemical reduce graphene oxide
R_{sol}	:	Electrolyte resistant
SEM	:	Scanning electron microscope
SLS	:	Sodium dodecyl sulfate
SPEs	:	Screen printed electrode
SWV	:	Square wave voltammetry
T	:	Thymine
tBHQ	:	Tert–butylhydroquinone
UPLC	:	Ultra-performance liquid chromatography
W	:	Warburg’s element

University of Malaya

CHAPTER 1: GENERAL INTRODUCTION

1.1 Electrochemical sensor

A chemical sensor is defined as a solid-state device that can transform a signal generated by a chemical interaction between an interest analyte with the device into a useful quantitative or qualitative type of analytical signal. A more specific definition of electrochemical sensor is the involvement of the signal from the sensor which is a current, voltage, or resistance change caused by the analyte composition or quality (Stetter et al., 2003). The development of electrochemical sensor began since 1930; when the study during that time was primarily focused on potentiometric sensor. One of the well-known potentiometric sensor developments is the pH electrode for the measurement of proton H^+ . Generally, potentiometric sensor can be divided into a few categories namely; ion selective (ISE), coated wire electrode (CWES) and field effect transistor (FETS). The working principle of potentiometric sensor is based on the measurement of potential difference across the sensor-solution; with the changes of ion concentration in the solution interface it will alter the sensor potential and this difference in potential is registered for further processing (Bakker & Qin, 2006). Other categories of electrochemical sensor include the amperometric and conductivity sensor. Table 1.1 summarises the type of electrochemical sensor and its working principle (Stradiotto et al., 2003).

Amperometric sensor was the most studied sensor till today. Various amperometric sensors have been developed and they can be sub-categorized into modified sensors, biosensors, screen-printed sensors, and microelectrodes. The working principle of amperometric sensor is based on the measurement of current. It operates by directly measuring the electron transfer that was generated through the reduction or oxidation process from electro-active substances such as ferricyanide and ascorbic acid. Alternatively, it also works by indirectly measuring the constant electron flow (or

current), which upon blockage through interaction such as between antigen and antibodies (biosensor coated), will interrupt the current flow measurement as a result of which the difference of the measured current can be quantified.

Table 1.1: Classification and type of electrochemical sensors (Stradiotto et al., 2003).

Classification	Type	Example
Potentiometric	Ion selective electrode	pH electrode for proton H ⁺ measurement
	Coated wire electrode	PVC electrode for surfactant analysis
	Field effect transistor	Enzyme electrode for immunoassay
Amperometric	Chemical modified sensor	Mercury coating electrode for metal, organic and anion analysis
	Biosensor	Fructose dehydrogenase enzyme on carbon sensor for fructose detection
	Screen printed sensor	Carbon screen printed sensor in ascorbic acid analysis
	Microelectrode	Nickel cobalt microelectrode in copper analysis
Conductivity	Conductivity	Copper oxide sensor in hydrogen sulfide detection
	Resistivity	Zeolite sensor in combustion gas detection

The conductivity sensor is the simplest when compared to the others. The working principle of this sensor is based on the measurement of resistivity. It also operates by either direct or indirect measurement, which the latter is by changing the solid state sensor resistivity to conductivity state in the presence of analyte of interest; whereas direct measurement is based on the conductivity interruption by the analyte. The drawback in conductivity sensor was limited by analyte selectivity, as a result, it was less popular for development (Stradiotto et al., 2003).

Among the electrical conductivity able material that have been extensively studied in sensor development, mercury remained the most classical substance that is preferred for electrochemical sensor particularly in amperometric analysis (Moreno et al., 2003). This is because mercury sensor allows every new surface to be renewable (fresh mercury drop), and possesses a good electrical conductance. However, mercury sensor is limited in applications because of the constraint in its applied potential window, especially towards higher anodic voltage, which itself can be oxidised at a potential greater than 0.1 V; besides mercury is also toxic and requires proper waste management after usage. This is due to the reason the development of mercury sensor has remained a drawback by many researchers. On other hand, the solid state sensor such as gold has emerged as one of the few materials that could be used as an alternative to mercury. Table 1.2 summarises the type of electrochemical base material with its advantages and limitations. Among these metals; gold, palladium and platinum are versatile substances for electrochemical sensor with excellent electrical conductivity and widely applied potential window but these materials are constrained by the intact surface (non-renewable), easy contamination after usage; high cost (expensive precious metal). As a result, it is not feasible to be used as an electrochemical sensor. Copper and silver have narrow applied potential window, with constraints at cathodic potential range (-volt), and, therefore, is not suitable for the analysis of most organic analytes, this has limited the potential to be used as electrochemical sensor.

Carbon based materials could be ideal for electrochemical sensor development. Although, the electrical conductivity is not as good as metal, but the surface of carbon could be modified for improvement. Most importantly, carbon materials are known for its wide applied potential window, renewable surface, non-toxic and low cost (Yang et al., 2015). The latter are much important factors for the development of a sensor, which it could afford as a disposable sensor after use. Some of the known carbon materials for

sensor development are graphite, carbon paste and glassy carbon. The latter two have been commercialized and extensively studied. However, they are not renewable and are subject to chemical attack such as acid or base due to the unstructured carbon molecule (Wissler, 2006).

Table 1.2: Type of electrochemical base materials with its advantages and disadvantages (Campbell & Compton, 2010; Wissler, 2006).

Electrochemical base material	Advantages	Disadvantages
Mercury	Renewable surface, flowable liquid, good electrical conductance, low cost.	Toxic, narrow potential window, scheduled waste.
Platinum	Good electrical conductance, wide potential window, non-toxic, electro-catalytic.	Solid state, non-renewable surface, high cost.
Gold	Good electrical conductance, wide potential window, non-toxic, electro-catalytic, bio-compatibility.	Solid state, non-renewable surface, high cost.
Palladium	Good electrical conductance, wide potential window, non-toxic, electro-catalytic.	Solid state, non-renewable surface, high cost.
Silver	Good electrical conductance, non-toxic.	Narrow potential window, non-renewable surface, high cost.
Copper	Good electrical conductance, non-toxic.	Narrow potential window, non-renewable surface, high cost, chemically instable (acid).
Carbon	Very wide potential window, soft surface, renewable (taping), low cost, non-toxic.	Solid state, moderate electrical conductance
Silica	Low cost, non-toxic, good surface energy.	Weak electrical conductance (semi conductance), narrow potential window.

1.2 Exploration of graphite as a new potential material for the working electrode/transducer in sensor development

The word 'graphite' was originated from the German word '*graphit*' meaning black lead, which is coined in year 1796 because of pencil development. Among the carbon allotrope such as diamond and fullerene; graphite is more crystalline in structure than the others and it possesses both properties of metal and non-metal that gives it the electrical

conductivity, inertness, high thermal resistance and soft surface. Graphite is in abundance and can be divided into synthetic or natural; with the latter categories at lower cost and can be further sub-categorized into flake, vein and amorphous (Wissler, 2006). Among these, vein possesses the best electrical conductivity properties but are rarely used in the industry because of resource constraint compared to the flake type; which the latter is more widely available and are mined in many countries including China, Brazil, Canada, Africa and others. Besides, natural flake graphite also possesses good electrical conductance properties and are widely used in the battery industry (Wissler, 2006). Amorphous graphite was also widely mined. In contrast to the rest it contains a much lower composition of crystalline graphite therefore limiting its applications. It is used mostly for the production of heating element, and is not suitable for the application of battery production because of its poor electrical conductivity properties.

A synthetic type of graphite is produced from both unstructured carbon such as petroleum coke and heating at high temperature of 2500°C. It can be further categorised into primary or secondary synthetic graphite depending on the process control condition, whereby a primary type production is more strictly controlled and the resulting graphites are more pure and consistent. This has incurred a higher price for the synthetic graphite than the natural type; therefore, it is hardly used in the industry except for high stream industry such as engineering material.

The structure of graphite is comprised of sp^2 hybridisation carbon which is arranged in a honeycomb laminar model and assumed a planar dimension, which is stacked and being held together by the bonding of the free valence electron of the carbon. Fig. 1.1 illustrates the bi-layer structure of graphite that comprises of an alpha and beta carbon. Here, the alpha carbon of the first (red line) and second layer (blue line) are held together by covalent bond that stabilises the graphite structure (Appy et al., 2014). The polymorph

structure of graphite has given it the properties of electrical conductivity through carbon π - π interaction in the hexagon ring, and also a stronger mechanical property. It consists of a unique free beta carbon that position on the void cavity of the honeycomb laminar. Since it is a sp^2 hybridised carbon, therefore it possesses a free valence electron that could readily form Van der Waals interaction with metal or other organic molecules. This has given the graphite special surface adsorption energy, which is ideal for surface modification. The alkali metal modification on graphite surface has been studied and widely applied in the field of catalyst such as in the production of biofuel.

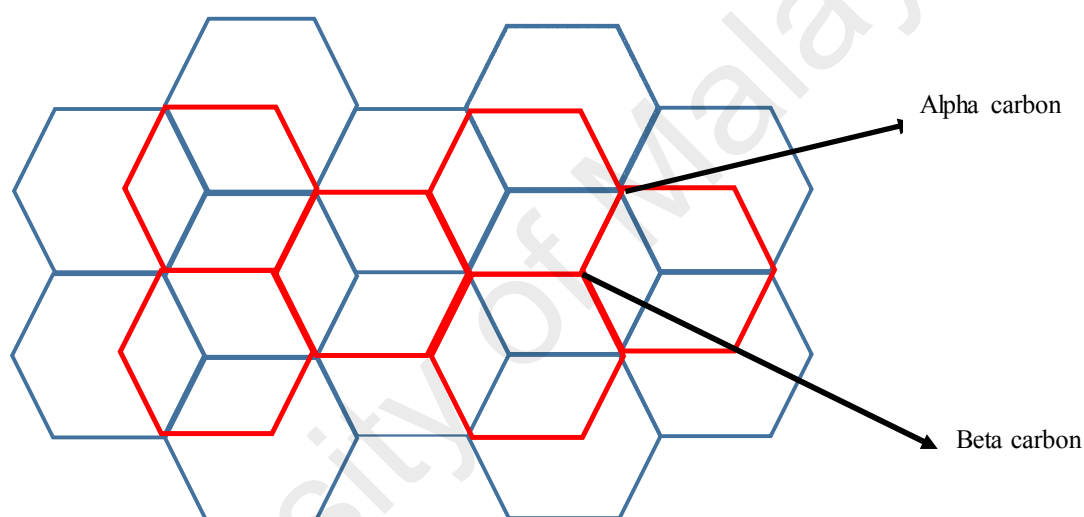


Figure 1.1: Honeycomb-laminar structure of bi-layer graphite.

Graphite has more advantages as an electrochemical sensor than metal and mercury in many approaches. The main factor for graphite preference is because of its applied potential window, which is much wider and could range from +1.4 V (anodic potential) down to -1.0 V (cathodic) (Gabriela et al., 2015; Niedzialkowski et al., 2015); compared to platinum electrode with a potential cut off at maximum of +1.0 V (Campbell & Compton, 2010). A wider anodic potential window is preferable especially in the analysis of anti-oxidant (Gil & Couto, 2013) and DNA bases (Švorc & Kalcher, 2014), which the detection is centered at the anodic potential range which depends on the oxidation properties of the analyte. As it is difficult to oxidise compound, it will require a higher

oxidation potential (anodic), with a limited potential range as it could impede the sensor application. The second important aspect of graphite over metal selection is the practicability of carbon surface to be renewed after usage (Ramesh et al., 2002); which is unlike the metal electrode, where the surface could be contaminated upon analysis and is difficult to be cleaned. This attribute of graphite material is due to the soft structure, from which the molecule is arranged in a layer by layer polymorph (Wissler, 2006) that could be easily stripped off; and it has been successfully demonstrated by Li et al. (2010) in obtaining a fresh surface of graphite rod by using a sticky tape (Li et al., 2010). Another important aspect of graphite based electrode against metal is the cost of carbon material, which is much cheaper (Sengupta et al., 2011) and with a promising electrical conductivity. Moreover, from a commercialised point of view, a disposable gold sensor is impractical for mass production compared to carbon. This point is rather more important when discussing about the development of a lab-on-a-chip concept. Other advantages of graphite based electrode include the inertness of carbon which is resistant to acid or alkali attack (Appy et al., 2014), unlike metal electrode that could be etched at acidic condition. In comparison to mercury or some other metal sensor, graphite is considered non-toxic and can be easily disposed or recycled after use. Moreover it could also be obtained from many available recycle sources such as battery, electronic devices, or pencil.

Spent graphite from batteries is often disposed after use. The study of the battery recycling process by Belardi et al. (2011) has shown that metal parts such as lithium, zinc, and manganese from household alkaline battery has been extensively recycled (Belardi et al., 2011), however parts such as graphite electrode and plastic material are of less valuable for recycling. This could be the other reason if spent graphite could be considered as the material for electrochemical sensor development. It is estimated that the world demand for battery in year 2016 will reach the market value of USD 132 billion,

and the production of batteries in China alone is estimated at 128×10^8 units (Sun et al., 2015). With this huge amount of batteries produced, it will pose a much concern on waste generation, and furthermore improper waste management of batteries could bring much harm to the environment. This dilemma has been a prime focus and numerous actions and law has been approved for the proper disposal and recycling of battery. Graphite from battery could be a potential source of used material that can be recycled into an electrochemical sensor, which not only reduces the waste generation but also converting them into something useful for the consumers. As mentioned, graphite from battery is derived from the flake type of natural graphite, which possesses a good electrical conductance than the other natural or synthetic graphite. Therefore, it is a potential source for the development of graphite sensor that is green and environmental friendly.

In comparison to the metal solid- state electrodes, graphite is still lacking in advantages especially in electrical conductivity. Apart from this, it is also limited in terms of the effective surface area, electrocatalytic and also electrode overpotential (Wring & Hart, 1992). The latter phenomenon, describes the application of a more positive potential in the oxidation process as predicted by thermodynamics (Campbell & Compton, 2010), which could impede the detection of difficult to oxidize substances such as DNA bases. These limitations in graphite can be overcome by surface modification.

1.3 Surface modification of graphite-based electrochemical sensor

Surface modification is a process of altering the chemical or physical properties of a material surface, which could affect the physisorption or chemisorption properties of the studied materials (Bélanger & Pinson, 2011). Depending on the substances, material-combination (composite) and method of surface modification applied, the outcome of which could affect the surface properties of an electrochemical sensor. Various materials could be used for surface modification ranging from a simple noble metal such as gold

nanoparticles to complicated organometallic substances such as ferrocene or polymer materials. Table 1.3 lists some of the surface modified materials and classification that can be used for surface modification.

Table 1.3: Type and materials used for surface modification (Bélanger & Pinson, 2011).

Type	Materials
Nanoparticles	gold, platinum, silver, palladium, nickel
Organic substances	carbon nanotubes, graphene, ethylenediamine, 3,4-dihydroxy phenylalanine (DOPA), 4-vinylpyridine
Organometallic	Aminoferrocifen, ferrocene
Biomolecules	glucose oxidase, ascorbate oxidase, horse radish peroxidase, antibodies
Polymer	polypyrrole, polyaniline, poly (3-methyl thiophene), chitosan, nafion

The type of materials used for the surface modification is dependent on the target analyte and objective of the sensor development. Some of the examples include ferrocene, which is commonly used as an electron or redox mediator in electrochemical sensor, and because ferrocene is compatible to aliphatic bases amines; it is often used in surface modification especially to graft macromolecule such as antibodies or enzyme (Wring & Hart, 1992). One such application is the glucose oxidase enzyme, which is used for the selective detection of glucose. Other applications of the surface modification with material such as noble metal has known to improve the electrochemical properties of the sensor including the electrical conductivity, surface area and electrode overpotential (Campbell & Compton, 2010), which could improve the sensor sensitivity.

The procedure used for surface modification remains a challenge for most researchers, as the method could be complicated or simple depending on the chemical and physical properties of the sensor; as well to the modifier and also the compatibility of both

materials. Some of the mentioned procedures for surface modification include spin coating, spray coating, heat casting, vacuum filtration, dip coating, and electro-deposition (Saha et al., 2014). Among these methods, heat casting, filtration and dipping remained the most direct procedure; which the modifier is directly bonded to the surface of the material and the medium or matrix is then being removed either by using vacuum force that is passed out through a porous material surface (such as polymer) or by evaporative loss through heating by oven. However, the latter method is inappropriate to heat sensitive material such as the protein, and enzyme. The dip coating method has been widely applied in industry such as glove industry, which the working principle is dependent on the material surface energy and must be compatible to the modifier substances. In most cases, the surface energy must be sufficient to bond the modifier substances otherwise it will not coat on the surface properly. Nevertheless, the dip coating method may be inappropriate for sensor, as the method is irreproducible due to agglomeration of the surface modified material (Yang et al., 2015). Other methods such as electro-deposition, spin coating and spray coating often require the use of instrument; eventually these methods are more consistent and controllable in contrast to the method mentioned earlier. For instance, in the spin coating and electro-deposition methods the amount of surface modifier substances, layer thickness, and repeatability are much controllable by the instrument. Besides, the electro-deposition method is also simpler in comparison to the others especially in the formulation of the deposition solution, which does not require complicated additive to optimise the solution viscosity and dispersity as compared to the spin or spray coating. The drawback to the electro-deposition method is associated with the requirement of an electro-active surface modifier agent; otherwise it is not possible to be deposited using this method.

1.4 **Electrochemical analysis for multiplex detection of anti-oxidants and nucleic acid bases**

Electro-active chemicals are substances capable of donating or receiving electron or both which are dependent on the functional group of the chemical structure. The compound containing functional groups such as phenyl, indole, or certain organometallic organic chemical usually possess the properties of redox site. These substances can be analysed by the electrochemical method, which depends on the ease of these substances in donating or receiving the electron. Other factors such as the electron transfer kinetic and electron transfer number can also affect the feasibility of such compounds which can be measured by electrochemical methods (Brewer, 2011; Eckermann et al., 2010; Estevão et al., 2011). Anti-oxidants and deoxyribose nucleic acid bases (DNA bases) are the two groups of chemical substances that could be benefited or have an impact on human physiology and health. Interestingly, both compounds are electrochemically active substances, which could potentially be analysed using electrochemical sensors.

1.4.1 **Anti-oxidants**

Anti-oxidant compounds can be categorised into natural or synthetic compounds (Brewer, 2011). Some of the known natural anti-oxidants including myricetin, epigallocatechin gallate (EGCG), ascorbic acid, resveratrol, gallic acid, melatonin, tryptophan, and serotonin. This class of anti-oxidants can be obtained from many natural resources such as fruits, herbs, vegetables or animal. Study has shown that anti-oxidants are an important source of human dietary intake and it is known to protect humans from diseases such as heart attack, diabetes, cancer and anti-inflammatory (Estevão et al., 2011; Gil & Couto, 2013); besides it can also be used as preservative additive in food for quality control purpose. On the contrary, synthetic anti-oxidant is synthesised in laboratory for the same purpose, some of the known synthetic anti-oxidants are butylated hydroxytoluene (BHT), propyl gallate, butylated hydroxyanisole (BHA), tert-

butylhydroquinone (TBHQ), indomethacin, etodolac etc. Synthetic anti-oxidants have the advantage of lower cost, higher purity, and better quality compared to natural anti-oxidants, besides the yield of these anti-oxidants is not subjected to seasonal harvest such as fruits. Fig. 1.2 and 1.3 illustrate the chemical structure of some natural and synthetic anti-oxidants respectively.

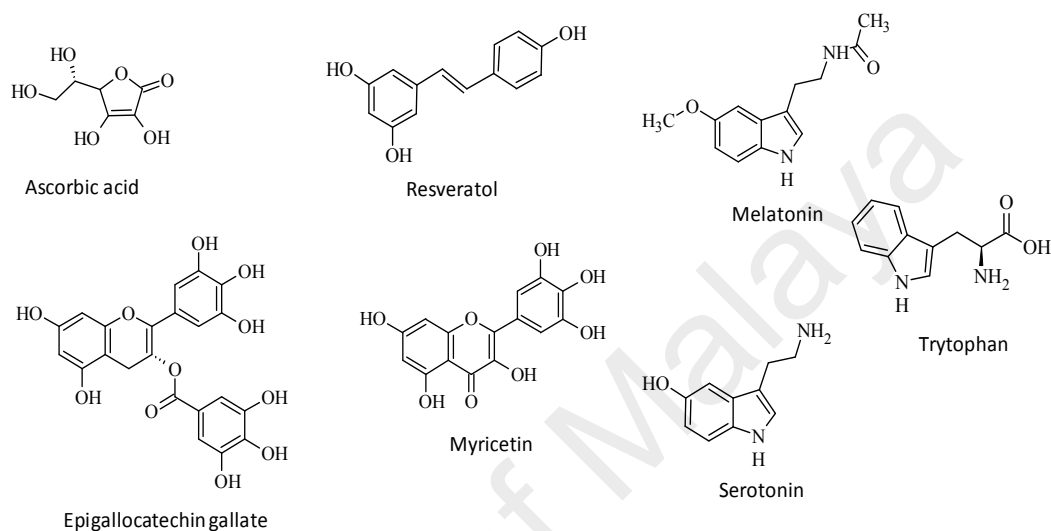


Figure 1.2: Chemical structure of natural anti-oxidants.

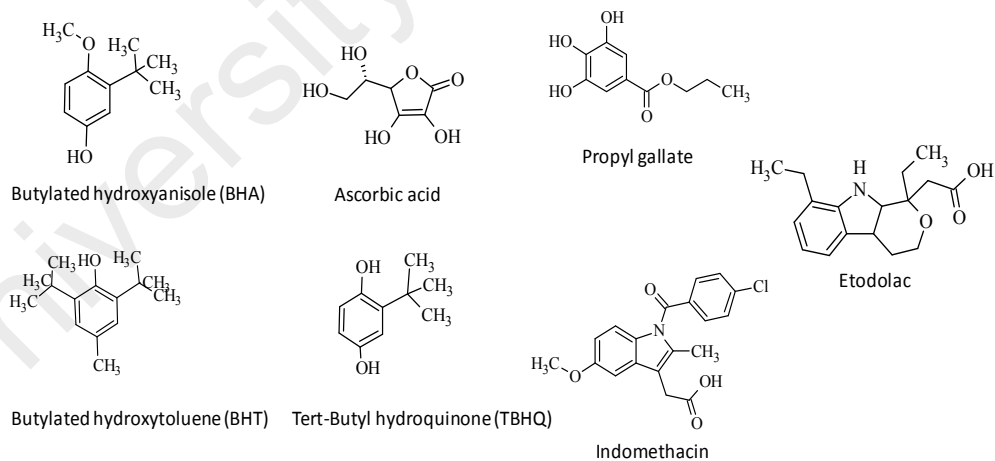


Figure 1.3: Chemical structure of synthetic anti-oxidants.

The capability of anti-oxidants as an electroactive compound has contributed to the radical scavenger properties especially in removing free radical substances such as superoxide anion, hydrogen peroxide, hydroxyl radical and singlet oxygen which was generated by many processes including lipid peroxidation, and body physiological

process such as aerobic metabolism and intercellular signaling (Asensi-Fabado & Munné-Bosch, 2010). When presented at high concentration, the free radical is capable to damage cellular lipid, protein and DNA. Besides, anti-oxidants can also function as a chelator that works by binding and deactivating oxidants such as metal ions (Carocho et al., 2015) and by donating electron to them. Failure to chelate these metal ions could initiate a peroxidation process such as lipid peroxidation in food products. Other functions of anti-oxidants include as quencher that works by deactivating high energy oxidant species; as a regenerator by activating anti-oxidants that has lost its proton; or as an oxygen scavenger that removes oxygen from a system (Carocho et al., 2015). These 5 mechanisms of anti-oxidant are important for both human and industry, either as a dietary supplement that benefits human health or as a preservative used to protect the quality of food products. The ability of these anti-oxidants to neutralise free radicals or oxidants is attributed by its chemical structure that comprises either of phenolic functional groups (Nijveldt, 2001) or indole moiety (Estevão et al., 2011). Both structures are illustrated in Fig. 1.2 and 1.3, whereby the ascorbic acid, gallic acid, EGCG, myricetin and resveratrol are the few examples that bear the structure of phenol; whereas melatonin, indomethacin, serotonin are the chemical substances that contain the structure of indole. Both functional groups are capable to donate proton and electron to the oxidant receiver (peroxide, ROS) and the resulting radical ion of anti-oxidant is stabilised by the phenol or indole ring groups.

Anti-oxidant usage is beneficial to our health and is also important for food preservation. Therefore, analysis of anti-oxidant is important either for the purpose of research study or as a quality control measure in food and supplements. Various analytical procedures have been developed for the determination of anti-oxidants compound. These include the high-performance liquid chromatography (Li et al., 2014), Fourier transform infrared spectroscopy (Goulart et al., 2014), and gas chromatography (Wang et al., 2014).

Although these methods are sensitive and selective, they are not suitable for on-site analysis and require expensive investment in instruments. Because of the sensitivity of anti-oxidant to environment oxidation, therefore on-site analysis is an important criterion to this application. In contrast, the electrochemical method is more simple, rapid, and sensitive (Campbell & Compton, 2010). Moreover, this method can be useful for portable real-time on-site analysis. The challenge that remains in the electrochemical methods still relies on the possibilities for multiplex detection of three or more anti-oxidants compound simultaneously. This attempt has so far not been successfully applied using electrochemical sensor.

1.4.2 Deoxyribose nucleic acid bases (DNA)

Human chromosome is a biopolymer that comprises of a complex combination of deoxyribose nucleic acid (DNA) that interacts between two DNA strands and coil into a double helical structure. It is vital to the human biochemical function that expresses through the function of protein biosynthesis forming various physiological substances such as enzyme. There are four types of nucleic acid bases including adenine (A), thymine (T), cytosine (C) and guanine (G); with the rule that A pairs with T, and G with C. The chemical structure of purines (A, G) and pyrimidine (T, C) contain a heterocyclic nitrogen group, in which the chemical properties resembled those of the indole functional group that is capable of donating proton or electron. In other words, these compounds are electrochemically active. Fig. 1.4 illustrates the chemical structure of A, G, C and T.

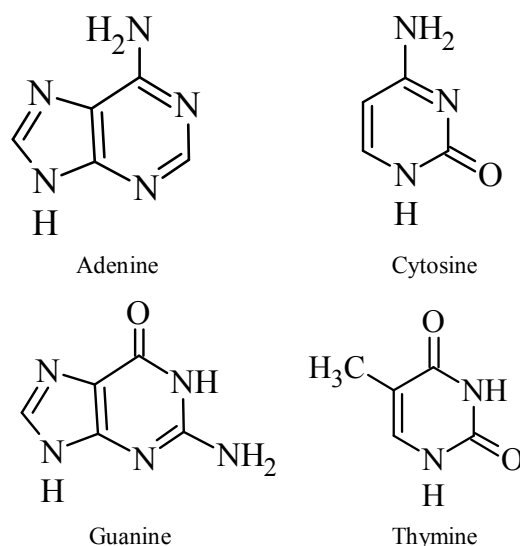


Figure 1.4: Chemical structure of A, C, G and T.

The analysis of DNA bases composition is important especially in the evaluation of DNA damages (Ferancová et al., 2010). Besides, it is also vital for the interaction study of DNA with molecules such as anti-oxidants (Mello et al., 2006). Other related studies include DNA structure changes and genotoxicity study of chemical on DNA substances (de Carvalho et al., 2016). The DNA damage study has been a focus recently, as changes in the composition of DNA bases can potentially impact the stability of double stranded DNA and also alter the genetic information; eventually this affects the protein expression, tumorigenesis, cell death (apoptosis), and genome instability (Sprung et al., 2015). These effects will result to an individual's health risk to disease such as cancer, Alzheimer's, cardiovascular, diabetes, and cataracts (El-Yazbi & Loppnow, 2014; Soares et al., 2015). Few factors have been investigated that could be associated to DNA damages. This includes exposure to ionizing radiation (El-Yazbi & Loppnow, 2014; Joshi et al., 2012; Sprung et al., 2015), reactive oxygen species (Joshi et al., 2012) and also individual dietary lifestyle (de Carvalho et al., 2016). To view the details of these damages, a comprehensive analysis of the A, G, C and T component is important. Moreover, a simultaneous detection of this nucleic acid is required, which is important to measure the

ratio of the DNA bases. Various analytical methodologies have been developed for this purpose including liquid chromatography (Moral *et al.*, 2005; Graven *et al.*, 2014), gas chromatography (Glavin *et al.*, 2006), fluorescent method (Pang *et al.*, 2016), capillary electrophoresis (Yang *et al.*, 2009) and electrochemical method (Gao *et al.*, 2014; Niedziałkowski *et al.*, 2015; Švorc & Kalcher, 2014; Yari & Derki, 2016). However, the challenge remained in DNA bases measurements including the attribute of a rapid detection, multiplexes, high sensitivity, accuracy and selectivity. Chromatographic techniques are accurate, precise, and selective but they require a complex sample preparation such as DNA enrichment or a derivatisation process (El-Yazbi & Loppnow, 2014; Glavin *et al.*, 2006; Švorc & Kalcher, 2014), which are time consuming. Nevertheless, the electrochemical method is rapid, simple, sensitive and compatible to biological samples, as it involves the use of electrolyte solution (salt) to resemble human physiological condition such as phosphate buffer (pH 7).

The electrochemical analysis of DNA, especially of pyrimidine bases (T, C), is difficult, because the pyrimidine bases are less potential to be oxidised as it requires a higher anodic potential (Oberacher *et al.*, 2015) application. Besides, the electron transfer kinetic of the DNA bases is slow (Švorc & Kalcher, 2014) as it impedes much electron transfer to the sensor resulting in lower current signal. Ample of sensors have been developed for the detection of DNA bases, however, the attempt was only successful in the purine bases (G, A) analysis; multiplexes detection of A, G, C and T by electrochemical sensor remained as a challenge for development. Hence, the electrochemical sensor used in the DNA bases study should possess the attributes of wide anodic potential window, electrocatalytic properties for current amplification, high sensitivity, and also chemically inert.

1.5 Scope and objectives of the study

The main objective of this Ph.D. thesis is to develop a simple, green and cost effective method for the fabrication of a graphite based sensor material from a used battery, in which it could be a potential source of recycled waste for electrochemical sensor development. Due to the many drawbacks of the graphite electro-properties such as high over potential and moderate conductivity; a surface modification of the fabricated graphite electrode is performed to improve the electrochemical properties of the fabricated graphite sensor including the effective surface area, electrocatalytic properties, fast electron transfers kinetic and electrode overpotential. The developed surface modified graphite is termed as the nanocomposite graphite sensor, and is subsequently applied in the methodology development for the multiplex measurement of natural and synthetic anti-oxidants and nucleic acids; this is to showcase the potential use of the graphite sensor in industry and laboratory testing. The structure of this thesis is divided into six chapters, in which three research articles are produced.

The first chapter of this thesis work is to give some background information and general discussion about sensor, graphite material and also the problem statement that is currently faced by the solid state electrode. In this chapter, the potential uses of the battery graphite material as a new source for electrochemical sensor development were discussed. Subsequently, the advantages and obstacles in the anti-oxidant and DNA base analysis using electrochemical sensor were also highlighted; especially on the attempt for multiplex analysis using electrochemical sensor; which remains a challenge to the development of electrochemical sensor.

The second chapter is to review on the recent research and literature work that has been contributed to the development of carbon bases sensor, and its application in electrochemical analysis. Besides, the details of the surface modification sensor and its

attributes to the development of electro analytical method were reviewed. To provide more comprehensive information of this thesis work, the analytical method of development on anti-oxidant and deoxyribose nucleic acid using various methods was also reviewed.

The third chapter is focused on the development of a graphite based sensor that is obtained from a used battery. Subsequently, a procedure for surface modification with gold nanoparticles is studied by optimising the deposition of gold nanoparticles on the graphite surface; with the acceptance performance taken into consideration by evaluating the morphology and electrochemical properties of the sensor using a field emission scanning electron microscope (FE-SEM), cyclic voltammetry (CV) and electrochemical impedance spectroscopy (EIS). To evaluate the practical use of the developed sensor in electrochemical analysis, a test on the standard ferricyanide redox solution and myricetin standard was performed. The fabricated sensor is termed as the gold-nanoparticles graphite (Au-NPs/graphite). In this chapter, the potential use of graphite from used battery as a sensor material will be addressed.

The fourth chapter of this thesis is centered on the application of Au-NPs/graphite sensor in synthetic anti-oxidants analysis. Here, an analytical methodology is developed for the multiplex determination of TBHQ, BHA and BHT using the Au-NPs/graphite sensor. These synthetic anti-oxidants are selected because it's widely used in the industry as a preservative and it is detrimental to health when used at high dosage usage. A linear sweep voltammetry procedure is proposed as the technique for the multiplex detection of the three anti-oxidants, in which presently this attempt has not been successfully performed before. Subsequently, the analytical performance of the method is validated and is compared with the liquid chromatography; in order to ensure the fitness use for regulatory control purpose. The developed method is used in the real sample analysis,

from which the TBHQ, BHA and BHT composition in the various market samples are determined. To evaluate the robustness of the method, various sample matrixes including fat, oil and emulsion based products are selected for evaluation; and spike recovery analysis is also performed to ensure the method reliability.

The fifth chapter of this thesis is focussed on the development and investigation of a layer-by-layer nano-composite graphite based sensor. This is to further expand the potential applications of the graphite in electrochemical analysis by using nanomaterial of multiwalled carbon nanotubes (MWCNT) deposition as the based layer. It is expected to improve the sensor effective surface area and electron conductive network. Successively followed with an intercalation layer of graphene and gold nanoparticles, an improvement in the electrocatalytic, overpotential and electrical conductivity of the sensor is expected. The layer-by-layer deposition procedure is studied and optimised; and the acceptable performance is taken into consideration by evaluating the morphology and electrochemical properties using Zeta-nanoparticle size analyser, FE-SEM, CV and EIS. The fabricated sensor is termed as the graphene-gold nanoparticles/multiwalled carbon nanotubes graphite sensor (Au–ErGO/MWCNT/graphite). The applications of the sensor in electrochemical analysis are further explored for the multiplex determination of A, G, C and T. Square wave voltammetry is proposed as the electrochemical technique for the detection of A, G, T and C simultaneously, in which the attempt has not been performed by any graphite sensor before. The developed method is validated and compared with the liquid chromatography method to ensure the analytical performance is fit for use in DNA damage study. The developed sensor should possess sufficient redox site to accommodate the multiple detection of A, G, T and C; besides it must also possess electro-catalytic properties to amplify the signal particularly in pyrimidine (T and C) detection. Other optimisation including the digestion procedure for hydrolysis of double stranded DNA into individual bases is also studied. The validated method is tested on real DNA samples

in order to assess the damage according to Chargaff's rules. Sample matrix of both plant and animal dsDNA is also studied to ensure the method is practically used in laboratory. Spike recovery is performed to evaluate the method reliability.

The final chapter of this thesis is to give a general conclusion on the extent of achievement of this research work from the intended research objective. Future study and development that can be further considered for the continuity of this work were also discussed in this chapter.

University of Malaya

**CHAPTER 2: A REVIEW ON THE GRAPHITE BASED COMPOSITE
WORKING ELECTRODE AND THE ANALYTICAL METHODOLOGY USED
IN ANTI-OXIDANTS AND DNA BASES ANALYSIS**

2.1 Introduction

The development flow in the electrochemical sensor study is particularly influenced by 3 factors, which are; the sensor development platform, electrochemical characterisation and targeted analyte detection. To accomplish this, an understanding of the different properties of the sensor platform such as carbon, metal, silica and composite is important. The challenge in getting this material into a solid state sensor which comprises of the working area, transducer and connector requires multiples steps of fabrication that includes different levels of surface material fabrication, cleaning, insulation and continuity test (electrical conductance test). The electrochemical performance of the fabricated sensor (analysis site) needs to be characterised, in order to understand the practical use of the sensor. Limitation in any of the electrochemical attributes (redox site, electron transfer rate, overpotential) could impede its application in the chemical analysis. Surface modification with nanomaterial can be employed to improve such limitation of the sensor, which involves a simple or complicated preparation steps that depends on the interaction between the modified material and sensor platform. The third factor in the sensor development is in the methodology development for the measurement of targeted analyte. This is an important factor that needs to be studied in detail to ensure the reliability of the sensor measurement. To achieve this, an understanding of the multiple processes that includes buffer/solvent preparation, detection technique, measurement and method validation is important.

To attain the above goal, various literature and research works have been carefully reviewed in this chapter. The focus is centered on the fabrication of graphite based sensor

including pencil graphite, graphite-epoxy based and commercial graphite. Besides, various surface modification procedures in improving the sensor performance were also reviewed by grouping into 4 different material categories, which includes noble metal nanoparticles, carbon nanoparticles, electro-polymer, and biomaterial. Finally, on the targeted analyte measurement, various sample preparation procedures, qualitative and quantitative analysis of anti-oxidants and DNA bases were also reviewed in this chapter.

2.2 Fabrication of graphite based sensor

Graphite is a suitable source of material for sensor development. There were ample studies which have been published utilising different resources of graphite including the graphite powder and pencil lead, which have been widely used for the fabrication of graphite sensor.

2.2.1 Graphite-epoxy sensor

Graphite powder was predominately used as the material for early sensor fabrication. A work described by Moreno-Baron et al. (2003) that using 50 mm particles size graphite powder and epoxy resin was used to develop graphite electrode. Both materials were mixed at a ratio of 1 to 4, and the resulting paste was filled into a polyvinylchloride (PVC) cylindrical tube of 6 mm diameter. Copper wire was inserted into the paste as an electrical contact point. Subsequently, the composite mixture was cured at 40°C to harden the epoxy; and the surface was polished with abrasive paper, followed by alumina silicate paper to obtain a smooth surface. The developed sensor was used for the analysis of lead (Pb), copper (Cu) and cadmium (Cd) in water (Moreno-Baron et al., 2003). A comparison study with the glassy carbon (GC) sensor has shown that the surface of the fabricated graphite sensor could be easily renewed using cello tape. The drawback of this sensor was particularly on the PVC housing, which is sensitive to organic solvent and also susceptible to acid attack. In a study by Pumera et al., (2005) a similar preparation step

using graphite powder but with a mixed ratio of 1:5 to epoxy resin was reported. The sensor was successfully used for the determination of gold nanoparticles in a water solution. The electrochemical characterisation using CV has shown that the fabricated graphite-epoxy sensor possesses more conducting surface (28.3 mm^2) than the standard glassy carbon electrode (7.1 mm^2), that contributes to the sensitivity of the graphite-epoxy in gold detection (Pumera et al., 2005).

In a separate study by Jayasari et al., (2006) a graphite epoxy electrode was fabricated but with additional silvercyanoferrate. The composite material was mixed thoroughly in a ratio of graphite powder to silvercyanoferrate and epoxy at 65:5:30 respectively, which was followed by packing it into a glass tube of 4 mm diameter. The composite mixture was cured and then removed from the glass tube; successively, the paraffin molten was used to insulate the sensor body and the surface was polished using white paper until it becomes glossy finish. The developed graphite-epoxy sensor was used as amperometric sensor for the detection of BHA. The advantages of silvercyanoferrate in the graphite epoxy electrode have shown improvement in the sensor response to BHA, which the silvercyanoferrate function as the redox mediator (Jayasri & Narayanan, 2006). Another study by the same author on the graphite-epoxy electrode was reported, but this time, with a different mediator using manganese (II) hexacyanoferrate. The described fabrication procedure was similar but with the substitution of manganese cyanoferrate instead of silvercyanoferrate. The electrochemical characterisation has shown an improvement in the sensor overpotential when compared to unmodified graphite wax, which could be attributed from manganese (II) hexacyanoferrate. The developed sensor was used for the analysis of BHA in food samples (Jayasri & Narayanan, 2007).

A fabrication of rutin anti-oxidant sensor was described by He et al. (2007) in which a disk type of graphite-epoxy sensor was fabricated by mixing graphite powder with molten

wax at a ratio of 5:2. The composite was thoroughly mixed and then poured into a hollow space of polyethylene strip plate. The graphite-epoxy disk was allowed to cure before being led out by a copper foil. The surface of the disk was then polished with emery paper to obtain a smooth and shining surface. The electrode was successfully employed for the determination of rutin (anti-oxidant). Besides, the author has also modified the sensor by drilling the disk with 9 holes, which is used for the study of UV-Vis spectral on the rutin upon changing the electric potential (He et al., 2007).

Although many studies on graphite-epoxy sensor have been published, however, most of the modification was not focused on the sensor surface; instead it is usually mixed with graphite and epoxy. As a result, it has restricted the availability of graphite structure on the surface, because of the surface dilution by epoxy material. Therefore, it is expecting such electrode to be less sensitive (lower effective surface area) when compared to pure graphite sensor. Besides, the inertness of epoxy material to chemicals such as solvent, acid and alkaline was not studied in detail.

2.2.2 Pencil graphite sensor

A typical pencil lead comprises of clay and graphite components (Alipour et al., 2013), as clay is a non-conductance material, which could affect the electrical conductivity of a pencil lead. The impact of clay component on sensor performance was demonstrated by Teepoo et al. (2012) when the author has extracted graphite lead from pencil of different grade that ranges from HB, 2B, 1H, 2H, 3H, 4H, 5H, and 6H. Higher numerical values of these grades indicate a higher content of the graphite component. The obtained pencil lead has a diameter of 2.0 mm; to prevent any lateral exposure of the pencil graphite to chemical, a high-density polyethylene layer was coated on the rod and the electrical contact point was made by inserting a wire into the pencil lead graphite (PG). The surface of the fabricated PG was polished with alumina silicate until a smooth surface is obtained.

An electrochemical characterisation of the I_{pa} / I_{pc} ratio for each grade of PG obtained from pencil was performed, which showed that PG with a low clay content gave a better reversibility property, with the ratio of I_{pa} to I_{pc} that is close to unity. The author concluded that grade 6H pencil was the best material for the sensor fabrication (Teepoo et al., 2012). In the same study, the author further modified the surface of the PG with chitosan, gold nanoparticles and horseradish peroxidase enzyme (HRP) in a layer-by-layer manner; and the fabricated sensor was used for the detection of hydrogen peroxide. In comparison to the GCE sensor (HRP/Ruthenium nanoparticles/chitosan/GCE, $0.798 \mu\text{A mM}^{-1}$) it was shown that the surface modified PG (HRP/gold nanoparticles/chitosan/graphite, $149 \mu\text{A mM}^{-1}$) gives a better sensitivity toward hydrogen peroxide detection (Teepoo et al., 2012).

In a separate study by Gabriela et al. (2015) a mechanical pencil lead (mPG) was used for the fabrication of the disposable graphite sensor. The diameter of the mPG used was measured at 0.5 mm. A mechanical pencil body was used to hold the pencil lead, and electrical contact point was soldered onto the metallic part of the mechanical pencil to provide connection to the potentiostat. The sensor design allowed a new mPG lead to be refreshed at 1 mm long for each measurement. No further modification on the surface was described by the author, as the graphite lead was fragile to be handled (Gabriela et al., 2015). The fabricated sensor was successfully used for the measurement of caffeic acid in tea samples. A comparison study of the sensor with other surface modified working electrode particularly the standard glassy carbon electrode (GCE). The study has shown that the performance of mPG is better in terms of detection limit and dynamic range; but is limited when compared to GCE that modified with MWCNT, in which the drawback of mPG detection limit could be explained by the superior electrochemical performance of MWCNT on GCE. Besides, the problem of high activation energy of over

potential in graphite material (Wring & Hart, 1992) was not addressed and studied by the authors.

A similar fabrication work utilising a mechanical pencil lead (mPG) was demonstrated by Rezaei et al. (2014) but using larger graphite lead diameter of 0.7 mm. The significant highlight in the study was the complexity in the surface modification of pencil graphite. The author has recognised the fragility part of the mechanical pencil lead and its limitation in the option for different surface modification method other than electrodeposition. The author has successfully developed a molecular imprinting sensor on the graphite lead using polypyrrole by electrodeposition method, which was used in the detection of lorazepam. The performance of the fabricated graphite sensor (polypyrrole@sol-gel/gold nanoparticles/MIP/graphite) exhibited a better detection limit (0.09 nmol L^{-1}) than chromatography (7.8 nmol L^{-1}) and the surface modified glassy carbon sensor (gold nanoparticles/orthophenylenediamine /MIP/GCE sensor, 0.2 nmol L^{-1}) (Rezaei et al., 2014). A study on the fabrication of quercetin modified pencil graphite (PG) was reported by Dilgin et al. (2013), which utilised a PG with diameter of 0.5 mm, and electrodeposition with quercetin. The developed sensor was used for the determination of nicotinamide adenine dinucleotide (NADH) and achieved a limit of detection of $0.15 \text{ }\mu\text{M}$ (Dilgin et al., 2013). All the studies have shown that the electrodeposition method is more suitable for the surface modification of pencil graphite (PG) with a diameter of less than 0.7 mm.

A multiplex analysis of dopamine and uric acid in biological sample was detected using PG. The sensor was fabricated from pencil lead with a diameter of 2.0 mm; Teflon tape was used to cover the lateral of the PG from exposure to chemical and the tip was polished with alumina silicate. Before the electrode was used for analysis, it was activated by CV with potential scanning between 1.5 to 2.0 V (versus calomel electrode) in

phosphate buffer pH 7.0 (Alipour et al., 2013). The author has described the importance of pretreating the graphite electrode upon usage; as inactivated pencil graphite electrode (untreated graphite) can impact the electron transfer kinetic as a result of which it could impede the oxidation of dopamine and uric acid. The formation of Oxide film was the factor that caused the graphite inactivation, which can be removed by applying CV at high anodic potential range. The developed graphite sensor showed a vast improvement in the detection limit of dopamine ($0.033 \mu\text{M}$) when compared to the surface modified glassy carbon (carbon nanofiber GC electrode).

Pencil graphite (PG) is a potential source of material for electrode fabrication; however the material is difficult to handle because of its brittleness that can be easily broken when dropped onto hard surface. Besides, PG does not contain 100% graphite as it is premixed with clay; therefore PG is expected to have a lower Eff A (redox site) than the pure graphite rod, which could impact the sensor sensitivity. The advantages of PG based sensor are attributed to its soft surface; which can be easily refreshed even by simple polishing using paper.

2.2.3 Industrial graphite sensor

The industrial grade graphite rod is a potential source of material for sensor fabrication because it comprises purely of graphite structure. The only drawback to the use of graphite rod is the price and its size dimension, which is expensive and usually comes in a large diameter that requires further cutting using a special tool. Few studies have been published, which employ the industrial graphite rod in sensor fabrication.

A glucose sensor has been developed by Natalja et al. (2014), which utilised a graphite rod purchased from commercial. The rod was cut into a diameter of 3 mm and the surface was polished with alumina silicate, a silicon tube was used to protect the graphite rod from lateral exposure to sample solution. The surface of the graphite was modified with

gold nanoparticles, followed with the immobilisation of glucose oxidase (GO). The fabricated graphite sensor was successfully used for the selective detection of glucose in human serum samples. Comparisons of the analytical performance between graphite with other sensors include the glassy carbon (GO/Au–NPs/GC), indium tin oxide (GO/Au–NPs/ITO) and gold electrode (GO/Au). This comparison has showed that the graphite possessed a wider detection range up to 10 mmol L⁻¹ (German et al., 2014). This could be attributed by the large surface area of graphite material, which provides more sites for enzyme immobilisation. The only drawback in this work is the use of silicon tube, which is sensitive to heat and organic solvent.

In a separate study by Li et al. (2010), a graphite electrode was fabricated in the same manner as described by Natalja et al. (2014) but the only difference is the use of Teflon tube instead of silicone. The surface of the graphite electrode was modified with 4–aminophenyl then followed with gold nanoparticles and polyaniline (Li et al., 2010). In another study by Lu & Zangari (2006), which also fabricated electrode material using graphite rod purchased from the industry with the surface modified with platinum particles (Lu & Zangari, 2006). Both studies were not extended to sensor application, as the interest was focused on the fabrication and characterisation of the working electrode preparation.

2.3 Surface modification of electrochemical sensor

The material used for sensor fabrication may not possess all the electrochemical attributes that fit for its intended application in chemical detection. Surface modification of sensor has been a promising method that could alter the physical or chemical properties of the sensor. Over a decade, many studies regarding surface modification of sensor have been published, and the study has shown success in improving the sensor electrochemical properties that fits to its purpose.

2.3.1 Noble metal nanoparticles

Among the many materials used for surface modification, metal nanoparticles are the substances that have been extensively used for modification of a sensor surface. The objective use of metal nanoparticles can be many including as an electron mediator that forms the connection between substrate and sensor (German et al., 2012); as an electrografting material, since gold is compatible to many biological materials (Bélanger & Pinson, 2011). Besides, metal nanoparticles such as gold and platinum also possess electrocatalytic properties that could amplify the electron transfer signal (Guo & Wang, 2007). Metal nanoparticles can also enhance the convergent mass transport properties, in which it improves the number of oxidation site, heterogeneous electron transfer rate and hence its sensitivity (Campbell & Compton, 2010; Streeter & Compton, 2007). Although, with the many interesting applications of metal nanoparticles, nevertheless the compatibility of these metal nanoparticles to the sensor substrate remained a challenge for many researchers to deposit the nanomaterial on the sensor surface. Various procedure can be used for the deposition of metal nanoparticles which includes electrografting (Bélanger & Pinson, 2011), electrodeposition (Hezard et al., 2012), drop-casting (Yin & Qin, 2013), and electro polymerisation (Li et al., 2010).

In general, gold nanoparticles are produced by reducing tetrachloride auric (HAuCl_4) acid with a reducing agent such as using sodium citrate and ascorbic acid. The type of reducing agent used will affect the particle sizes of gold nanoparticles. Up to date, seven different types of chemical reductants were investigated in the preparation of nanoparticles, including microorganism, plant extract, physiological substances, inorganic reagent, metal complexes, organic reagent, and polymer (Dumur et al., 2011). Among these substances, organic reagent has been extensively used as a reductant in the fabrication of sensor. In a work described by Natalija et al. (2015) sodium citrate was used as the reductant and capping agent for the preparation of gold nanoparticle solution

(German et al., 2014) in which, the gold anion (Au^{3+}) was reduced to elemental (Au^0). Since the OH group of citrate can adsorb onto the surface of gold particles, therefore, it renders the size of the gold particles and prevents them from aggregation (Dumur et al., 2011). The prepared gold nanoparticles were deposited onto the surface of a graphite electrode by applying a fix electrical potential, and the resulting gold-nanoparticles are used as the electron mediator for the immobilisation of glucose oxidase. Gold is well compatible to biological enzyme due to the favourable adsorption of functional groups such as NH, OH, and SH in the enzyme molecule (Dumur et al., 2011). The fabricated glucose oxidase/gold-nanoparticles/graphite sensor was used for the detection of glucose in human serum samples.

In a separate work by Lu et al. (2014) cysteines-fullerenes derivatives were used as the reductant (reduced HAuCl_4) and capping agent. The latter is important to stabilise the gold nanoparticles, which is possible through the adsorption interaction between the sulfur group of cysteines with the elemental gold particles (Dumur et al., 2011) that prevented further nuclei growth. The resulting Au-NPs-cysteines-fullerene products were casted onto the surface of the glassy carbon electrode and dried at room temperature (25°C) to obtain AuNPs@C60/GCE sensor. The sensor was successfully used for the individual determination of catechol (CC), hydroquinone (HQ) and p-cresol (PC). With the surface modification using gold nanoparticles and cysteine on the glassy carbon surface, the developed sensor has shown an improvement to the electron transfer rate and sensitivity. This has reflected a good detection limit in the CC and HQ analysis in contrast to other sensors such as Cds/ITO sensor by 1 magnitude (Lu et al., 2014).

An electrografting method was proposed by Li et al. (2010) using a 4-aminophenyl to adsorb the cationic gold (Au^{3+}). 4-aminophenyl was first immobilised on to the surface of the graphite, which was subsequently followed by dipping the sensor into a solution of

H₂AuCl₄. The adsorb Au³⁺ by the amino (NH) group of 4-aminophenyl was then reduced using a pulsed potential stepped from 0 to -0.8 V for 200 ms. As a result, the cationic gold is reduced to elemental Au (0). These processes were repeated again in order to grow the gold nuclei until certain particle size was obtained. In this work, a 100 nm size of gold particles was obtained. A controlled procedure on gold nanoparticles size distribution was proposed by the author, no application was tested using the sensor (Li et al., 2010).

A composite casting of gold nanoparticles was proposed by Liu et al. (2008). A composite solution of multiwalled carbon nanotubes (MWCNT) and gold nanoparticles was prepared prior to the deposition on the glassy carbon electrode. The gold nanoparticles solution was first prepared using 1% H₂AuCl₄, in which sodium citrate was added as a capping agent, and then followed by 0.75% of sodium boron tetrahydride (NaBH₄) as the reducing agent (inorganic molecule). Subsequently, a second solution of MWCNT was prepared by dissolving 1 mg of the black powder into DMF solution. Finally, both solutions of MWCNT and gold nanoparticles were mixed. The composite solution was deposited onto the glassy carbon electrode by direct casting and allowed to dry at room temperature (25°C) for one day. The developed sensor was used to detect the A and G in DNA, and the sensor has shown electro catalytic properties that were contributed by the gold nanoparticles. This has improved the sensor sensitivity and detection limit in A and G detection when compared to the bare glassy carbon electrode counterpart (Liu et al., 2008).

Electrodeposition is a simple and more direct procedure for deposition of metal nanoparticles. A method described by Hezard et al. (2012) has employed CV to reduce the cationic Au³⁺ to elemental Au (0). The resulting gold is deposited on the surface of glassy carbon with subsequent CV scanning the gold nanoparticle which has grown in size. In this way, the gold nanoparticle size was able to control that based on the number

of CV scan. The developed sensor is designated as Au-NPs/glassy carbon, and it has been used for the trace detection of mercury (II) (Hezard et al., 2012). The author has also established a relation of the sensor response towards the gold nanoparticle size, and found that at 36 nm (particle size) the sensor performance was the most optimised; and with the increase in the nanoparticle size the sensor response was found to be suppressed. A smaller nanoparticle is preferable, as it could enhance the convergent based diffusion of mass transport rather than the linear diffusion. The former diffusion could attribute to the improvement of active surface area, selectivity, and catalytic activity (Campbell & Compton, 2010). Electrodeposition is also preferred by many researchers, as the method is clean and does not contaminate the surface of the sensor with substances such as reductant (ascorbic acid, citrate, and NaBH_4) (Hezard et al., 2012).

Apart from gold nanoparticles, a similar approach has been performed by Lu et al., (2006) in which platinum nanoparticles were deposited on the graphite surface. A fix potential of 0.8 V vs. SCE was used in a solution of H_2PtCl_6 instead of using CV technique, and the particle size was controlled by the deposition time (Lu & Zangari, 2006). An alloy of gold and platinum nanoparticles was studied by Song et al., (2010) whereby an indium tin oxide (ITO) plate was immersed in a mix solution of H_2PtCl_6 and HAuCl_4 . The gold and platinum nanoparticles were electrodeposited on the ITO surface by using a CV. The developed sensor was used for the detection of nitrite, and a synergistic effect was demonstrated by the sensor, in which the current response (signal) has improved when compared to the mono-metallic sensor such as AuNPs/ITO and PtNPs/ITO (Song et al., 2010). A surface modification work with platinum nanoparticles was demonstrated by Jia et al. (2016), which a gold-glassy carbon electrode was immersed into a solution containing potassium chloroplatinate (K_2PtCl_4), and ascorbic acid was added to reduce Pt^{2+} ion to elemental Pt^0 that successively deposited to the surface of the glassy carbon electrode. The fabricated Pt nanoparticles-gold GCE was

used as an amperometry sensor for the detection of glucose. With platinum decoration on the gold GCE surface, the author has found vast improvement in the detection limit that was contributed by the electro catalytic effect of platinum (Jia et al., 2016).

In a separate study by Kumar et al. (2010) a copper nanoparticle (Cu-NPs) composite sensor was developed for the measurement of glucose by oxidation. The Cu-NPs was deposited on to the indium tin oxide (ITO) electrode by immersing the substrate into a solution of copper sulfate; and later the potassium perchlorate was added to reduce Cu^{2+} to elemental Cu^0 . Under a fix applied potential of -0.9 V vs. Ag/AgCl the copper metal was deposited onto the ITO. The developed sensor has shown excellent performance in its detection limit and electrocatalytic properties when compared to other sensors including Ni powder ceramic composite sensor, Chitosan-GCE, ZnO-gold sensor and bare graphite electrode. This study has shown that the surface modification, the electrochemical performance of the ITO have improved and are better than the bare graphite alone; suggesting the significance of surface modification in the sensor development (Kumar et al., 2010).

The polymer reducing agent has been used by Mehta & Umar (2011) in producing a zinc sulfide nanoparticles, using polyethylene glycol and thioacetamide to reduce zinc acetate (ZOAc) to zinc sulfide (ZnS) nanoparticles with the support of microwave energy (Mehta & Umar, 2011). Polymer are known to be a good reducing agent and stabiliser because of the macromolecules that can encapsulate the nanoparticles and prevent the particles from agglomerates (Dumur et al., 2011). The developed PEG-ZnS nanoparticles were deposited on the gold electrode, and the PEG-ZnS/Au sensor was used to measure cyanide. With the application of ZnS nanoparticles; the sensor detection limit and sensitivity have improved in comparison with the gold electrode (Mehta et al., 2012).

Other than gold, platinum, zinc and copper; silver nanoparticles are also extensively used for sensor development. A work published by Nia et al. (2015) who has utilised silver nanoparticles to decorate a polypyrrole-glassy carbon electrode (Py-GCE) for hydrogen peroxide sensing. A silver ammonia solution was prepared by dissolving a silver nitrate powder in a 1% ammonia solution. The silver nanoparticles were deposited on to the Py-GCE by the reduction of the silver ammonia solution using CV at a potential ranging from 0.6 to -0.3 V vs. SCE. The developed sensor has shown a high electro catalytic activity when compared to other modified GCE sensors (Nia et al., 2015). In another method proposed by Anamt et al. (2016) a drop casting method was used for the surface modification of silver nanoparticles on a GCE. A reduced graphene oxide-silver nanocomposite (GO-Ag) solution was prepared by mixing graphene oxide and ammonia silver solution at a ratio of 3:1. Subsequently, the solution was further exposed to microwave irradiation to obtain the final product. The developed nanocomposite particles were centrifuged and washed with deionised water. 5 μ L of the GO-Ag nanocomposite was dropped casted onto the GC surface and evaporated to dryness at room temperature (25°). The developed sensor was used for the analysis of 4-nitro-phenol. An improvement in the electron transfer rate was observed when silver nanoparticles was used (Anamt et al., 2016).

2.3.2 Carbon nanoparticles

In recent years, carbon nanomaterial has been extensively used in the fabrication of electrochemical sensor. Some of these carbon nanomaterials include carbon nanotubes (CNT), graphene (rGO), carbon dot (Cd) and fullerene (C60).

Among these materials, carbon nanotubes have been widely used for the surface modification of sensor; either it is of single walled (SWCNT) or multi walled carbon nanotubes (MWCNT). CNT has been a promising carbon-based nanoelectronic material

because of its exceptional chemical, physical and electrical properties; which gives the attributes of a large surface area to volume ratio, electrocatalytic properties, and enhanced electron transfer property (Lawal, 2016). Besides, it also possesses sp^2 hybridised carbon that can be functionalised with metal, polymer or organic substances that interact through π - π bonding. The presence of functional groups such as carboxylic (COOH) has enhanced the properties of CNT including the hydrophilicity improvement on sensor surface, or functional groups such as sulfur (S) or amine (NH) that can interact with biological substances such as enzyme (Yáñez-Sedeño et al., 2010). A study by Felix et al. (2016) has successfully deposited MWCNT on the surface of a gold substrate that was obtained from a conventional compact disk. The MWCNT was first prepared in dimethyl formamide (DMF) at a concentration of 1 mg mL^{-1} and $6 \text{ }\mu\text{L}$ of the solution was casted on to the surface of the gold sensor. The DMF was evaporated to dryness under room temperature (25°C) condition. The developed MWCNT/gold sensor was used for the determination of terbutaline and it has shown a vast improvement in the peak current signal, which was explained by the tremendous expansion of the Eff A (Felix et al., 2016). The centrifugation of the CNT solution is important, as the application of proper centrifugation force has observed the dispersion of CNT nanoparticle in water, whereas undesired carbon particles are spun down using the centrifugation force of 2500, which is sufficient to suspend the CNT (Xu et al., 2011). In another study by Zhao et al. (2011) a MWCNT sensor was used for the detection of luteolin. The MWCNT was deposited on GCE electrode with a similar preparation as described by Felix et al. (2016) using drop casting and evaporating the DMF to dryness. The fabricated MWCNT/GCE sensor has shown improvement on the surface area and also sensitivity towards luteolin oxidation (Zhao et al., 2011).

Graphene is a single nanosheet layer of carbon that possesses good electrical conductivity properties, electrocatalytic properties and also heterogeneous electron

transfer rate (Martín & Escarpa, 2014). It has been postulated that the graphene structure resembled closest to Lerf and Klinowski's model that comprises of a sp^2 hybridised carbon arranged into a single sheet of honeycomb polymorph, which the alcohol and epoxide group dominate the basal plane whereas the carboxylic and carbonyl moiety are located at the edge plane. These functional groups have contributed to the solubility of graphene in water, which was dispersed in aqueous solution and stabilised by the negative charge functional groups on surface. Furthermore, it also improves the hydrophilicity properties of the sensor surface that enhances interaction to those polar analytes (Wang et al., 2015). Graphene can easily undergo π - π interaction that stacked the graphene sheets together resulting in agglomeration, which alters the electro-properties of graphene through the loss of sp^2 carbon to sp^3 (Shi et al., 2016).

The electrocatalytic attributes of graphene were reported by Yin et al. (2011) where a graphene-chitosan composite glassy carbon sensor was fabricated for the detection of catechol (cc), resorcinol (rc) and hydroquinone (hq). Prior to the graphene deposition, a composite solution was prepared by mixing chitosan and graphene together (Chit-rGO); both substances were steady dispersed using ultra sonication and 5 μ L of the solution was dropped cast onto the glassy carbon surface and evaporated to dryness. The sensor performance was compared to the bare and chitosan-glassy carbon sensor, which showed excellent electro catalytic properties (Yin et al., 2011). In a different study by Chen et al., (2011) an electrodeposition method was used for the preparation of reduced graphene oxide on glassy carbon sensor. A CV scan was applied at a potential ranging from 0.5 V to -1.5 V vs. SCE, from which the glassy carbon was immersed in a graphene oxide solution that was prepared using phosphate buffer. The author has observed a cathodic peak position at -1.2 V, suggesting the reduction peak of graphene oxide (rGO). This reduced format of graphene (rGO) is more preferred than the graphene oxide (GO) alone; because of the higher percentage in sp^2 carbons than the sp^3 carbon whereas the former is

important for the attribute of heterogeneous electron transfer rate (Martín & Escarpa, 2014). The developed reduced graphene oxide/glassy carbon sensor was successfully used for the detection of catechol and hydroquinone; and the electron transfer rate was improved when compared to bare GCE, which was measured by comparing the anodic to cathodic peak separation potential (ΔE_p) (Chen et al., 2011).

The carbon dot is another type of carbon nanomaterial, which has been widely used to enhance the electrochemical properties of sensor. Carbon dot is unique and able to fluoresce when excited with radiation source (365 nm), which shows a green–blue, yellow or orange fluorescence depending on the particle size. The surface of the carbon dot always functionalised with the organic group such as carboxylic (COOH) or hydroxyl (OH). As a result, it gives the carbon dot superiority in water solubility (Esteves da Silva & Gonçalves, 2011); together with small particle size ranging from 2 to 3 nm. The structure is similar to graphene which has made the carbon dot an ideal material for surface modification especially as an electron mediator, electrocatalytic and geometric surface enhancer (Hasanzadeh et al., 2014).

The use of carbon dot as an electron mediator has been demonstrated by Wei et al. (2014), in which the carbon dot was used as a mediator between two MWCNT. The carbon dot was first synthesised by dissolving glucose into a polyethylene glycol and the mixture was irradiated with microwave at energy 530 W. The resulting carbon dot was then separated from the solution using dialysis. A layer-by-layer method was used to fabricate the sensor, with 5 μ L of MWCNT or the carbon dot was drop casted on a glassy carbon electrode following the order of MWCNT/carbon dot/MWCNT/glassy carbon. To prevent surface dissolution, nafion was casted on the sensor surface as a protector. The fabricated sensor was used for the simultaneous detection of catechol, hydroquinone and resorcinol. In which the carbon dot has shown an improvement to the sensor sensitivity

that efficiently connected the MWCNT together and enhanced the sensor surface area (Wei et al., 2014). In a separate study by Hashemzadeh et al. (2016) a carbon dot was deposited on to the surface of a glassy carbon sensor and used for the determination of doxorubicin. The carbon dot was first synthesised by pyrolysing citric acid, and subsequently dispersed into alkaline solution. The modification of glassy carbon was performed by casting a drop of the carbon dot to the surface and left to dry overnight. CV evaluation has shown that the fabricated CDs/GCE sensor possesses a fast electron transfer rate and electrocatalytic activity when compared to the bare glassy carbon counterparts. The sensor application in doxorubicin analysis was successfully tested in real human plasma samples (Hashemzadeh et al., 2016).

Fullerene is the third allotropes of carbon after graphite and diamond. It assumes the structure of a close cage carbon that contains pentagonal and hexagonal rings. Fullerenes can be represented by the formula of C_{20+m} , whereas the m being an integer number (Baena et al., 2002). The most studies on fullerenes in the electrochemical sensor belonged to the C_{60} homolog, which is known to possess multiple redox states and surface functionalised that could enhance sensor properties (Sutradhar & Patnaik, 2017). The former attribute is unique, as the reduction of fullerenes can be multiple stage that involves transient species, as a result, it allows for an ion exchange which has tremendously improved the electroactive surface area of the sensor (Rather & De Wael, 2013). Fullerene is also an effective electrocatalyst and also possesses good electrical conductivity.

A study by Rather & De Wael (2013) has described the fabrication of fullerenes C_{60} glassy carbon sensor for the detection of bisphenol-A. C_{60} was deposited onto the glassy carbon electrode by drop casting, with the solution dried under room temperature ($25^{\circ}C$) condition. A comparison study to the bare glassy carbon electrode has shown that the

fabricated C60/GCE possesses good electrocatalytic properties and also better electrode overpotential towards the detection of bisphenol A (Rather & De Wael, 2013). In another study by Brahman et al., (2016) a composite fullerene C60 sensor was fabricated and used for the detection of paracetamol. Fullerene C60 and MWCNT was mixed and dispersed in toluene; a drop of this mixture was casted on the surface of carbon paste electrode (CPE) and dried under room temperature condition (25°C). The sensor was then electrodeposited with copper nanoparticles to decorate the fullerenes and MWCNT; the developed sensor is designated as Cu-NPs/MWCNT-C60/CPE. An analytical evaluation of the paracetamol analysis using the fabricated sensor has shown tremendous improvement in the detection limit, when it overtakes the performance of other reported sensor. This was attributed to the high electroactive area of fullerene that improved the sensor sensitivity; and hence the detection limit (Brahman et al., 2016).

From the various studies of metal and carbon nanoparticles in the surface modification of sensor, it has evidenced the potential use of these materials in enhancing the electrochemical properties of an electrode. With the right balance and mixture of these nanomaterials, the performance of the sensor can be enhanced and fit for its intended use.

2.3.3 Conducting polymer materials

Conducting polymer is one of the few groups of surface modified materials that have been widely studied in the fabrication of electrochemical sensor. Various type of polymers are known to possess electrical conductivity properties, this includes; polyaniline, poly (3,4-ethylene dioxythiophene), polypyrrole, polyphenazine, poly (diallyldimethylammonium chloride), polyacridine orange and also some biopolymers such as chitosan and cellulose (Fratoddi et al., 2015). Among these conducting polymers, polyphenazine comprises the most number of homolog conducting polymer including poly azure, methylene blue, neutral red, phenosafranin, and thionine (Barsan et al., 2015). Many of these polymers have been used for the modification of the sensor surface, this is

because the material possesses the attribute of good electrical conductivity, large surface area, surface porosity, biocompatibility, stability and strong adherence to the surface (Barsan et al., 2015; Ciric-Marjanovic, 2013; Sun et al., 2013). Conducting polymer is rarely used as an individual material for the modification of sensor. This drawback is because of it slows electron transfer rate, high electrode overpotential and insufficient for electrocatalyst properties. Hence, conducting polymer is used as a composite to other sensitive material such as graphene that prevents agglomeration or lost through instability.

A composite polymer sensor was proposed by Ye et al. (2014) for the detection of A, G, and T. Poly (3,4-ethylenedioxythiophene) or PEDOT was used as the conducting polymer that composite with graphene (GO) and zinc sulfide nanomaterial on the surface of glassy carbon electrode. The monomer ethylenedioxythiophene was first mixed with graphene and stirred until it is well dispersed; iron (III) chloride was added into the solution as a polymerising agent and incubated for 12 h at 60°C. Blue precipitate (PEDOT-GO) was obtained from the polymerisation and removed from the solution by dialysis. Subsequently, it is mixed with zinc and thioacetamide, when the zinc sulfide nanoparticle (ZnS) was produced and the by-product of hydrogen sulfide (H₂S) from the reaction further reduced the PEDOT-GO to PEDOT-rGO. A black precipitate of ZnS-PEDOT-rGO was formed in this preparation, and it is deposited on a glassy carbon surface by drop casting and dried under ambient condition (25°C). The developed sensor has shown a wide linear range of A, G and T detection, which could be attributed by the large surface area of the PEDOT. Besides, it also showed good electron transfer properties and sensitivity that was contributed by the reduced graphene oxide (Ye et al., 2014). This work has shown the capability of the conducting polymer as a stable dispersion matrix for ZnS and rGO. However, a stability study of the sensor was not conducted by the

authors, which is an important study to ascertain the stability of the composite material adhesion to the glassy carbon surface.

Another study by Liu et al. (2008) has demonstrated the use of the electropolymerisation method to deposit conducting polymer on the sensor surface, which is proven to be simpler, effective and has better adhesion to the surface. Polythionine was used as the conducting polymer; prior to the electropolymerisation steps the glassy carbon surface was deposited with gold nanoparticles and multiwalled carbon nanotubes by drop casting. Subsequently, the sensor was immersed into a solution of thionine, and electropolymerised using CV with an applied scan in between -0.4 V to +0.4 V vs. SCE for 40 cycles. The fabricated sensor was used for the detection of A and G in DNA samples. Here the polythionine has improved the Eff A that provides more sites for redox process; hence improving the sensor sensitivity. Besides, it also shows a better stability and a lower detection limit (Liu et al., 2008).

One of the remarkable applications of conducting polymer is the development of molecular imprinting sensor (MIP); which utilises conducting polymer to create a three dimensional matrix surrounding a template molecule (analyte of interest). After the removal of this template the resulting space possesses a shape and functional group that resembles the analyte of interest (Tong et al., 2013). The fabrication of MIP sensor was demonstrated by Rao et al. (2017) in selective detection of melamine. A mixture of aniline, chloroauric acid and hydrogen peroxide was mixed into a glycol solution; and allowed for a static reaction for 24 h. Subsequently, it was separated by centrifuge and the supernatant (Au@PANI) was drop casted on a glassy carbon electrode. The fabricated Au@PANI/glassy carbon was immersed into a solution of methyl acrylic acid (MAA) and melamine, which the MAA is electropolymerised using CV for 30 cycles. Finally, the melamine molecule was stripped out from the sensor by soaking into a solution of

acetic acid, methanol and acetonitrile. A ferricyanide ion was used as the sensing probe, which in the presence of melamine the current signal of ferricyanide decreases because of the site blockage by melamine itself. The fabricated sensor has shown a good selectivity due to the molecular imprinting by the conducting polymer, and also a good sensitivity attributed by gold nanoparticles (Rao et al., 2017). In another study by Kiss et al. (2016) a more simple method was proposed for the fabrication of a dopamine MIP sensor. A mixture solution of ethacridine (monomer, MIPET) and dopamine (Da) was prepared and directly electropolymerised to the surface of glassy carbon using CV for a total of 5 scans; subsequently the template of dopamine was removed by immersing it in a sulfuric acid solution. The developed sensor was designated as MIPET–Da–GC, and used for the detection of dopamine in human serum. The developed sensor shows an excellent selectivity towards the detection of dopamine (Kiss et al., 2016).

Conducting polymer exhibits an excellent material for composite and MIP sensor; however, such electrode is not possible for reuse due to the unrenewable surface. Besides, the sensor preparation could be tedious because of the multiple steps in composite material preparation. Although, MIP sensor has shown a good selectivity, nonetheless, the electrode is impossible for detection of multiplex analytes.

2.3.4 Biomaterials

The use of biological based material in the surface modification of sensor has been widely studied; the application can be very selective depending on the intended use of the sensor. Various biological materials can be used for this purpose and, it can be categorised into enzymes (German et al., 2014), antibodies (Ma et al., 2015), and proteins (Sun et al., 2013). Among these, enzyme based sensor is the most extensively studied compared to the others. The main advantage of sensor that surface modify with biomaterials is the attribute of the selectivity, which can replace the current used method such as ELISA;

and with its rapid analysis, such sensor is important for clinical or hospital applications. The most challenging procedure in the fabrication of biosensor is the immobilisation of the biomaterials, which it is often sensitive to many conditions such as pH, and solvent used, as well the compatibility to the sensor surfaces (Wang et al., 2014; Yang et al., 2015).

Various types of enzyme can be immobilised on the surface of an electrode. Gold, MWCNT or graphene are often used as a composite material for the fabrication of biosensor. Such materials are known to be compatible to many biomaterials, because these materials possess functional groups such as COOH and OH that can bind with the biomaterials. The use of gold electrode is preferable for such application but due to the high cost; nanoparticles based gold are used instead. A simple fabrication study by Wang et al. (2008) has used gold nanoparticles as the electron mediator and also as the surface for the immobilization of glucose oxidase. This enzyme catalyzes the reduction of glucose and the resulting current response can be measured, which it can be used for the quantitation of glucose. Because of its specific binding to glucose, hence it improves the sensor selectivity. In the sensor fabrication work describe by the author, the gold nanoparticles (Au-NPs) were first deposited on the indium tin oxide (ITO) surface by electrodeposition. Subsequently, the Au-NPs/ITO was soaked into the cysteine solution followed by glucose oxidase which was self-assembled to the surface. The fabricated electrode was tested on human serum samples, which has shown a good selectivity and detection towards glucose (Wang et al., 2008). It has been known that the binding site of enzyme are often affected during the immobilisation of the enzyme to the sensor, therefore, fixing agent such as glutaraldehyde was used; this work was demonstrated by Teepoo et al. (2012), which showed a good immobilisation of the enzyme to the sensor surface (Teepoo et al., 2012). In another work by Kochana et al. (2015), an enzyme-based sensor was used for the detection of bisphenol A, which MWCNT was used as the site

for enzyme immobilisation. The sensor was prepared by mixing a composite solution of titanium dioxide, tyrosinase and multiwalled carbon nanotubes, which was homogeneously dispersed using sonicator. The dispersion was drop casted into a graphite sensor surface and dried for 20 h, subsequently the surface was protected with nafion. The fabricated tyrosinase sensor exhibits a good selectivity towards the detection of bisphenol A (Kochana et al., 2015).

The application of immune biological compound such as antibodies in sensor fabrication was also widely studied; sometimes it is also named as immunosensor. The procedure in adsorbing an immuno bio substance on the sensor surface can be challenging; as the adsorbing substrate need to be biocompatible to the antibodies for preserving its biological activity. The principle of an immunosensor is based upon the specific binding between the immobilized antibodies to its antigen. Comparing to the conventional Elisa method, an immunosensor is much sensitive, selective, low cost and also rapid detection. Similar to enzyme sensor; gold nanoparticles and graphene are the few materials that are preferable because of its compatibility to antibodies adsorption. A work by Ma et al. (2015) has shown the application of composite trimetallic nanoparticles with reduced graphene oxide for the immobilisation of nuclear matrix protein 22 antibodies (AB). The fabricated sensor was used for the detection of bladder cancer based on a known antigen marker (NMP22). A Trimetallic nanoparticle was produced by chemical reduction of HAuCl_4 , K_2PtCl_4 and Na_2PdCl_4 with ascorbic acid and consecutively after the reaction; antibodies (AB) was added into the solution and vibrated for 24 h to immobilise the AB on the nanoparticles surface. The nanoparticles were centrifuged and subsequently drop casted onto reduced graphene oxide-glassy carbon electrode (rGO/GCE) surface and allow to dry at 4°C to evaporate the matrix. Finally, the fabricated sensor (AB–AuPdPt NPS/rGO/GC) was incubated in BSA to eliminate the non-specific binding for antigen. A comparison of the analysis result performance using

the fabricated sensor to ELISA method, has shown a good result correlation, lower detection limit, higher selectivity and sensitivity of the proposed immunosensor (Ma et al., 2015). In a separate work by Hu et al. (2015) rGO–gold nanoparticles sensor was used for the immobilisation of HRP-anti *E. sakazakii*. The fabricated immunosensor was used for the detection of *Enterobacter sakazakii*, which showed a good selectivity and lower detection limit compared to other developed sensor. The improved detection limit up to 1.19×10^2 cfu/mL was attributed by the expanded surface area of graphene, which allows more antibodies to be immobilised (Hu et al., 2015).

Protein based sensor is another type of biomaterial that can be used for the surface modification of sensor. Most of the protein-based substances can be a short peptide or a complex protein structure depending on the intended use of the sensor. The amino acid that comprises the protein contains functional groups such as sulfur, carboxylic and amine. Therefore, it can be easily immobilised onto the surface, provided the binding platform is compatible. A study by Chammem et al. (2015) has demonstrated a procedure in the fabrication of a protein G sensor which is used for the detection of lipoprotein. Protein G was immobilised on a gold electrode, followed by Antibodies APOA1 using drop casting and finally dried under nitrogen. Subsequently, the fabricated G–protein/gold sensor was immersed into a solution of BSA to block the free spaces of the protein. The sensor was successfully used for the determination of HDL lipoprotein, which showed a very selective and sensitive detection of the HDL Lipoprotein and can even be differentiated from the reconstituted HDL lipoprotein particles (Chammem et al., 2015).

Although, biological based sensor showed a good selectivity toward analyte analysis, however, the range of analytes detection were limited and confined to those of biological based substances. Immobilised enzyme or antibodies on the sensor surface are usually sensitive to environment; as a result it has impeded biosensor development especially for

commercialised purpose. Moreover, alternate chemical sensor can also provide a selective and sensitive sensor for bio-analyte detection such as glucose. A work demonstrated by Kumar et al. (2010) has fabricated a copper nanoparticles/zinc composite sensor for the detection of glucose (Kumar et al., 2010), which is simple, stable and also sensitive. Apart from this, the fabrication of biosensor is also time consuming and always requires a long incubation time in a stable and controlled condition.

2.4 Analysis of anti-oxidants

In general, two forms of anti-oxidant substances can be extracted from food or natural product samples, which are the aglycone or glycone based compound. The latter form of anti-oxidant possess the glucoside groups and is more stable than the aglycones (Pandey & Rizvi, 2009). Anti-oxidant especially of aglycone is sensitive to environment oxidation and also to heating or chemical substances such as oxygen, salt, and organic acid. Therefore, in the extraction and preparation of samples containing anti-oxidant, these factor is crucial and requires consideration as to prevent any deterioration of the anti-oxidant that could impact on the quality of the analysis results (Brewer, 2011). Extracting of anti-oxidant from complex matrix can be challenging and depends on the technique, type of solvent used, pH, and temperature (Li et al., 2014). Studies have shown the temperature and solvent used for the preparation of samples for anti-oxidant detection that can affect the stability of the anti-oxidant substances. Using high temperature in anti-oxidant sample preparation of about 60°C, the oxidation activity of anti-oxidant (e.g., quercetin) has found to increase. As a result, high temperature has lowered down the stability of studied anti-oxidant within a week before it is completely dissociated. In contrary to the studied temperature controlled at 37°C, the anti-oxidant was found to have a longer stability. This study has suggested that the temperature used for sample preparation in anti-oxidant analysis is an important consideration factor (Pinelo et al., 2004). This is similar to the type of solvent used, which can also affect the anti-oxidant

stability. The use of hydro-alcohol solution (mixture of alcohol with water) has resulted to the instability of anti-oxidant compound over time. In contrast to pure solvent such as methanol, the stability of the anti-oxidant is much better (Pinelo et al., 2004). Both factors (temperature and solvent used) could vary depending on the type of preparation technique used. Therefore, understanding of the different techniques of anti-oxidant extraction from food samples is important, to assure a reliable analysis result. In this sub-chapter, some of the extraction procedures including sohxlet, solid phase, liquid-liquid and freeze drying will be reviewed, in order to give a more comprehensive selection on the different preparation techniques for anti-oxidant analysis.

The detection and measurement of anti-oxidant analysis can be divided into qualitative and quantitative analysis. Some of the commonly used qualitative methods include DPPH assay, ABTS assay and CV. These methods can provide qualitative information about the anti-oxidant such as the radical suppression activity, radical scavenging potential and also the pro-oxidant activity. However, qualitative method is always limited in the composition analyses; to patch this limitation, quantitative analysis is always performed together. Some of these methods include the chromatography and electrochemical methods. In this sub-chapter, both qualitative and quantitative methods were also reviewed to provide a more comprehensive study of the anti-oxidant.

2.4.1 Sample preparation of anti-oxidant

Various preparation procedure of anti-oxidant has been studied especially on the extraction of these substances from plant and food. Some of the common methods used for the preparation of anti-oxidants samples including liquid extraction, sohxlet extraction, reflux extraction, freeze drying, and solid phase extraction. In which, the procedure details, advantages and disadvantages will be review in this chapter.

2.4.1.1 Liquid extraction

Among the methods, liquid extraction is the most preferred because its simple, low cost, and a more diversified choice of solvents. With a suitable solvent, the anti-oxidant can be completely recovered from the samples and with intact structure without altering the properties of anti-oxidants. This is because the method is free from any heating or cooling process that could accelerate oxidation process. The principle of liquid extraction is based on the like-dissolve-like principle. The most important parameter is the choice of the solvent used, which depends on the properties of the target anti-oxidants (Amlashi et al., 2014); for example BHT, tocopherol, retinoate and BHA are known as oil soluble anti-oxidant (Dhiman et al., 2014). A study on the liquid extraction of oil soluble anti-oxidant has been demonstrated by Aladedunya et al. (2014) which employed a liquid extraction of oil soluble anti-oxidant in plants (*Prunus Virginiana*); the fruits were air dried and then ground in a mix solvent solution of acetone, water and acetic acid. The mixture was sonicated at 50°C and followed by filtration. Subsequently, the filtrate was further extracted with hexane, and successively with ethyl acetate and butanol. From the different extraction solvents, the author further analyse the composition using HPLC, which has successfully extracted 20 different types of anti-oxidants that was solubilised in fat or oil soluble solvent (Aladedunye et al., 2014). In food samples, liquid extraction is the preferred method for the analysis of anti-oxidants. One of the interesting study by Amlashi et al. (2014) was using a non-ionic surfactant based water solvent to extract synthetic phenolic antioxidants from edible oil samples (sunflower oil, soybean oil, grape seed oil, olive oil, sesame oil and almond oil). Surfactant is a good solvent for the extraction of anti-oxidants either hydrophilic or hydrophobic; this is because the latter type can be emulsified by the surfactant. In the procedure described, a non-ionic surfactant of polyoxoethylene lauryl ether was mixed with water at a concentration of 0.1 mol L⁻¹, and 30 µL of this solution was added to 5 mL of oil samples. Successively, the

solution was vortexed and centrifuged. The resulting supernatant was transferred out and injected into HPLC for the analysis of BHA, and TBHQ (Amlashi et al., 2014). Various studies have reported the same approach by using surfactant in the anti-oxidant compounds extraction; this includes the use of cetyltrimethylammonium bromide (CTAB) in extraction of TBHQ and BHA in biodiesel samples (Caramit et al., 2013); myricetin extraction using alkyl aryl polyether alcohol (Yao et al., 2014); TBHQ, propyl gallate and BHT in essence perfume using polyoxyethylene ether 9 (Li et al., 2014); and phenolic anti-oxidant using polyethylene glycol dodecyl ether in fruit juice (Sharma et al., 2015). The latter study has compared the extraction efficiency between surfactant and conventional solvent (water, ethanol and methanol) in anti-oxidant recovery from fruit juice. The result, of which, has shown the surfactant possessed a better effectiveness in extraction of anti-oxidants.

The use of conventional solvents in the extraction of anti-oxidants compound has been a long practice. Alcohol such as methanol, ethanol and isopropanol are the few choices of solvent used for the sample preparation of food samples. This procedure is of convenience especially for the detection method that based on chromatography techniques such as HPLC or GC, which the solvent is compatible to HPLC instrument. However, such solvent are usually not appropriate for the electrochemical detection method because of the electrolyte deficit that contributes to high ohmic resistant. A work by Freitas & Fatibello-Filho (2010) has shown the use of ethanol for extraction of BHA and BHT from mayonnaise samples, which showed that it is necessary to further dilute the extraction with potassium nitrate solution prior to electrochemical analysis (Freitas & Fatibello-Filho, 2010). Other similar studies including quercetin detection in fruits by methanol followed by a dilution with citric buffer prior to electrochemical analysis (Gao et al., 2014); luteolin detection in peanut hulls by ethanol extraction followed by dilution with Britton-Robinson buffer (Pang et al., 2014); and detection of eugenol in curry

powder by ethanol extraction followed by dilution with Britton-Robinson buffer (Lin et al., 2014).

A recent study has used ionic liquid as the solvent for anti-oxidants extraction. It is a cost effective and environmental friendly solvent, which has been widely used for the extraction of biopolymer, protein, starch and chitin (Jiao et al., 2013). The ability of the ionic liquid in degrading cellulose cell wall, and possessing the properties of surfactant has given this solvent a promising approach in the extraction of anti-oxidants; this is either hydrophilic or hydrophobic or both types of anti-oxidants (Jiao et al., 2013). A study by Larangeira et al. (2016) has used 2 buthyl-3-methyl-imidazolium chloride as ionic liquid to extract carotene from tomato samples and with the support of sonication it has successfully extracted the hydrophobic beta-carotene using a water based ionic liquid (Larangeira et al., 2016). In a separate study by Jiao et al. (2013) who investigated 4 different types of ionic liquid including 1-butyl-3-methyl-imidazolium bromide, 1-butyl-3-methyl-imidazolium chloride, 1-ally-3-methylimidazolium chloride and 1-ethyl-3-methylimidazolium acetate. These were used as the solvent liquid for the extraction of anti-oxidants from the *Dryopteris fragrans* plant, which the author successfully recovered 91.5% of the essential oil constituent and identified 18 components of anti-oxidants. 1-ethyl-3-methylimidazolium acetate showed the most optimal effectiveness in extraction compared to the other ionic liquids (Jiao et al., 2013).

Liquid extraction remains the most effective, simple and low cost method in the extraction of anti-oxidants from foods, plants, and oil samples. Many studies have shown the success of the liquid extraction method, and with the more recent work using surfactant and ionic liquid it has made the method more diversified in terms of the choice of solvent that could fit the requirement for further analysis and evaluation.

2.4.1.2 Soxhlet extraction

Soxhlet extraction is the most classical technique that can be used to extract anti-oxidants in solid sample prior to qualitative or quantitative analysis. In this method, the sample is weighed and placed into a filter thimble that fits into the soxhlet chamber; the extraction solvent is then heated until boiling, which is subsequently condensed and dripped onto the solid sample. Eventually, the condensed solvent will fill the soxhlet chamber, once full it will siphon back to the solvent reservoir and the process is repeated for a few cycles. The Soxhlet method is an efficient method in extracting anti-oxidant compounds from solid samples such as fruits, seed, and leaves.

A research work by Stojiljkovic et al. (2016) has made a comparison study between soxhlet, maceration and liquid extraction of anti-oxidant composition from wild apple fruit. The study has shown the conventional liquid extraction method which gave the highest recovery of anti-oxidant in terms of Gallic acid equivalent in most of the solvent used (ethanol, water, edible oil). When propylene glycol was used as the extraction solvent, the soxhlet method has shown the best recovery of anti-oxidants. In the same study, the author has also performed an anti-oxidant activity test on the extract, from which liquid extraction using ethanol showed the highest anti-oxidant activities (Stojiljković et al., 2016). In a similar study by Wen et al. (2015) he has compared the extraction methods between liquid and soxhlet technique, from which the antioxidant recovery are equivalent to both methods but with activities that are lower in soxhlet extraction (Hu et al., 2015).

Although, the soxhlet method is efficient in the recovery of anti-oxidant from solid samples; nevertheless, the study has shown a decrease in the anti-oxidant activities. This could be possibly explained by the heating step during extraction, which deteriorates the anti-oxidant activities by accelerating the oxidation process of the anti-oxidant. Indirectly,

this could contribute to the error in qualitative and quantitative analysis. Apart from this, the soxhlet extraction can be time consuming which requires at least 1–2 h for 4 cycles extraction.

2.4.1.3 Reflux extraction

Reflux extraction is similar to soxhlet with the difference in sample placement, when the sample is directly mixed with solvent instead of separating into a different sample platform. The advantage of reflux extraction is the compatibility of the technique to both liquid and solid type samples.

Conventionally, the heating element such as hotplate or heating mantle is used to heat the extraction solvent until boiling, this work has been demonstrated by Sultana et al. (2008) from which acidified methanol is used to extract anti-oxidant substances of various vegetable samples such as carrot, cabbage, onion, ginger and fruits. In brief, 1 g of the samples was weighed into a round bottom flask and 25 mL of the extraction solvent is added, the mixture was heated at 90°C for 2 h. The author has identified 3 major common anti-oxidants contained in most of the vegetables and fruits including myricetin, quercetin and kampeferol (Sultana & Anwar, 2008). In a separate study by Flores et al. (2015) who has employed the reflux method for the extraction of raspberry and blackcurrant using non-ionic surfactant (polysorbate). A composition analysis has shown that the extract contained a significant content of myricetin, quercetin and ellagic acid (Flores & Luisa, 2015). A comparison study between reflux, soxhlet and liquid extraction; when extracting *Lonicera japonica* has shown that the reflux method has a lower extraction amount of chlorogenic acid (3.4%) compared to soxhlet (3.7%) and liquid extraction (3.6%) (Hu et al., 2015); suggesting a lower effectiveness of reflux method, which could be caused by the interference from samples solid mass (insoluble starch or protein) with the extraction solvent.

Extraction of anti-oxidant using reflux method is time consuming, and overtime this could cause the oxidation of the anti-oxidant substances by the substances. Recently, a modified method was proposed by Li et al. (2016) that utilised microwave to assist the extraction of anti-oxidants from blackcurrant; which has successfully shorten the extraction time from conventionally 2 h process to 16 min.

2.4.1.4 Freeze drying

Freeze drying is another method that can be used for the extraction of anti-oxidant from food samples. However, this method is limited for liquid based samples, as for solid samples, it will require an additional extraction process such as soxhlet or liquid extraction. The principle of this method is divided into 2 steps. The first step is known as the freezing step when the samples are freeze by using the conventional -20 or -90°C refrigerator or with liquid nitrogen. Subsequently, the freeze samples are further dried under low vacuum where the generated heat will be sufficient to sublime the solvent of the samples; this step is known as primary drying. Some samples can be further dried (secondary drying) under room temperature (25°C) or elevated temperature (40°C) to further evaporate the residue solvent.

A work by Delpino-Rius et al. (2014) has shown the extraction of carotenoid in fruit juice by using freeze dryer, briefly 1.5 to 5.0 g of samples was first frozen at -80°C, which was then freeze dried under vacuum at 1.1 P for 24 h at -50°C. More than 90% of the carotenoid content was able to recover from this extraction procedure. In comparison to other extraction procedure, the freeze drying method is suitable for extraction of anti-oxidants, which is heat sensitive such as carotenoid (Delpino-Rius et al., 2014) and tocopherol (Conte et al., 2017). In a similar work by Girard et al. (2009), a freeze dryer technique was used to extract the anti-oxidants from fruits and vegetables, the samples was first grounded to obtain a liquid format which is then freeze dried at -80°C. The

composition in the extract showed a good anti-oxidant activity; which suggests that the freeze drying method is stable and does not alter the anti-oxidant properties of the extracts (Girard et al., 2009).

Freeze drying is a more preferred method than soxhlet and reflux; this is because the method operates at low temperature, which is important to preserve the properties of anti-oxidant substances. Besides, the final extract product is in powder format that allows the samples to be stored for a longer period of time prior to analysis and without affecting the anti-oxidant properties. In addition, it also inhibits the enzymatic degradation process that could be present in the raw samples such as fruits and vegetables (Thi & Hwang, 2016). However, this method can be time consuming, which could take up to 3 days for drying, and the method is constraint to liquid based samples.

2.4.1.5 Solid phase extraction

The working principle of solid phase extraction (SPE) is based on solid sorbent, which is functionalised with specific groups that are able to bind substance of interest either of polar or non-polar substances. The bound substances can then be eluted out with solvent that possesses polarity properties similar to the substances. The SPE method is only suitable for liquid based samples; as for solid sample it may require pre-extraction using soxhlet, or reflux extraction method that converts the sample into liquid phase.

A work by Kumar et al. (2009) has used a solid phase method for the extraction of anti-oxidants. The method was used for the analysis of anti-oxidants in tomato samples. A reflux extraction was first used to extract the anti-oxidants compound into a methanol. Subsequently, a solid phase extraction was employed whereby a carbowax resin fiber was used as the sorbent. The fibre was exposed to the sample solution that under stirring for few minutes, successively the fibre was removed and the bound anti-oxidants on the fibre is desorbed into solvent (70% citrate buffer and 30% acetonitrile). The same extraction

procedure was repeated for wine samples, except for the reflux steps. Analysis of the sample showed both wine and tomato samples contain myricetin and quercetin. By using the SPE preparation it has shown improvement in the detection limit (Kumar et al., 2009). In a separate work by Barnaba et al. (2015), an investigation on various types of SPE sorbent in the extraction of 56 different phenolic antioxidants in wine samples was studied. Among the different sorbent materials, polystyrene divinyl benzene that functionalized with urea showed the best retention for the phenolic anti-oxidants in comparison to other well-known sorbents such as C18 and hydroxyl functional polystyrene divinyl benzene (Barnaba et al., 2015).

SPE is a powerful sample preparation method for the extraction of anti-oxidant in food samples. It can be used as a pre-concentrator for improving the detection limit in anti-oxidant analysis (Masek et al., 2014). Besides, it can also use to clean up the unwanted substances by selectively retaining the anti-oxidant of interest such as polar from non-polar anti-oxidants. Although the use of SPE is versatile, however, the drawback is associated with its limitation in liquid phase samples, as solid sample will require further processing. Besides, SPE method is also expensive when compared to other mentioned methods (Li et al., 2014); and the choice of SPE sorbent used could be indecisive especially in the analysis of untargeted compounds (unknown anti-oxidants); which the retentive properties are unknown (Alvarez-Rivera et al., 2014).

2.4.2 Qualitative and quantitative analysis of anti-oxidants

The analysis of anti-oxidants could be divided into two objectives, either of qualitative or quantitative study. The latter is more important to determine the composition of anti-oxidants for the purpose to determine the nutrition value, stability or for regulatory compliance. As for the qualitative analysis, it is more associated to the study of the chemical and physical properties of the substances such as electron transfer kinetic rate,

radical scavenging power, or redox mechanism. Analysis of anti-oxidants can be performed by various procedures, depending on the objective of the study and the selection of the method needed to fit the purpose of the analysis.

2.4.2.1 Qualitative analysis of anti-oxidants

In qualitative analysis, the study of kinetic, redox mechanism and radical scavenging properties of anti-oxidant have become important information. This is because such input is important to understand the underlying properties of the anti-oxidants and also the effective use of the compound in applications such as health supplements, preservative, and cosmetic ingredient. Various methods including DPPH assay (2,2-diphenyl-1-picrylhydrazyl), pulse radiolysis, CV and ABTS assay (2,2-azino-bis-(3-ethylbenzothiazoline-6-sulphonic acid) diammonium salt) have been used for the qualitative evaluation of anti-oxidants (Gil & Couto, 2013; Schaich et al., 2015).

Among the many methods used for the qualitative assessment of the radical scavenging properties, DPPH assay is the earliest method; which is still widely used up to today. The principle of the method is based on the concentration point study of anti-oxidant in inhibiting the radical introduced; and in this case, the radical used is 2,2-diphenyl-1-picrylhydrazyl (Zhang et al., 2015). The DPPH is a stable free radical and in the presence of anti-oxidant, it will be scavenged through hydrogen donation reaction by the anti-oxidants. Consequently, this causes a change in the color of DPPH from purple to light yellow, which can be measured using spectrophotometer at a wavelength of 517 nm. By plotting a graph of efficient concentration (EC, equation 1) versus the anti-oxidant concentration; the efficiency of the anti-oxidant in scavenging the DPPH radical is reported as EC 50 (efficient concentration at 50%) (Potkonjak et al., 2012):

$$EC = \left(\frac{Ab - As}{Ab} \right) \times 100 \quad \text{----- (1)}$$

Whereby, Ab and As represent the absorbance of the blank and DPPH after reaction with anti-oxidants over a period of time. A work by Zhang et al. (2015) has performed DPPH assay on a list of synthetic and natural anti-oxidants; which the radical scavenging properties of these anti-oxidants from high to low can be sequence as propyl gallate > gallic acid > quercetin > caffeic acid > tocopherol l > tert-butylhydroquinone (TBHQ) > butylated hydroxylanisonle (BHA) > butylated hydroxytoluene (BHT) (Zhang et al., 2015). Although, the method has been proven as simple and versatile, however, the result was not correlated when the solvent used in the experiment was different. In a similar study by Zhang et al. (2015) it showed that the mentioned DPPH results did not correlate well when the anti-oxidants were used in fish lipid (Zhang et al., 2015). A similar study by Pinelo et al. (2004) has shown that the quercetin scavenging EC 50 in DPPH assay was affected by temperature and also solvent. The use of ethanol, methanol and water/ethanol mixture of quercetin have given a different value of EC 50, with ethanol solvent showing the highest anti-radical activity at $61.8 \text{ min}^{-1} \text{ mg}^{-1}$, compared to methanol at the value of $46.9 \text{ min}^{-1} \text{ mg}^{-1}$ (Pinelo et al., 2004). The contrast in results could be explained by the difference in reaction properties between the DPPH and also anti-oxidation, which remained a gap that requires further evaluation and study.

ABTS assay is another version of DPPH analysis. The difference in both methods is underlying on the type of radical use. In the case of ABTS, 2,2-azino-bis-(3-ethylbenzothiazoline-6-sulphonic acid) diammonium salt is used as the reacting radical. Prior to use, the ABTS is required to react with potassium persulfate over 16 h to generate the radical; and the difference in DPPH and ABTS radical is the solubility of ABTS in water instead of alcohol for DPPH (Jara-Palacios et al., 2014). In ABTS assay, the efficiency of anti-oxidant radical scavenging properties is expressed as

EC 50 which is similar to DPPH. One important consideration in both the methods is the solubility of the radical, as alcohol soluble anti-oxidant in DPPH can have a different performance in ABTS radical of water based. This study has been demonstrated by Kita et al., (2014) in the anti-oxidant analysis of polyphenol in potatoes. Although, the author did not conclude on the difference in the results between both ABTS and DPPH, however, from a comparison of the results it suggests the sequence of radical scavenging properties (anti-oxidant potential) of different potatoes using ABTS assay is different from DPPH assay. For instance, the potato variety from Vitelotte rank as the second highest property in anti-oxidant using DPPH assay, in contrast to ABTS that ranked fourth highest (Kita et al., 2014). This difference in results could cause a concern in the use of ABTS or DPPH method for anti-oxidant radical scavenging assessment. A study by Chu et al. (2013) has shown that the use of DPPH and ABTS radical may not be representative for the assessment of anti-oxidant activity in food; this is because both DPPH and ABTS are dissimilar to peroxy radical that is commonly found in actual physiological condition (Chu et al., 2013). According to Hurdles et al. (2015) the method for ABTS and DPPH is more suitable to distinguish electron transfer reaction mechanism by measuring the DPPH or ABTS absorbance response over time, instead of measuring radical quenching or scavenging properties. The author recommended ORAC (oxygen radical absorbance capacity) as the screening assay for anti-oxidant scavenging properties (Schaich et al., 2015).

The alternative ORAC method provides a more relevant free radical that resembles to peroxy radical, which is the most common free radical in the human body. Two types of radicals used in ORAC assay include fluorescein (3,6-dihydroxyspiro[isobenzofuran-1[3H]]) and pyrogallol red (Prior, 2014). The principle of ORAC is similar to DPPH or ABTS, which measures the decay of the fluorescein (pyrogallol) using plate reader or spectrophotometer. Subsequently, the area below the

fluorescence decay plot is measured, and correlated to a calibration curve that was constructed using known anti-oxidant standard such as trolox (6-hydroxy-2,5,7,8-tetramethylchroman-2-carboxylic acid) and caffeic acid (Castro et al., 2014; Prior, 2014). In ORAC assay the result is expressed in terms of μmol equivalent to the standard use (trolox or caffeic acid). A study by Kameya et al. (2014) has employed ORAC assay in the determination of anti-oxidant scavenging properties of various vegetables, when the analysis shows that the chrysanthemum, eggplant and parsley possessed the highest ORAC index than the other vegetables. The analysis was also correlated to other methods including electron paramagnetic resonance (EPR) (Kameya et al., 2014). The only drawback in the ORAC method is limited by the time consuming analysis that could take h for analysis, unlike to other instrument techniques that including EPR and electrochemical method using potentiometric. Besides, chemical assay based upon radicals including ABTS, DPPH, and ORAC could be sensitive to environment oxidation upon a long analysis time and will cause result deviation due to environmental oxidation and the biggest concern on these methods is the reactivity of the radicals (ABTS, DPPH and fluorescein) that not only cause steric hindrance to the anti-oxidants but also their reactivity toward phenolic substances by non-radical mechanism (Schaich et al., 2015).

Recently, electrochemical methods have been widely used for the study of anti-oxidants. It is more informative, practical and simple to use when compared to other methods (ABTS, DPPH, and ORAC). In the study of radical scavenging properties; electrochemical methods particularly CV has proven to be more rapid, cost effective, clean chemical, and tolerable to dirty sample matrix (Zieliński et al., 2012). A work by Samra et al. (2011) has employed CV for the study of anti-oxidant capacity (radical scavenger capacity) in ascorbic acid, caffeic acid, hesperatine, quercetin and catechin. The method is simple only by the immersion of carbon paste electrode directly into the

anti-oxidant sample solution of a known concentration; subsequently a CV analysis is performed by setting the scan range from -0.3 V to +1.2 V with scan rate of 50 mV s⁻¹. The radical scavenger capacity was evaluated based on the potential of the oxidation peak (E_p); the larger the potential (V) value the weaker anti-oxidant scavenger properties. From the CV analysis result, the author has sequenced the radical scavenger properties of the anti-oxidants from high to low as catechin > quercetin > hesperatin > caffeic acid > ascorbic acid. This finding was comparable to the DPPH results (Samra et al., 2011), suggesting the CV method is comparable to the chemical assay.

Apart from the study on anti-oxidant scavenging properties; one of the important applications using the electrochemical method is the ability to determine redox reversibility of the anti-oxidants; which is important for the study of oxidant and pro-oxidant properties (Samra et al., 2011; Santos et al., 2013). Such study is impossible to be measured using chemical assay (ABTS, DPPH and ORAC), which further explains the limitation of chemical assay in anti-oxidants analysis. A work by Santos et al. (2013) has shown the application of CV in the reversibility study of xanthenes using a glassy carbon electrode. An evaluation of the redox reversibility is performed by determining the cathodic and anodic peak potential, which corresponds to the reduction and oxidation of xanthenes. A cathodic peak infers the possibility of xanthenes to regain its original oxidised structure by accepting an electron or proton, by functioning as pro-oxidant (Santos et al., 2013).

The electron transfer rate of anti-oxidant is also an important area of study, as described by Lucarini et al. (2010) the kinetic rate of electron transfer is more important in determining the inhibition power of anti-oxidants; this is because in the peroxidation process the rate of peroxy radical generation is fast, and, therefore, the electron transfer rate of studied anti-oxidants should act faster to counteract the radical generation

(Lucarini & Pedulli, 2010). A study by Yin et al. (2011) on the electrochemical analysis of catechol and hydroquinone, have used graphene-chitosan composite glassy carbon electrode to measure the electron transfer rate of catechol and hydroquinone based on Laviron's equation. The kinetic rate obtained in the experiment corresponded to $2.1 \times 10^{-2} \text{ s}^{-1}$ and $1.47 \times 10^{-2} \text{ s}^{-1}$, respectively suggesting catechol is more faster than hydroquinone in the electron transfer rate (Yin et al., 2011). However, this procedure may be confined to the relative comparison between the anti-oxidants tested using the same composite electrode. As the diverse surface modified the electrode, different absolute kinetic rate values will be obtained for direct comparison between the two anti-oxidant substances. This limitation of sensor is governed by the different electrode overpotential; as a result it impedes the electron transfer rate.

Other important applications of the electrochemical method are the study of reaction mechanism in anti-oxidants. A study by Medeiros et al. (2010) has employed SWV and Nernst's equation to determine the ratio of electron to proton transfer in BHT and BHA, which inferred a total of 2 electrons which were involved in the oxidation process (Medeiros et al., 2010). This information is valuable in deducing the power of the anti-oxidant in donating electron, as more numbers of electron transfers suggests an effective anti-oxidant in neutralising radical. Although, electrochemical method is more diverse in application, rapid, simple and robust when compared to the chemical assay, nevertheless the sensor used in electrochemical analysis remained a challenge, particularly in the sensor overpotential. Some anti-oxidants will not be oxidised when the overpotential of the sensor is too high. This was demonstrated by Makhotkina & Kilmartin (2009) in sodium metabisulfite and ascorbic acid studies, which have shown the significance of electrode overpotential properties. Besides, the author has also inferred the importance of the electrode surface area in the analysis of multiple anti-oxidants that could saturate (adsorption) the redox site by easily oxidizing the anti-oxidants, and this could further

increase the electrode overpotential (in-situ) and subsequently impacting the oxidation of the next oxidised substance (Makhotkina & Kilmartin, 2009).

Application of chemical assay (ABTS, ORAC and DPPH) or electrochemical methods in the qualitative analysis of anti-oxidants are still debatable among many researchers. Although with the downfall comments on the use of DPPH and ABTS (Schaich et al., 2015); the application of both methods are still widely used even up to today (Stojiljković et al., 2016). One of the important trends that could be seen, is the emerging of instrumental methods that including electrochemical analysis using sensor, which is proven to be lower cost, rapid, effective and informative (Rebelo et al., 2013).

2.4.2.2 Quantitative analysis of anti-oxidants

The quantitative analysis of anti-oxidants in foods or plants is important. It can be studied for the purpose of anti-oxidant compositional profiling in fruits and plants (Carocho et al., 2015); for the stability evaluation of anti-oxidant in food over usage (Delfanian et al., 2015); or for legal compliance requirements (Caramit et al., 2013). The latter objective is more important especially when synthetic anti-oxidant is used as a preservative in food. Certain anti-oxidants, such as BHT and BHA could have detrimental effect to health when used at high dosage (above $3000 \mu\text{g g}^{-1}$) (Williams et al., 1999), therefore requires quality monitoring. The quantitative analysis can be performed by many methods including gas chromatography, high performance liquid chromatography, spectrophotometry and voltammetry method.

Folin Ciocalteu's assay (FC) or total phenolic contents is a general quantitative method that has been widely used for the determination of phenolic anti-oxidant based compounds. The method is performed by using folin ciocalteu's reagent that comprises a mixture of phosphomolybdate and phosphotungstate, which specifically reacts with phenolic groups and developed a blue colour solution; subsequently the absorption of the

colour is measured at 670 nm using UV–VIS spectrophotometer. Since the method is lacking in specificity therefore, an equivalent gallic acid standard is used as the calibration standard, and the result is reported as mg gallic acid equivalent/mL (mg GAE/mL) (Sharma et al., 2015). A work by Makhotkina et al. (2012) has performed an analysis of polyphenol compositions in juice; the FC analysis was performed on 26 juice samples to determine the total polyphenols for comparison purpose, and HPLC analysis was further employed to determine the individual component of the polyphenols in each sample (Makhotkina & Kilmartin, 2012). From the results, it suggests FC assay was still lacking in specificity; as the high content of total phenolic compound may not show the actual anti-oxidant potential in the juice. This is because FC assay will react with substances that is phenolic functionalised and also nitrogen containing compound such as hydroxylamine, which may not be an anti-oxidant (Ziyatdinova et al., 2014). As a result, it could give a false estimate of anti-oxidant compositions. However, FC assay is rapid and low cost for high throughput quantitative analysis of anti-oxidants, which can be a good tool for preliminary screening of anti-oxidant content during the plant extraction process or inline production monitoring (Ragubeer et al., 2010).

The liquid chromatography (LC) method is more specific and selective when compared to the FC assay. The principle of liquid chromatography is based on the separation of anti-oxidants through a pack column that is functionalised with chemical groups such as octyldecyl (C18), or divinyl benzyl sulfonate. This gives the column a different polarity property such as non-polar for C18 column. Subsequently, it is used to separate the anti-oxidant compounds by eluting with organic solvents such as methanol and acetonitrile. By altering this composition, the individual anti-oxidant will be separated from the others based on the principle of “like dissolve like”. The eluted anti-oxidant is then measured using a detector such as UV–VIS spectrophotometer, or mass spectrometry detector. A chromatogram of detector signal to elution time is plotted; and

each individual peak represents an anti-oxidant and the concentration can be measured by calibrating the peak area with a standard known amount. Using this method, multiple anti-oxidants can be determined in a single run, which is good for profiling the anti-oxidant composition content in food or plant extract samples (Castro et al., 2014; Kilmartin & Hsu, 2003; Sultana & Anwar, 2008). There are ample of studies in anti-oxidants analyses employing the LC approach for the composition analysis, the advantages of this method are associated to its multi-compounds detection capability. This was demonstrated by Aladedunya et al. (2014) by using a high performance liquid chromatograph with a mass detector (HPLC–MS) for the analysis of 20 polyphenol anti-oxidants in hawthorn extract (plant extract). The employed HPLC-MS method is selective due to the advantages of the mass detector that generates a unique mass spectrum in each individual anti-oxidant compound, which can be searched through a mass spectral library for identification (Aladedunye et al., 2014). Although, with the multi-compounds capability of HPLC method and specificity of MS detector, however, the use of HPLC is still restricted by the high operating cost and requirement of a specific laboratory condition such as space, clean environment, and solvent (Lin et al., 2014; Liu et al., 2016). With such requirements, it also impedes the possibility of this method to be used for on field analysis, this is particularly important as most anti-oxidants are sensitive to environment oxidation, therefore, in situ analysis of the samples is preferable (Ananingsih et al., 2013; Ioannou., 2012). Besides, the analysis time taken for HPLC analysis can be time consuming and not preferable for in process monitoring during manufacturing or plant extraction (Zhu et al., 2013).

Gas Chromatography is another technique that can be used for the quantitative analysis of anti-oxidant compounds. The operation principle of gas chromatography is similar to liquid chromatography. As the name ‘gas’ implies, the analysis of anti-oxidants by GC is based upon heating of the compounds into its gas state, which is then carried by the mobile

phase (helium, hydrogen) to the separating column. Since the temperature of column is controlled by an oven, the separation of the individual anti-oxidant can be achieved by optimising the oven temperature programme (isocratic or gradient temperature ramping), which allows the anti-oxidant of interest to be volatilised at a particular temperature condition and carried by the mobile gas to a detector, which is usually a flame ionisation detector (FID), mass detector (MS) or electron capture detector (ECD). The type of column used in GC is either a packed or capillary column that is functionalised with chemical groups such as phenyl arylene, cyanopropylphenyl, phenyl, and polyethylene glycol. The column different polarity properties are important for the selectivity criteria of the GC methods. An analysis of anti-oxidants using GC has been demonstrated by Masek et al. (2014) which employed a gas chromatography mass detector (GC-MS) for the analysis of anti-oxidants in hops extract (*Humulus Lupulus*). A total of 14 anti-oxidant compounds were detected and quantified by the GC-MS, and the identification is confirmed using mass spectral (Masek et al., 2014). Similarly, to HPLC-MS method, whereby both chromatography techniques (HPLC and GC) have the advantages of multi-compounds analyses capability, and selectivity. However, the method requires a heavy cost investment on the equipment; besides, it is also a time-consuming analysis, and is not suitable for on field analysis. In the case of GC, the use of high temperature may further cause degradation especially in thermally labile anti-oxidants (Masek et al., 2014). As a result, the use of GC is less preferable when compared to LC.

Recently, the application of electrochemical sensor in anti-oxidant analysis has been extensively studied. The principle of electrochemical sensor is based on the application of specific voltage (V) that caused the oxidation of anti-oxidant, when the resulting electron donated by the anti-oxidant is flowing through a counter electrode (usually platinum) and measured in the unit of ampere (A). A plot of A versus voltage (V) can be plotted, which the resulted graph known as voltammogram. The anodic peak from the

graph represents the oxidation of anti-oxidant, from which the peak area or height is proportional to the concentration of the anti-oxidants. By calibrating the anodic peak area or height with a known concentration, the amount of anti-oxidant in the samples can be determined. Various types of sensors including composite manganese hexacyanoferrate sensor for the determination of BHT anti-oxidant in food (Jayasri et al., 2007); polymer based on polyvinylpyrrolidone (PVP) sensor for BHA analysis in food (Wang et al., 2009); and gold nanoparticle and graphene sensor for the determination of hydroquinone (Hu et al., 2012) have been proposed.

One interesting application of electrochemical sensor is the multiplex analysis of anti-oxidants, which is demonstrated by Wei et al. (2014) in the quantitative determination of hydroquinone, catechol and resorcinol in river water. A composite sensor of nafion, MWCNT and carbon dot was modified on the surface of glassy carbon; and the sensor was successfully used for the multi determination of the mentioned anti-oxidants using a differential pulse voltammetry technique (DPV). The developed sensor showed a good linearity which ranges from 1 μM to 400 μM , and the limit of detection is below 0.1 μM for the three anti-oxidants (Wei et al., 2014). DPV is a sensitive technique that has been widely used for quantitative purpose unlike CV, which is used for qualitative analysis. In DPV, a modulation of the applied voltage in an increment pulse (staircase like) is used by the potentiostat to oxidise the anti-oxidants. Such method has the advantage in suppressing the capacitance current that was generated by the double layer (helmholtz's layer), as a result a more sensitive signal can be obtained. Other than DPV, other techniques including linear sweep voltammetry (LSV) was also widely used for the quantitative analysis of anti-oxidants. The principle of LSV is based on a linear ramping of potential (voltage) at a certain gradient that depends on the scan rate (V s^{-1}) of the method. A work by Caramit et al. (2013) has used MWCNT sensor with LSV technique for the determination of TBHQ and BHA in biodiesel samples. The developed method

showed a good linear ranging from 5×10^{-7} to 1.0×10^{-5} mol L⁻¹ for TBHQ and 3.4×10^{-7} to 1.7×10^{-5} mol L⁻¹ for BHA; with the detection limit for TBHQ and BHA which corresponded to 3.4×10^{-7} and 1.7×10^{-7} , respectively. LSV is simpler in comparison to DPV, and the method has advantages in its applied scan rate, which allows for a much higher value setting in comparison to DPV (Caramit et al., 2013).

Alternatively; the SWV technique is also widely used for the quantitative analysis of anti-oxidants. The principle of SWV is similar to DPV, which the applied potential is modulated in an incremental trend of a staircase like pulse, with a difference in the SWV which employed an additional negative pulse potential. The number of pulse is controlled by the frequency setting, which the complete frequency includes a cycle of both positive and negative pulse. The advantage of negative pulse allows the surface of the sensor to be conditioned each time upon oxidation. Combine with the effect of differential pulse; it reduces the capacitance current interference. As a result, SWV gives a sensitive technique that is comparable to DPV in the analysis of anti-oxidants (Ghoreishi et al., 2012). A work by Zhu et al. (2013) has employed the square wave technique in the quantitative analysis of quercetin in fruits. The proposed method was sensitive with a detection limit of 0.006 mg L⁻¹ that outstands other reported methods including HPLC and spectrophotometer (Zhu et al., 2013).

Electrochemical sensor is a rapid, low cost, simple to use and is also possible for field analysis (Caramit et al., 2013; Xu et al., 2012). These attributes have fitted to the criteria used for electrochemical methods in the analysis of anti-oxidants particularly when fast determination is required during in-line process monitoring (Ananingsih et al., 2013; Yao et al., 2014). Besides, with the multiple techniques available including LSV, CV, SWV, and DPV; they have given the flexibility of electrochemical sensors to be used in situ for either qualitative (by CV) or quantitative (LSV, SWV, and DPV) analysis of anti-oxidant

analysis, unlike to chromatography technique which is constrained by quantitative capabilities only. SWV has also proven to be more sensitive than HPLC in the quercetin analysis as shown in the work by Zhu et al. (2013) (Q. G. Zhu et al., 2013). Most importantly, the electrochemical sensor can also be used for the multi-compounds determination as HPLC or GC as demonstrated by Wei et al. (Wei et al., 2014), unlike chemical assay such as FC in total anti-oxidant analysis. Although, with the many advantages of electrochemical methods, however the drawback is still associated to its specificity and multiplex detection that is dependent on the fabrication and design of the sensor, which remains a challenge to many researchers.

2.5 Analysis of DNA bases

The analysis of DNA bases is important for the study of DNA damage, either for clinical or in-vitro studies. Few factors are required to consider when performing an analysis of DNA damages. First of all, it is the sample preparation procedure, since DNA is a biopolymer substance that is made up of a combination of DNA bases. To analyse its composition profile, the hydrolysis of the DNA is unavoidable. Various hydrolysis procedures have been studied, which includes biological or chemical approaches; in which an enzyme or acid is used respectively in each approach. In this chapter, both the advantages and disadvantages of the methods are reviewed to give a more comprehensive understanding about DNA bases analysis. Prior to DNA hydrolysis, preliminary isolation of DNA bases from samples matrix is also important in order to obtain pure DNA that is free from RNA and protein.

The analysis of DNA bases can be divided into qualitative or quantitative analysis; in which both methods are complementary to each other. The qualitative method is much simpler and direct, when compared to the quantitative procedure. However, the former approach is limited by its capability to measure DNA damage, and is often not selective

which is dependable on the purity of the DNA isolated. In contrast to quantitative method, this method is specific and hence more accurate in measurement. Some of these methods include electrochemical method (Yari & Derki, 2016), gel electrophoresis (Soares et al., 2015), high performance liquid chromatography (Zhou et al., 2015), and immunoassay (El-Yazbi & Loppnow, 2014). In this sub-chapter, each of these methods was reviewed in order to give a better comparison in terms of the method complexity, advantages and cost.

2.5.1 Preparation of DNA samples

In general, DNA preparation is much complicated in comparison to anti-oxidants depending on the approach of the detection method. It can be divided into three sections via; the DNA isolation, hydrolysis and enrichment.

2.5.1.1 DNA Isolation

The isolation of DNA is an important step to obtain a pure and free DNA from contamination such as protein, carbohydrate, lipid and RNA. To achieve this, the DNA in nucleus needs to be free from the cell matrix. Prior to isolation, preliminary preparation may be required depending on the nature of the samples. For solid samples, it needs to be homogenised first using a mortar and pestle. Whereas liquid samples, it can be directly extracted without preliminary preparation. The first step in DNA isolation is the lysis of cell membrane, which can be done by many procedures. The earliest method is by using surfactant such as sodium dodecyl sulfate (SDS) or cetyltrimethylammonium chloride (CTAB) to lyse the cell membrane, which comprises of phospholipid substances. SDS is the most common and effective surfactant used for this purpose and it is still widely used till today. Alternatively, other approaches using lysozyme enzyme was also proposed. At a concentration of 50 mg mL^{-1} it is sufficient to lyse the cell membrane immediately (Helden et al., 2001).

By lysis of the cell membrane, the content including lipid, RNA, DNA and protein are constituted into the mass solution. At this step, the extraction of DNA is the most crucial and the type of additives added to aid the extraction process will depend on the subsequent downstream processes (type of detection methods). Salting of DNA with sodium chloride is the most commonly employed method. With the addition of sufficient salt, the DNA biomolecule will precipitate out upon alteration of the solution polarity with solvent such as ethanol. Precipitated DNA can be removed by spooling with glass rod. A drawback to this method is associated to the salt residue, which could affect the performance of the detection step later. Therefore, in some cases de-salting of the DNA is required prior to extraction to obtain a pure DNA extract (El-Yazbi & Loppnow, 2014). Other extraction methods include phenol solution or alkaline solution was also used; from which it could selectively precipitate high molecular weight DNA, while leaving the circular DNA from bacterial in solution (Tan & Yiap, 2009), and followed by the segregation with spooling. Alternatively, the use of solid phase extraction (SPE) can be used for the purpose of DNA extraction. This method has proven to be simple and has also been widely commercialised, which allows a high throughput extraction of DNA samples. In principle, a solid sorbent was functionalised with chemical groups, in the case of DNA bases a positively charge diethylaminoethyl cellulose (DEAC) is modified on the silica bead surface. At pH condition between pH 6 to 9, negatively charged substances including anionic DNA will be bound to the functionalised sorbent and get trapped. The remaining matrixes including lipid and salt will pass through sorbent into the waste (Tan & Yiap, 2009). Among these methods, SPE has been widely used because of the ability to obtain a clean DNA from contaminants. The only drawback to this method is associated to the cost.

The final step in the DNA isolation is the purification of DNA extract. Contaminants such as salt, protein and lipid have been removed during the segregation either by

spooling or solid phase technique. Residues of contaminants are unavoidable, and further cleaning may be required depending on the method of detection. For instance, the use of the gel electrophoresis method in DNA detection may interfere by contaminant such as protein. To further purify the DNA extract, treatment using proteinase enzyme is performed to remove the protein (Shiomi et al., 2013). For salt contaminant, desalting step can be performed by using dialysis accessories, from which the solution flows through the surface of a dialysis membrane that allows the salt to pass through the membrane into a collector (deionized water). Alternatively, SPE can be further used to purify the DNA extract.

2.5.1.2 Hydrolysis or digestion of DNA

Hydrolysis or digestion of DNA is the process of breaking DNA biopolymer into its individual monomer bases which comprises of A, G, T and C or into smaller DNA strands (oligonucleotide). The extent of hydrolysis process depends on the requirements of employed detection methods. In general, there are a few approaches that have been widely used for this purpose including acid hydrolysis, thermal hydrolysis, and enzymatic digestion (El-Yazbi & Loppnow, 2014).

Among these methods, enzymatic digestion is widely used because of its specificity in hydrolysing a certain combination strand of DNA bases. Two types of enzymes can be used for this purpose including a more specific type known as restriction enzyme and a general type nuclease enzyme. A work by Shimelis & Giese (2006) has used nuclease P1 enzyme for the hydrolysis of calf thymus double stranded DNA. Briefly, the nuclease P1 enzyme was prepared in a 30 mM Trisbuffer at pH 7.5. Prior to use, the DNA sample was treated with zinc chloride before 40 μ L of the nuclease enzyme was added. The mixture was capped and incubated at 37°C for 2 h before it is collected by centrifugation; subsequently it is filtered and injected into high performance liquid chromatography for

detection. The analysis result was compared to other methods including acid digestion, which the author found a good result correlation between the two methods of digestion, and commented on the downfall of the UV absorbance assay as inaccurate (Shimelis & Giese, 2006). In a separate study by Mazloun et al. (2014) who has performed enzyme digestion of double stranded DNA using restriction enzyme known as BamHI, which specifically digested the DNA sequence of the combination GGATCC, and which is specifically found in the mitochondrial dehydrogenase gene. However, the described method is more specific and is designed for the detection of genes rather than for DNA damages study (Mazloun-Ardakani et al., 2014). Other similar work by William et al. (2013) has also used nuclease P1 enzyme for the digestion of oligodeoxyribosenucleotide into individual DNA bases and detection using liquid chromatography mass spectrometry (LC-MS) (Williams et al., 2013). It can be inferred that the use of nuclease enzyme is more suitable for the purpose of DNA damages study, whereby individual DNA bases quantification is required. On the other hand, the use of restriction enzyme is more specific and particularly meant for the assessment of explicit gene damages study.

Acid hydrolysis is another widely used method for the hydrolysis of double stranded DNA. Acid such as hydrochloric and sulfuric acid are used for the cleavage of the nucleotide bond between the DNA bases. A work by Svorc et al. (2014) has utilised hydrochloric acid for the digestion of double stranded DNA from fish sperm. Briefly, 3 mg of DNA samples was digested using 1 mL of 1 mol L⁻¹ hydrochloric acid at 100°C for 2–3 h. Subsequently the solution is neutralised with 1 mol L⁻¹ of sodium hydroxide. The author has successfully detected both A and G free bases from the hydrolysed DNA sample using electrochemical sensor. In the same study, a sample of DNA without hydrolysis was also measured using the sensor, from which the G and A were undetectable because of the steric hindrance posed by the double stranded DNA that prevents them from detection (through oxidation) by the boron doped diamond sensor

(Švorc & Kalcher, 2014). In a separate study by Moral et al. (2005) perchloric acid was used instead of hydrochloric acid in the digestion of bacteria sample, the digested samples was neutralised with potassium hydroxide. Upon cooling to room temperature (25°C), the samples were filtered and injected into HPLC. A and G were detected in the samples (del Moral et al., 2005). The advantage of acid hydrolysis compared to the enzyme method is associated to the final format of the DNA bases. The hydrolysis of DNA by enzyme will produce the final DNA bases of the monophosphate salt format such as adenine monophosphate (AMP) and guanine monophosphate (GMP). In comparison to acid hydrolysis a pure A and G compound is obtained (Shimelis & Giese, 2006). These considerations are important especially when the LC method is used for the detection, as the isomeric form of dAMP or dGMP may affect the retention time in LC chromatogram. Care has to be taken when performing acid hydrolysis of DNA especially on the applied temperature as severe heating may cause the deamination of cytosine to uracil (Shimelis & Giese, 2006).

Thermal hydrolysis of DNA is another alternative procedure for the hydrolysis or digestion of DNA. However, this method does not break the nucleotide bonding of the DNA bases instead only the hydrogen bond of double stranded DNA is broken to form a single stranded structure. This step is important for DNA enrichment; however, quantitative detection of DNA bases may not be appropriate. As a result, additional acid digestion may be performed for further digestion of the single stranded DNA. This approach has been demonstrated by Ferancova et al. (2010) from which a double stranded calf thymus DNA was thermal hydrolysed by heating at 100°C for 20 min and subsequently it is rapidly cooled in ice bath. The resulting single stranded DNA was further acid digested with 1 mol L⁻¹ HCl for 1 h and subsequently neutralised with sodium hydroxide prior to analysis using electrochemical sensor (cadmium sulfide/glassy carbon sensor) (Ferancová et al., 2010). The improvised thermal denaturation steps prior acid

digestion has shown the advantages in reducing the hydrolysis time from the conventional 3 h to 1 h, which could be attributed by the double stranded DNA that requires longer hydrolysis time. Thermal hydrolysis is important for the enrichment step of DNA, which is important for the detection technique such as gel electrophoresis and will be discussed in detail under Section 2.5.2.

Among the discussed hydrolysis methods, two major techniques that are based on enzyme and acid hydrolysis are the most widely used method. Acid hydrolysis is the most cost effective method and with preliminary thermal denaturation step; the method is much rapid than the enzyme digestion approach, which the latter requires 2–3 h incubation time. Contrary to temperature application, enzymatic digestion is gentler with the application at 36°C condition compared to the acid hydrolysis at 100°C that potentially affects the chemical structure of the DNA bases such as deamination of cytosine to uracil.

2.5.1.3 DNA enrichment

Enrichment is an additional procedure to pre-concentrate the DNA content in order to amplify the detection. This step is required when the employed analysis method is limited in detection response (sensitivity) such as gel electrophoresis or liquid chromatography method. Enrichment steps can be direct or in-direct depending on the detection method. The latter is associated to the use of polymerised chain reaction (PCR) to amplify the DNA biopolymer; whereas the direct enrichment utilised technique such as vacuum centrifugation to concentrate on the DNA bases.

PCR is a method of amplifying a copy of DNA into multiple copies. The step in PCR cycle can be divided into three steps; a double stranded DNA was first melted at high temperature to split them into individual single stranded DNA. This step is called denaturation step, whereby the single stranded DNA functioned as the template for multiplication. Subsequently, it enters the second step known as annealing and the

temperature was reduced down to 60°C. At this step, the primer of a specific DNA sequence adheres to the DNA template. The final step of the PCR is the extension or elongation process. In this step, polymerase enzyme is used to synthesize a new copy of DNA using the nucleotide source and is paired to the single stranded DNA template. This cycle is repeated until all precursors are consumed, and multiple copies of the DNA are produced. PCR only works for intact DNA, as hydrolyse DNA (into bases) is not possible to be amplified. A work by Senoo et al. (2016) has demonstrated the use of PCR to amplify the extracted mitochondrial DNA for 23 cycles, subsequently it is detected using gel electrophoresis (Senoo et al., 2016). In a separate study by Selbmann et al. (2011) PCR was used for the amplification of extracted Antarctic fungi DNA in which the fungi was exposed to ultraviolet radiation for DNA damage study. Successively, the amplified DNA is detected using gel electrophoresis (Selbmann et al., 2011).

Another procedure for the enrichment of DNA is by vacuum centrifugation, the method is only applicable for DNA bases samples. This method employed both vacuum force and centrifugation to evaporate solvent that constitutes the DNA bases. As a result, the DNA bases are pre-concentrated to a certain value which is sufficient for detection. A work by Zhu et al. (2010) has used vacuum centrifuge to pre-concentrate DNA extract from mouse. Formic acid was used to hydrolyse the DNA, and subsequently after pre-concentration the DNA bases was detected using liquid chromatography (Zhu et al., 2010). In a separate study by Shimelis & Giese (2006) vacuum centrifuge was used to concentrate the hydrolyse DNA bases by removing the acid solvent. Pre-concentrate DNA bases sample was detected using HPLC (Shimelis & Giese, 2006). Both studies have shown that the extracted DNA bases can be present at sufficiently low concentration for the detection using liquid chromatography, as a result the DNA enrichment procedure is required.

Both reviewed methods compliment to the different stages of DNA, which is either of biopolymer or individual monomer format. DNA enrichment may not be required for sample preparation, as it depends on the detection limit and sensitivity of the employed analysis method (quantitative).

2.5.2 Quantitative analysis of DNA

Analysis of DNA can be performed using a few methods and is categorised depending on the final format of the DNA during analysis. This is either by measuring the fragment of the DNA biopolymer of interest as a whole or quantifying the DNA monomer (DNA bases). The choice of the method is subjected to the objective and experiment design of the intended study. For instance, in the study of specific genes in DNA of certain bases combination; gel electrophoresis couple to PCR can be used for the selective study of these genes either for detection or DNA damages. The described method is more specific and targets on certain genes but does not give an overview of the whole genomes. Unlike electrochemical sensor or liquid chromatography that quantifies the DNA bases to give an overall view of the full DNA composition, hence it is more suitable for the study of DNA damage. In this chapter, the following methods including liquid chromatography, electrochemical sensor, gel electrophoresis and immunoassay (ELISA) that are used in DNA damage study will be reviewed.

2.5.2.1 Gel electrophoresis

Gel electrophoresis is a technique that employs a gel stationary phase to separate macromolecule substance using an electrical field. Subsequently, the separated macromolecule is stained with fluorescence-based dye such as ethidium bromide, and quantified based on fluorescence intensity according to Beer Lambert's law. The separation by gel electrophoresis is based on the charge density and size of the macromolecules such as deoxyribose nucleic acid, which can be charged under certain

pH condition. The gel used in the method is either of agarose or polyacrylamide, with the pores density adjusted by changing the concentration of the monomer. Small pores can be attained by increasing the monomer concentration, which is suitable for the separation of small DNA fragment. Electrical field is applied to a buffer solution usually of Tris or phosphate buffer at certain pH, whereby the gel is immersed and opposite electric field polarity to the charge of the DNA is applied. As a result, migration of the DNA molecule is achieved; and molecule with larger charge density (more charge with smaller molecular weight) will move faster and separated from the bulk DNA pool (Tan & Yiap, 2009).

A study by Hossain et al. (2013) has demonstrated the use of gel electrophoresis in the study of genotoxicity (DNA damage) of food flavouring such as curcumin, chamomile, etoposide and quercetin. In the experiment setup, P53R cells were used as the substrate and treated with various food flavouring substances for 30 min. Subsequently the cell was lysed with surfactant (sodium lauroyl sarcosinate and Triton X-100) and the DNA was extracted. A gel electrophoresis coupled with comet assay was used to assess the DNA damage. Briefly, the DNA is separated using gel electrophoresis, followed by staining with SYBR green; and the tailing of DNA fragment (Comet assay) is measured using comet score software. From the analysis result, the author has inferred few food flavouring including curcumin, quercetin, epigenin, chamomile, black tea and coffee showed positive to DNA damages of P53R cell upon exposure to certain concentration (Hossain et al., 2013). In a separate study by Selbmann et al. (2011) gel electrophoresis coupled with PCR was used to study the DNA damage after irradiation with ultraviolet radiation. The study objective was to correlate the potential damage of Antarctic fungi DNA by UV irradiation. The colonies of *Cryomyces antarcticus*, *Cryomyces minteri*, and *Saccharomyces pastorianus* were grown and subjected to UV irradiation. Subsequently, the DNA of these fungi was extracted and followed by enrichment using PCR at specifically three different DNA regions namely LSU, ITS and SSU; using primer LROR,

ITS5, and NS1, respectively. The amplified DNA samples were separated using gel electrophoresis, stained with ethidium bromide and the molecular weight of separated fragment was analysed using GeneRuler 100 base pair ladder. From the analysis result, the author concluded that the fungi was resistant to UV irradiation when contrasted to a positive control, and possibly the Antarctic fungi could produce UV irradiation substances (Selbmann et al., 2011).

Gel electrophoresis can be used for the study of DNA damages either on specific DNA region (genes) or the whole DNA biomolecule, as demonstrated by Selbmann et al. (2011) and Hossain et al. (2013) respectively. However, the limitation to the gel electrophoresis method is associated to its specificity and selectivity of the method. For instance the method does not give specific information with regard to DNA bases. Instead, it is based upon the structure damage of the DNA such as in comet score evaluation that is based upon the breakage of DNA. Besides, the method is also lacking in selectivity, as protein, and RNA contamination could contribute to the electrophoresis separation. As a result, it could give a false interpretation of the DNA fragment analysis. Gel electrophoresis is not suitable for high throughput analysis as the separation step is time consuming which requires 4 to 6 h.

2.5.2.2 Immunoassay

Immunoassay is another analysis method that can be used for the study of DNA damage. The principle of immunoassay is based on the detection of a byproduct that was produced by damaged DNA site, from which it (antigen) can bind specifically to antibodies. Few of these antibodies have been derived for this study purpose including CPD and 6-4PPs that binds to the antigen produced by DNA damage site. The detection of these interactions can be recognised by using ELISA, immunostaining and radioimmunoassay. The latter work by tagging the antibodies with radioisotopes

substances that emits ionising radiation upon positive interaction with the antigen; and similarly to immunostaining that is tagged with fluorescent substances such as fluorescein isothiocyanate. Among these detection assays, ELISA is the most commonly used method. From which the primary antibodies will interact with antigen produced from damaged DNA, subsequently secondary antibodies that is bound to an enzyme is used to detect the first antibody. By feeding the substrate to the bound enzyme; a product with intense absorption at specific wavelength is produced upon positive interaction (Cadet & Poulsen, 2010; El-Yazbi & Loppnow, 2014).

A work by Singh et al. (2014) has employed immunostaining method to study DNA damage through CARF binding. The author postulated a possible correlation between CARF to DNA damage response. Briefly, a cell line of U2OS was infected with a modified virus, which transfects the DNA of the cell with vector DNA from virus; as a result, it causes damage to the cell DNA. Subsequently, the cell was further treated with CARF, the positive binding of the antigen and CARF is visualised using a secondary immunostaining of ALEXA-488 conjugated goat anti-rabbit antibody. The positive or negative results were viewed and given a score under fluorescence microscope on both control and infected cell samples. The analysis result suggests the CARF has DNA damage inducible characteristic, which is either a damage sensor, signal transducer or checkpoint control required for further study (Singh et al., 2014). In a separate study highlighted by El-Yazbi & Loppnow (2014) has showcased the importance of 6-4PPs monoclonal antibodies. The ELISA method was used for the detection of 6-4PPs interactions; briefly a human cell was exposed to 12 and 24 h UV irradiation, successively it was treated with 6-4PPs antibodies. A secondary antibody was conjugated to alkaline phosphatase enzyme and used for the detection of 6-4PPs antibodies. From the analysis result, the author inferred that DNA damage can be detected and quantified efficiently at 24 h irradiation but not at 12 h (El-Yazbi & Loppnow, 2014).

Immunoassay method has proven to be specific and sensitive for the detection of DNA damage. However, the drawback in immunoassay method is associated by the limiting choice of antibody markers, which make the method too specific that typically limited to specific DNA site and localised damage only. Besides, the generation of antibodies can be tedious, difficult and a time-consuming process.

2.5.2.3 Liquid chromatography

The approach of liquid chromatography in DNA damage study is slightly different from the previously discussed immunoassay and gel electrophoresis methods. In this method, the measurement is based upon detection of individual DNA bases, instead of byproduct detection from damage DNA using immunoassay or DNA breakage as in gel electrophoresis method. According to Chargaff's rules, the ratio of C to G or T to A is equal to unity. Any deviation from this value is considered as DNA mis-matched and leads to the change in DNA double helical structure (Shamsi & Kraatz, 2013); resulting to the damage of DNA. By quantitating the amount of A, G, T and C; the Chargaff's ratio can be calculated and used for the detection of DNA damages. Liquid chromatography is a powerful method for the evaluation of DNA damage, due to its specific and selective detection of the DNA bases (Cadet & Poulsen, 2010).

The principle of liquid chromatography in DNA bases detection is based upon the separation of A, G, T and C using column such as octyldodecyl (C18) or HILIC column. Different types of column have distinctive separation ability which depends on the polarity properties of the column, for instance C18 is a non-polar column, which is suitable for use for the separation of non-polar substances. However, with the use of suitable mobile phase in the chromatography such as phosphate buffer, a C18 column can be used for the separation of ionic-based substances using a technique known as ion pairing. The column separating DNA bases are then individually recognised using

detectors such as UV-VIS spectrophotometer, mass spectroscopy, or refractive index. The choice of detector will affect the different sensitivity and selectivity of the liquid chromatography method.

A work by Zhu et al. (2010) has utilized the HPLC method for the study of carcinogenic properties of formic acid to DNA. Briefly, a male Kunming mouse was used as the subject of investigation, and was treated with sodium formate. After 24 h, the mouse was sacrificed and DNA was extracted from the liver, and further hydrolysed using nuclease P1 (enzymatic method). Subsequently, the hydrolysed samples were injected into HPLC equipped with C18 column for the separation of the DNA bases, and accelerator mass spectroscopy for the detection of the DNA bases (A, G, T and C). The author has inferred formic acid as non-genotoxic to human DNA, as no additional adduct of DNA bases can be observed and the Chargaff's ratio between the DNA bases was met (based on chromatogram) (Zhu et al., 2010). In a separate work by Inagaki et al. (2003) a study on genotoxicity of acetylaldehyde was performed using HPLC. Briefly, a HL 60 cells were cultured and treated with acetylaldehyde for 24 h. After which the DNA of the cell was extracted and hydrolysed using hydrochloric acid at 70°C for 4 h. Subsequently, the hydrolysed sample was injected into HPLC equipped with C18 column and a mass detector for the analysis of A and G. However, the author failed to recover C and T. From the analysis result, no changes was observed on the content of G bases when contrasted to blank control which the author has inferred that acetyl aldehyde was not genotoxic, but may require further evaluation using a more sensitive LC method (Inagaki et al., 2003).

In a study by Nagy et al. (2005) a HPLC method was also used for the study of urban air pollutants particularly 3-nitrobenzanthrone (3-NBA) and 2-nitrobenzanthrone (2-NBA) as potential genotoxin. Briefly, A549 cells were cultured and treated with 3-NBA and 2-NBA for 24 h. The treated cell was lysed with surfactant (Triton X 100) and

the DNA was extracted. Subsequently, the DNA was lysed with nuclease P1 enzyme, and the sample was injected into HPLC for analysis. A C18 column was used for the separation of the DNA bases and a UV detector used for analysis of the DNA bases and its possible adduct (derivatized). From the results, the author concluded that neither 3-NBA nor 2-NBA showed any damages to the DNA and no adduct of the format 8 oxo guanine is detected (Nagy et al., 2005).

Liquid chromatography method is a powerful method for the analysis of DNA damages. It is proven to be selective and specific which can detect the 4 DNA bases simultaneously and measure the degradation of these bases. Moreover, it can also be used to detect the DNA bases adducts or derivatives that might be oxidised or reduced when degradation of the intact DNA bases happened such as guanine to 8-oxoguanine. The drawback in the HPLC method is associated to its analysis time, which can be lengthy particularly per analysis will require approximately 10 min per sample. Besides, the investment and operation cost of HPLC instrument especially with mass spectroscopy detector can be expensive.

2.5.2.4 Electrochemical sensor

Electrochemical sensor is another method that can be used for DNA damage study; the approach of electrochemical sensor is similar to liquid chromatography, which the measurement is based upon the detection of individual DNA bases or corresponding adduct. The challenge of electrochemical sensor in DNA bases measurement is associated to the detection of C and T; this is because both nucleic acid bases are difficult to be oxidised (Verdolino et al., 2008). With recent advancement in electro-active materials such as nanomaterials and biopolymers, it has led to the breakthrough in the fabrication of surface modified sensor; in which the sensor is more sensitive, improved overpotential and possesses electro catalytic properties that can be used for DNA damage study.

The principle of electrochemical sensor is based upon the use of a dipping sensor or platform for samples. An oxidation potential (anodic voltage) is then applied to the sensor, which oxidises the respective DNA bases (G, A, T and C) and releases electron as the product of the oxidation. Subsequently, this electron (current) is measured and a voltamogram of current against potential can be plotted. Each of the DNA bases will be represented as a peak that is recognised based on its oxidation voltage, and the respective current height is proportional to the concentration. By measuring the peak height or current, the amount of the DNA bases can be determined.

A work by Yari & Derki (2016) has fabricated a surface modified sensor for the electrochemical detection of G and A. Briefly, a mix solution of MWCNT and Fe_3O_4 nanocomposite solution was prepared by dispersing MWCNT in distilled water under sonication for 20 min. Subsequently, FeCl_2 and FeCl_3 were mixed into a solution of HCl and stirred until dissolved. Both solutions were then mixed and stirred under nitrogen, and finally adjusted to pH 12 using ammonia solution. A polydopamine MWCNT- Fe_3O_4 paste was prepared by mixing the nanocomposite solution into a dopamine monomer solution. This final polymer precipitate was isolated and mixed with graphite powder and paraffin oil. The fabricated carbon paste was compressed into a polypropylene tube, whereby an electrical contact was established by pushing a copper wire into the tube. The fabricated sensor is designated as MWCNT- Fe_3O_4 @PDA/carbon paste; and the author has successfully used the sensor to detect A and G in fish sperm DNA after hydrolysis (Yari & Derki, 2016). In a separate study by Ferancova et al. (2010) a cadmium sulfide microsphere sensor was developed for the detection of G and A. A calf thymus DNA was subjected to UV-irradiation to induce damage. Subsequently the DNA was hydrolysed; G and A were detected using the sensor. The author inferred that at 60 min exposure to UV B, no damage in DNA was observed; but at 20 min exposure to UV C a total degradation of DNA bases was observed (Ferancová et al., 2010).

Most of the fabricated sensors have successfully measured G and A in DNA samples, but not for T and C. A recent work by Ye et al. (2014) has fabricated a nano zinc sulfide/PEDOT/rGO/GC sensor which is a thin layer of zinc sulfide-ethylenedioxythiophene-reduced graphene oxide film that was deposited on a glassy carbon platform; and the sensor was successfully used for the detection of A, G and T DNA bases. The author has successfully used the sensor for detection of 3 DNA bases in herring sperm DNA after hydrolysis (Ye et al., 2014).

Electrochemical sensor is a potential method use for DNA damages study; this is because the method is rapid, sensitive, and selective towards the detection of DNA bases. Unlike the immunoassay, chromatography and electrophoresis method, which is time consuming, moreover, the need for throughput analysis due to ample DNA samples screening have impeded the use of these established methods. On the other hand, with the rapid response of electrochemical sensor, it is fit for this purpose of study. However, the challenge remained in electrochemical sensor is still imparted by the ability to quantitate all the four DNA bases (A, G, T and C). Therefore, the application use of electrochemical sensors still requires much development especially to improve the sensors ability to perform multiplex detection of A, G, T, and C.

CHAPTER 3: ELECTROCHEMICAL PREPARATION AND CHARACTERISATION OF A GOLD NANOPARTICLES MODIFIED GRAPHITE ELECTRODE

3.1 Introduction and scope of work

Graphite has been known for its electrical conducting properties, and chemical inertness (Moreno-Baron et al., 2003), this has made it an attractive material for working electrode. Besides, it is also abundantly available from the recyclable source such as battery. It is estimated that the world market for batteries in year 2016 will reach USD132 billion, and the production of alkaline batteries in China alone is estimated at 128×10^8 units (Sun et al., 2015). This suggests that used batteries could be a potential source of graphite that can be recycled into working electrode. In general, a heavy-duty battery consists of 4 components namely; zinc (negative cathode), manganese (IV) oxide, ammonium chloride paste (electrolyte) and graphite (positive cathode). The recovery of manganese and zinc from spent battery has been extensively reclaimed, however, the feasibility of recycling graphite from used battery has not been in place (Belardi et al., 2011). In this chapter, a spent heavy-duty battery of grade “AA” was used for the sensor fabrication. A disposed battery from household was preferable, as this meets the study objective and falls within the scope of green chemistry. A typical grade “AA” battery consists of a graphite rod with diameter of 3 mm, which is ideal for sensor fabrication. Several studies on the electrochemical applications of disposable graphite electrode have been reported. The attempt was focused mostly on pencil graphite and mechanical lead; which have successfully demonstrated a low cost procedure in the fabrication of disposable working electrode and surface modification that transforms a graphite material into a sensitive and selective sensor. This approach could be applied to the graphite rod from a spent battery.

Flavonoid compounds extracted from various plants possess anti-oxidants, in which the properties can be studied using electrochemical method. Myricetin is one of the naturally occurring flavonoid that can be found abundantly in the skin of fruits such as tomato, grape, onion (Huang et al., 2010), and also in vegetables such as carrot, cabbage, spinach and cauliflower (Sultana & Anwar, 2008). The concentration of myricetin in various fruits and vegetables can be ranged between 150 mg kg^{-1} to 1700 mg kg^{-1} (Flores et al., 2008). The dietary intake of myricetin in our daily consumption is reported at 0.98 to 1.1 mg per day (Y. Li & Ding, 2012). Among the flavonoids, myricetin is one of the few that possesses a strong radical scavenging property (Samra et al., 2011) with a chemical structure that is similar to quercetin (Huang et al., 2010). Several studies have shown the significance of myricetin to health, including as an anti-oxidant, anti-carcinogenic, therapeutic potential in diabetes mellitus (Li & Ding, 2012), human keratinocytes protective effects (Huang et al., 2010) and also as an inhibitor in cancer cell proliferation (Shiomi et al., 2013). The analysis of myricetin can be performed by several analytical techniques such as liquid chromatography (Flores & Luisa, 2015; Sultana & Anwar, 2008), and gas chromatography (Kumar et al., 2009). Although these methods are accurate and precise; such analytical procedures often require tedious sample preparation, expensive equipment investment, and inappropriate for field-analysis. In addition, the stability of anti-oxidant compounds are sensitive and can be influenced by various conditions such as temperature, environmental oxygen, pH, and light (Ananingsih et al., 2013; Ioannou et al., 2012); therefore an on-field analysis is preferable. An electrochemical method is more attractive as an alternative method due to its sensitivity, rapid analysis, low expense, and possibility for field analysis (Gabriela et al., 2015).

The study of graphite sensor using pencil or mechanical lead has been widely demonstrated, however, the use of battery graphite has not been investigated before. In this chapter, a green, simple and cost-effective procedure in fabricating a graphite sensor

from a used battery is discussed. To overcome the high activation overpotential, an electrode surface modification by electrodeposition with gold nanoparticles using CV was performed. Furthermore, deposition of gold nanoparticles is optimised by determining the number of CV cycle that gives the best electrochemical performance. The optimisation procedures were carried out by determining the morphology and electrochemical characteristic of the gold-nanoparticles modified graphite sensor using CV, electrochemical impedance spectroscopy (EIS), scanning electron microscope (SEM) and energy dispersive X-ray fluorescence (ED-XRF). The optimised sensor is designated as Au-NPs/graphite sensor and used for the analysis of myricetin anti-oxidant in tea samples.

3.2 Experimental

3.2.1 Chemicals and apparatus

Potassium ferricyanide $K_3Fe(CN)_6$ powder was purchased from Acros (USA) and sodium nitrate was purchased from System (Selangor, Malaysia). Britton-Robinson buffer was prepared by mixing an equal amount of 0.04 mol L^{-1} phosphoric acid, 0.04 mol L^{-1} boric acid and 0.04 mol L^{-1} acetic acid. The pH of the Britton-Robinson buffer was adjusted to pH 2 with 1 M sodium hydroxide. All the chemicals used in the buffer preparation were purchased from Merck (Darmstadt, Germany). A myricetin $1000 \mu\text{g mL}^{-1}$ stock standard was prepared from pure powder which was purchased from King Herbs (China). The prepared myricetin solution was stored in a dark container and kept at $+4^\circ\text{C}$. A 1.0 mmol L^{-1} tetrachloroauric acid in 0.1 mol L^{-1} NaNO_3 solution was prepared from $\text{HAuCl}_4 \cdot (\text{H}_2\text{O})_3$ powder purchased from Sigma Aldrich (Steinheim, Germany). A 0.1 mol L^{-1} of potassium ferricyanide $K_3Fe(CN)_6$ solution (pH 7) was prepared for the electrode characterization. All the solutions were prepared using 18.2 M ohm deionised water.

Electrochemical measurements were performed using the Metrohm potentiostat system model PG Stat 202 (Utretch, Netherlands). The impedance measurements were performed using the FRA10V (Metrohm, Utretch Netherlands) interfaced to the PG Stat 202. A three-electrode system was employed throughout the experiments, in which a platinum rod was used as a counter electrode, and Ag/AgCl (3 mol L⁻¹ KCl) as the reference electrode, both electrodes were purchased from BASi (USA). The morphology analysis on the electrode surface was performed using Hitachi FE-SEM model SU8220 (Japan). The system was also hyphenated with energy dispersive X-ray (EDX) for elemental analysis which was obtained from Oxford instrument (United Kingdom).

3.2.2 Fabrication of graphite electrode

The graphite rod was extracted from a used battery of grade “AA” with the diameter measurement of 3 mm. A layer of starch material can be observed on the surface that coated the graphite, and was removed effectively by immersing the graphite rod in a hot water; upon sonication, this coating was removed from the surface. Trace manganese was also removed by immersing the rod in a solution of 1 mol L⁻¹ hydrochloric acid. The cleaned graphite was heated in an oven at 130°C to dry it overnight. Subsequently, the tip of the graphite was polished with emery paper grade P130, and then followed by grade P1000 and P2000 until a smooth surface is observed. PTFE tape was used to insulate the graphite body for approximately 5 layers, with the tip of the graphite exposed and a remaining 0.5 cm of the rod is unwrapped, which function as the connector to potentiometric. The exposed surface tip of graphite rod was polished with alumina slurry consisting of 1.0 µm particles, and then followed by particle-size of 0.3 µm and 0.05 µm on a Texmet pad. After polishing, the electrode was cleaned by sonicating with ethanol for 5 min, and followed by ultrapure water. The fabricated graphite electrodes were kept at room temperature (25°C) until further use. Fig. 3.1 shows the fabricated graphite rod, with connection and tip illustration. Since the graphite rod can be fragile and easily

broken, a 3 mm PTFE tube was used to support the graphite rod, and also to prevent the lateral exposure of the rod to electrolyte.

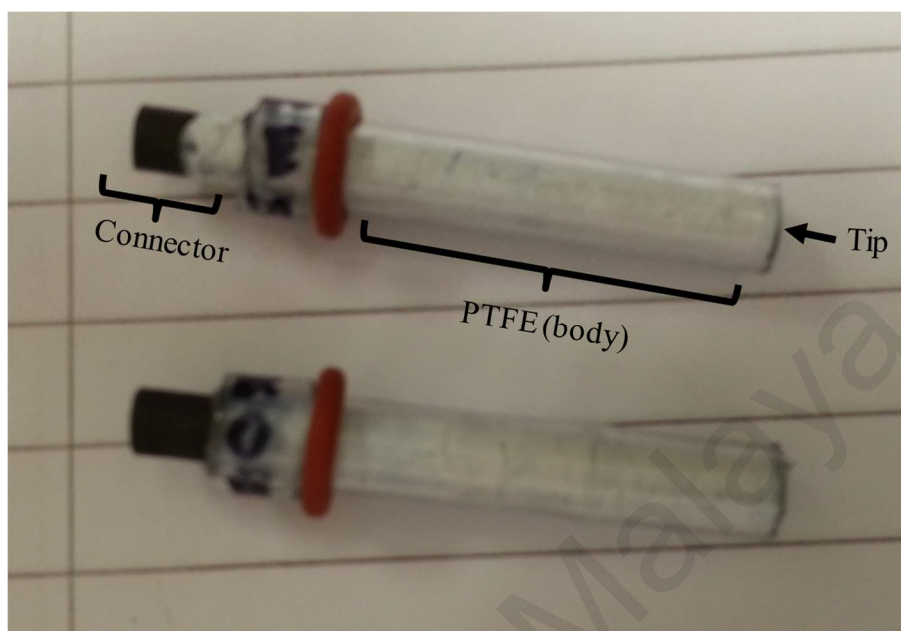


Figure 3.1: Fabricated graphite electrode from used battery.

3.2.3 Electro-deposition and activation of gold nanoparticles on the graphite electrode

The gold nanoparticles were deposited on the graphite electrode surface by using CV scanning. A solution of 0.1 mmol L^{-1} of tetrachloroauric acid at pH 3 was prepared by diluting 10 times the stock solution (subsection 3.2.1) with 0.1 M sodium nitrate. The following CV parameter was used for electro-deposition of gold nanoparticles; applied potential ranged from 0.900 to -0.300 V with fixed scan rates and potential steps of 0.05 V s^{-1} and 0.0025 V, respectively. To select the optimum deposition cycle of the gold nanoparticles on the graphite surface, a total of 6 preparations at 4, 8, 12, 16, 20 and 24 deposition cycle numbers were performed.

The electrodes were electrochemically activated by performing CV scan in a solution of 0.5 mol L^{-1} sulfuric acid. With the applied potential scanned from 0.2 to 1.6 V, a fixed

scan rate of 0.1 V s^{-1} and potential step of 0.0025 V , and a total of 20 repetition cycles were performed for each activation cycle. The surface modified electrode was designated as Au-NPs/Graphite electrode, and this abbreviation will be used throughout this thesis.

3.2.4 Electrochemical characterisation of Au-NPs/graphite

The activated Au-NPs/graphite sensor was characterised with CV and electrochemical impedance spectroscopy (EIS). Both experiments were performed using a 1.0 mmol L^{-1} ferricyanide solution prepared by diluting the stock solution 100 times with 1.0 mol L^{-1} NaNO_3 . To evaluate the effective surface area, and heterogeneous electron transfer rate, a CV scan was performed with the following parameter; applied potential from -0.150 to 0.650 V and across a range of scan rates from 0.020 to 0.800 V s^{-1} .

The EIS experiment was performed to evaluate the capacitance and electron transfer resistance. The following EIS parameter was used; applied potential was set at 0.2 V based upon the open circuit potential evaluation; the frequency range used was from 1.0 KHz to 0.1 Hz . Both the Nyquist and Bode plots were selected for data evaluation and the data was also fitted to a Randles circuit cell model.

3.2.5 Morphology analysis by field emission SEM

The tip of the surface modified graphite electrode was disengaged with a pair of cutters. The surface of the tip was positioned upward and the bottom was adhered onto the FE-SEM sample platform, a low vacuum mode was used, and the electron power was set at 30 K eV . For EDX measurement, a localised mode was used that selectively bombarded an area of gold nanoparticles with X-ray and elemental spectral was obtained.

3.2.6 Electrochemical analysis of myricetin using the Au–NPs/graphite electrode

3.2.6.1 Electrochemical characteristic of myricetin

The CV of myricetin was performed in a deaerated standard solution of $20 \mu\text{g mL}^{-1}$ in a 0.1 M Britton-Robinson buffer. Parameter used in the CV scan was set as followed, with the applied potential ranging from -0.15 to 0.90 V and a scan rate of 0.1 V s^{-1} was used.

3.2.6.2 Analysis of myricetin by SWV

The myricetin analysis was performed using a SWV technique in a deaerated Britton-Robinson buffer; with applied potential ranging from -0.2 to 0.8 V at a frequency and amplitude of 50 Hz and 25 mV, respectively. To assess the analytical performance of the SWV in myricetin analysis, a standard calibration curve of myricetin was constructed using the standard addition method; a $2 \mu\text{g mL}^{-1}$ concentration increment was used in each addition. The limit of detection (LOD) and limit of quantification (LOQ) of the myricetin were also determined by performing a two times serial dilution from concentration of $1 \mu\text{g mL}^{-1}$ (1.0, 0.5, 0.25, and $0.13 \mu\text{g mL}^{-1}$).

3.2.6.3 pH effect in myricetin analysis

Myricetin standard of $6 \mu\text{g mL}^{-1}$ was prepared in a different pH condition ranging from pH 2 to 7. Britton-Robinson buffer was used in the preparation which was adjusted to the required pH using 1.0 mol L^{-1} sodium hydroxide. A SWV method as described in section 2.6.3 was used for the detection of myricetin.

3.3 Results and discussion

3.3.1 Electrodeposition of gold nanoparticles on graphite electrode

The CV of gold nanoparticles deposition on the graphite electrode surface is illustrated in Fig. 3.2, with only the first, third and tenth CV scans being shown in the figure. In the reverse scan from 0.9 to -0.3 V, a cathodic peak was observed. This peak was associated with the reduction of gold (III) to elemental gold (Hezard et al., 2012). When analysing the CV results from first to the subsequent 3rd and 10th CV, the peak was shifted to a more positive potential, with the first scan and 10th CV scan recorded at 0.5497 and 0.7109 V, respectively. A similar observation was also reported by Hezard et al. (2012) and Maringa et al. (2014).

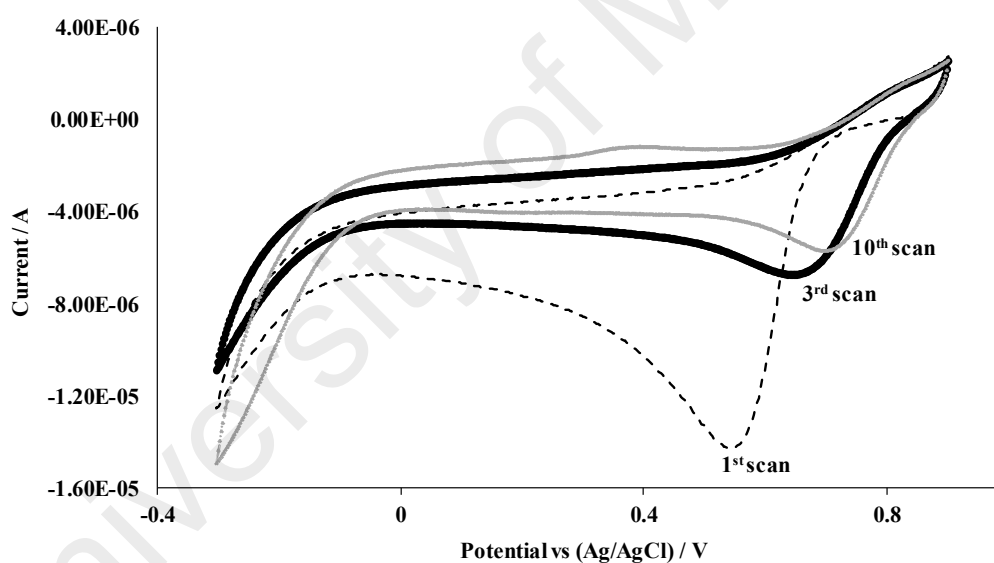


Figure 3.2: CV of gold nanoparticles deposition on graphite electrode.

No significant peak potential shift was observed after the 10th CV scan. The positive potential shift could be attributed to the favourable thermodynamic deposition of gold on the metal substrate itself (nucleation process) instead of on the carbon substrate, which requires more adsorption energy (Appy et al., 2014). Based on this evaluation, the electrodeposition of gold at 4th and 8th deposition cycles could result in less nucleation process with smaller and more consistent particle sizes as compared to the higher number

of deposition cycles. This is because, at 10th deposition cycles and above, nucleation process is more favourable with a continued growth of gold in the particle sizes leading to a wider distribution. This observation was further confirmed by the morphology analysis with field emission SEM. Fig. 3.3 illustrates the SEM results of the Au-NPs graphite surface prepared at 8th (image B), 16th (image C) and 24th (image D) deposition cycles. The size of the gold nanoparticles was measured and corresponded to diameter of 75 nm, 110 nm and 180 nm, respectively. A substantial increment of the gold nanoparticles size from the 8th to 24th deposition cycles suggested that nucleation process is favourable at higher deposition cycles. No gold particle was observed on the non electrodeposited graphite surface (bare graphite electrode).

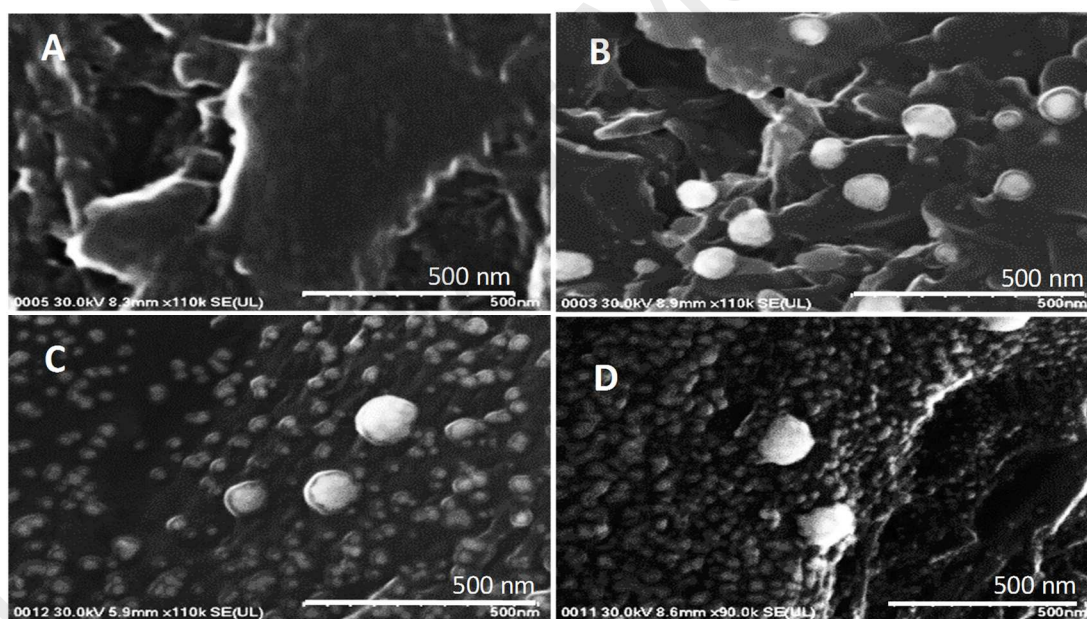


Figure 3.3: SEM of bare graphite (image A) and gold nanoparticles graphite electrode prepared at 8th (image B), 16th (image C) and 24th (image D) deposition cycles.

3.3.2 Activation of Au-NPs/graphite electrode

The Au-NPs/graphite electrode was activated using 20 cycles of CV scan in a 0.5 M sulfuric acid. The first and the last scan (20th scan) of the activation process are

superimposed as shown in Fig. 3.4. In the forward CV scan from 0.2 to 1.6 V, a large peak was observed in the region of 1.3 to 1.6 V. This region is broad due to the complex formation of Au oxide on the graphite surface (Gotti et al., 2014; Hezard et al., 2012; Maringa et al., 2014). On the reverse CV scan from 1.6 to 0.2 V, a peak was observed at potential 0.8714 V which corresponded to the reduction of the Au oxide (Gotti et al., 2014). A comparison of the first with the 20th CV scan showed a decrease in the current (Ampere) of reduction potential peak at 0.8714 V (Au oxide). Hence, it is suggested that with electrochemical activation the level of Au oxide formation on the graphite surface was suppressed, and this enhanced the performance of the electrode. I have demonstrated this performance improvement through the electrochemical characterisations, which is further discussed in section 3.3.4 and 3.3.5.

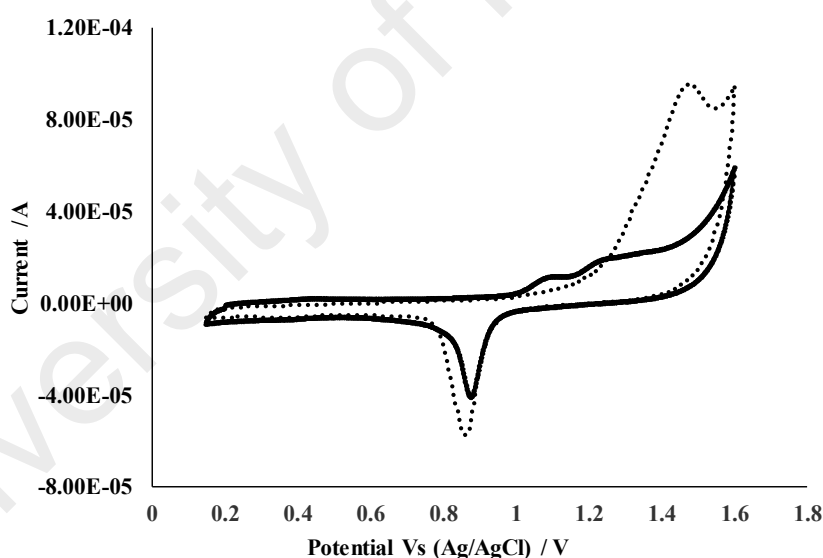


Figure 3.4: CV of Au-NPs/graphite during activation in 0.5 M sulfuric acid. The dotted and solid line corresponds to the first and 20th CV scan respectively.

3.3.3 Morphology characterisation by field emission SEM

The morphology of the bare and gold nanoparticles modified graphite electrode was characterised using FE–SEM. Fig. 3.5 illustrates the SEM images of the bare and gold nanoparticles modified graphite electrode, which were prepared at 8th, 16th and 24th

deposition cycle. The Au–NPs/graphite electrodes prepared at 16th (image C) and 24th (image D) deposition cycle showed a more nanoparticles coverage at 30 K magnification. In contrast, to the 8th (image B) deposition cycle, the gold nanoparticles were less consistent with a much narrower size distribution. With greater SEM magnification at 110 K (images C and D) as shown in Fig. 3.5, a mixture of small and large nanoparticles could be observed with the smaller nanoparticles on the electrode prepared at 16th and 24th deposition cycle measuring between 35 – 65 nm and 10 – 100 nm, respectively. The shapes of the smaller particles are irregular while the larger particles are spherical.

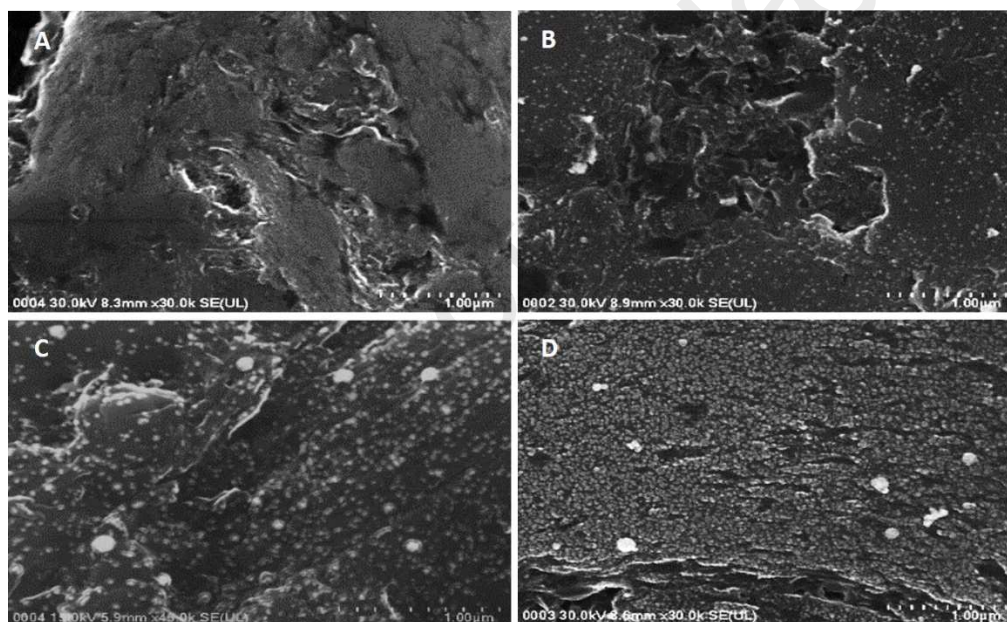


Figure 3.5: SEM of bare graphite (image A) and gold nanoparticles graphite electrode prepared at 8th (image B), 16th (image C) and 24th (image D) deposition cycles.

An energy dispersive X-ray analysis (EDX) was performed on a section of the Au–NPs graphite surface, which was prepared at 16th deposition cycles. The result is shown in Fig. 3.6, which confirms the presence of gold on the electrode surface.

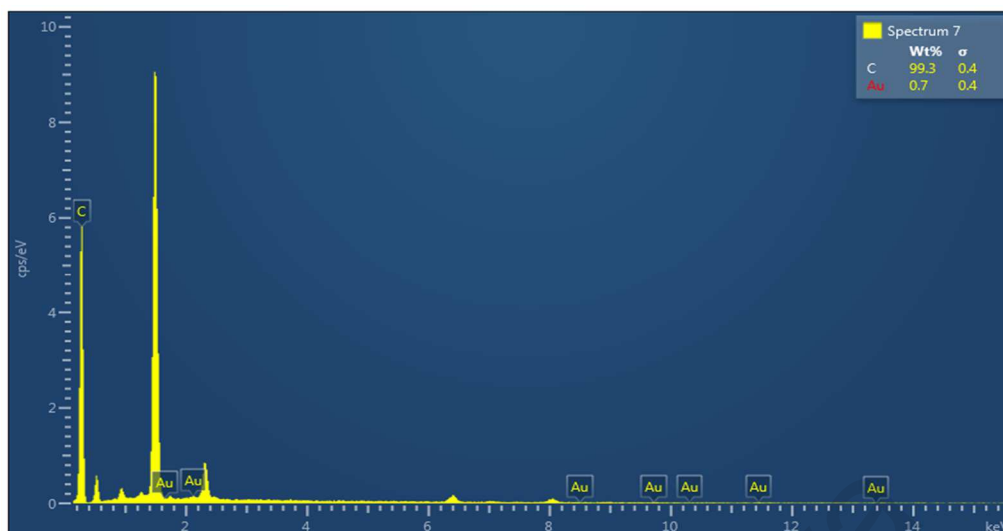


Figure 3.6: EDX spectral of Au–NPs/graphite surface electrode prepared at 16th deposition CV cycle.

3.3.4 Electrochemical characterisation of Au–NPs/graphite electrode by CV

3.3.4.1 Effective surface area

$$I_p = 2.69 \times 10^5 \times n^{\frac{3}{2}} \times A \times C \times D^{\frac{1}{2}} \times v^{\frac{1}{2}} \quad (\text{Eq. 1})$$

The effective surface area (Eff A) was calculated using the Randles-Sevcik equation (Eq. 1). Where, I_p , n , A , C , D and v correspond to peak current (A), the number of electron transfer, Eff A (cm^2), concentration (mol cm^{-3}), diffusion coefficient ($\text{cm}^2 \text{s}^{-1}$) and scan rate (V s^{-1}). By taking the diffusion coefficient of potassium ferricyanide in NaNO_3 as $6.20 \times 10^{-6} \text{ cm}^2 \text{s}^{-1}$, the Eff A of the bare graphite and Au–NPs/graphite electrode (surface modified) can be calculated from the slope of peak current versus square root of scan rate and both Eff A can be compared; it has been demonstrated by Arvand & Hemmati (2017) and Kalambate & Srivastava (2016) that compared the Eff A of different surface modified electrode using Randles-Sevcik equation (Arvand & Hemmati, 2017; Kalambate & Srivastava, 2016). Fig. 3.7 illustrates the CV of ferricyanide solution performed using bare graphite at various scan rates. By converting the value of scan rate to square root of scan rate, Fig. 3.8 shows the linear correlation of Randles–Sevcik equation, which indicates the Eff A of the graphite electrode.

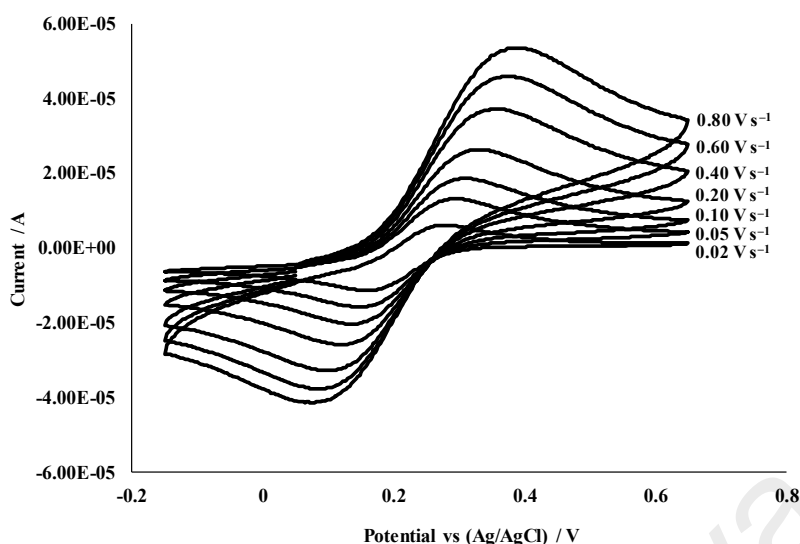


Figure 3.7: CV of 1.0 mmol L⁻¹ ferricyanide solution using bare graphite electrode at various scan rates.

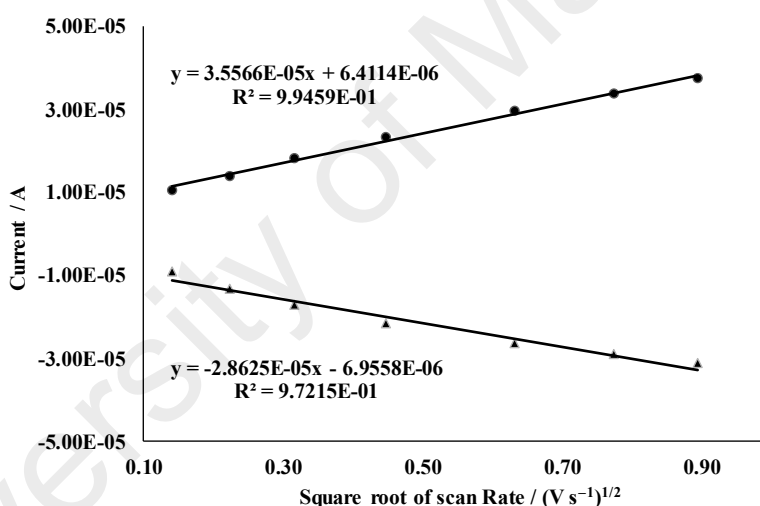


Figure 3.8: Correlation graph of current versus square root of scan rate measured using bare graphite electrode.

These values are important as it determines the number of site that is redox active and capable to oxidise or reduce the analyte of interest. Tables 3.1 to 3.3 summarise the Eff A of bare graphite, inactivated Au-NPs/graphite and activated Au-NPs/graphite electrode, respectively. The Eff A of activated Au-NPs/graphite showed a much larger surface area when compared to their bare graphite counterpart, with the activated Au-NPs/graphite electrode prepared at 16th deposition cycles having the largest Eff A of 0.165

cm², in comparison to its bare graphite at 0.048 cm². Fig. 3.9 illustrates the surface area trend across different deposition cycles of the graphite electrodes. Based on the figure, the Eff A of the inactivated Au-NPs/graphite electrodes is the same as the bare graphite electrodes. This suggests the inactivated Au-NP/s graphite could be impeded by the Au oxide nanoparticles. Upon activation in acidic solution by multiple CV scanning, the Eff A of the activated Au-NPs/graphite electrodes were expanded, due to a reduction of the gold oxide to gold.

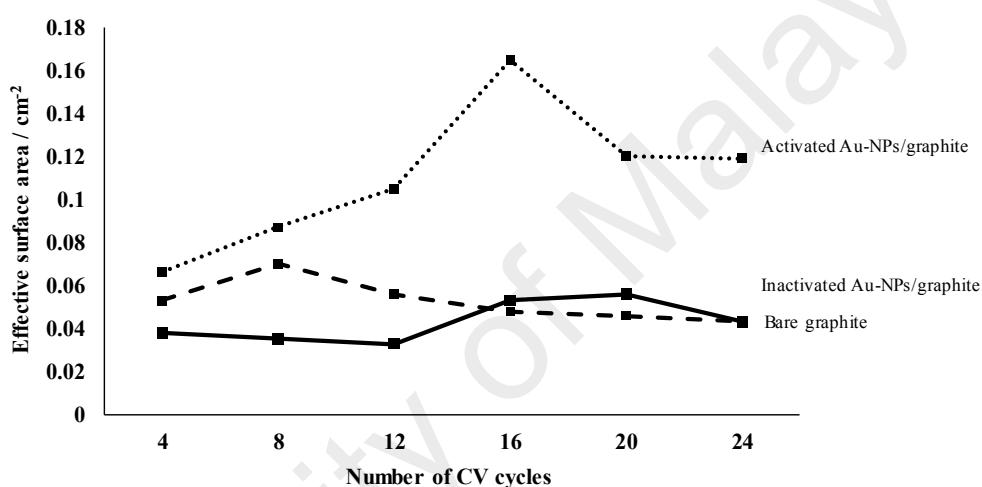


Figure 3.9: Eff A versus deposition cycle of gold nanoparticle using CV, and comparison made between activated, inactivated and bare graphite electrode.

Table 3.1: Electrochemical characterisation of bare graphite electrode by CV.

No	Electrode	¹ Eff A/cm ²	² k _s /s ⁻¹	³ R _{ct} / ohm cm ²	⁴ C _{dl} /μF	⁵ DP cycle
1	Graphite 1	0.053	2.0778	1020	2.11	4
2	Graphite 2	0.070	3.1565	822	3.57	8
3	Graphite 3	0.056	2.8409	1540	2.69	12
4	Graphite 4	0.048	2.1674	2450	2.07	16
5	Graphite 5	0.046	1.8146	2470	1.96	20
6	Graphite 6	0.043	1.9243	2130	2.31	24

¹ Effective surface area

² Heterogeneous electron transfer rates

³ Electron transfer resistance

⁴ Double layer capacitance

⁵ CV deposition cycle without gold

Table 3.2: Electrochemical characterisation of inactivated Au–NPs/graphite electrode by CV.

No	Electrode	¹ Eff A/cm ²	² k _s /s ⁻¹	³ R _{ct} / ohm cm ²	⁴ C _{dl} /μF	⁵ DP cycle
1	Graphite 1	0.038	1.7357	2420	1.45	4
2	Graphite 2	0.035	1.4434	3540	2.20	8
3	Graphite 3	0.033	1.6580	3500	3.14	12
4	Graphite 4	0.053	1.7933	2860	1.73	16
5	Graphite 5	0.056	2.8081	2310	1.56	20
6	Graphite 6	0.043	1.7234	2790	1.84	24

¹ Effective surface area

² Heterogeneous electron transfer rates

³ Electron transfer resistance

⁴ Double layer capacitance

⁵ CV deposition cycle

Table 3.3: Electrochemical characterisation of activated Au–NPs/graphite electrode by CV.

No	Electrode	¹ Eff A/cm ²	² k _s /s ⁻¹ (CV)	³ Γ /mol cm ⁻²	⁴ R _{ct} /ohm cm ²	⁵ C _{dl} /μF	⁶ DP cycle
1	Graphite 1	0.066	3.9823	5.8203	1210	6.44	4
2	Graphite 2	0.087	4.7005	5.8563	475	11.7	8
3	Graphite 3	0.105	8.1767	5.9055	265	10.1	12
4	Graphite 4	0.165	9.8908	6.0113	156	23.8	16
5	Graphite 5	0.120	7.7094	5.9385	281	8.01	20
6	Graphite 6	0.119	12.2476	5.7689	145	10.9	24

¹ Effective surface area

² Heterogeneous electron transfer rates

³ Surface coverage

⁴ Electron transfer resistance

⁵ Double layer capacitance

⁶ CV deposition cycle

3.3.4.2 Surface coverage

$$I_p = n^2 F^2 A \Gamma \frac{v}{4RT} \quad (\text{Eq. 2})$$

The surface coverage of Au–NPs on graphite can be calculated using equation 2 (Eq. 2), where, I_p , n , F , A , Γ , R , V and T corresponds to peak current (A), the number of electrons transfer, Faraday constant (C mol⁻¹), Eff A (cm²), surface coverage (mol cm⁻²), gas constant (J mol⁻¹ K⁻¹), scan rate (V s⁻¹) and temperature (K) (Martinez et al., 2005; Pillay et al., 2010). By taking the value of A as equal to the Eff A of the activated

Au-NPs/graphite, the surface coverage in terms of mol per area (cm^{-2}) can be calculated from the slope of the plot of current against scan rate (Arvand & Hemmati, 2017). Table 3.3 summarises the gold surface coverage at various deposition CV cycles which was calculated using Eq. 2. In this study, the surface coverage was used as a method to evaluate the gold nanoparticles deposition. Based on the calculation, at 16th deposition cycle, the surface coverage was the highest at $6.01 \times 10^{-10} \text{ mol cm}^{-2}$. At subsequent deposition above 16 cycles, the surface coverage of the gold was found decreasing. This observation could be a result of gold nanoparticles nucleation process instead of deposition on the fresh graphite surface. This further confirms our earlier findings on the nucleation process over higher deposition CV cycles as observed during the CV electrodeposition and SEM evaluation (Section 3.3.1). At 24th cycles, the densely packed gold nanoparticles (Fig. 3.3, image D) were observed started to overlap each other at the edge side, resulting in a larger volume to surface ratio that affecting the surface coverage.

3.3.4.3 Heterogeneous electron transfer rate (k_s)

$$E_p = E_0 - \frac{2.303RT}{\alpha nF} \log \frac{RTk_s}{\alpha nF} + \frac{2.303RT}{\alpha nF} \text{Log}v \quad (\text{Eq. 3})$$

$$\text{Log} k_s = \alpha \log(1 - \alpha) + (1 - \alpha) \log \alpha - \log\left(\frac{RT}{nFv}\right) - \frac{\alpha(1-\alpha)nF\Delta E_p}{2.303 RT} \quad (\text{Eq. 4})$$

$$k_s = \frac{\alpha nFv_c}{RT} = \frac{(1-\alpha)nFv_a}{RT} \quad (\text{Eq. 5})$$

The heterogeneous electron transfer rate (k_s) was calculated using the Laviron equation (Eq. 3), where, E_p , E_0 , R , T , n , F and v correspond to peak potential (V), formal potential (V), gas constant ($\text{J mol}^{-1} \text{K}^{-1}$), temperature (K), number of electron transfer, Faraday constant (C mol^{-1}) and scan rate (V s^{-1}). The term α is a dimensionless constant which measures the symmetry of the energy barrier of the redox reaction (German et al., 2014). The alpha value is determined from the slope of the plot of ferricyanide peak potential

versus logarithm of scan rate. The Laviron equation was applied by Sun et al. (2013) for the determination of heterogeneous electron transfer rate on a graphene-platinum nanocomposite sensor performed in a diffusion controlled and quasi-reversible system (Sun et al., 2013); and Sutradhar & Patnaik (2017) that used ferricyanide solution for the heterogeneous electron transfer rate measurement of fullerenes-goldnanoparticles/GCE (Sutradhar & Patnaik, 2017). Since the obtained CV (Fig. 3.7) illustrates a shift of peak potential with scan rate; therefore Laviron equation is applied in measurement of k_s . Fig. 3.10 illustrates a correlation plot of potential versus logarithm of scan rate that was obtained using bare graphite electrode in 1.0 mmol L^{-1} ferricyanide solution.

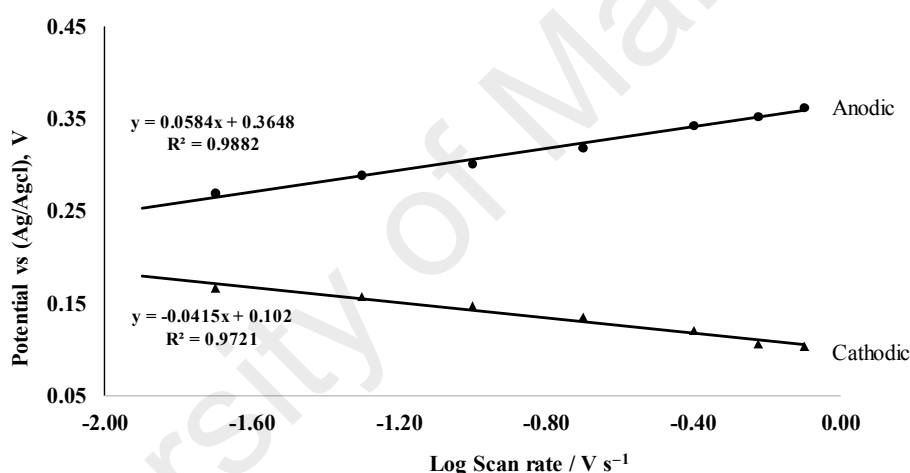


Figure 3.10: Linear correlation graph of peak potential versus logarithm of scan rate that performed using CV and bare graphite electrode in 1.0 mmol L^{-1} ferricyanide solution.

Two linear lines corresponding to anodic and cathodic peak are obtained with the slope value of 0.0584 and -0.0415, respectively; α value can be calculated from the slope. The formal potential E_0 can be determined from the intercept of the graph of peak potential versus scan rate. With the inputs of α and E_0 , the k_s can be calculated from the rearrangement of Laviron's equation (Eq. 4) (Dilgin et al., 2013; Eckermann et al., 2010), where ΔE_p is equal to the difference of $E_p - E_0$. When the overpotential is equal to zero i.e., $\Delta E_p = 0$, the k_s can be calculated from the simplified formula (Eq. 5), where V_c and

V_a correspond to the scan rate of cathodic or anodic process, respectively. At $\Delta E_p = 0$, the V can be extrapolated at $Y = 0$ in the linear graph of peak potential versus log of scan rate.

In this study, the heterogeneous electron transfer rate (k_s) is calculated from the anodic process of the ferri/ferro cyanide redox. The k_s of bare graphite, inactivated Au-NPs/graphite and activated Au-NPs/graphite were calculated using the equation above, and the results were tabulated in Table 3.2 and 3.3, respectively. Overall, the heterogeneous electron transfer rate of the activated Au-NPs/graphite is the highest as compared to its bare graphite electrode counterpart. The electrode prepared at 24th deposition cycles showed the highest k_s with a rate constant of 12.2476 s^{-1} , this is followed by electrode prepared at 16th deposition cycles with k_s of 9.8908 s^{-1} . The significance of electrode activation towards the performance of Au-NPs/graphite electrode was also investigated by comparing the k_s performance; Fig. 3.11 shows the trend of k_s between activated and inactivated Au-NPs/graphite electrode. From the graph, the inactivated Au-NPs/graphite has the lowest k_s value when compared to the bare graphite. This can be explained by the Au oxide surface (subsection 3.3.2), which impedes the electron transfer process.

From the CV characterisation of Eff A, surface coverage, and heterogeneous electron transfer rate studies, Au-NPs/graphite electrode prepared at 16th deposition cycle and after activation gives the best attribute in electrochemical properties. In other words, 16th deposition cycle gives the optimum conditions for the preparation of Au-NPs/graphite electrode.

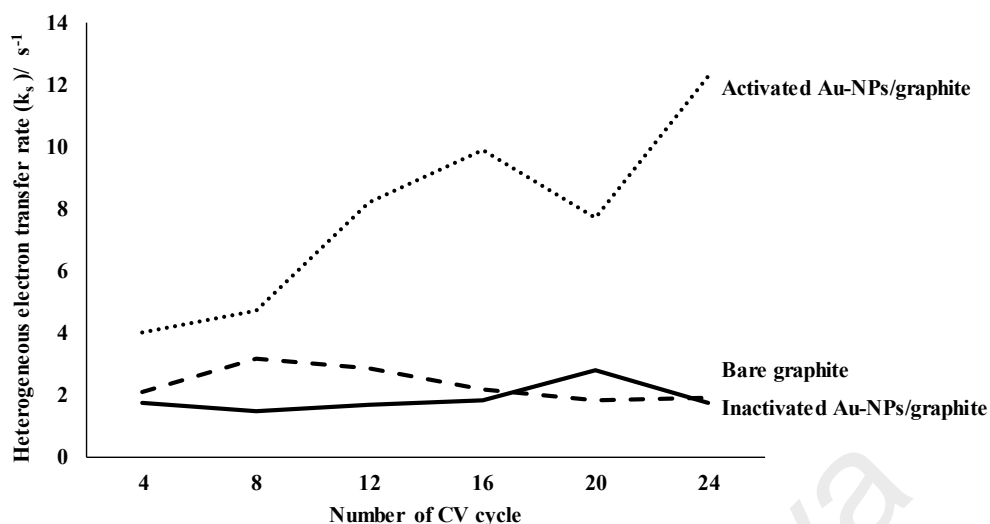


Figure 3.11: Heterogeneous electron transfer rate (k_s) versus deposition cycle of gold nanoparticles using CV and comparison between activated, inactivated and bare graphite.

3.3.4.4 Electron transfer efficiency

The electron transfer efficiency of the activated electrode prepared at 16th deposition cycle was further evaluated with CV which was based upon Nernstian equation. The resulting voltammogram is illustrated in Fig. 3.12. The potential difference (ΔE_p) between the anodic and cathodic peak of the electrode was separated by 78.1 mV. This value is close to the theoretical value of 59 mV in a Nernstian reversible system, hence, suggesting an efficient electron transfer process when compared to the value 183 mV that was obtained using bare graphite. The peak separation of the electrode (activated at 16th deposition cycle) was also monitored throughout a range of scan rates from 0.02 to 1.25 V s⁻¹. The results are summarised in Table 3.4 based on the peak potential difference, the electron transfer efficiency of the activated Au-NPs/graphite (16th deposition cycle) in a reversible redox process could be attained up to a scan rate of 0.4 V s⁻¹, above this value the peak difference was getting wider suggesting that the electrochemical reversibility of the electrode is not favourable. The change in the ΔE_p could be also due to ohmic drop; which was not considered in this study as the cell geometry, electrolyte concentration and ferricyanide concentration was constant throughout the experiment.

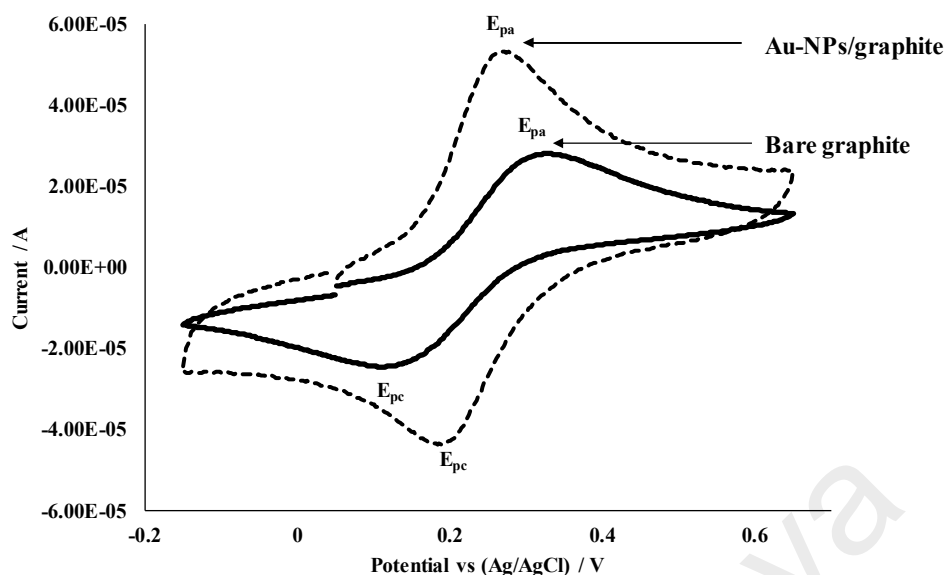


Figure 3.12: CV of 1.0 mmol L⁻¹ ferricyanide solution performed using bare graphite versus Au-NPs/graphite electrode prepared at 16th deposition cycle.

Table 3.4: Peak potential difference (ΔE_p) of Au-NPs/graphite (16th deposition cycle) at various scan rates.

Scan Rate / V s ⁻¹	Peak potential difference $\Delta E_p (E_{pa} - E_{pc}) / V$
0.02	0.0708
0.2	0.0781
0.4	0.0781
0.8	0.0928
1.0	0.0855
1.25	0.0952

3.3.4.5 Electrode overpotential

Electrode overpotential is described as the application of a more positive potential in the oxidation process than predicted by thermodynamics. To evaluate the overpotential performance of Au-NPs/graphite, a CV experiment using ferricyanide solution was performed. Fig. 3.12 illustrates the ferri/ferro cyanide redox process using activated Au-NPs graphite electrode (prepared at 16th deposition cycle) versus its bare graphite counterpart. From the voltammogram it has shown a decrease in the anodic peak potential

from 0.3210 V (bare graphite) to 0.2698 V (Au–NPs/graphite). The reduction in the anodic peaks potential by 51 mV suggests an improvement in the overpotential of Au–NPs graphite electrode. An improved overpotential is important for the analysis of anti-oxidants and nucleic acid bases, especially for those difficult to oxidise substances such as butylated hydroxyl toluene (BHT).

3.3.5 Electrochemical characterisation of Au-NPs/graphite electrode by electro impedance spectroscopy

The Randles-circuit model was used in the EIS study of the fabricated Au-NPs/graphite sensor. Fig. 3.13 illustrates the Randles-circuit model, in which 4 components of R_{sol} (Resistance of electrolyte), R_{ct} (charge transfer resistance), C_{dl} (double layer capacitance) and W (Warburg's element) are connected in series or parallel manner.

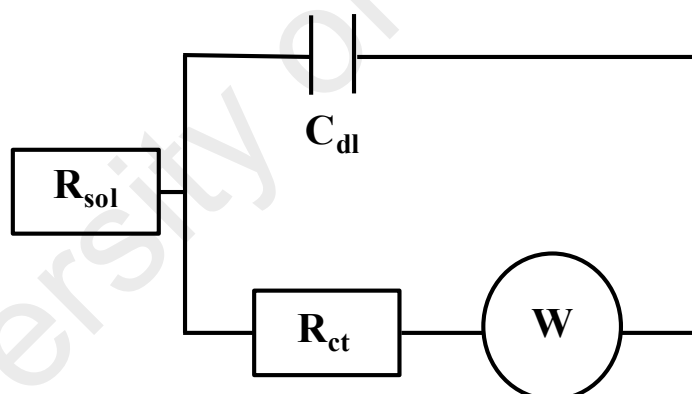


Figure 3.13: Randles-circuit model that represents an electrochemical interface of a working electrode with bulk solution.

From the analysis data obtained from EIS, a Nyquist graph was plotted and fitted to a Randles-circuit model. The 4 component values were estimated for all sensors prepared at different gold deposition cycles; and the results are summarised in Table 3.1 to 3.3. The R_{ct} values for the bare graphite, inactivated Au–NPs/graphite and activated Au–NPs/graphite prepared at 16th deposition cycle were estimated at 2450 ohm cm², 2840 ohm cm² and 156 ohm cm², respectively. This observation can infer that after sensor activation with sulfuric acid, the Au–NPs/graphite sensor showed the lowest electron

transfer resistance. In which, the result is consistent to the heterogeneous electron transfer rate findings; and both the bare graphite and inactivated Au–NPs/graphite showed a higher and constant R_{ct} values. This again suggests the importance of sensor activation upon usage. Fig. 3.14 illustrates the Nyquist plot of activated Au–NPs/graphite, bare graphite and inactivated Au–NPs/graphite electrode which was prepared at 16th deposition cycle of gold nanoparticles.

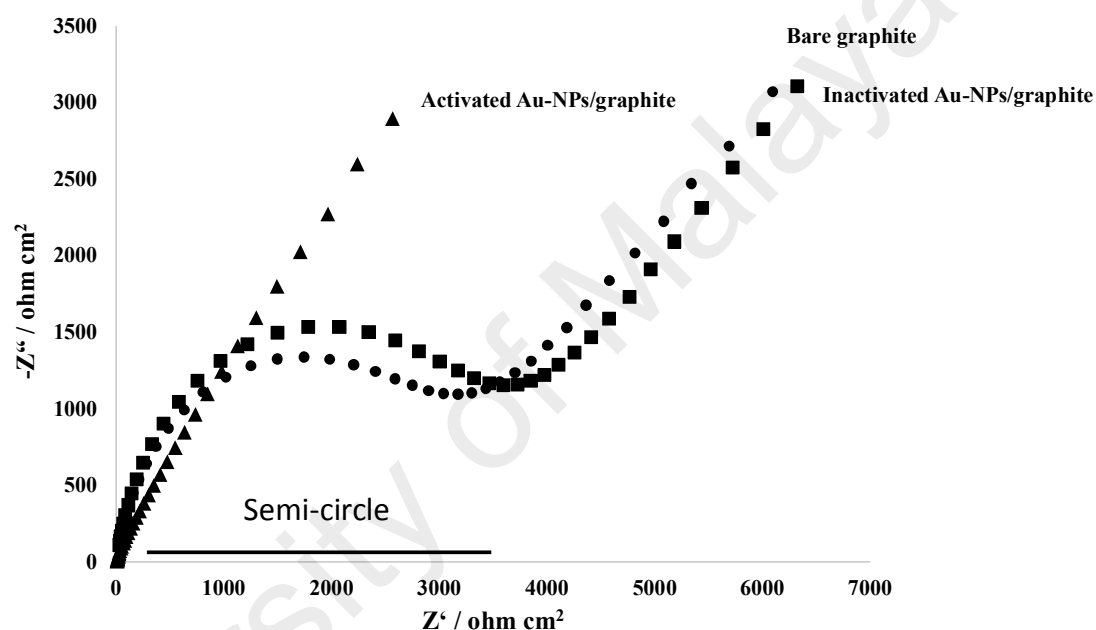


Figure 3.14: Nyquist plot of bare graphite (sphere marker), inactivated Au–NPs/graphite (square marker) and activated Au–NPs/graphite (triangle marker) which was prepared at 16th CV deposition cycle.

The diameter of the semi-circle portion in the Nyquist plot corresponds to the electron transfer resistance. Based on the Nyquist plot as shown in Fig. 3.14, the inactivated Au–NPs/graphite has a semi-circle diameter that is comparable to the counterpart bare graphite electrodes. In contrast to the activated Au–NPs/graphite a linear line is observed instead of a semi-circle, which suggests that after activation the electrode exhibits a lower electron transfer resistance.

Fig. 3.15 illustrates the double layer capacitance (C_{dl}) properties trend across the different CV gold deposition cycle numbers. From the graph, both inactivated Au-NPs/graphite and bare graphite sensor at various CV deposition cycles does not show any significant change in the C_{dl} trend. On the other hand, the C_{dl} values of the activated Au-NPs/graphite were increased from 4th to 16th CV cycle, after which the values started to decrease.

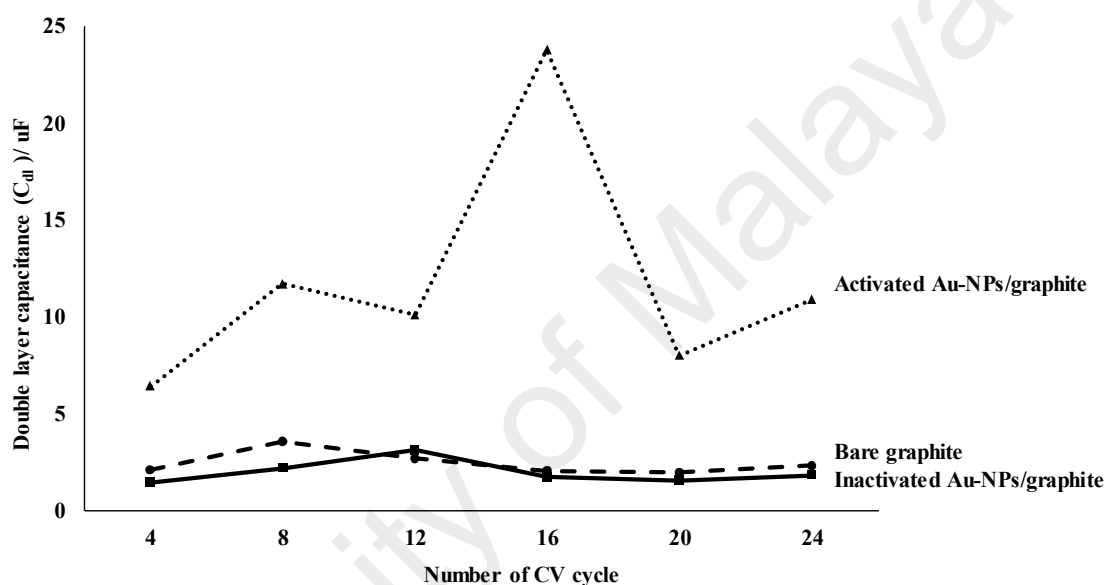


Figure 3.15: Graph of double layer capacitance (C_{dl}) versus the number of CV gold nanoparticles deposition cycles.

This observation could be explained by taking into account the surface roughness of the electrode (Kerner & Pajkossy, 2000; Daikhin et al., 1997; Pajkossy, 2005). From the SEM images (image B, C and D) as shown in Fig. 3.3, it showed at low deposition cycles (below 16 cycles) the gold nanoparticles deposited on the graphite surface were more homogeneously deposited (less roughness). However, upon reaching 16th deposition cycles the gold nanoparticles deposition was accompanied by the nucleation process, in which a mix of small and large particles started to produce, hence a rougher surface with higher double layer capacitance. At deposition cycles greater than 16, the coalescence of the gold

nanoparticles into a more homogenous sheet was observed, therefore resulting in a lower double layer capacitance.

To measure this surface roughness, a factor (R) can be measured by determining the ratio of Eff A (Au–NPs/graphite) to its bare graphite counterpart. These values were calculated for all the gold nanoparticle modified graphite sensors which was prepared at different deposition cycles, and the results are tabulated in Table 3.5. The calculation showed at 16th deposition CV cycles, the R value was the highest suggesting a much rougher surface in comparison to the 20th and 24th deposition cycles.

Table 3.5: Surface roughness factor (R) and constant phase fitting (CPE) of activated Au–NPs/graphite that prepared at different CV deposition cycles.

No	Electrode	Surface roughness (R)	¹ CPE fitting (N)	² DP cycle
1	Graphite 1	1.2453	0.871	4
2	Graphite 2	1.2429	0.05	8
3	Graphite 3	1.8750	0.601	12
4	Graphite 4	3.4375	0.879	16
5	Graphite 5	2.6087	0.929	20
6	Graphite 6	2.7674	0.906	24

¹CPE means Constant phase element.

²DP means CV deposition cycle.

To determine the impact of surface roughness on the electrochemical sensor performance, the capacitive impedance of Au-NPs/graphite electrode was studied. According, to Pajkossy et al. (2000) the rough surface could affect the sensor capacitance dispersion. As a result, it could affect the sensor sensitivity. From the Randles circuit model illustrated in Fig. 3.13, the modification of the model was made by replacing the ideal capacitance (C_{dl}) with a constant phase element (CPE). From the EIS experiment fitting, the capacitive impedance (Kerner & Pajkossy, 2000) can be determined using the following relation i.e., the power-law of frequency of capacitance [$C(\omega^N)$]. An N value that is close to 1 denoted that the sensor exhibits an ideal capacitive impedance (Kerner

& Pajkossy, 2000; Pajkossy, 2005). The N values for each gold nanoparticles modified sensor prepared at different deposition cycles are calculated and summarised in Table 3.5. From the results, the Au-NPs/graphite prepared at 16th deposition cycle has the N-value of 0.879. Accordingly, the CPE of most solid electrode are generally ranged from 0.7 to 0.9 (Kerner & Pajkossy, 2000). Although, the rough surface of the Au-NPs/graphite could impact on the capacitive impedance, however the CPE fitting suggested that Au-NPs/graphite prepared at 16th deposition cycle was still close to the ideal condition.

From the EIS characterisation, the Au-NPs modified graphite electrode prepared at 16th deposition cycle was found to be the optimum. Besides, it also showed the lowest electron transfer resistance after activation. Although, the surface could be rough that could potentially impact the capacitance properties, nevertheless EIS analysis suggesting the N values was still acceptable. Based on the EIS and CV studies, the activated Au-NPs/graphite electrode prepared at 16th deposition cycle was selected for further application studies.

3.3.6 Electrochemical analysis of myricetin using the Au-NPs/graphite electrode

3.3.6.1 Analysis of myricetin using CV

The CV of the myricetin was performed using the activated Au-NPs/graphite (16th deposition cycle) electrode at various scan rate (Fig. 3.16 (a)). Subsequently, Fig. 3.16 (b) shows a linear correlation of peak current (anodic and cathodic) vs. square root of scan rate for myricetin that was performed using Au-NPs/graphite suggesting it is a diffusion-controlled process (Yari & Derki, 2016; Zhu et al., 2013).

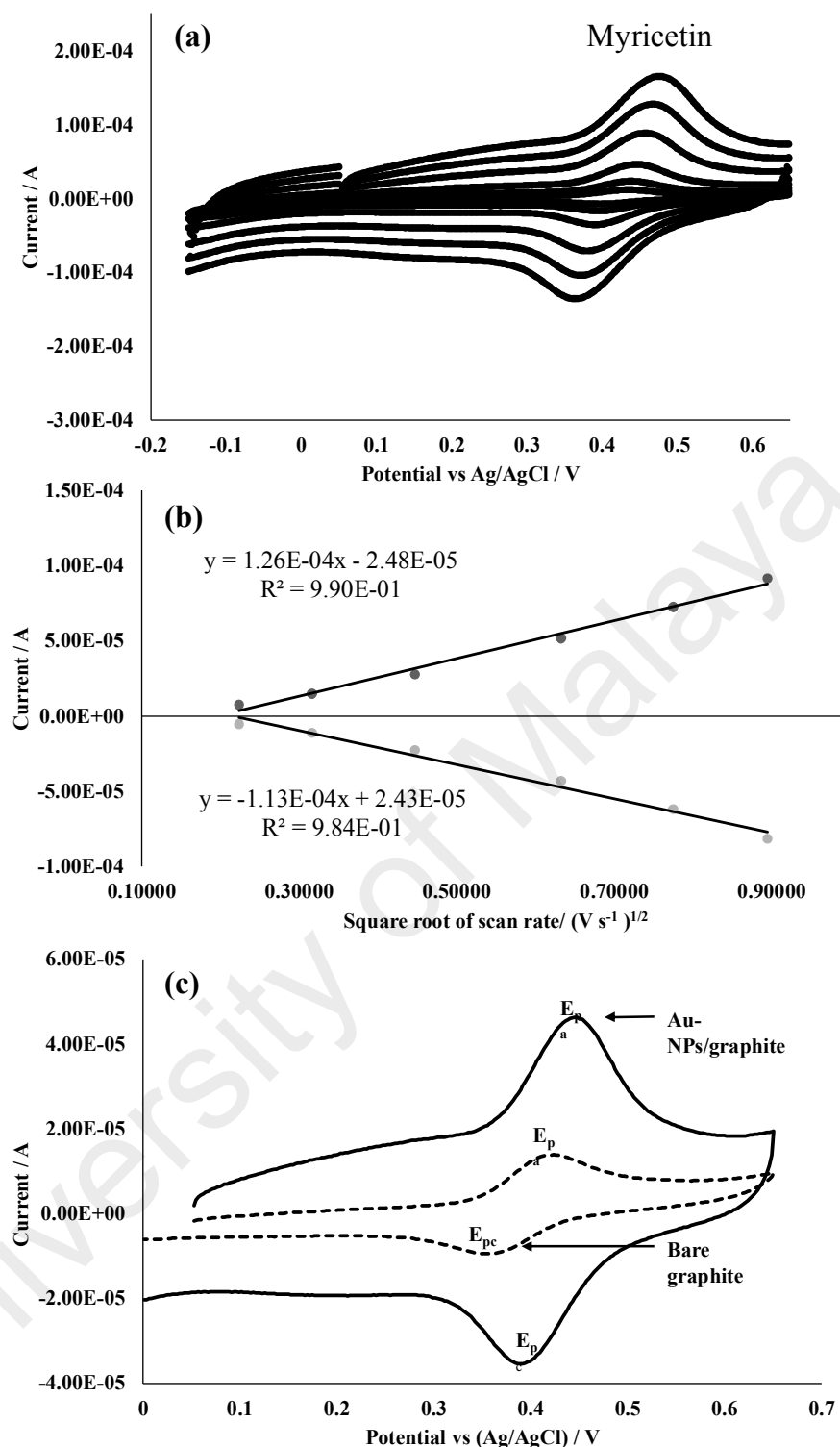


Figure 3.16: (a) CV of myricetin at various scan rates (0.05, 0.10, 0.20, 0.40, 0.60 and 0.80 $V s^{-1}$) (b) Graph of peak current versus square root of scan rate of myricetin that performed using Au-NPs/graphite (c) CV of myricetin performed using Au-NPs/graphite versus bare graphite in 0.1 mol L^{-1} Britton Robinson buffer.

Fig. 3.16 (c) illustrates the CV results of the myricetin that performed using Au-NPs/graphite and bare graphite, which a reversible redox process was observed in

myricetin, with the anodic and cathodic peak potential of the Au–NPs/graphite were measured at 0.4480 and 0.3919 V, respectively. The potential difference between the anodic and cathodic peaks was measured at 56.15 mV, which is close to the theoretical value of 59.16 mV (Nernstian behaviour). From the Nernst equation, the number of electrons involved (n) in the myricetin redox process is given by $59.16/n$, which in this evaluation yield a value of 1 which suggested that the myricetin redox process involved a one electron and proton transfer process. A similar experiment was performed using the bare graphite electrode, in which a reversible redox process was also observed.

From the CV shown in Fig. 3.16 (c), the peak currents of the myricetin that was performed using the Au–NPs/graphite electrode were more intense as compared to its counterpart bare graphite, thus suggesting the Au–NPs/graphite was more sensitive than its bare graphite counterparts. A similar observation on the reversible process of myricetin was also reported by Komorsky-Lovric & Novak (2013) using a paraffin impregnated graphite rod, with the anodic and cathodic peak potentials measuring at 0.409 and 0.307 V, respectively (Komorsky-Lovrić & Novak, 2013).

From the Randles-Sevchik equation (Eq. 1), the diffusion coefficient of myricetin was calculated by plotting a graph of peak current versus the square root of scan rate, which is illustrated in Fig. 3.16 (b). By assuming the Eff A of the Au–NPs/graphite electrode as 0.165 cm^2 , the diffusion coefficient of myricetin to Au–NPs/graphite interface was calculated at $2.049 \times 10^{-5} \text{ cm}^2 \text{ s}^{-1}$. Apart from this, the heterogeneous electron transfer rate (k_s) was also calculated using Laviron equation, which showed the k_s of myricetin on Au–NPs/graphite obtained was 2.45 s^{-1} .

3.3.6.2 pH effect in myricetin analysis

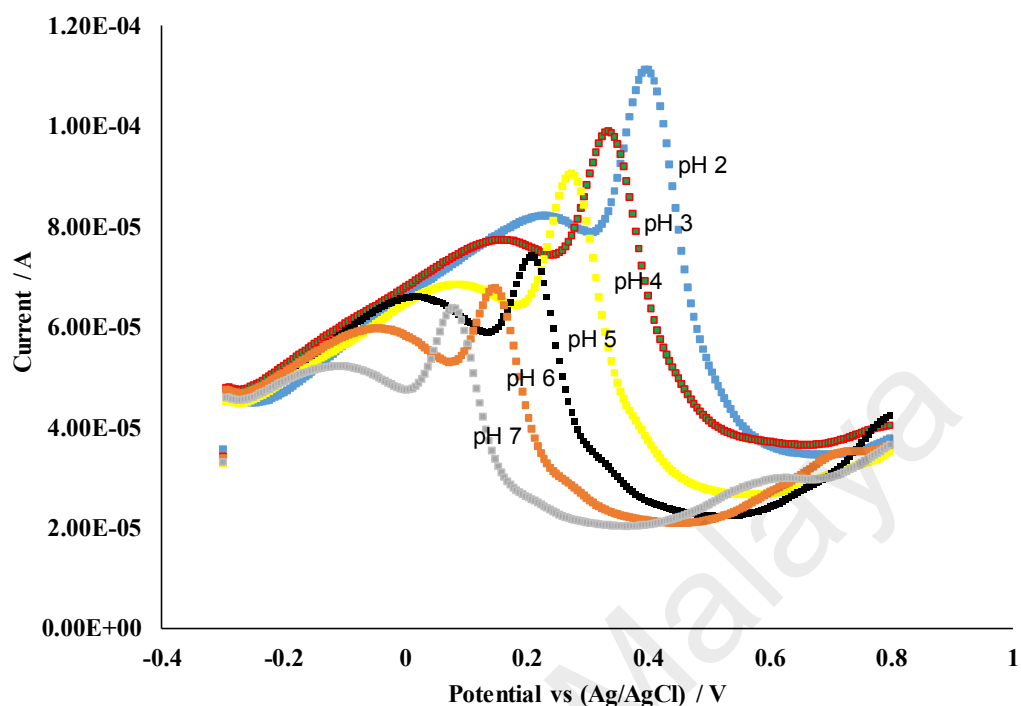


Figure 3.17: SWV of 6.0 µg mL⁻¹ myricetin measured at pH 2, pH 3, pH 4, pH 5, pH 6 and pH 7 in a 0.1 mol L⁻¹ Britton Robinson buffer.

A SWV method was used in the myricetin analysis. An Au–NPs/graphite prepared at 16th deposition cycle was used as the working electrode. Fig. 3.17 illustrates the SWV of myricetin at various pH values using the Au–NPs/graphite prepared at 16th deposition cycle. The peak potential of myricetin was shifted to less positive potential with increasing pH values. This shifting could be attributed by the difference in ratio between the protonated myricetin in the bulk solution to un-protonated species on electrode surface which is according to the Nernst's equation.

$$E = E_{ref} - \frac{RT}{nF} \text{Log} \frac{A}{AH} \quad (\text{eq. 6})$$

Whereby, the E , E_{ref} , R , T , n , F , A and AH corresponded to peak potential, reference potential, gas constant, temperature, number of electron transfer, Faraday's constant, unprotonated anti-oxidant and protonated anti-oxidant. Therefore, at a lower pH (e.g., pH

2), the concentration of protonated myricetin (AH) in the solution will be much greater because of excess proton from acidic condition. When $AH > A$ (unprotonated myricetin), the reaction quotient will be less than 1, as a result the peak potential shifted to a more positive potential following equation (6) (logarithm of $< 1 =$ negative value).

A graph of anodic peak potential against pH is plotted as shown in Fig. 3.18, resulting in a linear correlation between the anodic peak potential and pH with a linear regression and slope value of 0.9996 and 0.0639 V/pH, respectively. From the Nernst equation, the slope of potential (V) versus pH is equivalent to $0.0591 \text{ V}/n$, where n is equal to the number of electrons transfer. Therefore, this showed that a single electron and proton was transferred in the myricetin oxidation process, which could be ascribed to the pyrogallol group.

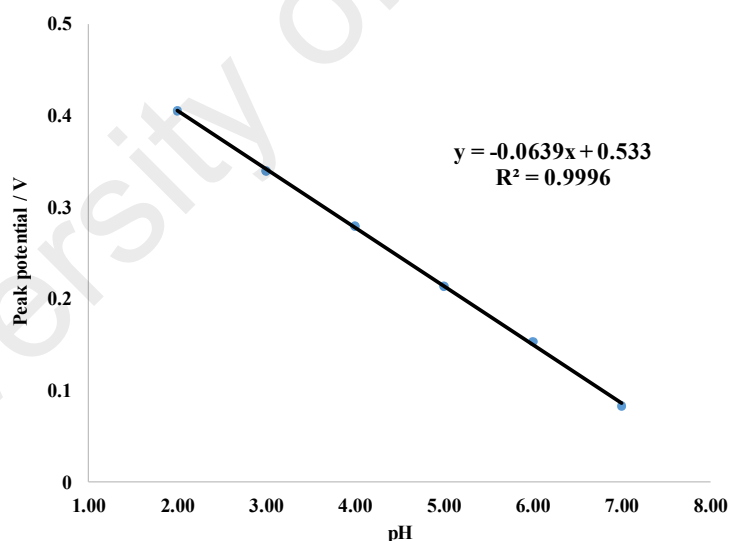


Figure 3.18: Correlation graph of myricetin anodic peak potential versus pH.

Fig. 3.19 illustrates the possible schematic reaction of the myricetin oxidation. The slope value is also in agreement with the result reported by Komorsky–Lovric & Novak (2013), in which the slope value obtained in their work was 0.06 V using a paraffin impregnated graphite rod. From Fig. 3.17, the myricetin peak current is highest at pH 2,

suggesting an optimum pH condition for the quantitative analysis of myricetin. This pH condition was selected for further studies of myricetin.

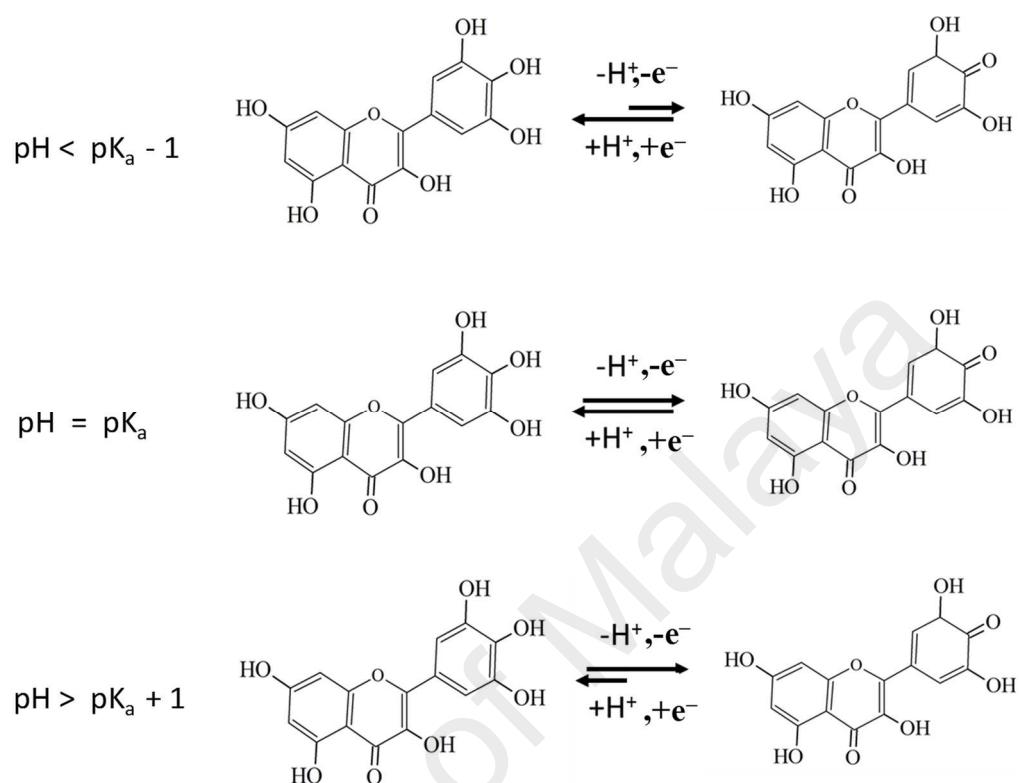


Figure 3.19: Schematic illustration of myricetin oxidation (deprotonation) and reduction (protonation) under different pH conditions, with pK_a referring to the dissociation constant of myricetin.

3.3.6.3 Quantitative determination of myricetin by SWV

Fig. 3.20 illustrates the SWV of myricetin at various concentrations with the myricetin anodic peak potential at 0.4251 V (versus Ag/AgCl, 3 M KCl). The peak area was observed to increase constantly with each concentration increment. The anodic peak potential has remained unchanged, without shifting to negative or positive potential suggesting the myricetin oxidation on Au-NPs/graphite surface is a mass diffusion controlled process. This attribute is important especially for quantitative analysis. From the anodic peak current measurement of each myricetin standard, a calibration curve of anodic peak current against myricetin concentration is plotted as shown in Fig. 6 (b). The

linear regression of the myricetin calibration curve using Au–NPs/graphite was greater than 0.99, with linearity ranged from 2.0 to 10.0 $\mu\text{g mL}^{-1}$.

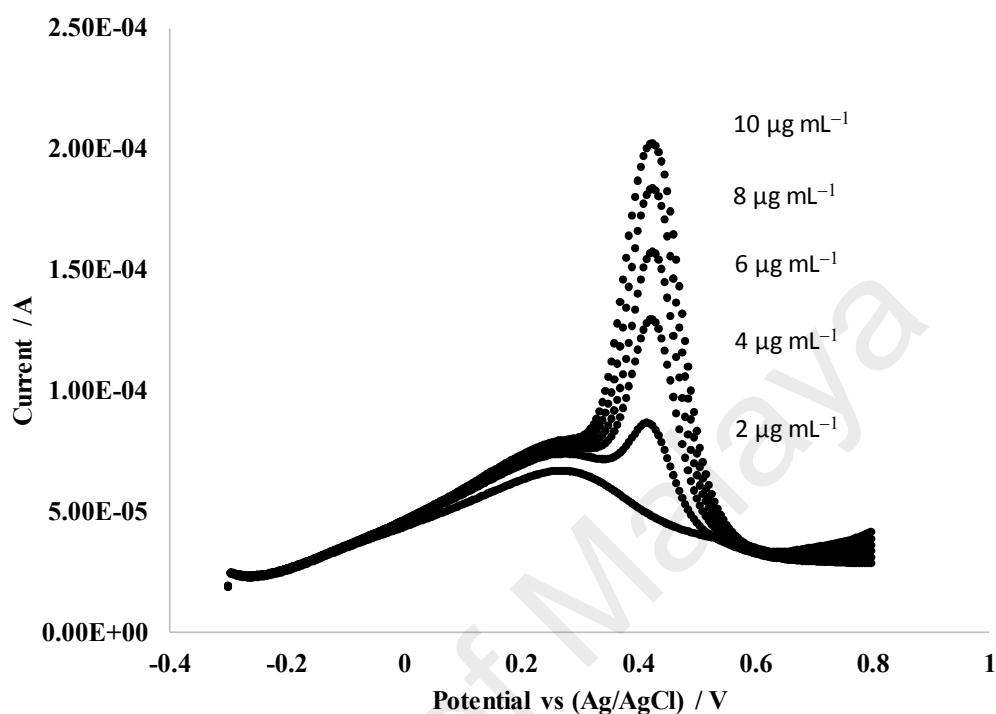


Figure 3.20: SWV of myricetin at blank, 2.0, 4.0, 6.0, 8.0 and 10.0 $\mu\text{g mL}^{-1}$ of myricetin standard.

To assess the performance of Au–NPs/graphite in myricetin analysis, a same experiment was repeated using bare graphite sensor. The calibration curves of bare graphite and Au–NPs/ graphite sensor were compared as shown in Fig. 3.21. The results suggested that Au–NPs/graphite electrode was more sensitive to myricetin with a higher response factor (slope = 1.6499×10^{-6} ampere/ $\mu\text{g mL}^{-1}$) of one magnitude when compared to the bare graphite electrode (slope = 4.5477×10^{-7} ampere/ $\mu\text{g mL}^{-1}$). A higher response factor is preferable as it allows a much higher signal current per concentration, hence a more sensitive detection. This is important especially for the detection of low myricetin concentration; for instance, at 2 $\mu\text{g mL}^{-1}$ standard, the response obtained using Au–NPs/graphite was 2.6161 ampere/ $\mu\text{g mL}^{-1}$, in contrast to bare graphite with the response at 0.5618 ampere/ $\mu\text{g mL}^{-1}$.

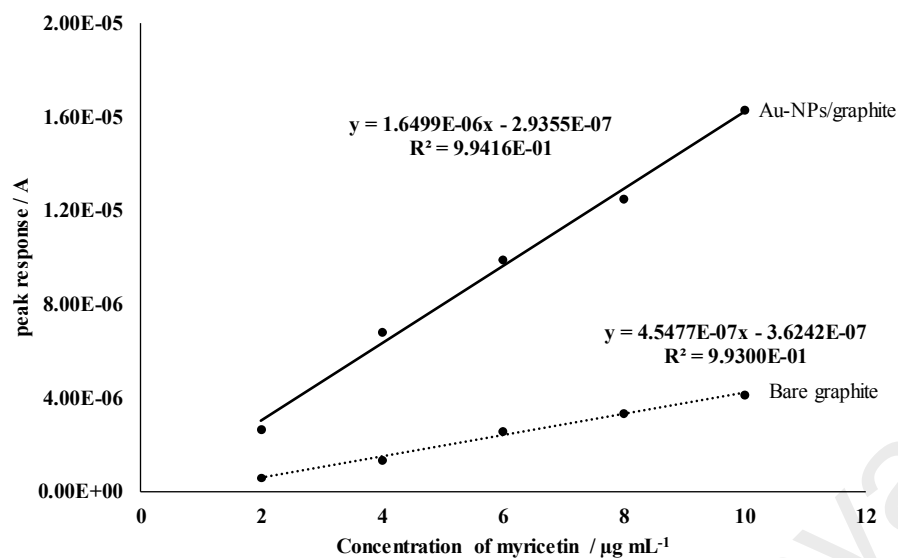


Figure 3.21: Calibration curve of peak response (current) versus concentration of myricetin.

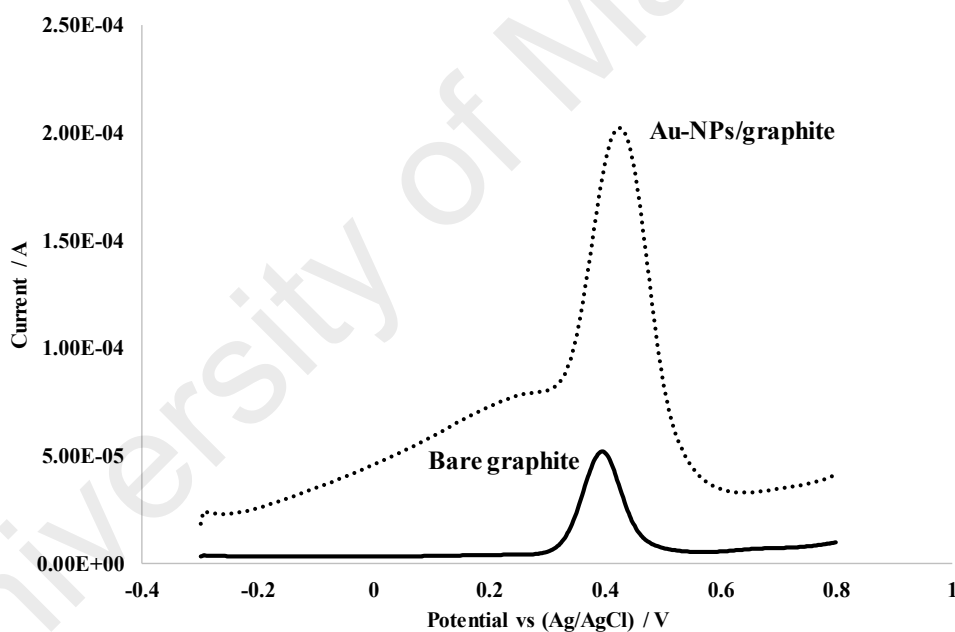


Figure 3.22: SWV of $10 \mu\text{g mL}^{-1}$ myricetin analysis using Au-NPs graphite prepared at 16th deposition cycle (dotted line) and bare graphite (solid line).

Fig. 3.22 illustrates the SWV of myricetin which was measured using bare graphite and Au-NPs/graphite working electrode. A comparison of both SWV, the peak current (ampere) of myricetin measured by Au-NPs/graphite electrode showed a 2.5-fold increase in the response as contrasted to that obtained using bare graphite electrode. This infers that with a gold nanoparticles modification on graphite surface, the electrochemical

properties of graphite have significantly improved. This was particularly attributed by the improved Eff A and the heterogeneous electron transfer rate.

3.3.6.4 Limit of detection (LOD) for myricetin detection in Britton Robinson buffer.

The limit of detection (LOD) of myricetin was determined by the serial dilution of a 1 ppm standard using Au-NPs/graphite, Fig. 3.23 illustrates the SWV of myricetin peak at concentrations of 0.2 to 1.0 $\mu\text{g mL}^{-1}$. The LOD of myricetin was found at 0.4 $\mu\text{g mL}^{-1}$, at concentration of 0.2 $\mu\text{g mL}^{-1}$ and below, the myricetin peak was not detectable.

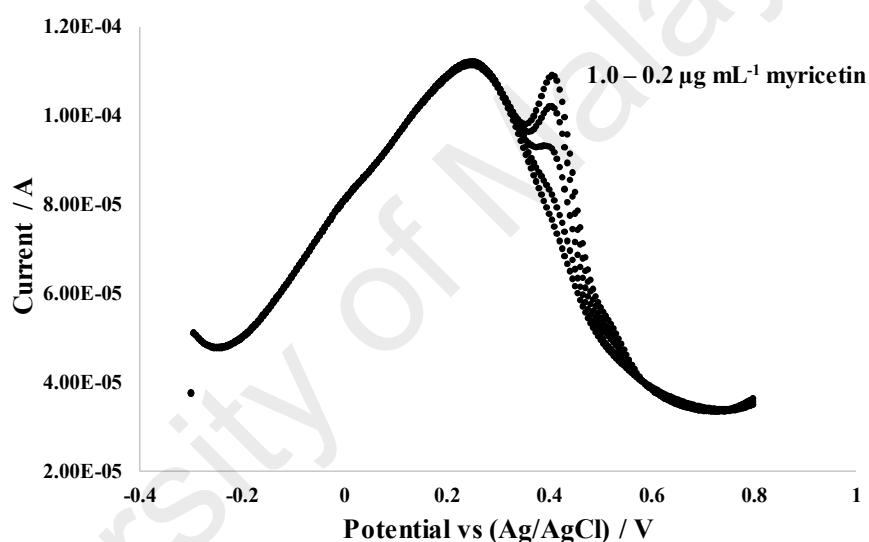


Figure 3.23: SWV of myricetin with concentration increment order correspond to 0.2, 0.4, 0.6, 0.8 and 1.0 $\mu\text{g mL}^{-1}$ in Britton Robinson buffer.

3.3.6.5 Analysis of myricetin in tap water samples

The developed SWV method was used for the analysis of myricetin in water. Myricetin is often found in tea, where the water is often used to extract the myricetin from the tea (Huang et al., 2010). An external calibration curve was used to quantify the amount of myricetin in the samples. The determination results were summarised in Table 3.6. An analysis of myricetin in spiked water sample (0.40 $\mu\text{g mL}^{-1}$) has shown that the percentage recovery was lower than 90.0%, but at a concentration of 0.60 $\mu\text{g mL}^{-1}$ and above, the recovery of myricetin was greater than 90.0%. The lower recovery of myricetin

in water samples could be due to the detection limit of the Au–NPs/graphite. This finding has shown that the developed Au–NPs/graphite sensor can be applied for the rapid analysis of anti-oxidants in food (beverages) samples such as tea, as the preparation method was simple and detection time was less than 3 min.

Table 3.6: Determination of myricetin in tap water samples using Au–NPs/graphite sensor.

No	Samples	Detected/ $\mu\text{g mL}^{-1}$	Recovery/%
1	0.40 $\mu\text{g mL}^{-1}$ myricetin spiked water	0.34	85.00
2	0.60 $\mu\text{g mL}^{-1}$ myricetin spiked water	0.55	91.67
3	0.80 $\mu\text{g mL}^{-1}$ myricetin spiked water	0.80	100.00
4	1.00 $\mu\text{g mL}^{-1}$ myricetin spiked water	1.07	107.00

3.4 Conclusion

In this chapter, a simple, green and cost effective procedure have been successfully devised for the fabrication of gold nanoparticles modified graphite electrode from a used alkaline AA battery. The Eff A, heterogeneous electron transfer rate, electrode overpotential and electron transfer resistance of the Au–NPs/graphite electrode were significantly improved when compared to its counterpart bare graphite electrode. It can be inferred that at 16th deposition cycle of 0.1 mM tetrachloroauric acid, the performance of the Au–NPs/graphite electrode have reached an optimum. Further electrode surface characterisation by FE–SEM, has evidenced that the gold nanoparticles sizes were measured at the range of 35–65 nm, and homogeneously distributed on the graphite electrode surface at 16th deposition cycles.

The fabricated Au–NPs/graphite electrode was also used for the determination of natural antioxidant myricetin. The CV experiment suggested that the myricetin exhibited a reversible redox process with anodic and cathodic peak potential corresponding to 0.448 and 0.3919 V, respectively, in which a single electron and proton transfer process is involved. The diffusion coefficient of the myricetin was calculated at $0.0975 \text{ cm}^2 \text{ s}^{-1}$. The optimum pH condition for myricetin was also investigated and pH 2. Besides, the anodic peak current was linear proportional to the concentration of myricetin in the range from 6.28×10^{-6} to $3.14 \times 10^{-5} \text{ mol L}^{-1}$ with a limit of detection of $1.26 \times 10^{-6} \text{ mol L}^{-1}$. Last but not least, a SWV method was successfully used for the determination of spiked myricetin in tap water samples. In short, the developed Au–NPs/graphite sensor from a used battery can be practically used as a rapid sensor or method for anti-oxidant analysis (myricetin) in beverages samples.

CHAPTER 4: ELECTROCHEMICAL MULTIPLEX ANALYSIS OF SYNTHETIC ANTI-OXIDANTS IN FOOD SAMPLES USING GOLD NANOPARTICLES MODIFIED GRAPHITE ELECTRODE

4.1 Introduction

Butylated hydroxyanisole (BHA), butylated hydroxytoluene (BHT), *tert*-butylhydroquinone (TBHQ), and propyl gallate (PG) are examples of common synthetic antioxidants (Brewer, 2011; Iverson, 1995; Tomášková et al., 2014). These are commonly used in food as preservative additive, which ensures the good quality and appearance, odour, and taste perception to the consumers. This has become a concern, especially with the rapid growth of the processed food market that requires a long and stable shelf life, therefore the use of synthetic anti-oxidant is unavoidable. Synthetic antioxidants are preferred to naturally occurring ones due to the polar nature of the latter, which limits their solubility, especially in oil- and fat-based products (Iverson, 1995). Moreover, synthetic antioxidants are more affordable in comparison with their natural counterparts (Brewer, 2011). According to the USFDA (Food Drug Administration, USA) regulations, the permissible levels of BHT or TBHQ in food (either alone or in combination with BHA) are limited to $200 \mu\text{g g}^{-1}$ (Brewer, 2011). On the other hand, the levels of BHA alone are limited to $2\text{--}1000 \mu\text{g g}^{-1}$. Safety assessment studies have shown that the use of BHA and BHT at high concentrations (above $3000 \mu\text{g g}^{-1}$) potentially promotes cancer proliferation in animals (Iverson, 1995; Williams et al., 1999; Chao et al., 2009). Hence, the determination and monitoring of these unavoidable additives in processed products are important for food safety. Various analytical procedures have been developed for the determination of these antioxidants, including high performance liquid chromatography (Li et al., 2014; Wang et al., 2014), Fourier transform infrared spectroscopy (Goulart et al., 2014), and gas chromatography methods (Wang et al., 2014). Although these methods are sensitive and selective, they are not suitable for on-field analysis and require

expensive investment in instruments. The alternative electrochemical method is more simple, rapid, and sensitive. Moreover, this method can be adapted to novel technologies, such as screen-printed electrodes (SPEs), which can be useful for portable real-time on-site analysis.

Several electrochemical methods for the determination of BHA, BHT, and TBHQ have been reported. Goulart et al. (2014) proposed a glassy carbon electrode for the determination of TBHQ in soybean biodiesel (Goulart et al., 2014), while Wang et al. (2015) reported the determination of BHA using a highly selective and sensitive sensor based on a gold nanoparticle-polyvinylpyrrolidone (PVP)-graphene nanocomposite electrode (Wang et al., 2015). Both studies have successfully demonstrated the possibility of sensitive detection of synthetic antioxidants. However, these methods are limited to the determination of a single compound and are therefore, not applicable in real food analysis, since the preservative used could be a combination of any of these antioxidants (BHA, BHT, and TBHQ). Hence, the multiplex detection of synthetic antioxidants is preferable for rapid and hassle-free analysis without the need to exchange different working electrodes or involve tedious sample preparation procedures.

In this chapter, a gold nanoparticle/graphite (Au-NP/graphite) electrode was utilised for multiplex detection of BHA, BHT, and TBHQ in food samples using a linear sweep voltammetry (LSV) technique, which has not been reported before. The proposed method presents a simple and green procedure that can be used to solve the multiplex detection of the BHA, BHT and TBHQ in food samples using a single analysis step, which so far has not worked successfully using graphite electrode. On the other hand, CV was also used to study the electrochemical properties of these antioxidants, such as their efficacy and electron transfer ratio, which are important for understanding the oxidation mechanism of those studied synthetic antioxidants.

4.2 Materials and methods

4.2.1 Chemicals and apparatus

Standard stock solutions of BHT, BHA, and TBHQ ($1000 \mu\text{g mL}^{-1}$) were prepared in acetonitrile. A 0.04 mol L^{-1} Britton-Robinson (BR) buffer was prepared by mixing equimolar amounts of 0.04 mol L^{-1} acetic acid, boric acid, and phosphoric acid and adjusted to pH 2 using 1 mol L^{-1} sodium hydroxide. All chemicals used for the preparation of standards and buffers were of analytical grade and were purchased from Merck (Darmstadt, Germany). Tetrachloroauric acid (1 mmol L^{-1} , HAuCl_4) was prepared from the powder obtained from Sigma Aldrich (Steinheim, Germany) and was dissolved in 0.1 mol L^{-1} sodium nitrate solution. The acetonitrile used for the mobile phase in chromatographic analysis was purchased from Merck (Darmstadt, Germany). A 0.005 mol L^{-1} solution of sodium dodecyl sulphate (SDS) was prepared from the pure solid purchased from Merck (Darmstadt, Germany). All solutions were prepared using $18.2 \text{ M}\Omega$ ultrapure water from Millipore.

Electrochemical measurements were performed using a Metrohm potentiostat system model PG Stat 202 (Utrecht, Netherlands) interfaced to NOVA software. A three-electrode system was used for analysis, comprising an Ag/AgCl (3 M KCl) reference electrode and a platinum rod counter electrode. These electrodes were purchased from BASi (USA). The determination of synthetic antioxidants by liquid chromatography analysis was conducted using a WATERS ultra-performance liquid chromatography (UPLC) system (USA) equipped with a photodiode array detector (PDA), quaternary pumps, and an ethylene bridged hybrid (BEH) octadecylsiloxane C18 column ($50 \text{ mm} \times 2.1 \text{ mm}$). Images of the electrode surface were captured with a Hitachi field emission SEM (SU8220, Japan).

4.2.2 Preparation of the Au-NP/graphite working electrode

The graphite rod was obtained from a used alkaline AA battery, and the Au-NP/graphite working electrode was fabricated according to the procedures as described in Chapter 3 of the thesis. Sixteen deposition cycles were used to prepare the above electrode, which was activated by running a full CV scan in 0.5 mol L⁻¹ sulphuric acid. The surface of the activated electrode was subsequently characterised by scanning electron microscopy (SEM) at 30 keV under high vacuum.

4.2.3 Individual CV analysis of BHA, BHT, and TBHQ

Individual CV analysis of BHA, BHT, and TBHQ was performed at an applied potential between -0.4 and 1.2 V. The effect of scan rates (0.1 to 1.0 V s⁻¹) on the individual BHA, BHT, and TBHQ oxidation currents (I_{pa}) was studied, and the heterogeneous electron transfer rate was calculated based on Laviron's equation. The individual pH responses of BHA, BHT, and TBHQ (pH 1 to 7) were also studied by using CV method at a scan rate of 0.1 V s⁻¹. All CV experiments were performed using 0.04 mol L⁻¹ Britton-Robinson buffers, which was adjusted to the required pH by 1.0 mol L⁻¹ sodium hydroxide.

4.2.4 Multiplex detection of TBHQ, BHA, and BHT using LSV analysis

An LSV method was used for the simultaneous analysis of a mixed standard containing BHA, BHT, and TBHQ (40 µg mL⁻¹). (Note: this concentration was selected for comparing the Au-NP/graphite electrode to bare graphite. At concentrations below 40 µg mL⁻¹, TBHQ was not detectable with the bare graphite electrode). The applied potential ranged from 0 to 1.2 V, with a potential step of 0.0024 V and a scan rate of 0.1 V s⁻¹ was used in this study. The linearity range and calibration curves were determined using six standards with concentrations ranging between 5 and 120 µg mL⁻¹. The limit of detection (LOD) was determined by serial dilution of a 1 µg mL⁻¹ standard until reaching a

concentration at which the antioxidant was undetectable. The limit of quantification (LOQ) was calculated as five-fold LOD signal-to-noise standard deviation. All analyses were performed using a de-aerated supporting electrolyte mixture (0.04 mol L⁻¹ Britton-Robinson buffer: acetonitrile, 80:20 v/v). The detection sensitivity was determined from the slope of the calibration plot.

4.2.5 Optimisation of sodium dodecyl sulphate solution

The effect of sodium dodecyl sulphate (SDS) concentration in multiplex detection of BHA, BHT and TBHQ was investigated. A 40 µg mL⁻¹ mixed TBHQ, BHA and BHT standard was prepared using 0.04 mol L⁻¹ Britton-Robinson buffer (pH 2); subsequently, 0.06 mmol L⁻¹ of SDS was added into the solution and LSV was measured according to the procedure described in subsection 4.2.4. The experiments were repeated using different concentration of SDS at 0.12, 0.20, 0.26 and 0.33 mmol L⁻¹.

4.2.6 LSV analysis of food samples

A total of three different food sample matrices were selected for this study, including oil-based (sunflower oil), fat-based (ghee), and emulsion-based (salad dressing). These products were purchased from local supermarkets in Kuala Lumpur.

Some simple preparation steps were needed, since the oil-based food samples do not allow for electron flow, and no current peak could be detected in the LSV analysis. Simple dilution steps were required for certain samples, such as solid fat (e.g., ghee). The food sample (1 g) was dissolved in 10 mL of the mixed supporting electrolyte (0.04 mol L⁻¹ Britton-Robinson buffer: acetonitrile, 80:20 v/v), vortexed for 1 min, and centrifuged for 5 min at 2600 g rotational centrifugation force (RCF). An aliquot of the upper layer extract (5 mL) was diluted to 15 mL using the same supporting electrolyte, which was pre-adjusted to pH 2 and spiked with 600 µL of 0.005 mol L⁻¹ sodium dodecyl sulphate. A standard addition LSV method (analytical condition as described in Section 4.2.4) was

used for the quantitative analysis of synthetic antioxidants. A recovery study was conducted for all food samples by spiking with a known antioxidant standard at three concentration levels: low, medium, and high (100, 200, and 300 $\mu\text{g mL}^{-1}$, respectively).

4.2.7 Method validation using UPLC-PDA analysis

The food sample (1 g) was dissolved in 10 mL of an acetonitrile: water mixture (80:20 v/v), vortexed for 1 min, and centrifuged at 2600 g (RCF) for 5 min. The upper layer was filtered through a 0.22 μm nylon syringe filter, and 2- μL aliquots were injected into the UPLC instrument. A two-solvent system was used, with the A and B mobile phases corresponding to methanol (Merck) and ultrapure water (Millipore). A gradient elution mode was employed, with the methanol ratio initially set at 5% and held for 0.3 min, then ramped to 95% in 6 min and maintained for 2 min. After 8.3 min, the methanol/water ratio was adjusted back to its initial value and equilibrated for 2 min before the next injection. A constant flow rate of 0.35 mL min^{-1} was used throughout the gradient elution, and the resulting chromatogram was extracted at 280 nm. A recovery study was conducted for all food samples by spiking with a known antioxidant standard at three concentration levels: low, medium and high (100, 200, and 300 $\mu\text{g mL}^{-1}$, respectively). The analytical performance (e.g., sensitivity, linearity, LOD, and LOQ) of the UPLC-PDA method was carefully studied and compared to that of the newly developed electrochemical sensor.

4.2.8 Selectivity and stability study of Au-NP/graphite sensor

The stability of the developed electrode was evaluated by testing the analytical performance of the sensor at different intervals (1, 3, 7, 14, 21 days) at room temperature (25°C) and elevated temperature (45°C). A mixed solution of 60 $\mu\text{g mL}^{-1}$ TBHQ, BHA and BHT was used as the standard to monitor the performance of the sensor. The

percentage peak response (current) was calculated for each stability measurement that is relative to its initial day.

The selectivity of Au–NPs/graphite sensor towards BHA, BHT and TBHQ detection were investigated using other potential antioxidants (interferences) possibly present in real food samples, such as vitamins, phenolic acids, and food additives. These interferences include tocopherol, ascorbic acid, quinic acid, benzoic acid, phenoxyethanol, niacinamide, glycerine, sodium, chloride, potassium, sulphate, acetate and magnesium. A mixed solution of 40 $\mu\text{g mL}^{-1}$ TBHQ, BHA and BHT was prepared as the standard, in which the peak current response (ampere) was firstly measured. Subsequently, 40 $\mu\text{g mL}^{-1}$ of the interference was added into the standard and the current response was measured again.

4.3 Results and discussion

4.3.1 Enhancement of individual antioxidant electrochemical characteristics using the Au–NP/graphite electrode

The electrochemical characteristics of BHA, BHT, and TBHQ were studied using CV technique, with the resulting voltammograms of each individual TBHQ, BHA, and BHT standard (40 $\mu\text{g mL}^{-1}$) obtained as illustrated in Fig. 4.1, 4.2 and 4.3, respectively. Single anodic peaks were detected for BHT (anodic peak potential, (E_{pa}) = 0.79 \pm 0.01 V), BHA (E_{pa} = 0.50 \pm 0.01 V), and TBHQ (E_{pa} = 0.28 \pm 0.01 V) when the Au–NP/graphite working electrode was used, suggesting the presence of a single oxidation site. Antioxidants with an E_{pa} close to 0 V possess a greater electron–donating ability (i.e., greater antioxidant potential) than the ones with higher E_{pa} values (Samra et al., 2011; Gil & Couto, 2013). When the Au–NP/graphite electrode was used, the E_{pa} of TBHQ shifted closer to 0 V compared to BHA and BHT values, and the antioxidant potential order could be expressed as TBHQ > BHA > BHT.

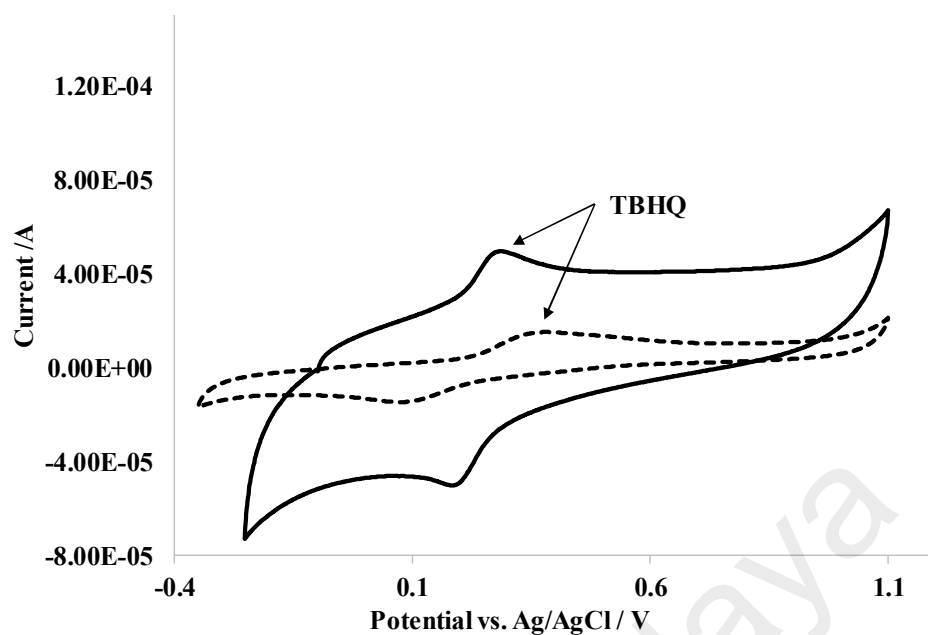


Figure 4.1: CV of $40 \mu\text{g mL}^{-1}$ TBHQ obtained using Au-NP/graphite electrode (solid line) and bare graphite (dotted line).

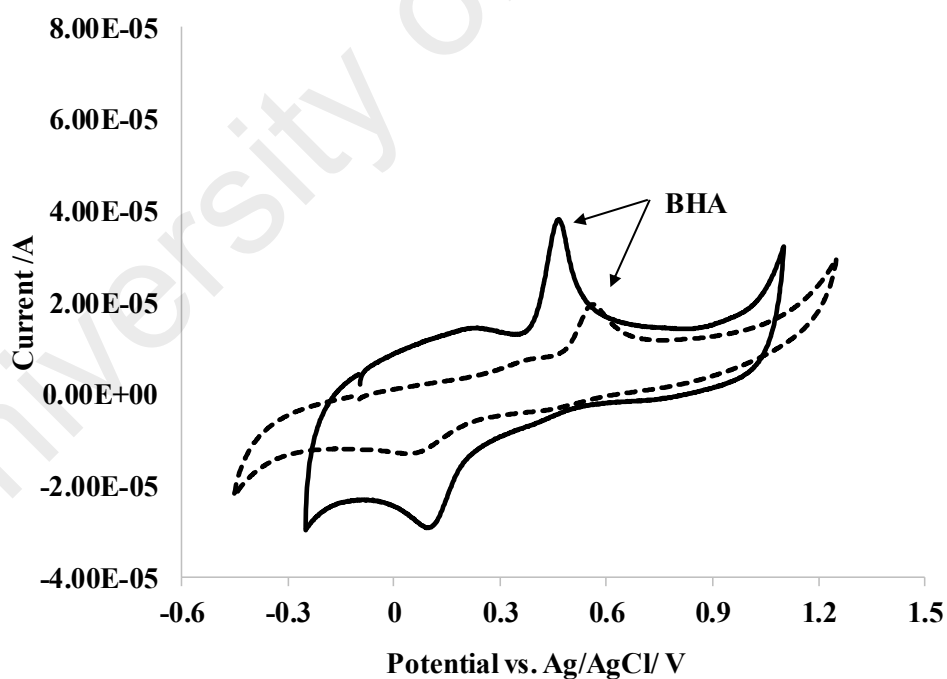


Figure 4.2: CV of $40 \mu\text{g mL}^{-1}$ BHA obtained using Au-NP/graphite electrode (solid line) and bare graphite (dotted line).

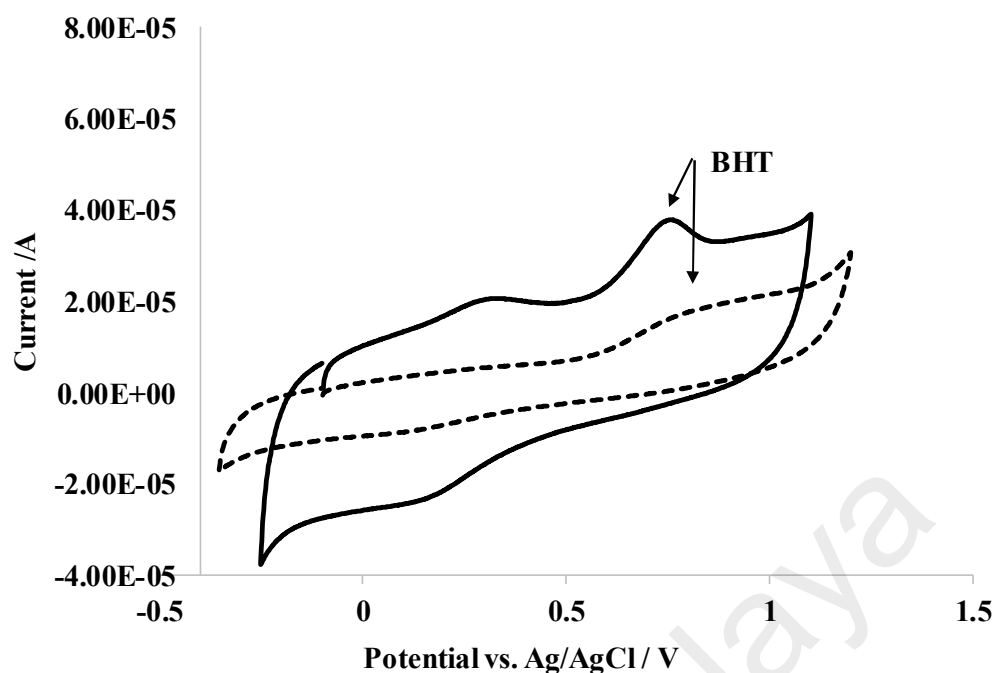


Figure 4.3: CV of 40 $\mu\text{g mL}^{-1}$ BHT obtained using Au-NP/graphite electrode (solid line) and bare graphite (dotted line).

Fig. 4.1 and 4.2 show that a single cathodic peak was detected for TBHQ and BHA when the Au-NP/graphite electrode was used, with the cathodic potential (E_{pc}) being equal to 0.19 and 0.20 V, respectively. This suggests that both TBHQ and BHA exhibit redox reversibility. CV analysis using the bare graphite electrode revealed similar reversibility for TBHQ and BHA. No significant cathodic peak was detected for BHT, although Fig. 4.3 shows a weak cathodic peak at a potential of 0.16 V. However, this peak was also found in the blank control sample that could be due to surface oxide such as reduction of COOH functional groups.

To assess the electron transfer rate of the Au-NP/graphite composite, a series of CV analyses at various scan rates were performed, and individual BHA, BHT, and TBHQ heterogeneous electron transfer rates (k_s) were calculated using Laviron's equation as described in Chapter 3 of the thesis and the calculated results were summarised in Table 4.1. BHA exhibited the highest k_s of $2.11 \pm 0.05 \text{ s}^{-1}$, followed by TBHQ ($1.95 \pm 0.04 \text{ s}^{-1}$) and BHT ($0.72 \pm 0.01 \text{ s}^{-1}$). Fig. 4.4 illustrates the cyclic voltammogram of TBHQ, BHA

and BHT at various scan rates that were used for k_s calculation. Compared to bare graphite, the k_s values of BHA and TBHQ were improved 1.3–fold when the Au-NP/graphite electrode was used. This improvement could be explained by the electrocatalytic effect of gold nanoparticles on the graphite surface. No comparison of BHT k_s values was possible for the bare graphite electrode, due to the insignificant anodic peak of this antioxidant at increasing scan rates. The E_{pa} was difficult to integrate when running at higher scan rates, as the peak shifted towards more positive potentials, and eventually the anodic peak was not detectable. Hence, the plot of peak potential vs. logarithm of scan rate was not linear and the k_s was not able to be determined.

Table 4.1: Electrochemical characterisation of individual BHA, BHT, and TBHQ that was performed using Au–NP/graphite and bare graphite electrodes.

Analyte	Electrode	* k_s / s^{-1}	**Slope / mV pH ⁻¹
BHT	Au–NPs/graphite	0.72 ± 0.01	-36.31
BHA	Au–NPs/graphite	2.11 ± 0.05	-39.41
TBHQ	Au–NPs/graphite	1.95 ± 0.04	-61.49
BHT	Bare graphite	–	–
BHA	Bare graphite	1.69 ± 0.05	-40.99
TBHQ	Bare graphite	1.53 ± 0.08	-52.87

[†] Results based on three replicate analyses

* Heterogeneous electron transfer rate (k_s) calculated using Laviron's equation

** Slope of a plot of peak potential against pH (1–7)

On the other hand, the bare graphite electrode overpotential for TBHQ, BHA, and BHT detection was obviously improved by modification with gold nanoparticles. Fig 4.1, 4.2, and 4.3 show the CV voltammograms of TBHQ, BHA, and BHT, respectively, where a comparison made between an Au–NP/graphite versus bare graphite electrode. The antioxidant anodic peaks were shifted towards less positive potential (0.366 to 0.278 V for TBHQ, 0.559 to 0.503 V for BHA, and 0.791 to 0.747 V for BHT) when using Au–NP/graphite instead of bare graphite, providing an overpotential improvement of 88,

56, and 44 mV, respectively. This phenomenon has also improved the detection response (current) by 9.96 μA of the BHT anodic peak (E_{pa} at 0.747 ± 0.009 V), which was only weakly detectable by the bare graphite electrode.

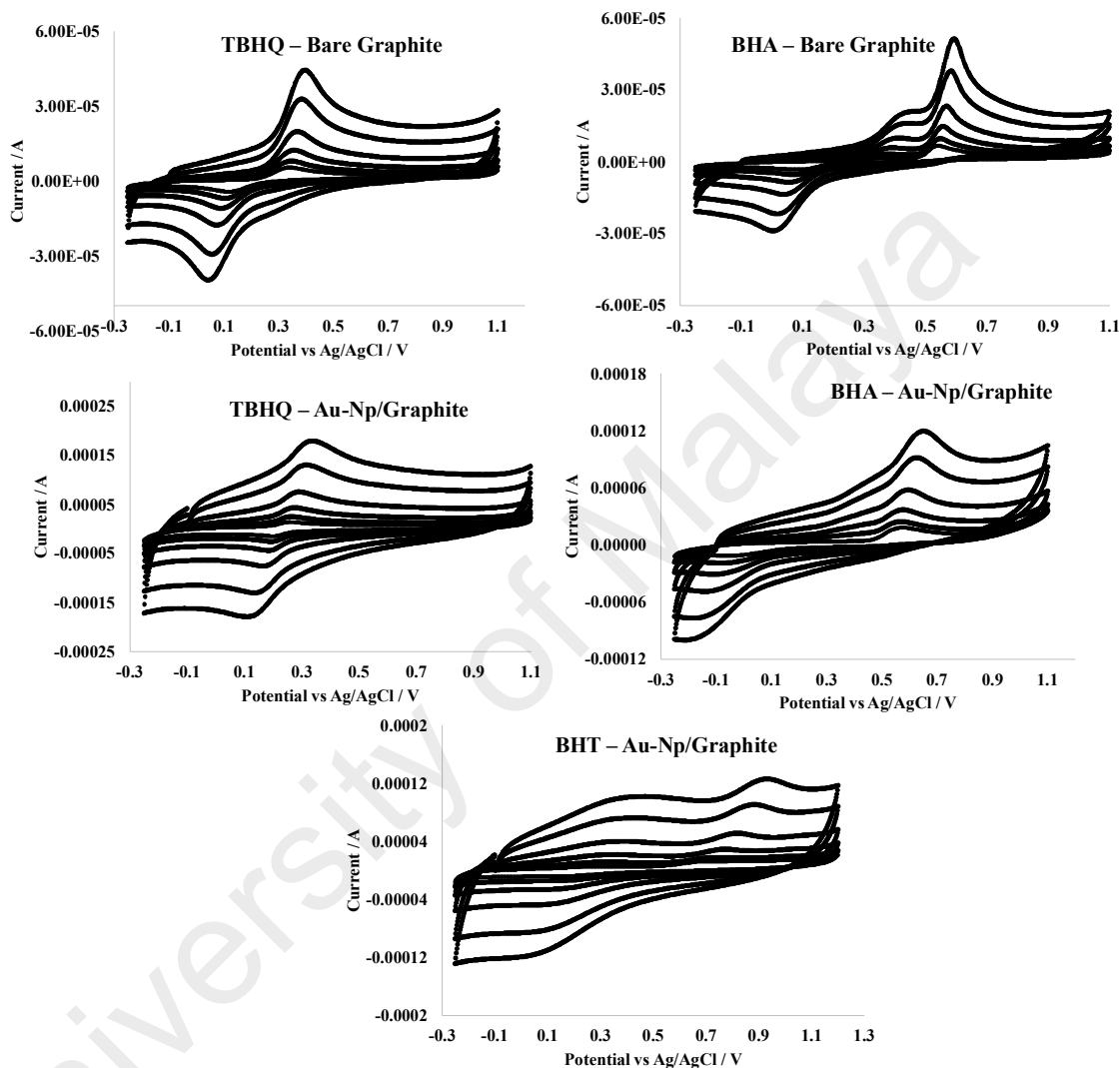


Figure 4.4: CV of TBHQ, BHA and BHT that perform at various scan rates (0.05, 0.1, 0.2, 0.4, 0.8 and 1.2 V s^{-1}) using bare graphite and Au-NP/graphite sensor.

Fig. 4.5 shows a plot of I_{pa} vs. the square root of scan rate for the Au-NP/graphite electrode. It can be seen that the anodic peak current of TBHQ, BHT, and BHA is linearly correlated to the square root of scan rate, suggesting that oxidation at the electrode interface is diffusion-controlled. Hence, quantitative analysis of TBHQ, BHA, and BHT using the fabricated Au-NPs/graphite electrode is possible.

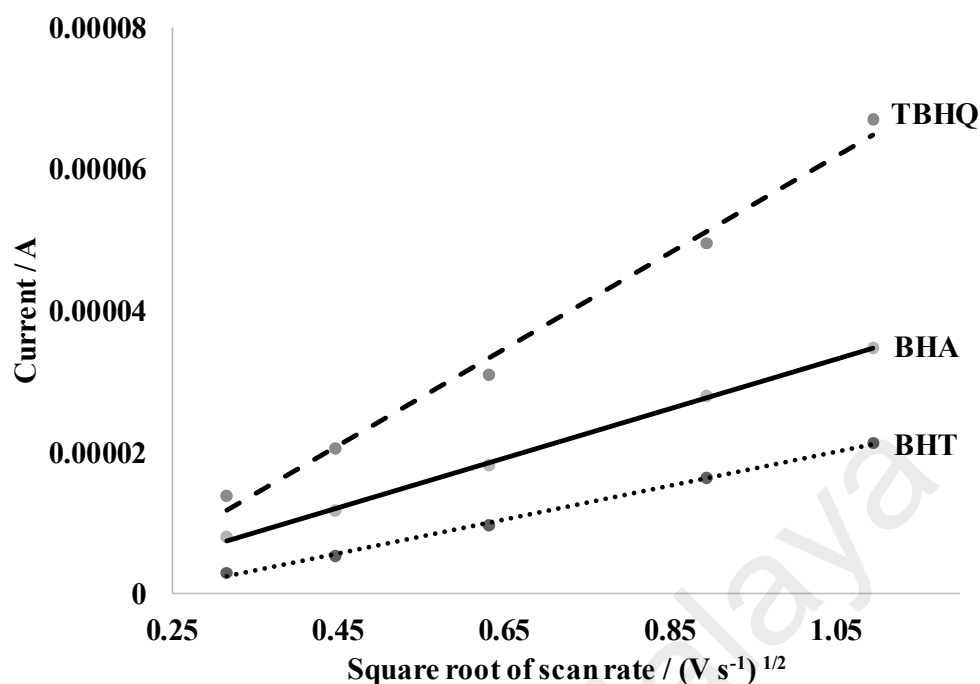


Figure 4.5: Linear correlation plot of individual TBHQ, BHA, and BHT anodic peak current (I_{pa}) against the square root of scan rate that was performed using Au-NP/graphite sensor.

4.3.2 Morphology of the Au-NP/graphite working electrode

Fig. 4.6 (a) and (b) show the SEM images of the fabricated Au-NP/graphite electrode surface. Image (a) proves that the gold nanoparticles are homogeneously deposited on the graphite surface, which is important to prevent the appearance of bare (uncovered) areas, since two different sites (with and without deposited Au NPs) could exhibit different electrochemical properties, such as electron transfer rates and surface areas.

SEM imaging showed that the gold nanoparticles were 80 to 120 nm in size and had a spherical shape, with the latter possibly contributing to expansion of the electrode surface area. This was further confirmed with a CV experiment conducted, where the Eff A of the Au-NP/graphite electrode was calculated using the Randles-Sevchik equation. The results showed a four-fold expansion of the Au-NP/graphite electrode surface area as compared to the bare graphite electrode.

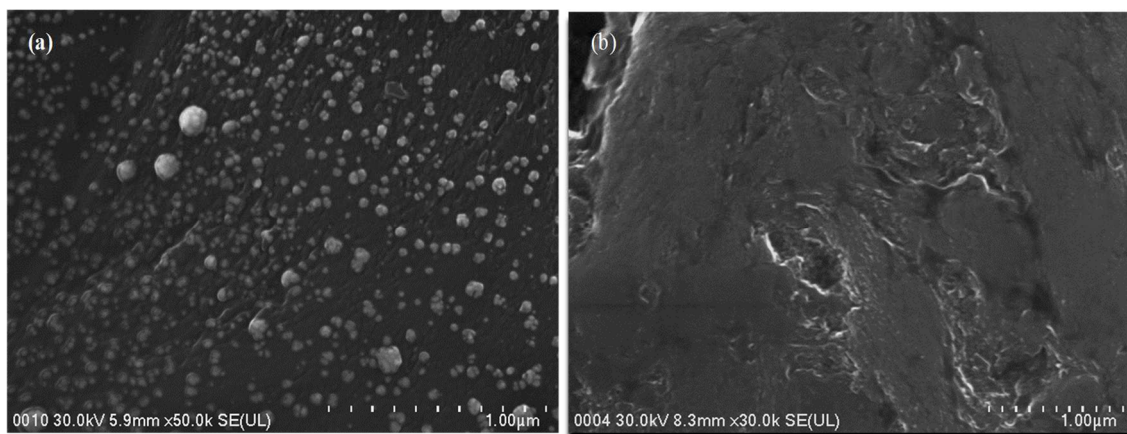


Figure 4.6: SEM images of (a) Au–NP/graphite electrode surface and (b) bare graphite at 35000 magnifications.

The significant improvement of the E_{eff} and k_s values of the Au–NP/graphite electrode has enhanced its response to antioxidants analyses, as evidenced in Fig. 4.1, 4.2 and 4.3. The I_{pa} values of BHA (1.88×10^{-5} A), TBHQ (1.85×10^{-5} A), and BHT (5.57×10^{-6} A) for the newly developed nanocomposite electrode were found to have increased two–fold as compared to bare graphite electrode (TBHQ = 7.83×10^{-6} A, BHA = 9.42×10^{-6} A, BHT = 2.69×10^{-6} A).

4.3.3 Effect of pH on the electrochemical characteristics of individual BHA, BHT, and TBHQ investigated by CV

According to the Nernst equation, the slope of the peak potential versus pH plot should correspond to $59.16 \text{ mV pH}^{-1}/n$, where n is the number of electrons involved in the oxidation process. Fig. 4.7 illustrates the plot of oxidation peak potential (E_{pa}) versus pH for individual BHT, BHA, and TBHQ, with the slopes being equal to 36.31, 39.41, and 61.49 mV pH^{-1} , respectively.

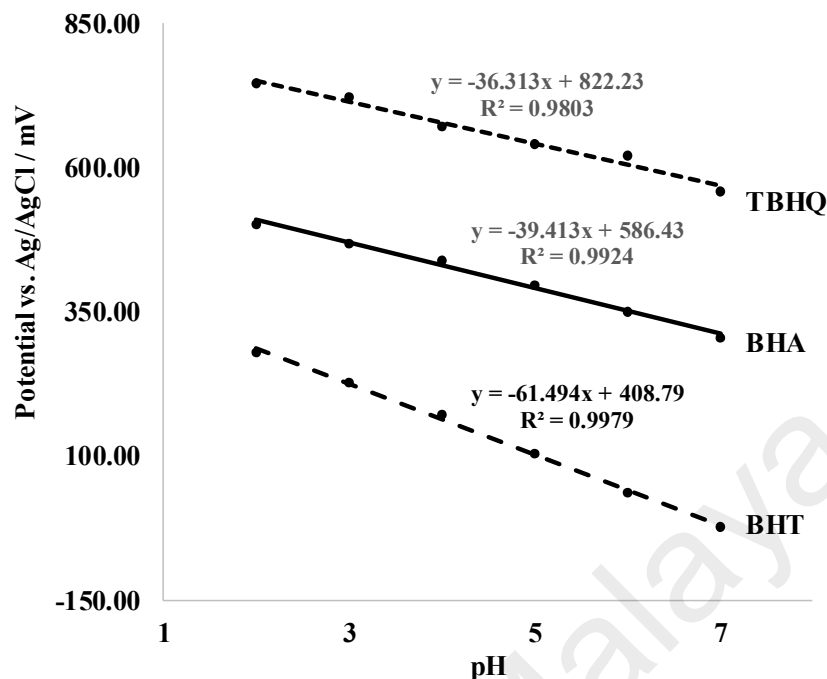


Figure 4.7: Linear correlation graph of individual BHA, BHT, and TBHQ anodic peak potential (mV) versus pH. The experiment was performed using Au–NP/graphite electrode.

The obtained values can be used to estimate the ratio of electrons to protons transferred in the oxidation process. The slopes of both BHT and BHA are approximately half of 59.16 mV pH^{-1} , suggesting two-electron single-proton transfer (Barsan et al., 2015). For TBHQ, the slope value (61.49 mV pH^{-1}) obtained was found close to 59.16 mV pH^{-1} , indicating a single-electron single-proton transfer. Based on the electron/proton transfer ratio, a possible mechanism for BHT, BHA, and TBHQ oxidation on the Au–NP/graphite electrode surface is proposed and shown in Fig. 4.8. Both BHA and BHT exhibit a similar oxidation mechanism, involving a single-proton two-electron transfer at the hydroxyl groups. Since TBHQ possesses two hydroxyl groups, two electrons and two protons are involved in the oxidation process.

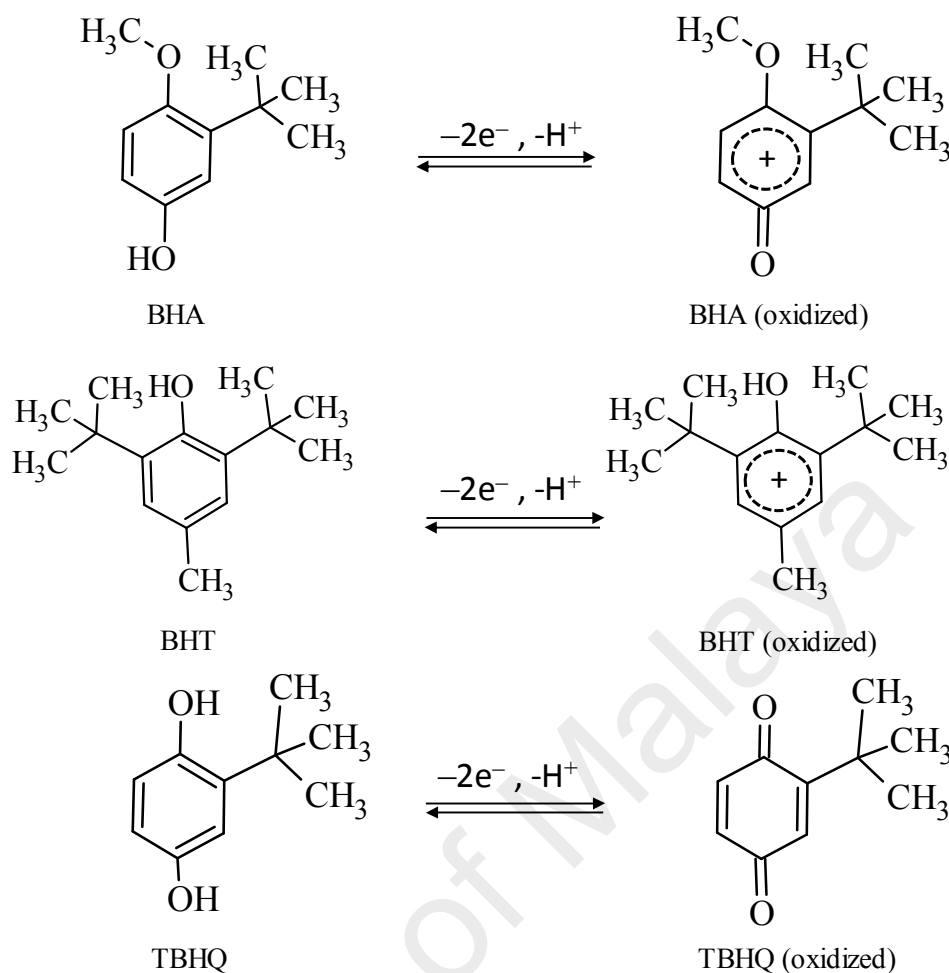


Figure 4.8: Possible mechanism of BHA, BHT and TBHQ oxidation on the Au-NP/graphite electrode surface.

Fig. 4.9 illustrates the individual dependence of BHA, BHT, and TBHQ ($40 \mu\text{g mL}^{-1}$ standard) oxidation currents under different pH conditions. BHT exhibited the lowest I_{pa} among the three antioxidants at all pH values, being less susceptible to oxidation. Therefore, this could be a limiting factor for the simultaneous detection of the above-mentioned antioxidants. At pH 2, the I_{pa} was most optimised for both BHA and BHT. Despite BHT exhibiting the highest I_{pa} at pH 7, this value was not selected due to the lowest I_{pa} values exhibited by BHA and TBHQ (response reduction of 30%). Besides, the BHT peak (based on CV) was found widened and partly interfered with the BHA peak at pH 7. To enable multiplex detection of the three synthetic antioxidants, pH 2 was selected and used in further studies.

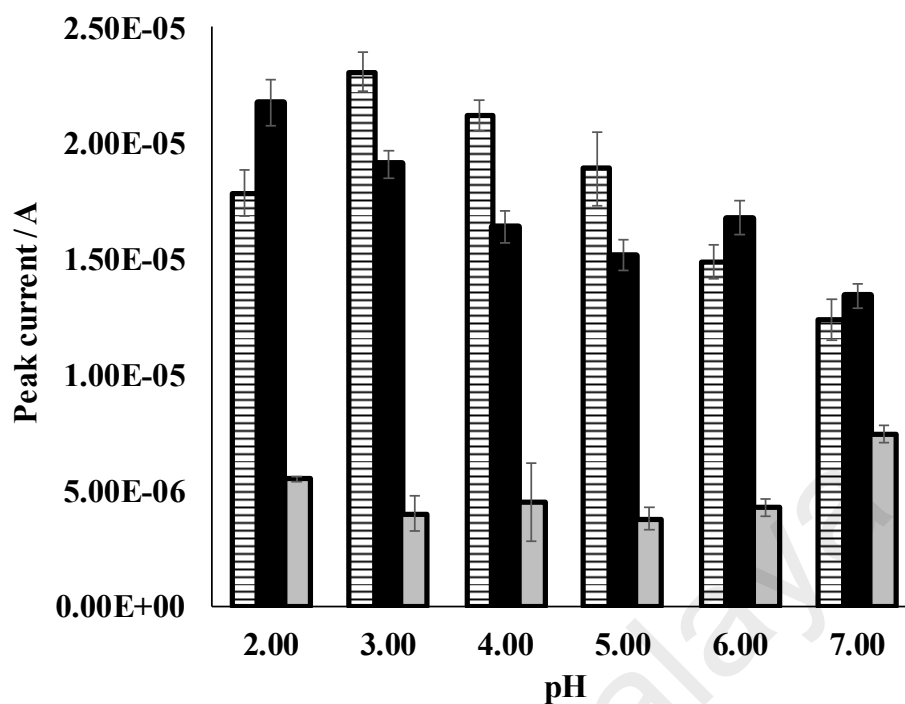


Figure 4.9: Comparison of the anodic peak current of TBHQ (striped), BHA (black), and BHT (grey) at pH values of 2–7.

4.3.4 Simultaneous determination of BHA, BHT, and TBHQ using LSV

LSV was used for the simultaneous detection of BHA, BHT, and TBHQ in a mixed standard ($40 \mu\text{g mL}^{-1}$) using a Britton-Robinson buffer (0.04 mol L^{-1}) at pH 2. Fig. 4.10 illustrates the LSV voltammogram for the multiplex detection of three synthetic antioxidants using the newly developed Au-NP/graphite electrochemical sensor. The peak potentials (E_{pa}) obtained for TBHQ, BHA and BHT were corresponded to 0.34, 0.54, and 0.74 V, respectively.

As compared to the individual CV scan using the same Au-NPs/graphite electrode (Fig. 4.1, 4.2 and 4.3), these anodic peaks recorded for each individual antioxidant was found shifted towards a more positive potential by 0.04 V, and the peaks are still well separated from each other. A comparison of the LSV voltammograms (for multiplex detection) recorded between Au-NP/graphite and bare graphite electrodes. The results showed that the overpotentials of TBHQ, BHA, and BHT peaks were improved, since the

peaks shifted towards less positive potential when Au–NP/graphite electrode was used. The BHT anodic peak showed a significant shift from 0.86 to 0.72 V; BHA (0.59 to 0.54 V) and TBHQ (0.42 to 0.34 V). All anodic peaks were negatively shifted from 0.05 V to 0.14 V. This exciting finding again showed that the graphite electrode overpotential was significantly improved by modification with gold nanoparticles.

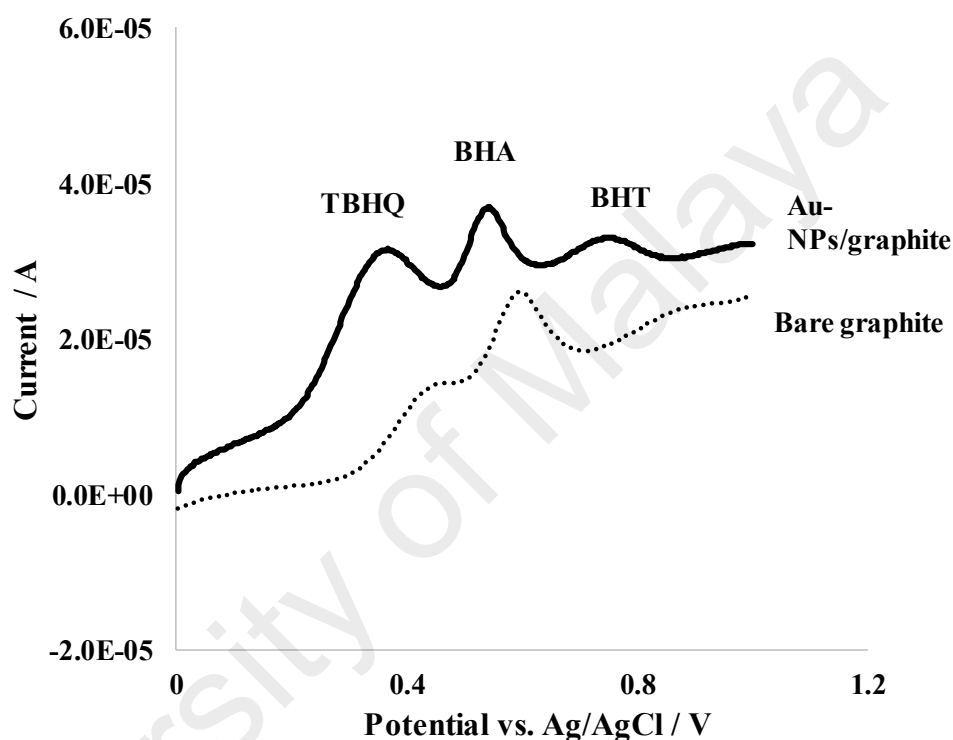


Figure 4.10: LSV voltammograms obtained for simultaneous determination of TBHQ, BHA, and BHT performed using Au–NPs/graphite electrode and bare graphite electrode.

The effect of the scan rate on the I_{pa} was studied to optimise the LSV method. Fig. 4.11 shows a linear sweep voltammogram of a mixed BHA, BHT, and TBHQ standard recorded at various scan rates. At 0.1 V s^{-1} , the antioxidant peaks were well separated; however, at a scan rate of 0.4 V s^{-1} and above, the TBHQ anodic peak was positively shifted and eventually merged with the adjacent BHA anodic peak, whereas the BHT peak was moved aside without interfering with BHA. The anodic peak was found shifted towards a more positive potential with the increment of scan rate. Such behaviour

indicates possibly a EC (electron–chemical) mechanism, in which the process involving an electron transfer process first, and subsequently followed by a chemical reaction (proton or methyl groups transfer) on the electrode surface (Abdel-Hamid & Newair, 2011; Masek et al., 2014). As a result, it limits the diffusion potential as a function of increasing scan rate, with the chemical transfer process as the limiting factor. Based on these results, an optimum scan rate of 0.2 V s^{-1} or below ($\geq 0.05 \text{ V s}^{-1}$) was used for the multiplex detection of TBHQ, BHA, and BHT.

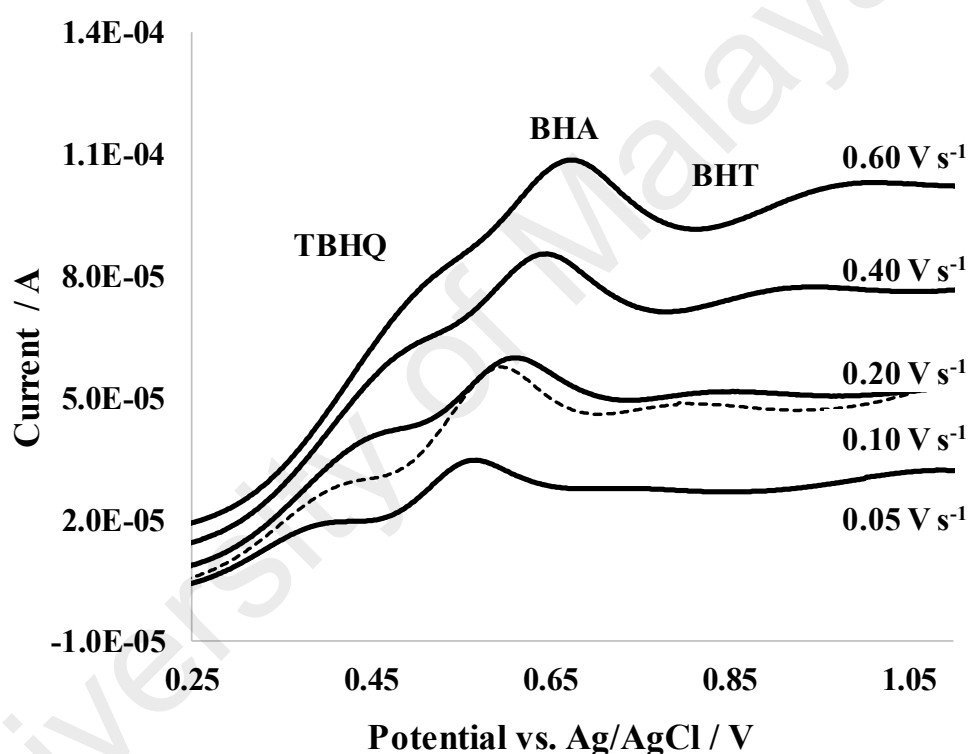


Figure 4.11: Multiplex LSV detection of TBHQ, BHA, and BHT using the Au–NP/graphite electrode at different scan rates. Note: for a clearer comparison, the LSV performed at 0.1 V s^{-1} is represented with a dotted line to prevent confusion from the LSV of 0.2 V s^{-1} .

4.3.5 Impact of sodium dodecyl sulfate on the multiplex detection of TBHQ, BHA, and BHT

The analysis of fatty samples (edible oil, emulsion) could affect the wettability of TBHQ ($\log p = 2.26$), BHA ($\log p = 3.50$), and BHT ($\log p = 5.19$) which could be detected simultaneously on the Au–NP/graphite electrode surface. This is particularly

true if fatty matter from the sample matrices affects the solubility of the above mentioned antioxidants (Chen et al., 2013). A method proposed by Caramit et al. (2013) using cetyltrimethylammonium bromide (CTAB) surfactant and a multi-walled carbon nanotube solid-phase electrode improved the detection of TBHQ and BHA (Caramit et al., 2013). Conversely, sodium dodecyl sulphate which acts as a surfactant was also used in this study, which has improved the detection of BHA and BHT by emulsifying the fatty matter from physically absorbing on the sensor electrode surface and also improving the antioxidants solubility. Fig. 4.12 illustrates the impact of SDS concentration on the multiplex detection of TBHQ, BHA, and BHT.

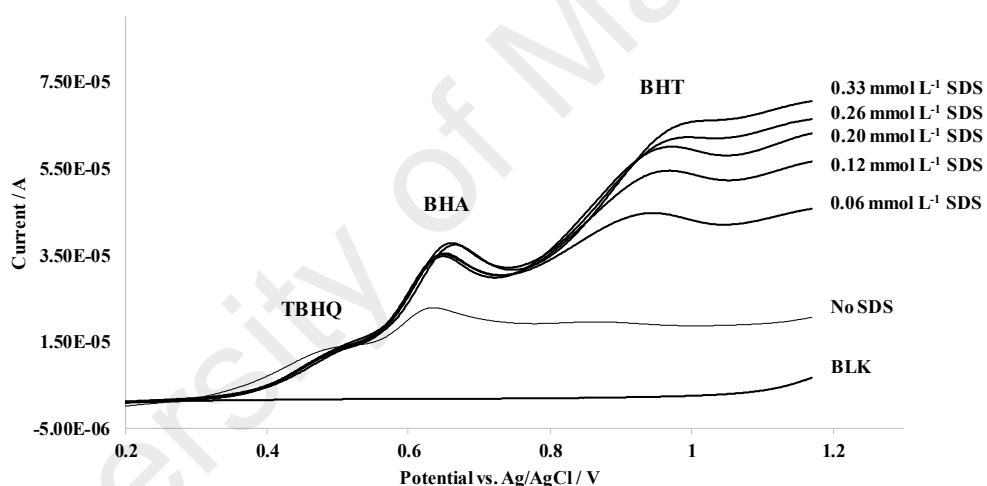


Figure 4.12: LSV curves for a $40 \mu\text{g mL}^{-1}$ mixed TBHQ, BHA, and BHT standard at different SDS concentrations.

At 0.06 mmol L^{-1} SDS, the BHA and BHT peak currents were improved two- and ten-fold, respectively. The subsequent addition of up to 0.20 mmol L^{-1} SDS resulted in no further improvement of the BHA peak current. However, in the case of BHT the peak response continued to increase, exceeding the original value 20-fold. The increased BHA and BHT peak responses could be due to their improved solubility in the electrolyte solution, leading to better detection at the Au-NP/graphite electrode surface. SDS did not have any influence on the TBHQ peak response, which could be explained by the

hydrophilic properties of this antioxidant (lower log p value). At a higher SDS content (above 0.26 mmol L^{-1}), saturation of the BHT peak response was observed. Thus, the addition of 0.20 mmol L^{-1} SDS to the supporting electrolyte was selected and used for the multiplex detection of TBHQ, BHA, and BHT.

4.3.6 Analytical performance of the Au-NP/graphite electrode for multiplex detection of BHA, BHT, and TBHQ

Fig. 4.13 shows the LSV voltammograms of TBHQ, BHA, and BHT (mixed standards) at concentrations of 5, 10, 20, 40, 60, and $80 \text{ }\mu\text{g mL}^{-1}$. All peaks were well separated at $5 \text{ }\mu\text{g mL}^{-1}$ and even at higher concentration of $80 \text{ }\mu\text{g mL}^{-1}$. A linear regression plot of I_{pa} versus antioxidant concentration is illustrated in Fig. 4.13. The linearity (R^2) of the TBHQ, BHA, and BHT plots obtained were found equal to 0.9985, 0.9995, and 0.9971, respectively, suggesting a good correlation between the current response and analyte concentration.

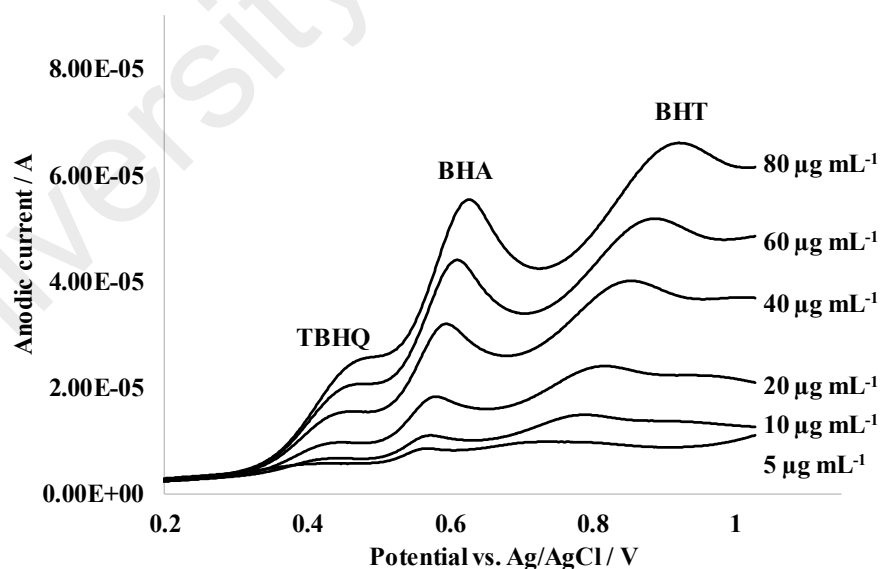


Figure 4.13: Multiplex detection of TBHQ, BHA, and BHT by LSV at concentrations between 5 and $80 \text{ }\mu\text{g mL}^{-1}$ with addition of 0.2 mmol L^{-1} SDS.

The BHT peak potentials (V) were found positively shifted with concentration increment, which could be explained by the limiting diffusion potential of BHT that due

to higher amount of the analyte, which impeded the chemical transfer mechanism process (methyl group of BHT as compared to proton in BHA and TBHQ) resulting to a resistivity increase in its potential. Alternatively, the peak shift could possibly be caused by ohmic drop during measurement; however this was not considered in this study because it was only observed in BHT peaks but not on TBHQ and BHA.

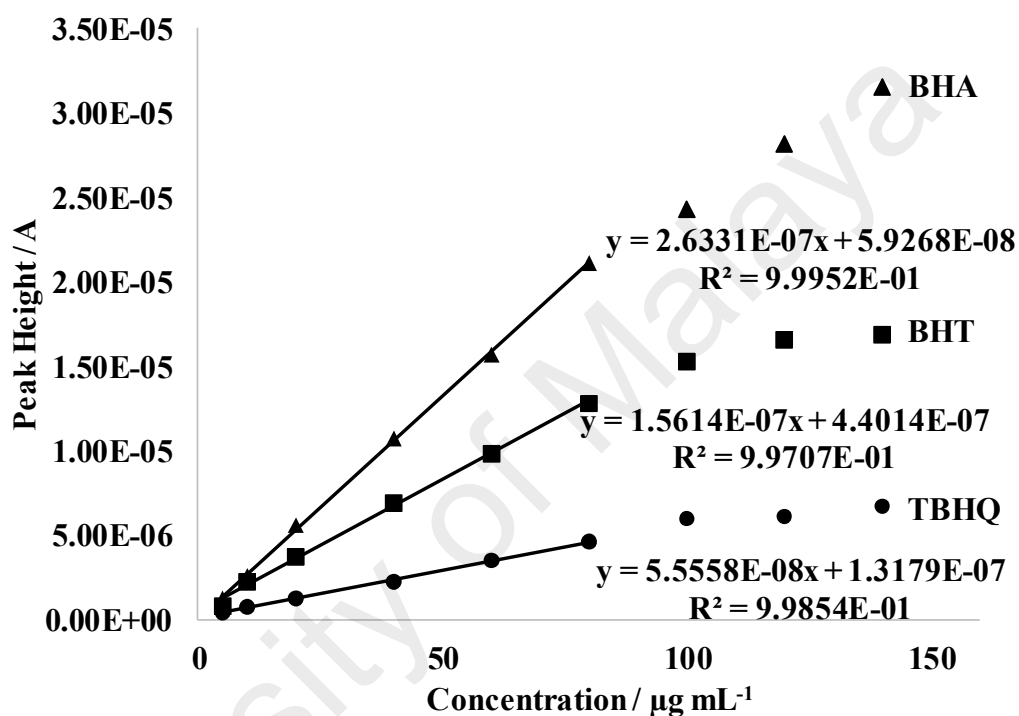


Figure 4.14: Linear regression plot of antioxidant anodic peak current responses against concentration (5 to 140 $\mu\text{g mL}^{-1}$) with the presence of 0.2 mmol L^{-1} SDS.

Among the three antioxidants, BHA (Fig. 4.13) exhibited the highest response (slope), suggesting that the Au-NP/graphite electrode is more sensitive towards BHA, with the order of sensitivity being BHA ($2.63 \times 10^{-7} \text{ A}/\mu\text{g mL}^{-1}$) > BHT ($1.56 \times 10^{-7} \text{ A}/\mu\text{g mL}^{-1}$) > TBHQ ($5.55 \times 10^{-8} \text{ A}/\mu\text{g mL}^{-1}$). The dynamic range of the analysis was also shown in Fig. 4.14, which indicates that the dynamic ranges of the studied antioxidants ranged from 0.6 to 80 $\mu\text{g mL}^{-1}$. Outside this range, the calibration linearity (R^2) fell below 0.99. A slight cloudiness was observed in the mixed standard solution when its concentration was prepared above 100 $\mu\text{g mL}^{-1}$, indicating the limit of antioxidants solubility in the

supporting electrolyte solution (80% Britton-Robinson buffer, 20% acetonitrile, and 0.20 mmol L⁻¹ SDS). A similar experiment using the Au-NP/graphite electrode was repeated without SDS addition and the results obtained as shown in Fig. 4.15. As predicted, the resulting linear regression plot for each studied antioxidant showed a much lower response signal (Fig. 4.16), which could be due to a decrease in antioxidant wettability on the electrode surface. This is particularly reflected in the BHT peak, as compared to LSV between BHT in the presence of SDS (Fig. 4.13) or without SDS (Fig. 4.15); the BHT peak response was found to have improved in the presence of 0.20 mmol L⁻¹ SDS.

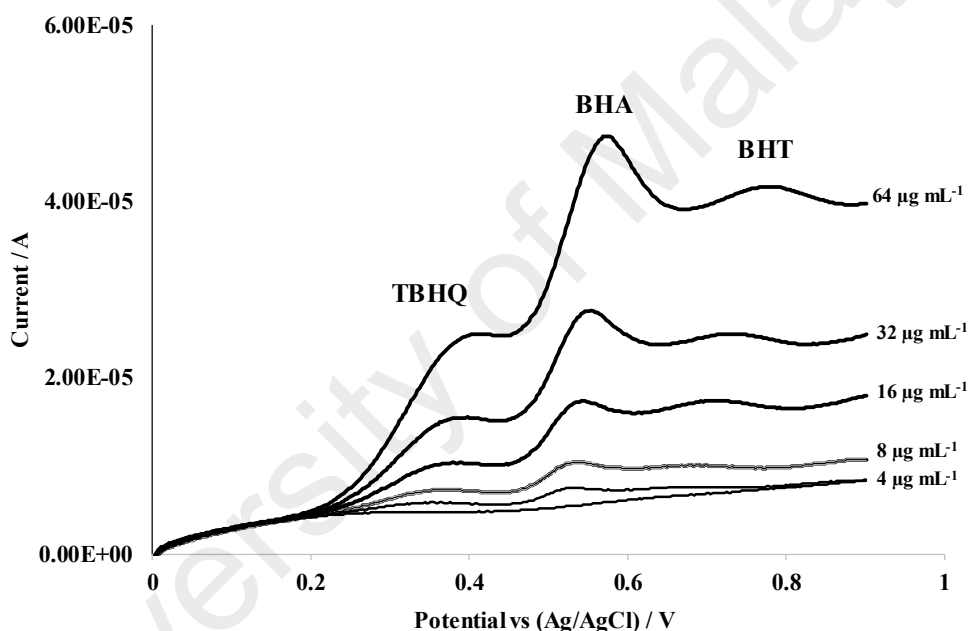


Figure 4.15: Multiplex detection of TBHQ, BHA, and BHT by LSV technique at concentrations ranged between 5 and 80 µg mL⁻¹ without addition of SDS.

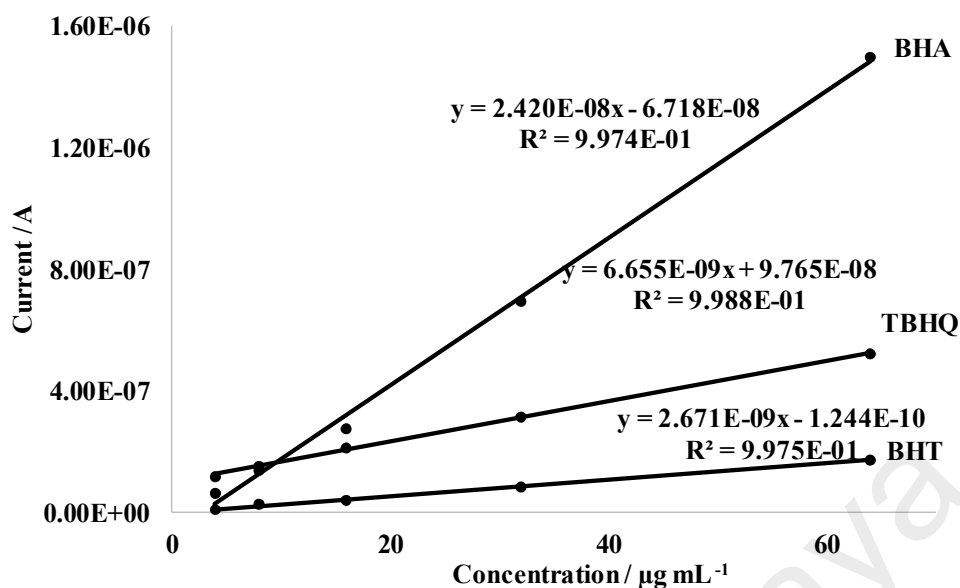


Figure 4.16: Linear regression plots of antioxidant anodic peak current responses against concentration (5 to 140 $\mu\text{g mL}^{-1}$) without addition of SDS.

The LODs of TBHQ, BHA, and BHT were determined by the serial dilution of a 1.0 $\mu\text{g mL}^{-1}$ mixed standard (until the antioxidant peak became undetectable by LSV) and were equal to 0.4, 0.1, and 0.6 $\mu\text{g mL}^{-1}$, respectively. Fig. 4.17 illustrates the LSV from the LOD study. The LOQs of TBHQ, BHA, and BHT were calculated as the five-fold standard deviation of the corresponding LODs, being equal to 0.5, 0.3, and 0.7 $\mu\text{g mL}^{-1}$, respectively. The LODs, LOQs, dynamic range, and linearity values are summarised in Table 4.2. In short, the LSV method used together with the newly developed Au-NPs/graphite electrochemical sensor showed an excellent dynamic range, LOD, and LOQ, thus being suitable for regulatory control usage, where the maximum permitted level of the above antioxidants is set at 200 $\mu\text{g g}^{-1}$. At five- to ten-fold sample dilution, this value falls within the dynamic range of the LSV approach used as was carefully described in this thesis chapter.

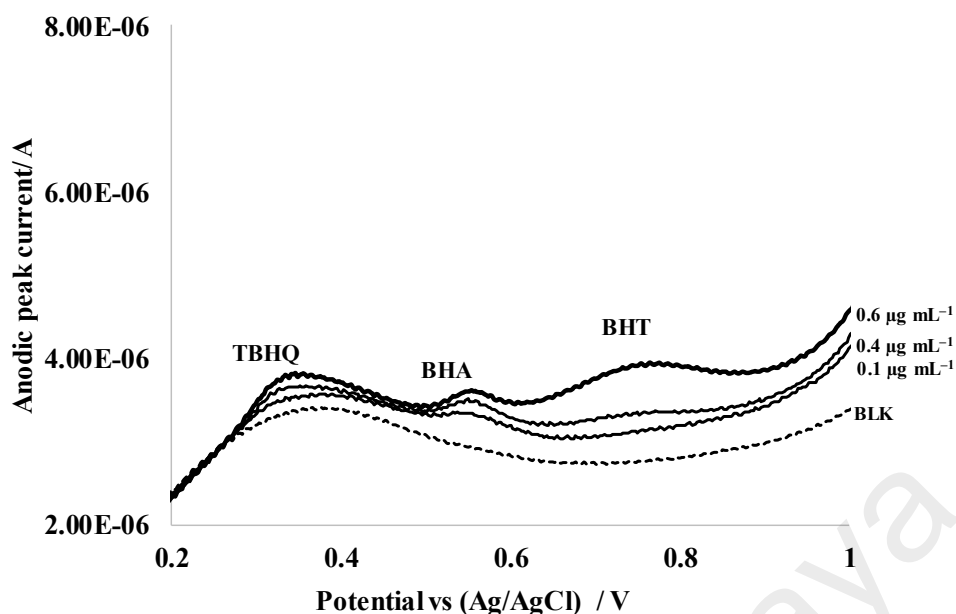


Figure 4.17: LSV for multiplex detection of BHA, BHT and TBHQ using Au-NPs/graphite. Analysis performed at concentration of 0.1, 0.4 and 0.6 $\mu\text{g mL}^{-1}$ for limit of detection (LOD) study.

Table 4.2: Comparison of the analytical performance made between UPLC-PDA and LSV Au-NP/graphite methods for the multiplex analysis of TBHQ, BHA, and BHT.

Analyte	Method	¹ LOD	² LOQ	Dynamic Range	Linearity	³ Sensitivity
		$\mu\text{g mL}^{-1}$	$\mu\text{g mL}^{-1}$			unit signal/ $\mu\text{g mL}^{-1}$
TBHQ	LSV	0.4	0.5	0.5–80.0	0.9985	0.081
	UPLC	0.8	0.9	0.9–800.0	0.9999	0.081
BHA	LSV	0.1	0.3	0.3–100.0	0.9995	0.092
	UPLC	0.4	0.5	0.5–800.0	0.9996	0.084
BHT	LSV	0.6	0.7	0.7–80.0	0.9971	0.066
	UPLC	0.4	0.5	0.5–800.0	0.9999	0.082

¹ Limit of detection

² Limit of quantitation

³ Normalize response factor that relative to 10 $\mu\text{g mL}^{-1}$ standard analyte (by divide calibration slope with signal response of the standard)

4.3.7 Analytical performance of UPLC-PDA in multiplex detection of BHA, BHT, and TBHQ

Fig. 4.18 illustrates the UPLC-PDA chromatogram for multiplex detection of TBHQ, BHA, and BHT, with retention times of 5.03 ± 0.01 , 6.15 ± 0.01 , and 7.64 ± 0.01 min,

respectively. The antioxidant linear regression plots are illustrated in Fig. 4.18, showing linearities (R^2) above 0.999. The LODs of TBHQ, BHA, and BHT determined by UPLC corresponded to 0.8, 0.4, and 0.4 $\mu\text{g mL}^{-1}$, respectively, while the corresponding LOQs were calculated as 0.9, 0.5, and 0.5 $\mu\text{g mL}^{-1}$, respectively. Table 4.2 compares the analytical performance of LSV and UPLC methods, and the data suggests that the former method exhibits better LODs and LOQs for TBHQ and BHA detection than the latter, while BHT is better detected using the UPLC–PDA method.

The dynamic detection range is found to be wider using the UPLC–PDA method, which could be explained by the limiting effect of sensor surface area on oxidation, which reaches saturation at 100 $\mu\text{g mL}^{-1}$ of the three antioxidants. In terms of analysis speed, the LSV method is much faster, requiring approximate 2 min per sample analysis, while UPLC–PDA requires 10 min per run.

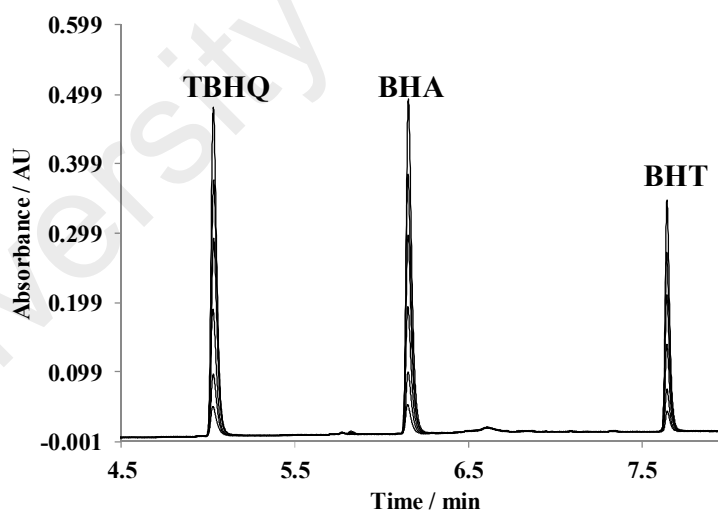


Figure 4.18: UPLC–PDA chromatogram for multiplex detection of TBHQ, BHA, and BHT at concentrations ranging between 10 and 100 $\mu\text{g mL}^{-1}$.

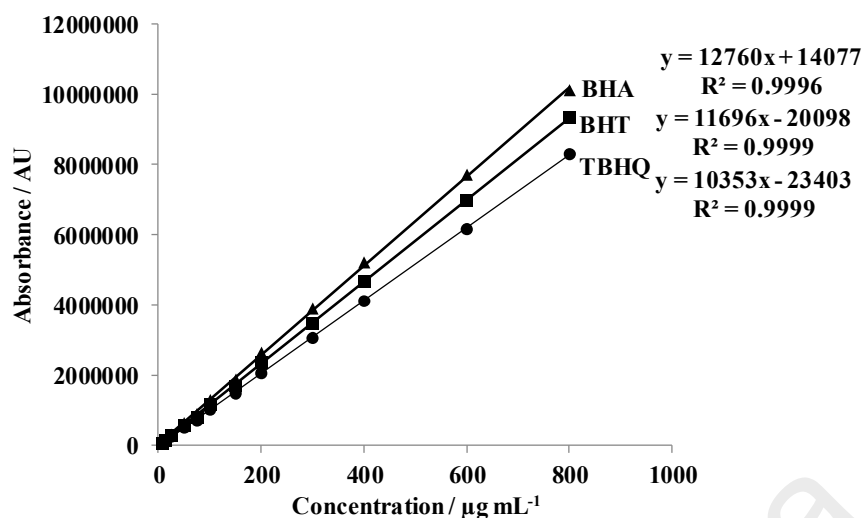


Figure 4.19: Linear regression plot of peak area (AU) versus concentration of TBHQ, BHA, and BHT standard performed using UPLC–PDA.

Fig. 4.19 shows the UPLC–PDA calibration curves of TBHQ, BHA, and BHT. The UPLC sensitivity (slope) is in the following order BHA (1.27×10^4 AU/ $\mu\text{g mL}^{-1}$) > BHT (1.17×10^4 AU/ $\mu\text{g mL}^{-1}$) > TBHQ (1.04×10^4 AU/ $\mu\text{g mL}^{-1}$). Since both LSV and UPLC-PDA methods have different slope magnitudes due to dissimilar signal responses (i.e., ampere and absorbance), a direct comparison is not possible. Hence, the sensitivity of these two methods was compared by normalising the calibration slope relative to the antioxidant signal response at $10 \mu\text{g mL}^{-1}$, affording a standardised unit signal per concentration. Table 4.2 summarises the sensitivity responses of LSV and UPLC methods. A comparison of these values shows that LSV is a more sensitive technique used for the detection of BHA (0.092 unit signal/ $\mu\text{g mL}^{-1}$) but less sensitive for BHT detection (0.066 unit signal/ $\mu\text{g mL}^{-1}$) as compared to UPLC (BHA = 0.084 unit signal/ $\mu\text{g mL}^{-1}$ and BHT = 0.082 unit signal/ $\mu\text{g mL}^{-1}$), while equal sensitivities are observed for TBHQ detection (LSV = 0.081 unit signal/ $\mu\text{g mL}^{-1}$ versus UPLC = 0.081 unit signal/ $\mu\text{g mL}^{-1}$). This suggests that the sensitivity of the LSV method is comparable to UPLC.

4.3.8 Analysis of antioxidants in real food samples and method validation with UPLC–PDA

The antioxidant concentrations in actual food samples were analysed by LSV method and validated using the UPLC–PDA technique, and the results are summarised in Tables 4.3 and 4.4, respectively.

Table 4.3: Simultaneous determination of TBHQ, BHA, and BHT content in food and spiked food samples using LSV method (Au–NP/graphite electrode).

Sample	Spike ($\mu\text{g mL}^{-1}$)	TBHQ		BHA		BHT	
		Result ¹ ($\mu\text{g g}^{-1}$)	Recovery ¹ (%)	Result ¹ ($\mu\text{g g}^{-1}$)	Recovery ¹ (%)	Result ¹ ($\mu\text{g g}^{-1}$)	Recovery ¹ (%)
Ghee	0	-	-	101.6 \pm 0.5	-	62.8 \pm 0.6	-
	100	100.2 \pm 2.5	100.2 \pm 2.5	202.5 \pm 0.7	100.9 \pm 0.7	161.7 \pm 1.1	98.9 \pm 1.1
	200	201.1 \pm 3.2	100.6 \pm 1.6	300.4 \pm 1.2	99.4 \pm 0.6	260.6 \pm 0.6	98.9 \pm 0.28
	300	300.2 \pm 0.7	100.1 \pm 0.2	402.7 \pm 1.3	100.4 \pm 0.4	361.7 \pm 1.9	99.6 \pm 0.6
Sunflower Oil	0	200.2 \pm 2.3	-	-	-	-	-
	100	297.4 \pm 1.9	97.2 \pm 1.9	98.7 \pm 1.2	98.7 \pm 1.2	98.9 \pm 2.4	98.9 \pm 2.4
	200	400.4 \pm 3.7	100.1 \pm 1.9	203.9 \pm 3.4	101.9 \pm 1.7	202.3 \pm 2.2	101.1 \pm 1.1
	300	501.7 \pm 1.5	100.5 \pm 0.5	302.3 \pm 0.3	100.8 \pm 0.1	302.2 \pm 2	100.7 \pm 0.1
Salad Dressing	0	-	-	37.3 \pm 0.6	-	-	-
	100	102.6 \pm 1.6	102.6 \pm 1.6	136.6 \pm 1.3	99.3 \pm 1.3	99.1 \pm 0.7	99.1 \pm 0.7
	200	200.4 \pm 2.0	100.2 \pm 1.0	237.4 \pm 0.5	100.1 \pm 0.3	199.6 \pm 1.7	99.8 \pm 0.8
	300	301.2 \pm 2.2	100.4 \pm 0.7	336.3 \pm 0.5	99.7 \pm 0.2	300.6 \pm 1.4	100.2 \pm 0.5

¹ Three replicate ($n = 3$) analyses with standard error at 95% confidence limit.

A total of three different types of food sample matrices including oil-, fat-, and emulsion-based samples were purchased and tested using the Au–NP/graphite working electrode. For a quantitative measurement, a standard addition method was used. BHA and BHT were simultaneously detected in ghee (butterfat) at levels of 101.6 \pm 0.5 and 62.8 \pm 0.6 $\mu\text{g mL}^{-1}$, respectively. Individual TBHQ and BHA antioxidant was detected

in sunflower oil and salad dressing (emulsion) samples, at levels of 200.2 ± 2.3 and $37.3 \pm 0.6 \mu\text{g mL}^{-1}$, respectively.

Table 4.4: Simultaneous determination of TBHQ, BHA, and BHT content in food and spiked food samples using UPLC-PDA method.

Sample	Spike ($\mu\text{g mL}^{-1}$)	TBHQ		BHA		BHT	
		Result ¹ ($\mu\text{g g}^{-1}$)	Recovery ¹ (%)	Result ¹ ($\mu\text{g g}^{-1}$)	Recovery ¹ (%)	Result ¹ ($\mu\text{g g}^{-1}$)	Recovery ¹ (%)
Ghee	0	-	-	99.8 ± 1.5	-	61.5 ± 1.8	-
	100	106.5 ± 2.4	106.5 ± 2.4	200.3 ± 2.1	100.5 ± 2.1	151.8 ± 1.6	90.3 ± 1.6
	200	202.9 ± 1.8	101.4 ± 0.9	301.6 ± 0.4	100.9 ± 0.2	256.2 ± 1.2	97.4 ± 0.6
	300	304.7 ± 1.9	101.6 ± 0.6	394.6 ± 4.3	98.3 ± 1.5	360.5 ± 2.3	99.7 ± 0.9
Sunflower Oil	0	199.1 ± 0.4	-	-	-	-	-
	100	300.1 ± 2.1	100.9 ± 2.1	100.2 ± 1.2	100.2 ± 1.2	100.3 ± 2.1	100.3 ± 2.1
	200	399.9 ± 2.1	100.4 ± 1.0	199.8 ± 1.4	99.9 ± 0.7	199.8 ± 1.2	99.9 ± 0.6
	300	500.7 ± 2.9	100.5 ± 1.0	299.5 ± 3.9	99.8 ± 1.3	298.3 ± 4.2	99.4 ± 1.4
Salad Dressing	0	-	-	36.7 ± 0.5	-	-	-
	100	103.1 ± 2.9	103.1 ± 2.9	133.7 ± 0.6	97.0 ± 0.6	103.8 ± 1.3	103.8 ± 1.3
	200	205.6 ± 0.7	102.8 ± 0.4	235.7 ± 0.7	99.5 ± 0.4	203.9 ± 0.3	101.9 ± 0.1
	300	306.3 ± 1.7	102.1 ± 0.6	325.4 ± 1.9	96.2 ± 0.6	300.5 ± 4.0	100.2 ± 1.3

¹ Three replicate ($n = 3$) analyses with standard error at 95% confidence limit.

The LSV results were compared to the one obtained from the UPLC–PDA method to determine their reliability. A standard addition technique was employed, and the analysis results are summarised in Table 4.4. All LSV results agreed with the ones from the UPLC method, and the LSV to UPLC level ratio was taken as the accuracy of this method (%). Based on this, the BHA and BHT content in ghee constituted 101.8 and 102.1% of the corresponding UPLC values, whereas the TBHQ and BHA content in sunflower oil and salad dressing corresponded to 100.5 and 101.6%, respectively. This suggested that the LSV results were close to those of UPLC–PDA, with the accuracy of the former method being $100.0 \pm 3.4\%$ relative to UPLC, with the standard error located at a confidence limit of 95%.

To further evaluate the reliability of LSV as compared to UPLC–PDA method, a recovery study of food samples spiked with three different concentration levels at 100, 200 and 300 $\mu\text{g mL}^{-1}$ of the mixed antioxidant standard was performed, with the results as summarised in Tables 4.3 and 4.4. All antioxidants were multiplex–determined using the Au–NP/graphite electrode where a standard addition method was utilised. TBHQ was detected in sunflower oil, BHA in ghee and salad dressing, and BHT in ghee. In other words, both BHA and BHT were detectable simultaneously using the Au–NP/graphite LSV method within a single test run. Further, the percentage recoveries of the spiked TBHQ, BHA, and BHT in ghee (fat), sunflower oil, and salad dressing (emulsion) were found between 97.2 and 102.6%. On the other hand, the UPLC–PDA recoveries were found between 97.0 and 106.5%, suggesting that the Au–NP/graphite LSV method is as good as the standard UPLC–PDA method.

To study the correlation between LSV and UPLC methods, linear regression analysis was performed by mapping the LSV results against those of UPLC–PDA (including spiked samples), with the resulting linear plot as shown in Fig. 4.20. The graph shows that the results of both methods were distributed linearly (correlation coefficient of 0.9988), suggesting a good correlation between these two methods.

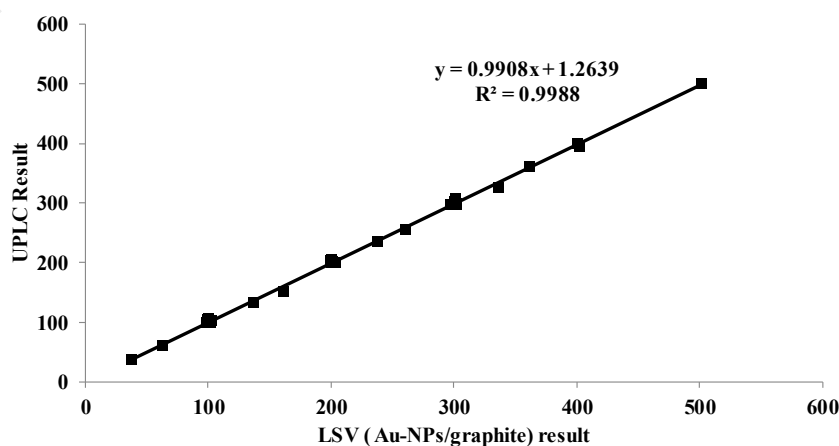


Figure 4.20: Correlation plot of samples and spike result that performed using LSV and UPLC methods.

The performance of the Au–NP/graphite sensor in synthetic anti-oxidant analysis was compared to other developed sensors. Table 4.5 summarizes the analytical performance of other studied sensor. In which it shows the proposed Au–NP/graphite sensor has the advantages for the simultaneous detection of TBHQ, BHA and BHT. In overall, the detection limit of Au–NP/graphite was comparable to the others sensors, while the detection range was found wider; except for the AuNPs–PVP-graphene/GCE sensor, which was more sensitive and wider detection range but the detection was restricted to BHA analysis only.

Table 4.5: Comparison of the analytical performance shown by different reported electrochemical sensor for the analysis of TBHQ, BHA and BHT.

Electrodes	Analyte	Method	Detection limit, (mol L ⁻¹)	Linear range (mol L ⁻¹)	Notes	Reference
Pt/PPY/NiPcTs ^a	TBHQ	CV	2.3 x 10 ⁻⁵	1.8 x 10 ⁻³ – 2.0 x 10 ⁻⁴	Only BHA and TBHQ were detected	Fuente et al., 2008
	BHA		1.2 x 10 ⁻⁵	2.0 x 10 ⁻³ – 2.0 x 10 ⁻⁴		
MCCE–Cu ₃ (PO ₄) ₂ -poly ^b	BHA	SWV	6.8 x 10 ⁻⁷	4.1 x 10 ⁻⁵ – 3.4 x 10 ⁻⁷	Only BHA and BHT were detected	Freitas et al., 2010
	BHT		9.1 x 10 ⁻⁷	4.1 x 10 ⁻⁵ – 3.4 x 10 ⁻⁷		
MWCNT-SPE ^c	TBHQ	LSV	5.7 x 10 ⁻⁶	1.0 x 10 ⁻⁵ – 5.0 x 10 ⁻⁷	Only TBHQ and BHA were detected	Caramit et al., 2013
	BHA		1.7 x 10 ⁻⁷	1.0 x 10 ⁻⁵ – 5.0 x 10 ⁻⁷		
GCE ^d	TBHQ	DPV	3.7 x 10 ⁻⁶	6.3 x 10 ⁻⁴ – 1.3 x 10 ⁻⁶	Only TBHQ was detected	Goulart et al., 2014
AuNPs–PVP–graphene/GCE ^e	BHA	LSV	4.0 x 10 ⁻⁸	1.0 x 10 ⁻⁴ – 2.0 x 10 ⁻⁷	Only BHA was detected	Wang et al., 2015
Au–NPs/graphite ^f	TBHQ	LSV	2.4 x 10 ⁻⁶	4.8 x 10 ⁻⁴ – 2.0 x 10 ⁻⁶	BHA, BHT and TBHQ were detected	Ng et al., 2017 (this thesis study)
	BHA		5.5 x 10 ⁻⁷	5.5 x 10 ⁻⁴ – 1.5 x 10 ⁻⁷		
	BHT		2.7 x 10 ⁻⁶	3.6 x 10 ⁻⁴ – 2.7 x 10 ⁻⁶		

^aPlatinum/polypyrrole/nickel phthalocyanine p–toluenesulphonate

^bModified composite carbon electrode with copper phosphate immobilized in polyester resin

^cMultiwalled carbon nanotubes/screen printed electrode

^dGlassy carbon electrode

^eGold nanoparticles polyvinylpyrrolidone/reduce graphene oxide/glassy carbon electrode

^fGold nanoparticles graphite electrode

4.3.9 Interference and stability study of the Au–NP/graphite sensor

The selectivity of the Au–NP/graphite sensor for multiplex detection of TBHQ, BHA, and BHT was challenged by the addition of common interferents occurring in food samples, including anti-microbial preservatives (benzoic acid (Ding et al., 2015; Pohanka et al., 2011), phenoxyethanol), vitamins (ascorbic acid, tocopherol (Brennan et al., 2011; Carocho et al., 2015; Shahidi & Ambigaipalan, 2015), and niacinamide (Athar et al., 2006)), phenolic acids (quinic acid) (Bakhouché et al., 2014; Shahidi & Ambigaipalan, 2015), glycerine (Tan et al., 2013), and ions (sodium, potassium, magnesium, acetate, chloride) (Mendil et al., 2009). The recovery percentages of BHA, BHT, and TBHQ (40 $\mu\text{g mL}^{-1}$) after addition of individual interferent are summarised in Table 4.6.

Table 4.6: Recovery percentages of the 40 $\mu\text{g mL}^{-1}$ TBHQ, BHA, and BHT standard in the presence of individual interferent using the Au–NP/graphite electrode.

NO	Interference	Concentration ($\mu\text{g mL}^{-1}$)	40 ppm TBHQ recovery (%) ¹	40 ppm BHA recovery (%) ¹	40 ppm BHT recovery (%) ¹
1	Tocopherol	40	98.5 \pm 1.2	98.7 \pm 0.7	98.8 \pm 2.0
2	Ascorbic acid	40	98.4 \pm 0.5	100.0 \pm 0.2	102.0 \pm 3.2
3	Quinic acid	40	99.2 \pm 1.7	98.5 \pm 1.1	94.7 \pm 3.4
4	Quercetin	20	93.1 \pm 0.9	98.8 \pm 0.8	108.1 \pm 2.1
5	Gallic acid	20	97.3 \pm 1.2	99.8 \pm 0.3	105.5 \pm 3.2
6	Benzoic acid	40	101.0 \pm 0.2	95.4 \pm 2.7	103.0 \pm 1.1
7	Phenoxyethanol	40	99.1 \pm 0.5	97.6 \pm 1.1	99.5 \pm 3.8
8	Niacinamide	40	97.1 \pm 2.2	92.0 \pm 1.6	93.4 \pm 1.1
9	Glycerine	40	98.0 \pm 1.1	99.5 \pm 2.0	101.0 \pm 1.3
10	Sodium	40	95.1 \pm 3.8	104.0 \pm 1.1	105.0 \pm 1.2
11	Chloride	40	95.4 \pm 3.7	103.2 \pm 1.9	101.0 \pm 1.2
12	Potassium	40	98.4 \pm 3.6	101.0 \pm 2.1	108.0 \pm 2.1
13	Sulphate	40	98.0 \pm 3.7	103.0 \pm 2.0	99.1 \pm 2.0
14	Acetate	40	99.0 \pm 1.1	97.1 \pm 1.0	100.1 \pm 1.3
15	Magnesium	40	97.6 \pm 1.0	98.9 \pm 0.9	99.7 \pm 1.5

¹ Three replicate ($n = 3$) analyses with standard error at 95% confidence limit.

In most cases, the recoveries of BHA, BHT, and TBHQ were above 95%, with the exception of niacinamide, where the BHA and BHT recoveries were 92 and 93%, respectively, while the TBHQ recovery was not affected. In the presence of phenolic interferences (gallic acid and quercetin) at 40 $\mu\text{g mL}^{-1}$ the detection of BHA and BHT

was recovered above 120%, and TBHQ was less than 50%. However, if the concentration of these phenolic interferences were reduced half from $40 \mu\text{g mL}^{-1}$ to $20 \mu\text{g mL}^{-1}$ or below, the recovery was found close to 100%. This limitation does not impact on the application of Au-NPs/graphite in complex food samples analysis, as the total phenolic contents (as expressed as gallic acid and its equivalent) detected in ghee, salad dressing and most edible oil is below $10 \mu\text{g GAE mL}^{-1}$ (Ghazani et al., 2013; Siger et al., 2008; Sreeramulu, 2011), which after sample preparation (30 times dilution) the concentration is below $3 \mu\text{g mL}^{-1}$. Moreover, this evaluation does not take into consideration the phenolic compounds degradation or lost during manufacturing processing such as refinery. The overall results suggest that the Au-NP/graphite electrode exhibits a good selectivity for the multiplex detection of BHA, TBHQ, and BHT.

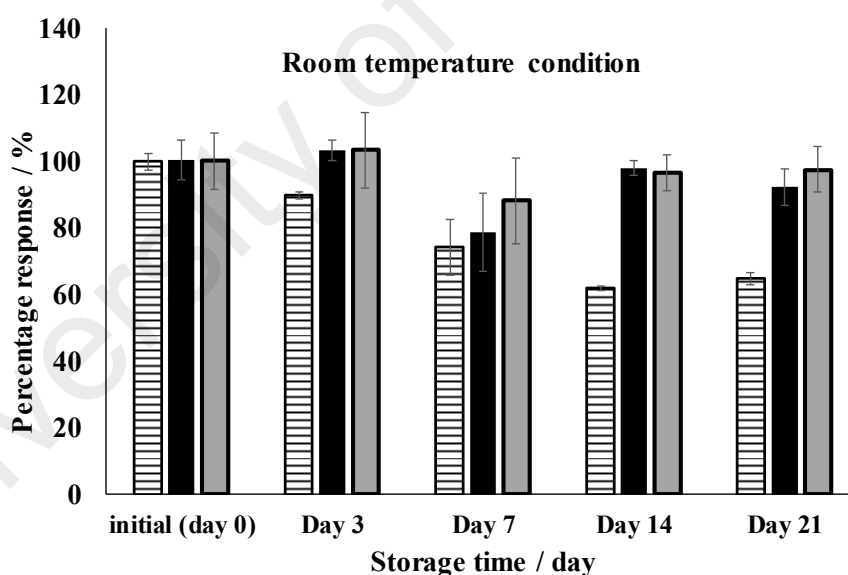


Figure 4.21: Stability analysis of the Au-NP/graphite electrode performed over 21 days for multiplex detection of TBHQ (striped), BHA (black), and BHT (grey) under storage conditions at room temperature (25°C).

The stability of the Au-NP/graphite electrode for use in the multiplex detection of antioxidants was monitored for 21 days at 45 and 25°C (room temperature), in which the results are shown in Fig. 4.21 and 4.22, respectively. The performance of this electrode

for multiplex detection of TBHQ, BHA, and BHT was monitored at intervals of 0, 3, 7, 14, and 21 days.

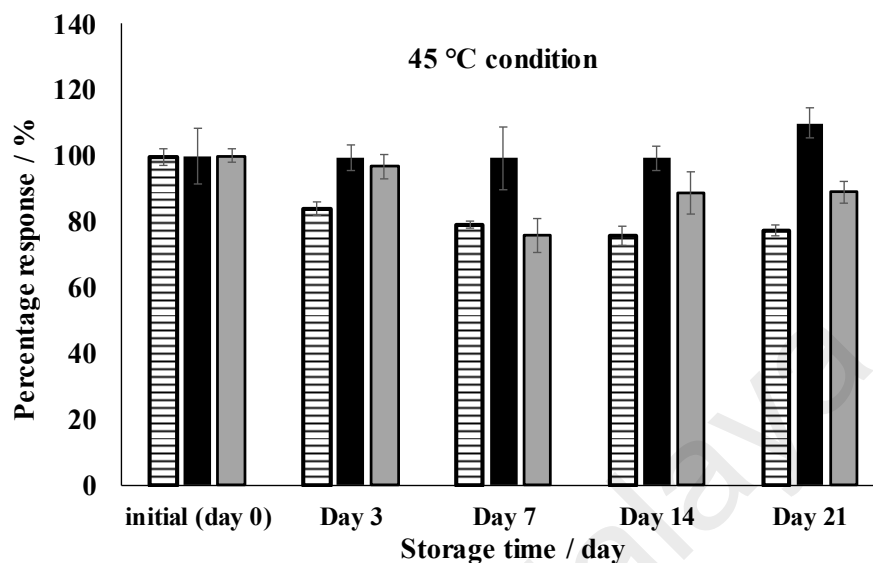


Figure 4.22: Stability analysis of the Au-NP/graphite electrode performed over 21 days for multiplex detection of TBHQ (striped), BHA (black), and BHT (grey) under storage conditions at 45°C.

The electrode current response (I_{pa}) to TBHQ, BHA, and BHT ($40 \mu\text{g mL}^{-1}$) was normalised and expressed as a percentage. Based on the graph (Fig. 4.20), no large deterioration of current response was observed for BHA and BHT after 21 days, either at 45 or 25°C, while a slight decrease in the sensor performance was observed for TBHQ detection (25% after 7 days at 25°C, subsequently stable until 21 days). In contrast, when the Au-NPs/graphite electrode was stored at 45°C, the performance of the Au-NP/graphite electrode in TBHQ detection deteriorated by 20% in day 3, subsequently remain stable for up to 21 days under storage. This observation suggested that the Au-NP/graphite sensor is stable for up to 21 days even at extreme temperature conditions such as storage temperature of up to 45°C.

4.4 Conclusion

A green, cost-effective, and simple procedure was successfully developed for rapid, sensitive, specific, and quantitative multiplex determination of BHA, BHT, and TBHQ in food samples using LSV technique with an Au–NP/graphite modified electrode. Surface modification with gold nanoparticles significantly enhances the electrochemical properties (electron transfer rate, E_{eff} , and overpotential) of the graphite electrode, hence enabling simultaneous LSV analysis of three synthetic antioxidants within a single test. This newly developed method was successfully tested in three different food matrices, including liquid oil, solid fat, and emulsion-based food samples. The obtained LSV analysis results on the real samples yielded a good linear correlation value which is above 0.99, as compared to the UPLC–PDA method. These outstanding findings justified the good analytical performance of the proposed method and its practical use for real sample analysis. The recovery studies of spiked TBHQ, BHA, and BHT into the sample matrix at concentrations of 100, 200 and 300 $\mu\text{g mL}^{-1}$, respectively, have shown a recovery of the anti-oxidant above 97%. Besides, a wide dynamic range of BHA, BHT and TBHQ multiplex detection was obtained using the LSV method (0.6 to 80 $\mu\text{g mL}^{-1}$), being optimal for purposes of regulatory control in food safety (200 $\mu\text{g mL}^{-1}$), although the control concentration is higher than the calibration range, nevertheless, after sample preparation and dilution (10 times); the values will fall in the range (20 $\mu\text{g mL}^{-1}$). The Au–NP/graphite electrode was found to be selective towards TBHQ, BHA, and BHT even in the presence of common interferents (e.g., benzoic acid, tocopherol, ascorbic acid, niacinamide, quercetin and gallic acid). On the other hand, the Au-NPs/graphite electrochemical sensor also exhibited high sensitivity, LODs, and LOQs as compared to those results obtained from the UPLC–PDA method.

CHAPTER 5: DEVELOPMENT AND CHARACTERISATION OF AU- ErGO/MWCNT/GRAPHITE NANOCOMPOSITE SENSOR FOR THE DETERMINATION OF DNA BASES IN PLANT AND ANIMAL DNA

5.1 Introduction

In the recent development of electrochemical sensor, the use of composite nano-material for surface modification has been getting much attention. The hyphenation of different characteristic material could give a synergistic effect to the fabricated sensor. As a result, this could diversify the electrochemical performance and characteristic of the sensor that could be fit for a wider application use. The choice of material used in the composite nano-material can be quite diversified; which depends on the intended application and also the performance criteria to be built on the sensor. Some of these nanomaterials are multiwalled carbon nanotubes (MWCNT), metal nanoparticle, graphene and carbon dot.

In this chapter, the feasible use of graphite substrate as the material for sensor development is further investigated and improvised. A simple preparation procedure that utilises two simple steps; starting with heat casting for the preparation of MWCNT/graphite and subsequently co-electrodeposition technique to intercalate reduced graphene oxide and gold particle on the surface of MWCNT-graphite is studied and the developed sensor is designated as Au-ErGO/MWCNT/graphite. A study reported by Fotouhi et al. (2012) using MWCNT/GCE in sulfaguanidine detection (Fotouhi et al., 2012); Tran et al. (2011) in polyaniline/MWCNT for papilloma virus detection (Tran et al., 2011); and Yari & Derki (2016) in MWCNT/Fe₃O₄/polydopamine on GCE for G and A detection (Yari & Derki, 2016) have shown improvement to the Eff A and electron conductive network; which suggested a more active site for the electro-oxidation process, hence it increases the flow of current (electron) and improves the graphite sensitivity.

However, the preparation procedure for MWCNT attachment on the silica or carbon substrate was not discussed, particularly the hydrodynamic size of MWCNT that could potentially affect the number of nano-tube junction and the electron transfer efficiency. The degree of sonication and pH condition of the MWCNT could be a factor that requires further investigation.

An additional approach to incorporate graphene oxide on the graphite electrode is to improve the electrocatalytic attribute of the sensor (Liu et al., 2013). A recent sensor development (Zinc sulfide-ethylenedioxythiophen-reduced graphene oxide) by Ye et al. (2014) has successfully utilized the graphene oxide in the multiplex detection of G, A and T (Ye et al., 2014), which has evidenced the electrocatalytic oxidation improvement of the 3 studied DNA bases. However, the sensor failed to detect C, the drawback could be associated to zinc sulfide oxidation potential (anodic) that limits its application to C detection required at higher potential value of above +1.4 V. This could be improved with the properties of gold nanoparticles instead of zinc, as gold (+1.50 V) possesses a higher standard oxidation potential than zinc (-0.76 V). Besides, the graphene agglomeration was not assessed by the author, which could potentially affect the conductivity performance of reduced graphene oxide (Liu et al., 2011). This issue could be resolved by the intercalation of the graphene layer with gold nanoparticles, which could prevent the graphene agglomeration.

It is expected that the fabricated Au-ErGO/MWCNT/graphite sensor as detailed in this thesis will have an improved electrochemical property which includes sensitivity, overpotential and electrocatalysis. These characteristics are important for the development of a high throughput, multi analyte, rapid and sensitive sensor. The developed electrochemical sensor is then used for the multiplex detection of DNA bases of A, G, T and C. The main application is to focus on the feasibility use of this

electrochemical sensor as an alternative, rapid, and high throughput method for the study of DNA damages. Many sensors have been successfully developed but the attempt was confined to limited measurement of A and G only, which failed to provide a comprehensive detail of the entire DNA component (A, G, T and C). The reliability and applicability of the developed sensor is then tested using real samples of calf thymus and onion DNA, respectively. Both samples were chosen, to test the practicability of the developed electrochemical sensor in measurement of DNA that was derived from animal and plant source respectively. A secondary alternative method using the UPLC method is also employed to validate the reliability of obtained results.

5.2 Experimental

5.2.1 Chemicals and apparatus

Britton-Robinson buffer of concentration 0.04 mol L^{-1} was prepared from an equal volume mixture of 0.04 mol L^{-1} phosphoric acid, acetic acid and boric acid, the pH of the buffer was adjusted to value 2, 3, 4, 5, 6, 7, 8 and 9 using 1.0 mol L^{-1} sodium hydroxide. All the chemicals used for the buffer preparation were purchased from Merck (Darmstadt, Germany). For electrode surface modification, 3 mg mL^{-1} solution of carboxylic functionalised multiwalled carbon nano-tubes (MWCNT) was prepared in the Britton-Robinson buffer at pH 7; and 0.5 mg mL^{-1} of graphene oxide (GO) was dispersed in ultrapure water using an ultra-sonic bath. A tetrachloroauric acid solution of 1 mmol L^{-1} was prepared in a sodium nitrate solution (0.1 mol L^{-1}). For modified electrode surface characterisation, a stock solution of 0.1 mol L^{-1} potassium ferricyanide $\text{K}_3\text{Fe}(\text{CN})_6$ was prepared in sodium nitrate solution of concentration 0.1 mol L^{-1} . The graphite rod used in this study was obtained from used battery, which was pretreated according to Chapter 3 (Section 3.2.2).

For DNA bases characterisation study, a Britton-Robinson buffer concentration of 0.04 mol L^{-1} was prepared from an equal volume mixture of 0.04 mol L^{-1} phosphoric acid, acetic acid and boric acid, the pH of the buffer was adjusted to value 2, 3, 4, 5, 6, 7, 8 and 9 using 1.0 mol L^{-1} sodium hydroxide; subsequently used to prepare the different pH condition of A, G, C and T standard. A 0.1 mol L^{-1} phosphate buffer of pH 7 was prepared by mixing 0.6025 g of potassium dihydrogen phosphate and 0.9707 g of potassium hydrogen phosphate salt together in 1 Liter of ultrapure water. For DNA bases measurement, $1000 \text{ } \mu\text{g mL}^{-1}$ stock standard of A and G were prepared in 0.1 mol L^{-1} sodium hydroxide solution; for C and T, the solutions were prepared in the phosphate buffer of pH 7 (0.1 mol L^{-1}). The calf thymus DNA sample was obtained from Sigma Aldrich and was used directly. For the DNA extraction work, pure sodium dodecyl sulfate, sodium chloride and absolute ethanol were used. The hydrolysis of the DNA into its individual bases was performed using either sulfuric acid or hydrochloric acid (8 mol L^{-1}). All chemicals used for the sample preparation work were obtained from Merck (Darmstadt, Germany). Ultrapure water (Merck Milipores) of 18.2 Mohm was used for the preparation of all the chemicals.

The electrochemical measurement was performed using Metrohm potentiostat/galvanostat model PG Stat 202 (Utrecht, Netherlands). A three electrode system was employed with the counter and the reference electrode corresponded to the platinum rod and silver-silver chloride electrode (3 M KCl), respectively. Both electrodes and electrochemical sample cells were purchased from BASi (USA). For the liquid chromatography analysis, the UPLC system from WATER inc. (USA) equipped with photo diode array (PDA) detector and auto injector was used. The separating column used in the UPLC is a BEH C18 column of 50 mm (length) \times 2.1 mm (diameter) dimension which was purchased from WATER. The hydrodynamic particles size distribution and zeta potential of the MWCNT solution were measured using the Malvern Zetasizer

(USA). The surface morphology of the modified graphite electrode was characterised using the Hitachi field emission SEM model SU8220 (Japan) which was also equipped with energy dispersive X-ray for the purpose of element composition analysis.

5.2.2 Particle size analysis of MWCNT suspension using dynamic light scattering method (DLS)

The particle size of the MWCNT in liquid was characterized using DLS, follow the method as proposed by Xu et al. (2011). but with slight modification (Xu et al., 2011). A solution of 1 mg mL^{-1} MWCNT-COOH was prepared in Britton-Robinson buffer. Subsequently, the suspended particles were centrifuged at $2000 \times g$ to remove the large carbon particles. The clear layer solution was pipetted into a cuvette. The zeta potential and particle size distribution of the carboxylic functionalised MWCNT particles was measured using the Malvern Zetasizer. The experiment was repeated for different pH conditions at values of 2, 4, 7, and 9 which had been adjusted using 1 mol L^{-1} sodium hydroxide solution.

5.2.3 MWCNT/graphite preparation

1 mg mL^{-1} solution of MWCNT-COOH was prepared using Britton Robinson buffer pH 7, subsequently the solution was centrifuged at $2000 \times g$; and $200 \mu\text{L}$ of this solution was pipetted onto the tip of the graphite. The casted solution was evaporated to dryness at 105°C for 3 h in the oven and the surface was cleaned with ultrapure water. Prior to use, the fabricated MWCNT/graphite sensor was kept in dry condition at room temperature (25°C).

5.2.4 Co-electrodeposition of gold nanoparticles and graphene oxide on MWCNT/graphite electrode

The gold and graphene oxide were electrodeposited onto the MWCNT/graphite electrode using the CV method. The following CV condition was used; applied potential

range from 0.9 to -1.3 V at a scan rate of 0.05 V s^{-1} for 16 cycles. The deposition solution used was $50 \mu\text{g mL}$ of graphene oxide and 0.1 mmol L^{-1} solution of tetrachloroauric acid prepared in 0.1 mol L^{-1} sodium nitrate. This prepared electrode is designated as Au–ErGO/MWCNT/graphite composite electrode and kept at room temperature (25°C) until further used.

5.2.5 Electrochemical characterisation of Au–ErGO/MWCNT/graphite electrode

The electrochemical properties of the Au–ErGO/MWCNT/graphite electrodes were characterised using the CV and electrochemical impedance spectroscopy (EIS) method. A 1.0 mmol L^{-1} solution of ferri/ferro cyanide was diluted 100 times from the stock solution using 1.0 mol L^{-1} sodium nitrate; and the solution was used as the redox species for the electrochemical characterisation. The CV experiment was performed using the following conditions; applied potential which begins at -0.2 V , with the first and second vertex potential corresponding to 1.0 and -0.4 V , respectively. Six different scan rates ranging from 0.1 to 1.0 V s^{-1} were performed for each CV study.

The EIS experiment was performed using Autolab potentiostat at the following conditions; applied potential at the electrode open circuit potential (OCP), and frequency range from 1.0 KHz to 0.1 Hz . The electrochemical characterisation experiment was also performed on the MWCNT/graphite and bare graphite. A 1.0 mmol L^{-1} solution of ferri/ferro cyanide solution was used as the redox species.

5.2.6 Morphology characterization of Au–ErGO/MWCNT/graphite sensor

The tip of the surface modified graphite electrode was disengaged with a pair of cutter. The surface of the tip was positioned upward and the bottom was adhered to the SEM sample platform using a carbon conductance tape. A low vacuum mode was used and the electron power was set at 2 keV ; the surface was observed at two different magnifications.

5.2.7 CV evaluation of DNA bases

Individual CV analysis of A, T, C and G were performed at an applied potential range from -0.4 to 1.9 V, with stop potential at -0.5 V and scan rate of 0.1 V s^{-1} . A 0.1 mol L^{-1} phosphate buffer (pH 7) was used as the supporting electrolyte. Prior to analysis, a blank scan was performed on the electrolyte and subsequently $300 \mu\text{L}$ of the individual DNA bases was spiked into the 15 mL of the supporting electrolyte to obtain a $20 \mu\text{g mL}^{-1}$ concentration of DNA bases. The experiments were performed using Au–ErGO/MWCNT/graphite and bare graphite for comparison purpose.

5.2.8 SWV analysis of nucleotide bases using Au–ErGO/MWCNT/graphite electrode

A SWV method was used for the determination of A, G, C and T. The following conditions were applied in the SWV method; with the scan potential beginning at 0.2 V , and end potential set at 1.9 V . The method frequency was set at 25 Hz , with a deposition potential of 0.2 V for 5 s . The SWV method was used in both individual and multiplex determination of DNA bases.

5.2.9 pH response study of individual A, G, T and C

The pH response study of individual A, G, T and C was performed using Britton Robinson buffer which was adjusted to the required pH using 1 mol L^{-1} of sodium hydroxide. A blank scan at a specific pH was performed first prior to the DNA bases analysis. In which $300 \mu\text{L}$ from the $1000 \mu\text{g mL}^{-1}$ stock standard of individual DNA bases was added later into the 15 mL blank solution and the SWV was performed using the Au–ErGO/MWCNT/graphite sensor. A linear correlation graph of peak potential (E_{pa}) versus the different pH conditions was plotted to deduce the possible oxidation mechanism on the sensor surface.

5.2.10 Impact study of different supporting electrolyte in multiplex determination using SWV with Au–ErGO/MWCNT/graphite sensor

The impact of electrolyte solution in multiplex detection of DNA bases was studied in four commonly used electrolytes which include Britton Robinson buffer, phosphate buffer, potassium chloride, and sodium nitrate. The concentration of the supporting electrolyte and DNA bases used in this study were corresponding to 0.1 mol L^{-1} and $20 \text{ } \mu\text{g mL}^{-1}$, respectively. The measurement was performed using SWV method as described in Section 5.2.8.

5.2.11 Analytical performance study for the multiplex determination of DNA bases using SWV with Au–ErGO/MWCNT/graphite sensor

The calibration linearity and dynamic range were performed by standard addition using a variable volume of a mixed DNA bases standard; the dynamic range for each DNA bases were assessed up to $150 \text{ } \mu\text{g mL}^{-1}$. For the limit of detection (LOD) study, a serial dilution of a $2 \text{ } \mu\text{g mL}^{-1}$ mixed DNA based standard was performed down to $0.1 \text{ } \mu\text{g mL}^{-1}$. The limit of quantification (LOQ) of the method was calculated at 5 times the standard deviation of the LOD. All the measurements were performed using the SWV method as described in Section 5.2.8. 0.1 mol L^{-1} phosphate buffer at pH 7 was used as the supporting electrolyte.

5.2.12 Acid hydrolysis and DNA composition analysis in real sample

For the DNA extraction work from the real samples (onion), 40 g of chopped onion was suspended in a 500 mL of ultrapure water. Subsequently, 1.0 g of sodium dodecyl sulfate and 3.0 g of sodium chloride were added, and the solution was blended using homogeniser. The solution was filtered, and the clear solution was transferred into a test tube; whereby absolute ethanol was used to precipitate the DNA. Subsequently, the DNA

was collected from the ethanol layer (upper) by spooling using a glass rod and then dried overnight.

For acid hydrolysis work, 8 mg of DNA samples was hydrolysed in 4 mL of sulfuric acid (8 mol L^{-1}). The solution was sonicated at 60°C for 10 min and heated in boiling water for 5 h. The obtained clear solution was neutralised with 8 mL of sodium hydroxide solution (8 mol L^{-1}), and filled up to 30 mL with phosphate buffer pH 7 (0.1 mol L^{-1}) solution. The sample solution was further diluted to 5 folds with electrolyte solution (0.1 mol L^{-1} phosphate buffer, pH 7.4) and the DNA bases composition of the prepared samples were determined using the SWV method as described in Section 5.2.8. A standard addition method was used to determine the concentration of all four DNA bases (A, C, G, T) in the samples. To further evaluate the method reliability, a standard of 25, 50 and 75 mg L^{-1} DNA nucleic acid bases standard were spiked into the samples and the percentage recovery was determined.

5.2.13 Validation of DNA nucleic acid bases analysis in real samples using ultra-performance liquid chromatography with photo diode array detector (UPLC-PDA)

Calf thymus and onion DNA were prepared according to Section 5.2.12. The prepared sample was cleaned with a $0.2 \mu\text{m}$ syringe nylon filter and transferred into a 1.5 mL vial. A standard addition method was used by adding a known amount of A, C, T, and G into the samples. A total of 7 standard additions that range from 0 to $40 \mu\text{g mL}^{-1}$ were prepared for the sample analysis. The following analytical conditions were used for the analysis of the A, G, T and C; ultrapure water was used as the mobile phase line A and phosphate buffer (pH 7) of concentration 0.1 mol L^{-1} was used as the mobile phase B. An isocratic mode was employed with the ratio of A to B was set at 90:10; a flow rate of 0.25 mL min^{-1} and injection volume of $2 \mu\text{L}$ were set in the UPLC system. The chromatogram for

simultaneous detection of the 4 DNA nucleotide bases was extracted at 254 nm. The calibration linearity and dynamic range was performed using a mixed standard prepared from 0.4 to 50 $\mu\text{g mL}^{-1}$. For LOD determination, a serial dilution of a 2 $\mu\text{g mL}^{-1}$ was prepared by further diluting down to 0.1 $\mu\text{g mL}^{-1}$. The LOQ of the UPLC method was determined at 5 times the standard deviation of the LOD. To further evaluate the UPLC method reliability, a recovery study of the spiked standard at 25, 50 and 75 mg L^{-1} DNA nucleic acid bases standard into the real samples matrix was studied.

5.2.14 Selectivity and stability evaluation of Au–ErGO/MWCNT/Graphite electrode

The selectivity of the Au–ErGO/MWCNT/graphite in detection of A, G, T and C was performed by studying the current response of the DNA bases in the presence of common interferences; including uracil, niacinamide, pantothenic acid, L–cysteine, L–serine, L–glutamine, L–tyrosine, glucose and minerals such as sodium, potassium and chloride. Prior to the interference analysis, the current response of a 20 $\mu\text{g mL}^{-1}$ mix standard of A, G, T and C was measured using SWV method as described in Section 6.2.3. Subsequently, 20 $\mu\text{g mL}^{-1}$ of the individual interference was added into the solution, and the current response for each DNA bases was measured again. The recovery percentages of the DNA bases were calculated using the following formula, whereby I_b and I_a are corresponding to the current response of the individual DNA bases in the presence (I_b) and absence (I_a) of interference substances, respectively:

$$\% \text{ recovery} = I_b \div I_a \times 100$$

The electrode stability was also evaluated by measuring the current response of the DNA bases throughout the one month duration. The study was performed under two different conditions: at room temperature (25°C) and 45°C; with the measuring frequency

set at interval day of 1, 3, 5, 7, 14, 21, and 28 days. A SWV method as described in Section 6.2.3 was used for the measurement of the current response.

5.3 Results and discussion

5.3.1 Characterisation of MWCNT–COOH particles

In search for an optimum pH condition for the deposition of MWCNT–COOH nanoparticles on graphite surface, a dynamic light scattering (DLS) analysis was performed across the different pH conditions of MWCNT-COOH solution. DLS is often used for the measurement of spherical particles and surface charge; nevertheless, it can still be used for the determination of hydrodynamic diameter, which takes into account the MWCNT–COOH particle length (Xu et al., 2011). Fig. 5.1 illustrates the particle size and surface charge of the MWCNT-COOH particles across the different pH conditions that were measured using DLS. With the increased of pH from 2 to 7, the hydrodynamic particles size was observed to increase from 174 nm (pH 2) to 397 nm (pH 7) and eventually drop at pH 9 (66 nm). This showed that at pH 7 the hydrodynamic particle size of the MWCNT–COOH was optimal. A larger hydrodynamic particle size suggests a longer length of the MWCNT and this is preferable as it could reduce the degree of the nano–tubes junction on the electrode surface, in comparison to the shorter length, the MWCNT particle has a tendency to bundle together; as a result, higher numbers of nanotubes junction will be created on the electrode surface, which could reduce the electrode conductivity properties (Saha et al., 2014).

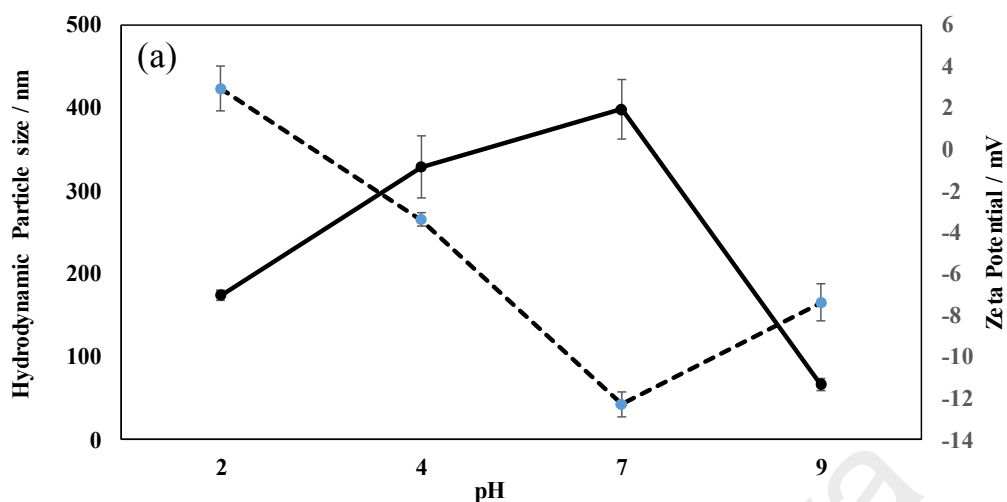


Figure 5.1: Hydrodynamic particle size (solid line) and surface zeta potential (dashed line) of MWCNT–COOH particles suspended in Britton Robinson buffer across pH 2, 4, 7 and 9.

At the same pH 7, the surface charge of the MWCNT particles were also observed to be the highest (negative values) with zeta potential of -12.3 mV, in comparison to pH 2 (2.9 mV), 4 (-3.4 mV) and pH 9 (-7.4 mV). A greater surface charge (negative charge) on the MWCNT is preferable, as the repulsive hindrance between the charged particles could improve the dispersion of the colloid particles (Liu et al., 2011). This surface charge could be explained by the de-protonation of the functionalised carboxylic group (COOH) to carboxylate (COO⁻), which depends on the dissociation constant (pK_a) of the carboxylic functional groups. At pH 7, the surface charge (negative) was also the highest which suggests a more stable suspension than that at pH 9, which is evidenced by the largest hydrodynamic particle size of the MWCNT–COOH nanomaterial with less breakage and hence is more stable. Whereas, at pH 9 the particles are less charged and could be subject to inter-particle collision that leads to breakage into smaller particle. At pH 9 also, the surface charge of MWCNT was lower than expected, which could be explained by the removal of the OH or COOH functional groups from the MWCNT-COOH to form an activated MWCNT (Kashyap et al., 2014). As a result, it has a lower COO⁻ anion and surface charge (negative) on the surface.

5.3.2 Surface casting and electrochemical characterisation of MWCNT/graphite sensor

To further evaluate the performance of MWCNT particles on the graphite sensor, a dry casting method was employed to deposit the nanomaterial onto the graphite surface and subsequently the solution was heated to dryness that allows the MWCNT particles to deposit on the graphite surface. This fabricated sensor was designated as MWCNT/graphite. Fig. 5.2 illustrates the schematic flow of the MWCNT/graphite sensor fabrication.

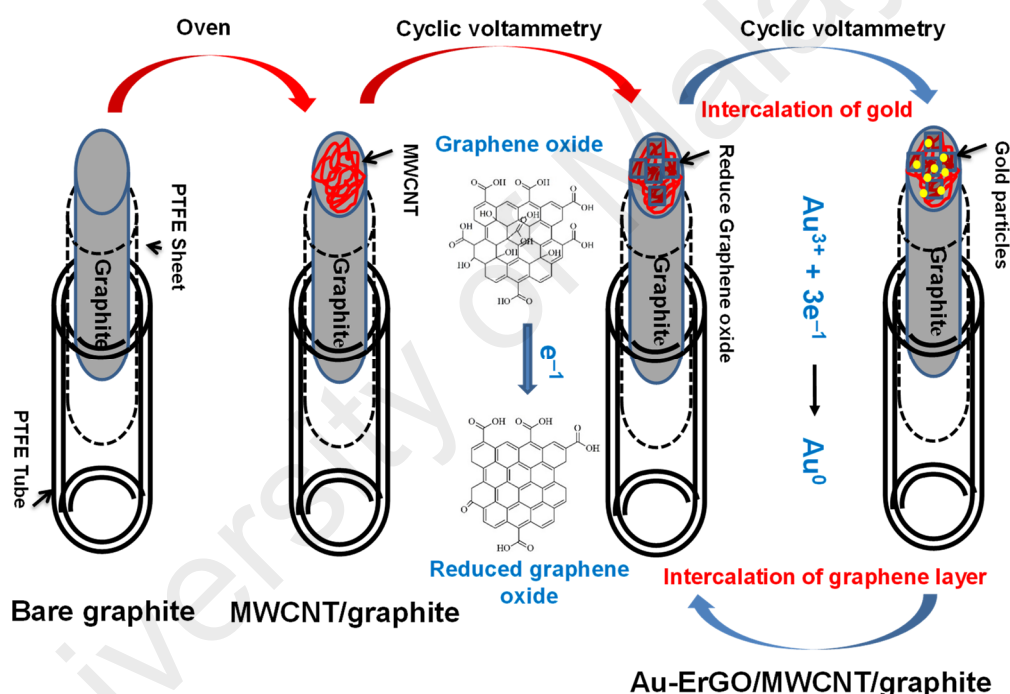


Figure 5.2: Schematic flow of Au–ErGO/MWCNT/graphite sensor fabrication.

The electrochemical characteristic of the MWCNT/graphite sensor was assessed using CV, with ferricyanide used as the redox species. The Eff A, and heterogeneous electron transfer rate (k_s) of the MWCNT/graphite were determined using Randles-Sevchik's and Laviron's equation, respectively. The procedure and principle of the equation were elaborated in detail under Chapter 3, Section 3.3.4.3. For a more comprehensive evaluation of the MWCNT deposition, the characterisation was assessed across the

different pH conditions in MWCNT solution, which the CV versus various scan rates were illustrated in Fig. 5.3. This is for a better correlation to the DLS finding that discussed in subsection 5.3.1.

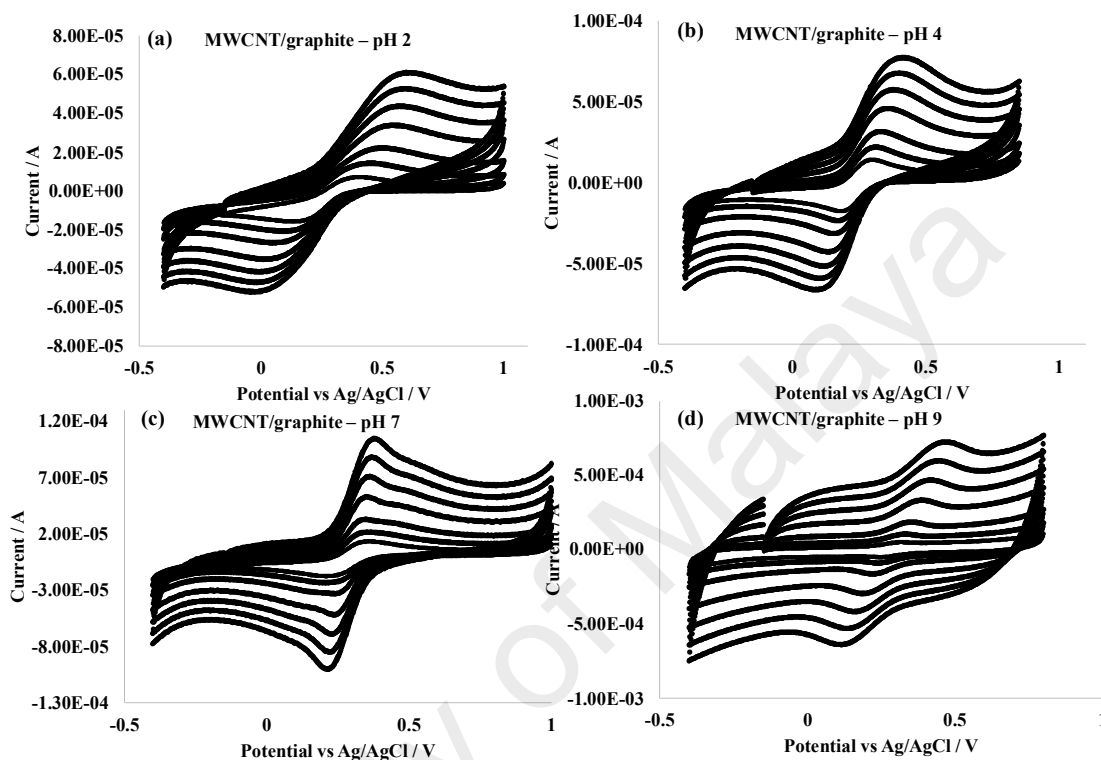


Figure 5.3: CV of MWCNT/graphite that prepared at different pH. The experiment was performed in a 1 mmol L^{-1} ferricyanide solution at scan rate of (0.05, 0.10, 0.20, 0.40, 0.60, 0.80 and 1.00 V s^{-1}).

Fig. 5.4 illustrates the heterogeneous electron transfer rate (k_s) of the surface modified graphite electrode across the different pH conditions preparation of MWCNT-COOH electrode, which was calculated based on Laviron's equation (Cretu et al., 2006). At pH 4, the k_s of MWCNT-COOH/graphite were found to be slightly higher as compared to the bare electrode. However, at pH 2 and 9, no improvement in k_s was observed (Fig. 5.4). This could be associated to the bundling of the MWCNT-COOH particles on the graphite surface, as both conditions have shown a lower hydrodynamic particle size (Fig. 5.1); as a result it has formed a densely packed nano-tubes junction on the graphite surface that impeded the electron transfer properties of the MWCNT/graphite sensor. In contrast, a significant increase in the k_s was observed at pH 7, with the

heterogeneous electron transfer rate at $8.1 \pm 0.6 \text{ s}^{-1}$ showing a much-improved conductivity of the MWCNT modified graphite electrode, which could be associated to the length and nanotubes junction of the MWCNT–COOH particles. The bare graphite does not show any significant change in the k_s throughout the different pH conditions prepared using blank solution (buffer only) from pH 2 to 9. Table 5.1 summarises the k_s values of the MWCNT/graphite sensor that was prepared under different pH conditions.

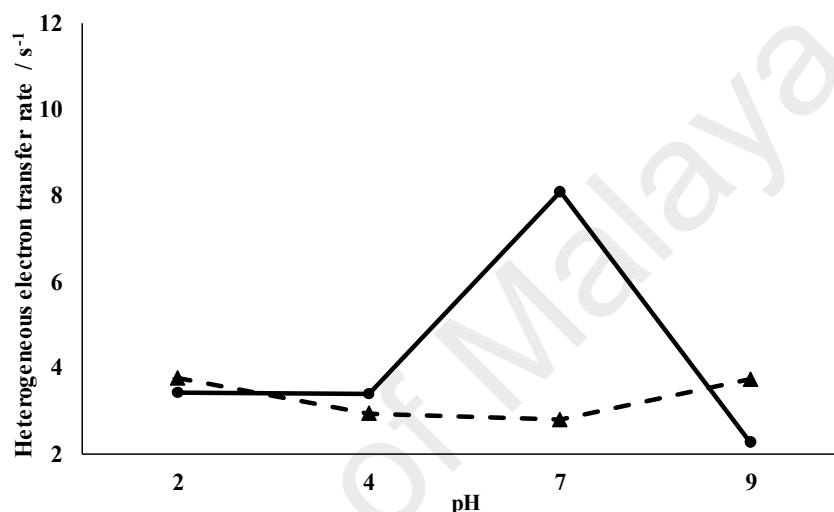


Figure 5.4: Heterogeneous electron transfer rate of the bare graphite (dashed line), and MWCNT–COOH/graphite (solid line) that was prepared at different pH conditions.

On the other hand, the highly nanotubes junction of MWCNT–COOH at pH 9 prepared electrode has also shown an increase in the capacitance current, which could associate to its rougher surface (Pajkossy, 2005). Fig. 5.5 (a) illustrates the CV of ferri/ferrocyanide performed using MWCNT-COOH/graphite prepared at pH 7 and 9 at a scan rate of 0.2 V s^{-1} . The thickness of the CV obtained for pH 9 is much thicker than pH 7, which indicates a higher capacitance current on the modified electrode surface that could potentially affect the sensor sensitivity (Pajkossy, 2005). To the MWCNT/graphite preparation at pH 2 and 4 the resulting ferricyanide CV are illustrated in Fig. 5.5 (b), which was also performed

at a scan rate of 0.2 V s^{-1} . The thickness of CV obtained at pH 2, 4 and 7 does not show any significant difference in terms of the capacitance current.

Table 5.1: Electrochemical characterisation of MWCNT/graphite electrode by CV.

No	pH	¹ Eff A, cm^2	² k_s , s^{-1}	³ ΔE_p , mV
1	2	0.032 ± 0.002	3.4 ± 0.21	418 ± 24
2	4	0.062 ± 0.001	3.4 ± 0.04	249 ± 4
3	7	0.108 ± 0.004	8.1 ± 0.56	93 ± 1
4	9	0.318 ± 0.070	2.3 ± 0.02	116 ± 3

¹ Effective surface area

² Heterogeneous electron transfer rate

³ ΔE_p = anodic potential (E_{pa}) – cathodic potential (E_{pc})

The electron transfer efficiency (ΔE_p) can be calculated from the potential (Volt) difference between anodic (E_{pa}) and cathodic (E_{pc}) peak. According to Nernst's equation (Chapter 3, Section 3.3.6.2) for a single electron transfer process, the difference in the peak potential is equivalent to 59.16 mV. The ΔE_p values was determined for the MWCNT/graphite prepared at each pH 2, 4, 7 and 9 (refer Fig. 5.5 (b)), which were corresponded to 418 mV, 249 mV, 93mV and 116 mV, respectively. This could infer that at pH 7, the prepared MWCNT/graphite shows better electron transfer efficiency, with the ΔE_p obtained was found to be closer to 59.16 mV.

The effective surface area of the MWCNT–COOH/graphite electrode was determined using the Randles-Sevcik equation. Fig. 5.6 illustrates the plot of Eff A versus the different pH preparation conditions of the MWCNT–COOH/graphite electrode. The Eff A of bare graphite was found to be constant regardless of the pH conditions with an average Eff A value of $0.037 \pm 0.005 \text{ cm}^2$. At acidic pH conditions (pH 2 to 4), the Eff A of the MWCNT–COOH/graphite does not show much improvement when compared to the bare graphite, only the sensor prepared at pH 4 shows a slight increment of Eff A to $0.062 \pm 0.001 \text{ cm}^2$. In contrast to the MWCNT/graphite that was

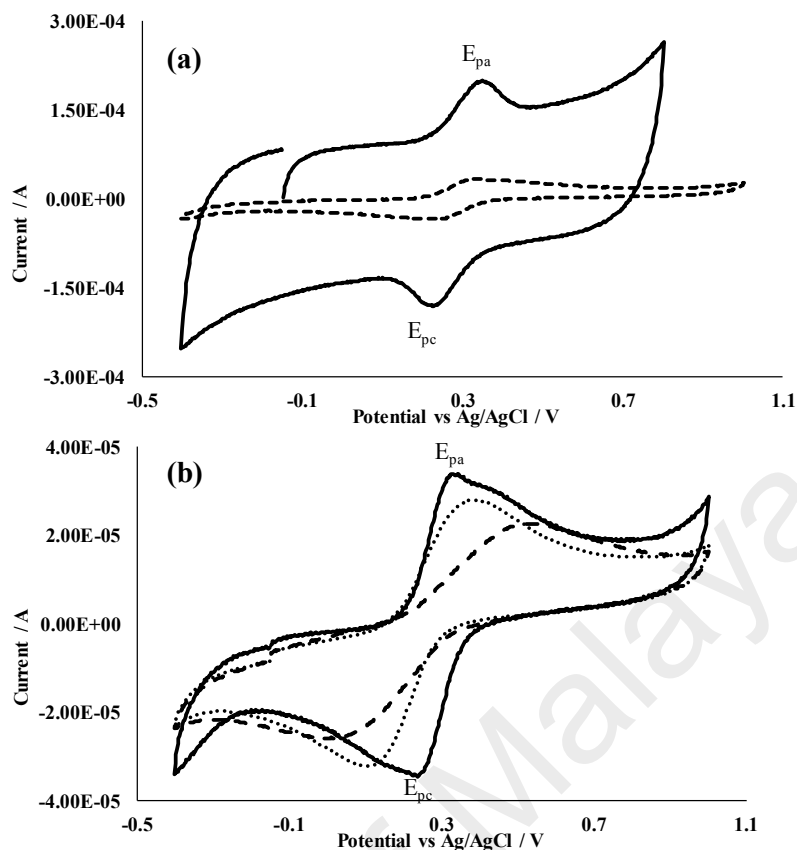


Figure 5.5: (a) CV of ferricyanide that was performed using MWCNT-COOH/graphite electrode prepared at pH 9 (solid line) and pH 7 (dashed line) conditions. (b) CV of ferricyanide that was performed using MWCNT-COOH/graphite electrode prepared at pH 7 (solid line), pH 4 (dotted line) and pH 2 (dashed line) conditions.

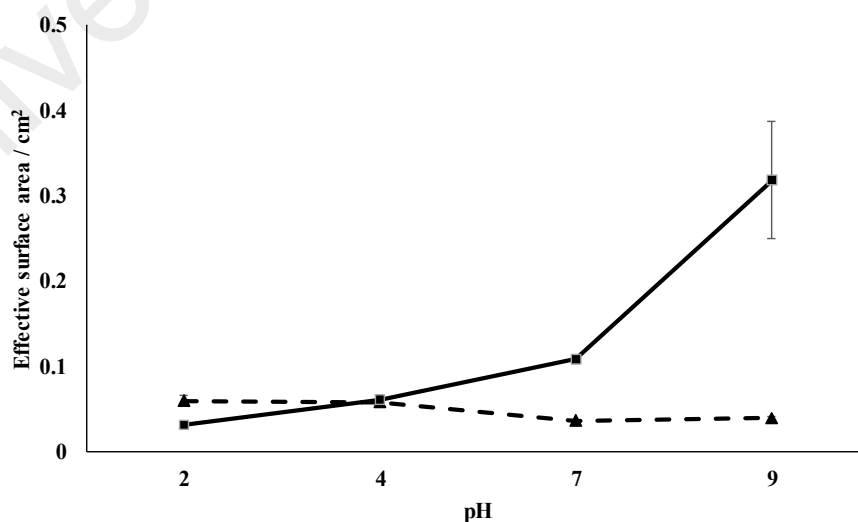


Figure 5.6: Eff A of bare graphite (dashed line) and MWCNT-COOH/graphite electrode (solid line) that was prepared at different pH condition.

prepared at pH 7 and 9, the Eff A expanded to $0.108 \pm 0.003 \text{ cm}^2$ (3 folds) and $0.318 \pm 0.069 \text{ cm}^2$ (9 folds), respectively. MWCNT/graphite prepared at pH 9, showed the greatest expansion on the surface area than pH 7, 4 and 2; which could be explained by the bundle deposition of activated MWCNT (MWCNT without the COOH functional group) instead of COOH-MWCNT, which the former contained more redox site (site for electron transfer takes place) that has been freed from the previous occupied COOH or OH group on the MWCNT surface. At alkaline condition (pH 9), the defunctionalisation of COOH and OH functional groups from MWCNT could occur (to become activated MWCNT) (Kashyap et al., 2014). Greater Eff A is preferable in the electrode fabrication, as this attribute could increase the availability of electro-active site for redox reaction and contribute to the current amplification (Liu et al., 2014; Radhakrishnan et al., 2015), as a result it could improve the electrode sensitivity. However, at pH 9 an enormous surface area of activated MWCNT will contribute to the greater charging of the electrode-electrolyte interface (Helmholtz layer); consequently increase the capacitance current, which can be observed in Fig. 5.5 (a). As a result, it could impede the faradaic current and therefore not favourable to the sensor development. Besides, an activated MWCNT (without functionalized) is not favourable in comparison to MWCNT-COOH, as it becomes unstable over times and agglomeration due to the absent of charge repulsion by the COO⁻ group (Liu et al., 2011); this is consistent to the DLS result as discussed in Section 5.3.1. Table 5.1 summarises the Eff A values, k_s and ΔE_p of the MWCNT/graphite sensor that was prepared under different pH conditions.

The first layered MWCNT-COOH/graphite electrode possesses the properties of good electron transfer rate and also large surface area, which is an important criteria to form an electron conductive network and greater deposition area for graphene and gold. pH 7 was selected as the optimum pH condition for the preparation of MWCNT-COOH/graphite electrode; this is because the k_s and ΔE_p of the electrode was the most optimum. Although

the Eff A of the electrode was lower as compared to pH 9, nevertheless the electron transfer properties and capacitance are the most optimum; moreover the electrode prepared at pH 9 shows a high capacitance current (Fig. 5.5) that could mask the faradic current, and affects the electrode sensitivity. As a conclusion, MWCNT/graphite prepared at pH 7 was selected for further investigation study on Au–ErGO/MWCNT/graphite sensor.

5.3.3 Co-electrodeposition of gold and graphene oxide on MWCNT-COOH/graphite surface

The gold and graphene oxide (Au–ErGO) were co-electrodeposited as a second layer to the MWCNT-COOH/graphite electrode using CV. The deposited ErGO is referring to the characteristic of an electrochemically reduced graphene oxide (ErGO).

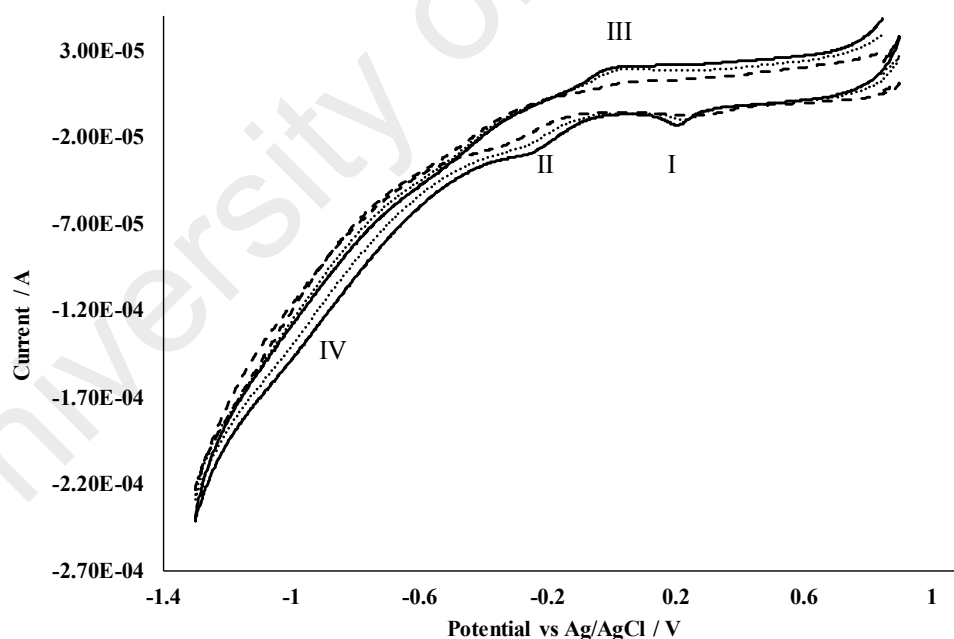


Figure 5.7: CV of the co–electrodeposition of gold and graphene oxide on MWCNT–COOH/graphite surface at 1st cycle (dashed line), 8th cycle (dotted line) and 16th cycle (solid line).

Fig. 5.7 illustrates the CV of the Au–ErGO deposition on MWCNT–COOH/graphite, the CV scan was performed from anodic (0.9 V) to cathodic potential (-1.3 V); which

observed a series of cathodic peak at potential of 0.23 V (I), -0.23 V (II) and -0.95 V (IV); and anodic peak at potential 0.01 V (III). At peak (I) of potential 0.23 V, the cathodic current had shown an increment trend on the subsequent CV scan (deposition), which suggests a reduction (electrodeposition) of the tetrachloroauric acid to its elemental gold on the MWCNT-COOH/graphite surface. The other cathodic peak (II and IV) and anodic peak (III) were belong to the graphene deposition (Chen et al., 2011), with peak II and III which could possibly be a reversible redox process of graphene functionalised oxide group (O, OH). At peak IV, the cathodic peak current was increased with a subsequent CV scan, which could be associated to the irreversible reduction of graphene oxide (ErGO) on the MWCNT-COOH/graphite surface. The gold particle was postulated to intercalate with ErGO, when performing CV scan from a positive (0.9 V) to negative potential (-1.3 V); suggesting the gold was deposited first, which was followed by graphene. Therefore, with a subsequent CV scan the gold particle was intercalated in between the ErGO sheet (Fig. 5.6). This is evidenced from the study conducted on Au-NPs/graphite electrode preparation which was described in Chapter 3, Section 3.3.1, whereby the Au cathodic peak was shifted to a higher positive potential with subsequent CV scan, because of the thermodynamically favour of gold deposition on its substrate (nuclei growth) instead of carbon (Chapter 3, Section 3.3.1). However, in the deposition of Au-ErGO on MWCNT/graphite surface, the Au was found to have been reduced at a potential of 0.24 V (1st deposition) to 0.23 V (16th deposition) without any significant shift to the lower positive potential; at the meantime, the peak showed an increasing trend in cathodic current (I_{pc}) over the subsequent CV scan (Fig. 5.7). This could infer that the gold could have been reduced at a new carbon substrate site instead of the gold substrate itself (no shifting of peak potential); and has evidence the possibility of intercalation of gold in between the graphene layers. This unique polymorph could prevent the graphene from agglomeration among themselves that eventually converted into graphite, beside

such polymorph has also improved the signal response of the electrode, which the gold can function as an electron transporter between the graphene sheet (Liu et al., 2011). The agglomerated graphene sheet that forms graphite will change the electrochemical properties of graphene, which as a result will lose its electro-catalytic properties in the Au–ErGO/MWCNT/graphite fabrication. The slight negative potential shift (10 mV) observed in the Au peak (Fig. 5.7) could be explained by the subsequent increase in the graphene layer that could improve the overpotential of Au reduction on the Au–ErGO/MWCNT/graphite electrode surface.

The gold deposition is also evidenced by the electrochemical reduction of the electrode using a 0.5 mol L^{-1} sulfuric acid (H_2SO_4), as shown in Fig. 5.8. The characteristic Au peak was reduced at a potential of 0.85 V. To confirm this, a solely gold nanoparticles deposition was prepared on MWCNT/graphite (Au–NPs/MWCNT/graphite); in which a similar voltammogram was observed that could also exhibit a single gold cathodic peak at the same potential (0.85V).

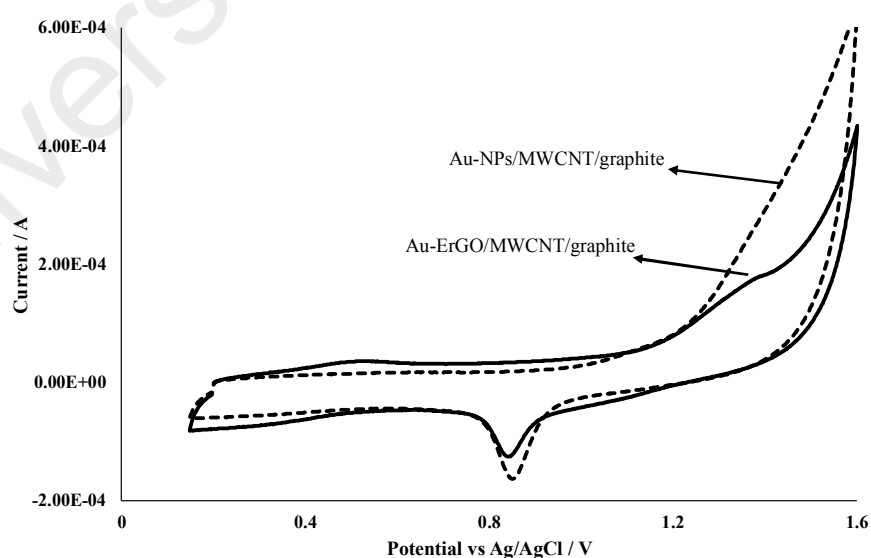


Figure 5.8: CV of gold nanoparticles/MWCNT–COOH/graphite versus Au–ErGO/MWCNT–COOH/graphite tested in 0.1 mol L^{-1} sulfuric acid solution.

5.3.4 Optimization of Au–ErGO deposition cycle

To optimise the number of Au–ErGO deposition cycle on the MWCNT/surface; the electrochemical performance of the resulting Au–ErGO/MWCNT/graphite sensor was assessed; and Fig. 5.9 show the CV of the prepared sensor at various scan rates.

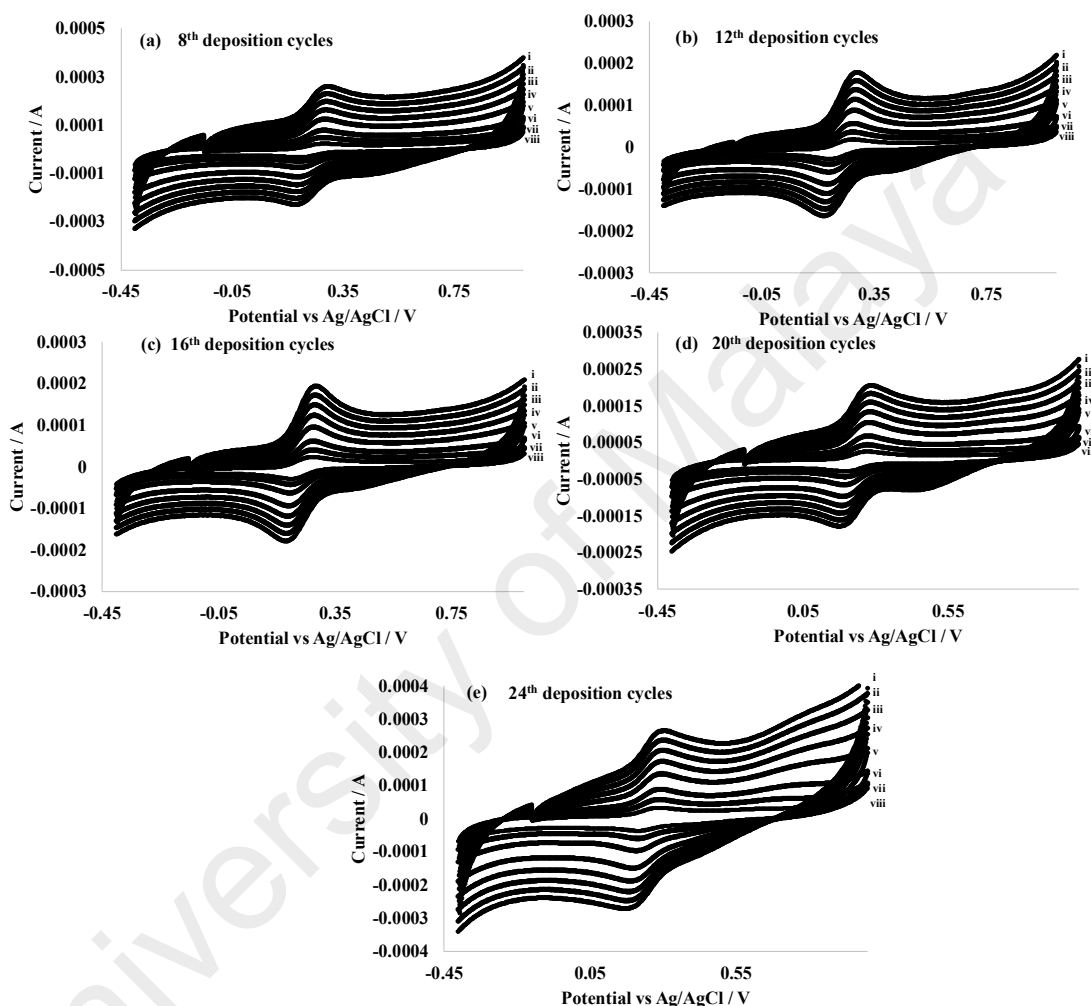


Figure 5.9: CV of Au–ErGO/MWCNT/graphite prepared at (a) 8th; (b) 12th; (c) 16th; (d) 20th; (e) 24th deposition cycles. The experiments were performed at 1.0 mmol L⁻¹ ferricyanide solution at various scan rate from i to viii corresponds to 0.05, 0.1, 0.2, 0.4, 0.6, 0.8, 1.0 and 1.2 V s⁻¹.

Subsequently; Fig. 5.10 illustrates the electro–deposition cycle number versus the Eff A and heterogeneous electron transfer rate (k_s) of Au–ErGO/MWCNT/graphite electrode, both electrochemical properties were calculated using the Randles Sevcik and Laviron equation respectively. From 8th to 16th deposition cycles, the effective surface and k_s had

shown an increased trend, with 16th deposition cycle giving the most optimum values of both Eff A and k_s with values of 0.15 cm² and 27 s⁻¹, respectively.

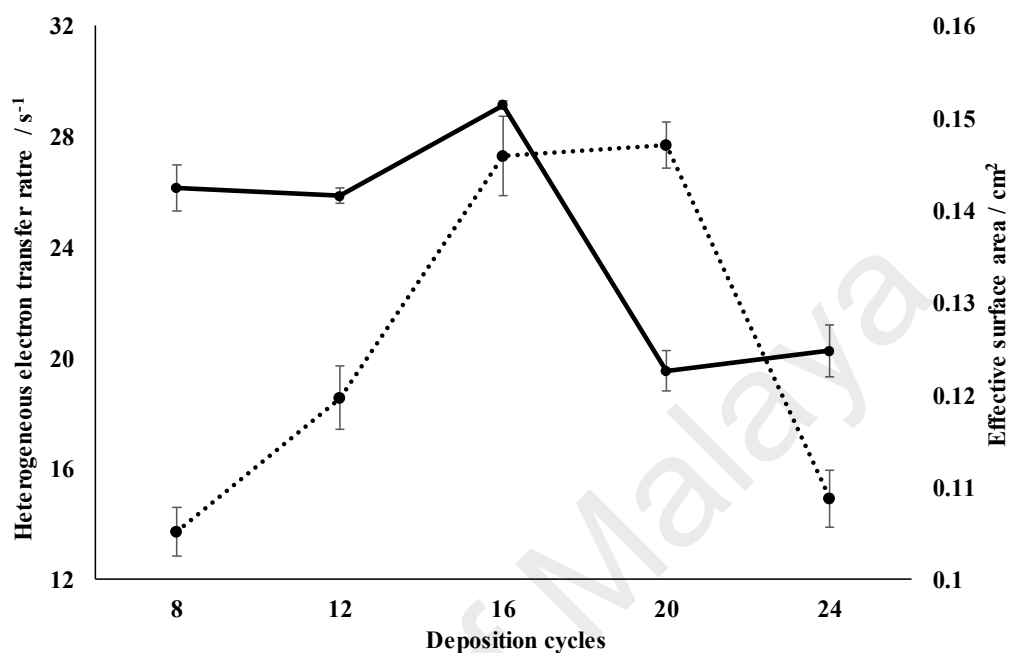


Figure 5.10: Graph of heterogeneous electron transfer rate (solid line) and effective surface area (dotted line) versus the co-electrodeposition cycle number of gold and graphene oxide.

However, with the subsequent deposition of above 20th cycles, a drop in the Eff A was observed. It was postulated that with a higher cycle number, the graphene had possibly agglomerated due to over deposition that stack the graphene together, and this impeded the electrode surface area. Nevertheless, the k_s was still optimum which could be contributed by the gold nanoparticles. Table 5.2 summarises the electrochemical attributes of Au–ErGO/MWCNT/graphite electrode over the different deposition cycles. From this evaluation 16th deposition cycles were selected as the optimum co–electrodeposition condition and the developed working electrode was designated as the Au–ErGO/MWCNT/Graphite composite electrode.

Table 5.2: Electrochemical characterization of Au–ErGO/MWCNT/graphite electrode over the different deposition cycle by CV.

No	¹ DP cycle	² Eff A, cm ²	³ k _s , s ⁻¹	⁴ ΔE _p , mV
1	8	0.142 ± 0.003	13.7 ± 0.9	77 ± 0.8
2	12	0.141 ± 0.001	18.6 ± 1.1	77 ± 1.6
3	16	0.151 ± 0.001	27.3 ± 1.5	73 ± 1.4
4	20	0.122 ± 0.002	27.7 ± 0.8	75 ± 1.6
5	24	0.125 ± 0.003	14.9 ± 1.0	74 ± 0.5

¹ Deposition cycle

² Effective surface area

³ Heterogeneous electron transfer rate

⁴ ΔE_p = anodic potential (E_{pa}) – cathodic potential (E_{pc})

5.3.5 Electrochemical impedance spectroscopy analysis of Au–ErGO/MWCNT/graphite

The electron transfer resistance of the fabricated electrode was evaluated using electrochemical impedance spectroscopy (EIS). Fig. 5.11 shows the Nyquist plot of Au–ErGO/MWCNT–COOH/graphite electrode, in which a two-small semicircle line can be observed. A semicircle graph in the EIS plot suggests that a measurable resistance of electron transfer between the electrode-electrolyte interface, which was obviously observed in the bare graphite electrode (Fig. 5.11). The two semi-circle lines of Au–ErGO/MWCNT/graphite, suggest the developed nanocomposite Au–ErGO/MWCNT/graphite has a low resistance to electron transfer. To further investigate the electron transfer resistance of Au–ErGO/MWNCT/graphite, a fitting to the modified Randles circuit model was performed.

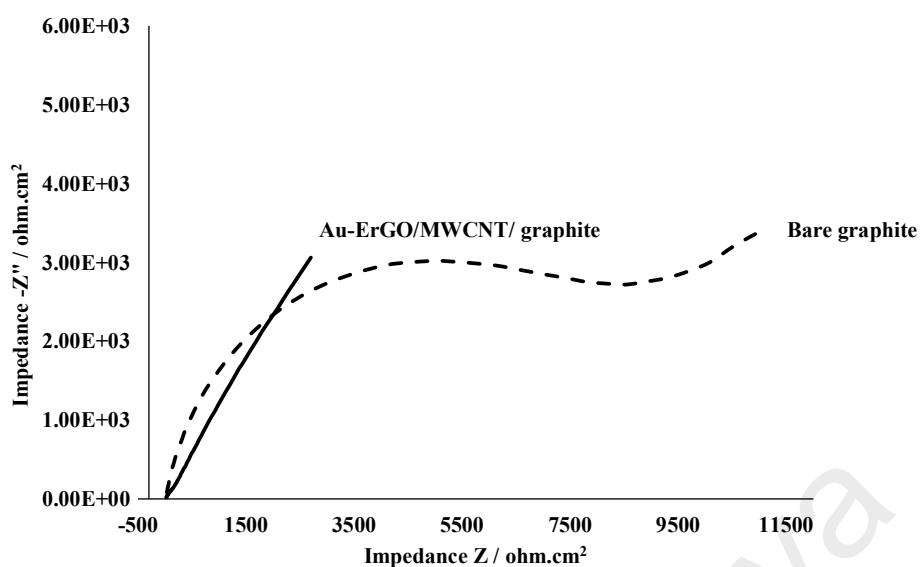


Figure 5.11: Nyquist plots of Au–ErGO/MWCNT–COOH/graphite (solid) and bare graphite (dotted) electrode performed in ferricyanide solution (1 mmol L^{-1}).

The developed nanocomposite Au–ErGO/MWCNT/graphite sensor is fitted to the circuit model as illustrated in Fig. 5.12. With the R_{sol} , R_{ct} , C_{dl} , and W corresponded to the electrolyte resistance (ohm), the electron transfer resistance (ohm cm^2), the double layer capacitance (F), and Warburg's diffusion. The fitted circuit is slightly different from the Randles circuit (as discussed in Chapter 3, Section 3.3.5), with a slight modification that includes additional R_{ct} and C_{dl} element that connect in serial to the Randles circuit

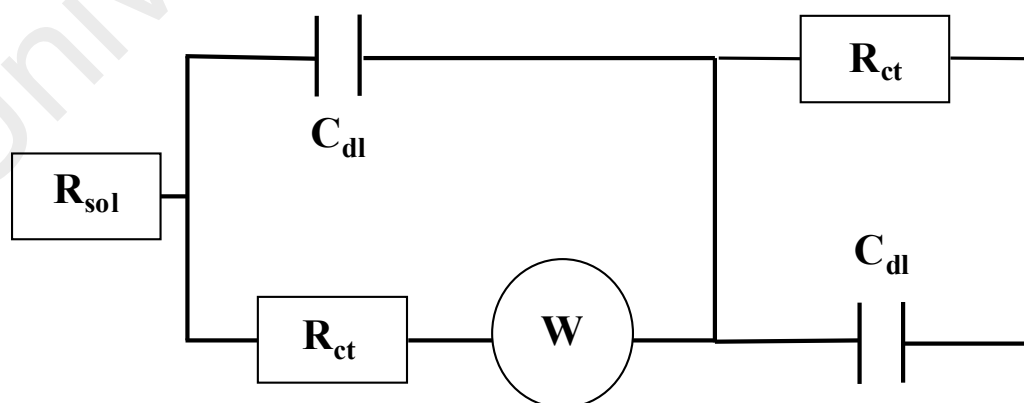


Figure 5.12: Modified Randles-circuit model that represents an electrochemical interface of Au–ErGO/MWCNT/graphite sensor.

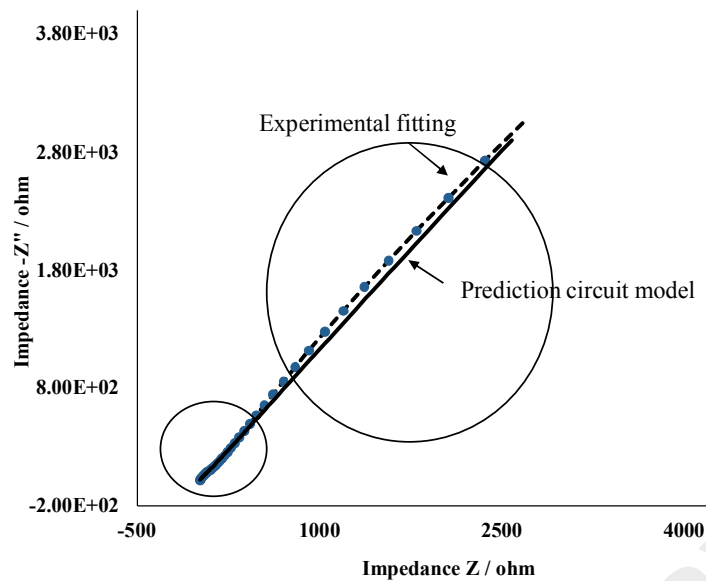


Figure 5.13: Nyquist plot fitting between the experimental data and the prediction model of Nyquist plot which was performed using Au–ErGO/MWCNT/graphite.

This additional circuit is related to the additional capacitance of the nanostructure, which could be MWCNT (first layer) in the sensor and the circuit is without any diffusion element; as the MWCNT function as the electron mediator (Hrady et al., 2013). Fig. 5.13 illustrates the Nyquist plot of the circuit fitting, that fit between experimental data obtained and circuit prediction data (theoretical data), which the result showed a good correlation between the two set of data, with the chi square fitting (χ^2) of 0.0978.

From the circuit model fitting, the electron transfer resistant (R_{ct}) of Au–ErGO and MWCNT layer were corresponded to 189 Ohm cm^2 and 2.6 Ohm cm^2 , respectively. This suggests the electron transfer process on the sensor-electrolyte interface (Au–ErGO) is favourable with a low resistance (189 Ohm cm^2); and the resistance between the MWCNT mediator with Au-ErGO layer is almost insignificant (2.6 Ohm cm^2). The bare graphite fit to Randles's circuit (as discussed in Chapter 3, Section 3.3.5) with R_{ct} values of 2450 Ohm cm^2 , suggests that the fabricated Au–ErGO/MWCNT/graphite is 13 folds much improved in the electron transfer properties.

5.3.6 Morphology evaluation of the Au-ErGO/MWCNT/graphite

The electrode surface of the AU-ErGO/MWCNT-COOH/graphite was studied using a field emission scanning electron microscopy (FE-SEM). Fig. 5.14 illustrates the SEM image of the (a), bare graphite (b) MWCNT/graphite and (c) composite Au-ErGO/MWCNT/graphite electrode. The electrochemical reduced graphene oxide sheet (ErGO) and gold nanoparticles were evidenced in Fig. 5.14 (c), while the ErGO is shown to be a wrinkled and flexible sheet like appearance. The surface of the bare graphite (Fig. 5.14, image a) was smooth, and with clean surface without any particle as can be observed. From the Fig. 5.14 (d) the image of the MWCNT is evidenced to be a tubular long shape structure, and it is observed to be distributed homogenously on the surface.

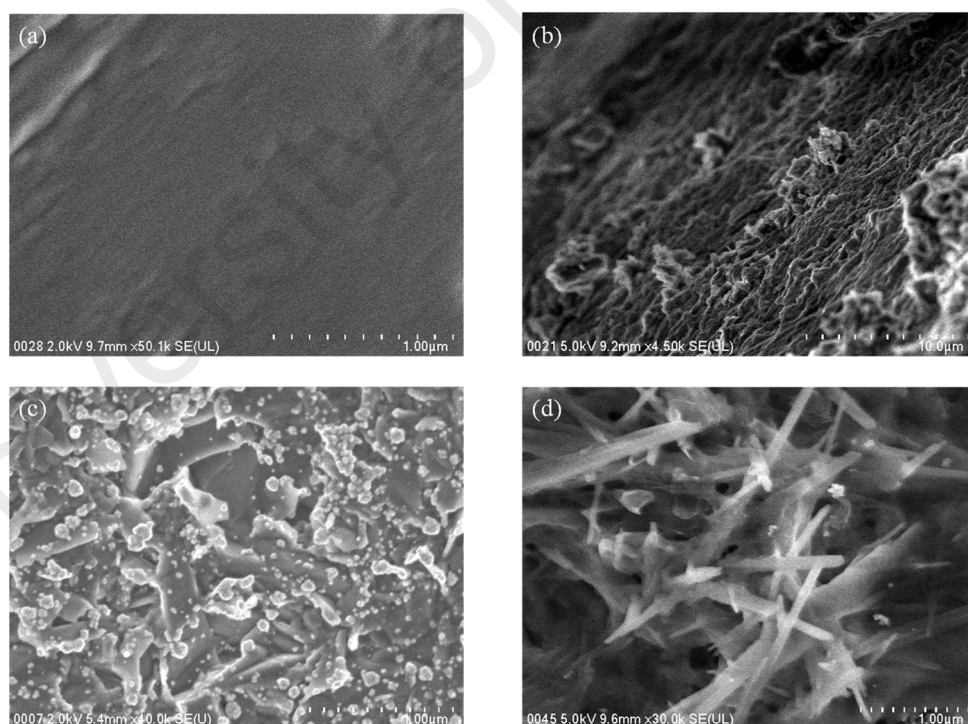


Figure 5.14: SEM images of (a) bare graphite electrode. (b) MWCNT-COOH/graphite electrode at 4500x magnification. (c) Au-ErGO/MWCNT-COOH/graphite electrode at above 30,000x magnification. (d) MWCNT-COOH/graphite electrode at 30,000x magnification.

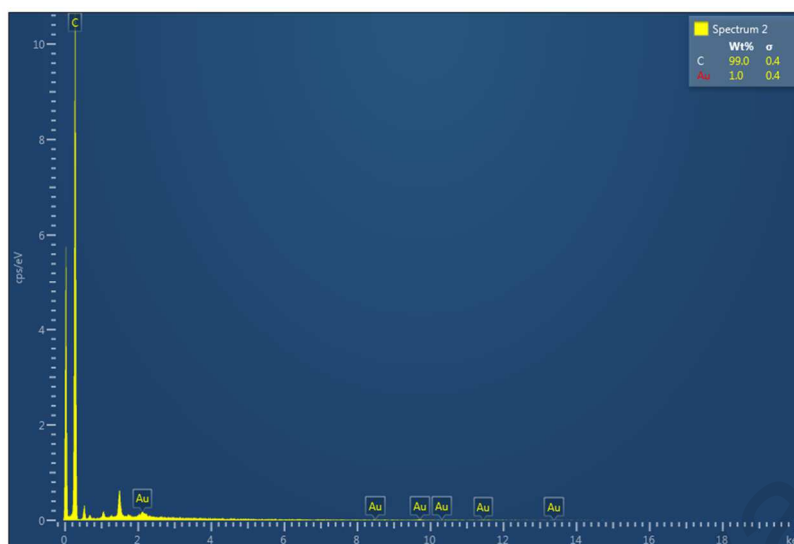


Figure 5.15: EDX spectral of Au–ErGO/MWCNT/graphite surface sensor.

The gold nanoparticle on the Au–ErGO/MWCNT/graphite surface was confirmed using EDX analysis. The EDX spectrum is illustrated in Fig. 5.15, which shows the amount of gold and carbon at an approximate 1.0% and 99%, respectively. The gold nanoparticles were observed under the SEM (Fig. 5.14, image C) as irregular shape and with an average diameter measured in between 70 to 130 nm.

5.3.7 Electrochemical characteristic of Au–ErGO/MWCNT/graphite nanocomposite electrode in comparison to other surface modified graphite sensor

The electrochemical characteristic of Au–ErGO/MWCNT/graphite was evaluated, including the Eff A, k_s , and electrode overpotential. This attribute was also compared to the other graphite modified electrode including MWCNT/graphite, Au–NPs/graphite (Chapter 3, Section 3.3.4) and bare graphite. The Eff A of the Au–ErGO/MWCNT/graphite was improved to 0.151 cm², which corresponds to the 4 folds improvement in Eff A than its counterpart bare graphite (0.037 cm²). In comparison to the other surface modified graphite electrode; the surface area of Au–ErGO/MWCNT/graphite was better than the MWCNT/graphite (0.108 cm²) by 1.4

folds. This could be the attribute of the gold nanoparticles that further improved the Eff A; with the possibilities of ErGO in contributing to the Eff A was ruled out, because of its 2 dimensional structure (Wang et al., 2009) unlike the MWCNT or gold, which assumes a 3 dimensional properties. Nevertheless, the Au–NPs/graphite (Chapter 3, Section 3.3.4) has the highest Eff A of 0.165 cm², which is slightly better than the Au–ErGO/MWCNT/graphite. This drawback could be possibly explained by the surface of the graphene layer that intercalate with gold nanoparticles on the MWCNT/graphite surface, in which it embedded the gold nanoparticles and as a result, impeding the Eff A outcome of Au–ErGO/MWCNT/graphite.

The electron transfer efficiency of the Au–ErGO/MWCNT/graphite was calculated, which was based on the potential difference (ΔE_p) between anodic and cathodic peaks of the ferri/ferrocyanide cyclic voltammogram. According to Nernst's equation, this ΔE_p is corresponding to 59.16 mV for a quasi-reversible reaction that involves a single electron transfer. From Fig. 5.16 the peak potential differences (ΔE_p) of Au–ErGO/MWCNT/graphite, MWCNT/graphite, Au–NPs/graphite and bare graphite can be calculated; in which these values corresponded to 73.5 mV, 92.0 mV, 78.1 mV, and 355.0 mV, respectively. The Au–ErGO/MWCNT/graphite showed the nearest value (73.5 mV) to 59.16 mV, indicated good electron transfer efficiency than its counterpart bare graphite and other surface modified electrode.

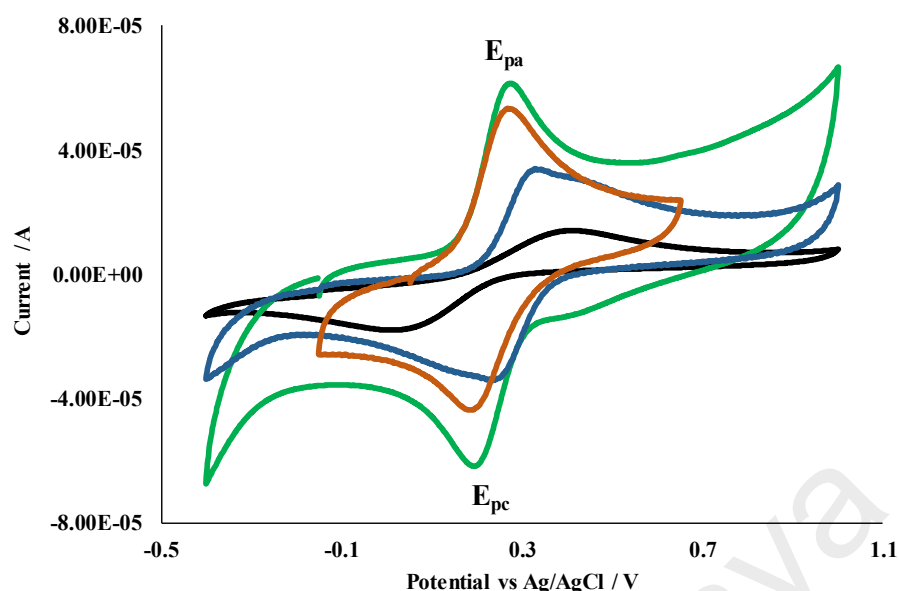


Figure 5.16: CV of 1 mmol L⁻¹ ferri/ferrocyanide that was performed using MWCNT-COOH/graphite (blue), Au-NPs/graphite (brown), Au-ErGO/MWCNT/graphite (green) and bare graphite (black) at scan rate of 0.2 V s⁻¹.

The heterogeneous electron transfer rate (k_s) of the Au-ErGO/MWCNT/graphite sensor was also evaluated; among this sensor (Table 3.3, 5.1 and 5.2) the order of greater k_s can be sequenced as Au-ErGO/MWCNT/graphite (27.3 s⁻¹) > Au-NPs/graphite (9.8 s⁻¹) > MWCNT/graphite (8.1 s⁻¹) > bare graphite (2.2 s⁻¹). This had shown that the Au-ErGO/MWCNT/graphite possessed greater electron transfer kinetic properties than the other surface modified graphite sensor, which is 12 folds the k_s of bare graphite; and 3 folds of Au-NPs/graphite and MWCNT/graphite electrode. This could be attributed by the electrocatalytic properties of reduced graphene oxide (ErGO). A fast electron transfer (k_s) is an important criteria for sensor application especially in the electro-analytical study; which is to ensure a diffusion limiting process that is according to Fick's Law.

To further test on the electrode performance, a CV experiment using 1 mmol L⁻¹ ferri/ferrocyanide redox species were performed and the result is illustrated in Fig. 5.16. From the anodic peak height of the CV, the current response (I_{pa}) of the Au-ErGO/MWCNT/graphite; MWCNT/graphite; Au-NPs/graphite and bare graphite

can be measured, these values corresponded to 4.6×10^{-5} , 2.9×10^{-5} , 4.1×10^{-5} , and 1.8×10^{-5} Ampere, respectively. Suggesting the Au–ErGO/MWCNT/graphite sensor is more sensitive, with the current response of Au–ErGO/MWCNT/graphite was greater by 2.6 and 1.6 folds when compared to the bare graphite and MWCNT/graphite respectively. In comparison to Au–NPs/graphite, the current response has improved by 10% although the Eff A (redox site) of Au–ErGO/MWCNT/graphite is much lower than the Au–NPs/graphite, nevertheless the current response is much higher; which could be explained by the electrocatalytic and k_s attribute of the graphene and gold nanoparticles.

The electrode overpotential of the prepared Au–ErGO/MWCNT/graphite was evaluated from the CV that shown in Fig. 5.16. The anodic peak potential of the ferri/ferrocyanide peak that was performed using Au–ErGO/MWCNT-COOH/graphite ($E_a = 0.2675$ V) was shifted towards a less positive potential by 2.3 mV, 75.7 mV and 136.7mV corresponding to the Au–NPs/graphite ($E_{pa} = 0.2698$ V, Chapter 3, Section 3.3.4.4); MWCNT/graphite ($E_{pa} = 0.3432$ V) and bare graphite electrode ($E_{pa} = 0.4042$ V) respectively. This shift of peak potential suggests an improvement in the Au–ErGO/MWCNT/graphite overpotential, which indicated a much easier oxidation of the ferricyanide. This improvement could be attributed by the electro-catalytic properties of reduced graphene oxide and gold.

Based on the electro characteristic evaluation of Au–ErGO/MWCNT/graphite; it can be inferred that few important attributes of the sensor were improved particularly on the Eff A, k_s , and electro-catalytic properties; which gives better sensitivity and improved electrode overpotential than those of single nanomaterial modified sensor (MWCNT/graphite and Au–NPs/graphite).

5.3.8 Electrochemical characteristic of A, G, C and T using Au–ErGO/MWCNT/Graphite

The redox properties of the DNA bases were determined using the CV. Fig. 5.17 and 5.18 illustrate the CV for each individual A, C, T and G bases that was performed in 0.1 mol L⁻¹ phosphate buffer (pH 7) at concentration of 20 µg mL⁻¹.

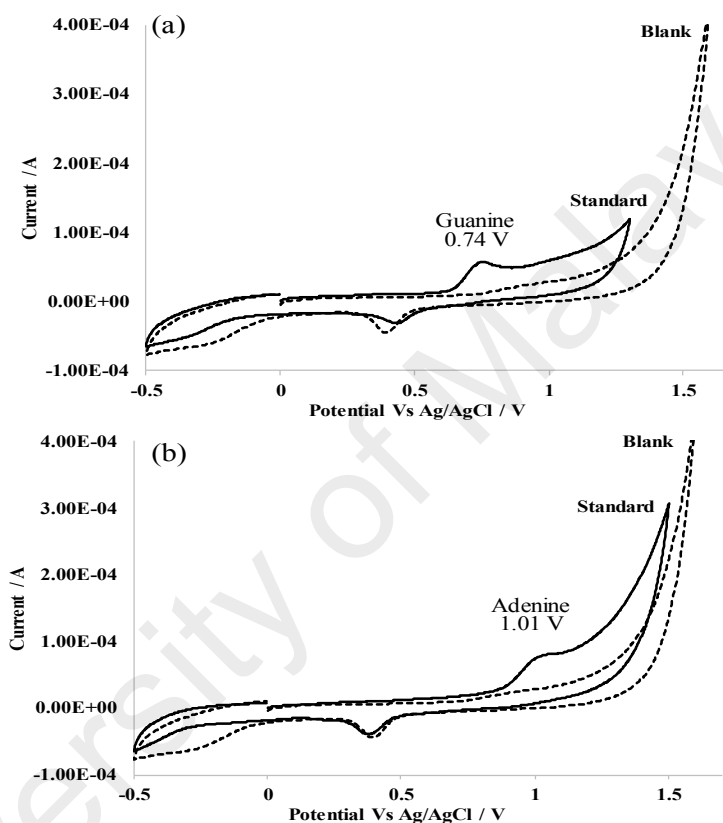


Figure 5.17: CV of guanine (a) and adenine (b) performed using Au–ErGO/MWCNT/graphite. The solid line and dotted line correspond to the 20 µg mL⁻¹ standard and blank solution CV scan respectively that was performed in phosphate buffer (0.1 mol L⁻¹, pH 7).

Only a single anodic peak (oxidation) was detected in the DNA bases suggesting that the redox process of the G, A, T and C was chemically irreversible; with their respective anodic peak potential corresponding to 0.74, 1.01, 1.15 and 1.36 V.

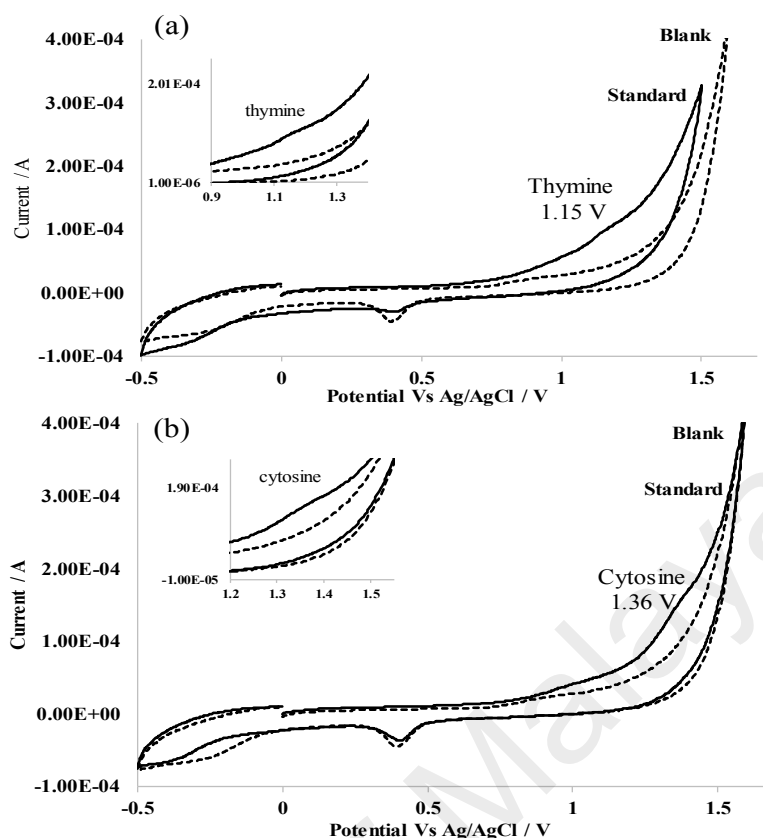


Figure 5.18: CV of T (a) and C (b) was performed using Au–ErGO/MWCNT/graphite. The insets illustrate the enlarged version of the T and C peaks, respectively. The solid line and dotted line correspond to 20 μg mL⁻¹ standard and blank solution CV scan, respectively that was performed using phosphate buffer (0.1 mol L⁻¹, pH 7).

No oxidation peak was detected in the blank scan, and the reduction peak (cathodic) that was observed in the blank at 0.45 V could be due to a reduction of gold oxide (Hezard et al., 2012). This was formed on the deposited gold nanoparticles as explained in Chapter 3 (Section 3.3.2); where the peak is also detected in each individual standard DNA bases prepared in 0.1 mol L⁻¹ phosphate buffer (pH 7), as showed in the CV scan (Fig. 5.17 and 5.18). The current response of the C and T DNA bases were weak when compared to A and G (Fig. 5.17 and 5.18) because it is less favourable to be oxidized. Therefore, to improve the detection of C and T, a SWV method was used in this study. Since SWV is using a modulated differential pulse potential, therefore it has the ability to eliminate the

background capacitance current or Helmholtz double layer charge that can improve the faradaic current (measured current) (Sochor et al., 2013).

5.3.9 Impact of pH to DNA bases oxidation on Au–ErGO/MWCNT/graphite

Various pH conditions were studied on the DNA bases that were prepared at $20 \mu\text{g mL}^{-1}$ using Britton-Robinson buffer which was adjusted to the required pH using sodium hydroxide. At different pH conditions, it will affect the oxidation properties of A, G, T and C. It is preferable to have a more oxidative condition to the DNA bases, as this gives a higher current response signal.

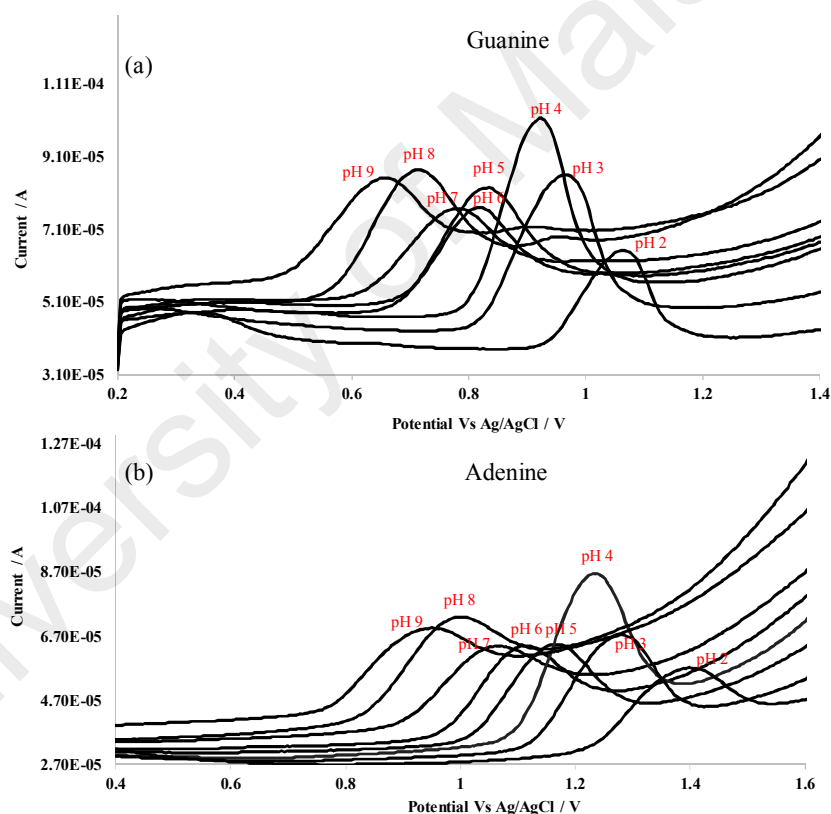


Figure 5.19: SWV of guanine (a) and adenine (b) performed using Au–ErGO/MWCNT/graphite at various pH conditions.

Fig. 5.19 and 5.20 illustrate the plots of SWV anodic current response (I_{pa}) versus the applied anodic potential of G, A, C and T; each voltammogram of different pH conditions were superimposed for better comparison.

At pH 2, G and A can be detected, but not for C and T. At pH 3 and above, all DNA bases were able to be detected by using the Au–ErGO/MWCNT/graphite electrode, however at pH 3 and 4 the peak current was weak for both C and T. Therefore, the ideal pH condition for the optimised anodic current response (I_{pa}) of the DNA bases ranged from pH 5 to 9.

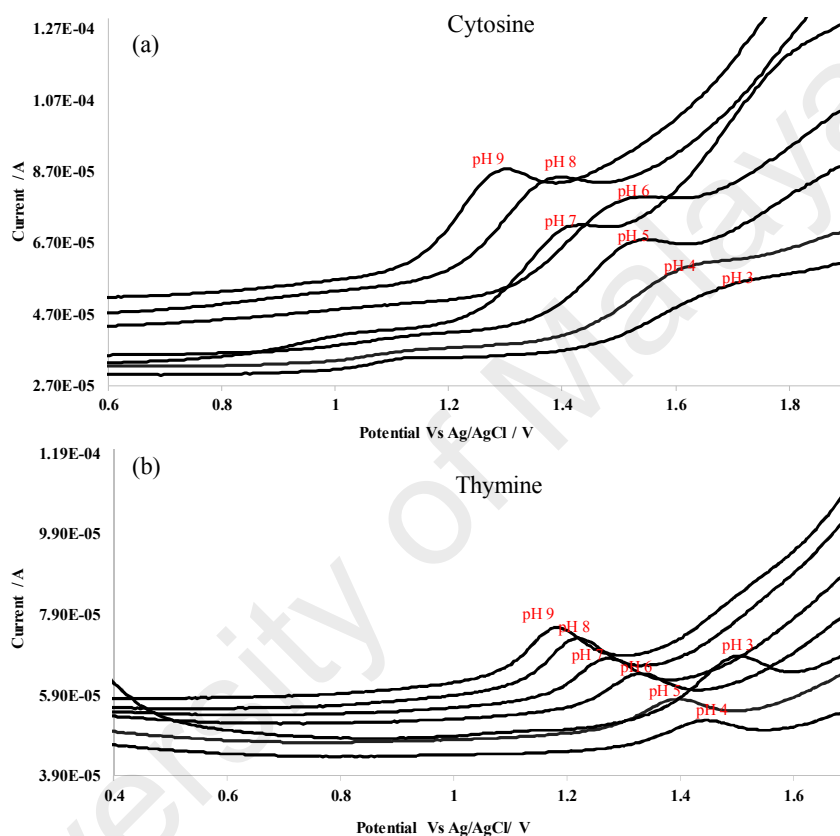


Figure 5.20: SWV of cytosine (a) and thymine (b) performed using Au–ErGO/MWCNT/graphite at various pH conditions.

Fig. 5.21 shows the graph of the anodic peak current response at different pH conditions. Both G and A have the highest current response at pH 3 and 4, however, it is not an optimum pH because of the weak response of C and T that limits the detection sensitivity. An analysis of the peak current response also suggests that both G and A were more oxidisable at moderate acidic condition (pH 3 to 5) giving higher current response; in contrast, to C and T which is more oxidisable at moderate alkaline condition (pH 8 to 9).

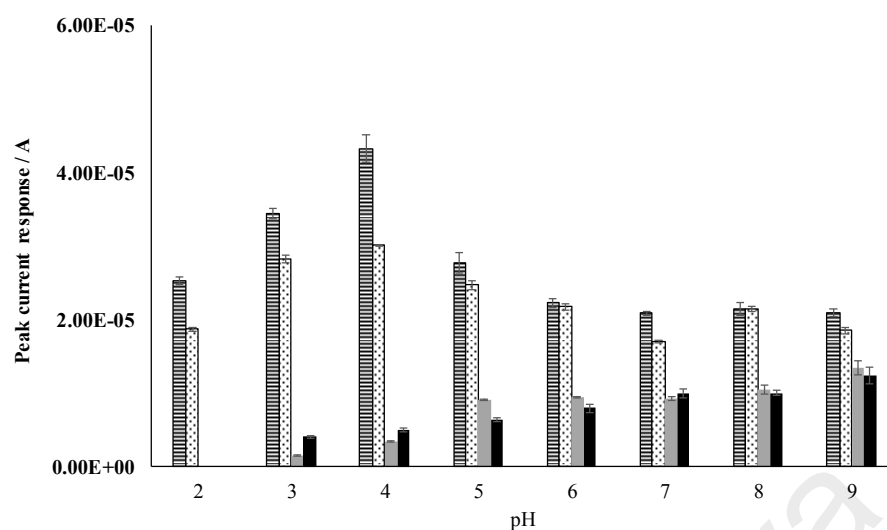


Figure 5.21: Graph of anodic peak current response of G (lines), A (dotted), C (grey) and T (black) versus pH of the prepared standard solution ($20 \mu\text{g mL}^{-1}$) for effective pH selection study.

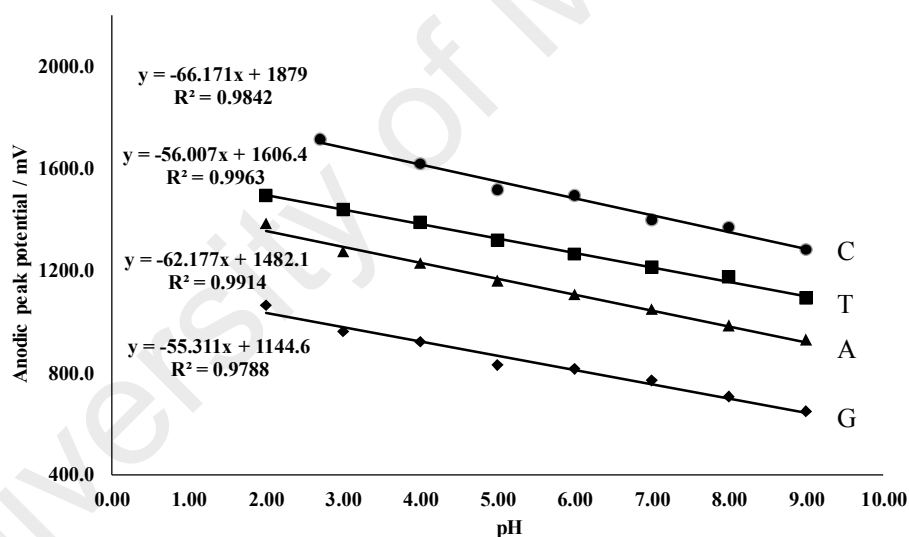


Figure 5.22: Linear correlation graph of anodic peak potential of C, T, A and G that was performed using Au–ErGO/MWCNT/graphite at various pH conditions. The slope of G, A, T and C were corresponding to $-55.31 \text{ mV pH}^{-1}$, $-62.18 \text{ mV pH}^{-1}$, $-56.00 \text{ mV pH}^{-1}$, and $-66.17 \text{ mV pH}^{-1}$, respectively.

Based on the pH optimization study, pH 7 was selected for the multiplex study of the four DNA bases, because pH 7 is reported to be ideal for biological sample analysis (Ferancová et al., 2010). It is, therefore, recommended that pH 7 be used as the measurement condition for DNA bases study.

Fig. 5.22 illustrates a graph of anodic peak potential against the pH values, which the slope can be used to determine the number of electron transfer. The slope value corresponds to 59.16 mV/decade suggests a one electron and one proton transfer process according to Nernst's equation. Based on linear curve graph (Fig. 5.22) the slope of G, A, T and C corresponded to $-55.31 \text{ mV pH}^{-1}$, $-62.18 \text{ mV pH}^{-1}$, $-56.00 \text{ mV pH}^{-1}$, and $-66.17 \text{ mV pH}^{-1}$, respectively. Which suggest an equal electron and proton transfer process. It is postulated that the electrochemical reaction of the four DNA bases on the surface of Au-ErGO/MWCNT/graphite electrode involved an electron (one) and a proton (one) transfer process, with the postulated oxidation reaction as shown in Fig. 5.23 that bases upon the oxidation reaction at pH 7 that involve a single electron or oxidation stages, which is also postulated by verdolino et al. (2008) that based on density function theory calculation (Verdolino et al., 2008). Multiple oxidation stages on the sensor surface could be happened at different pH conditions, however at pH 7 study condition, it is postulated to involve 1 oxidation stage on the sensor surface.

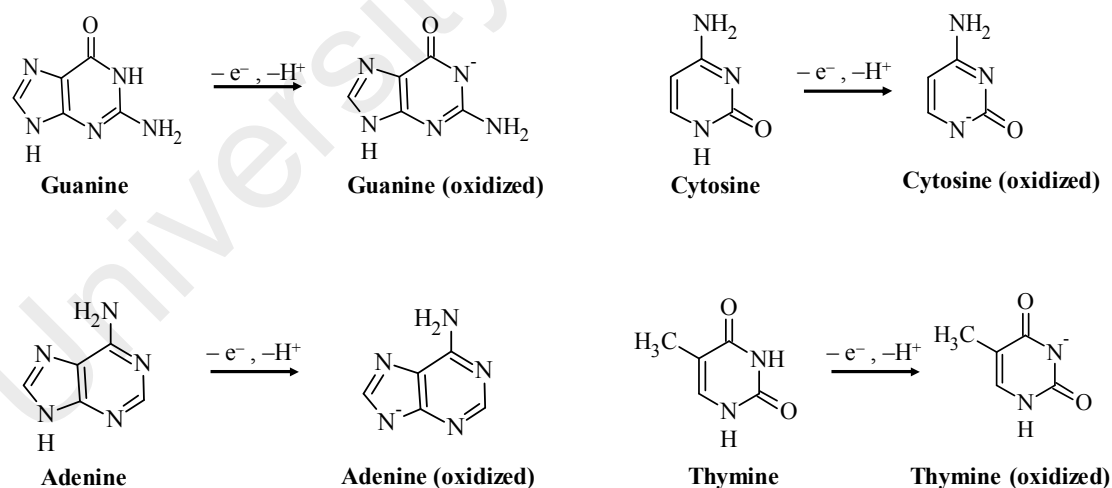


Figure 5.23: Oxidation reaction of G, A, T and C on Au–ErGO/MWCNT/graphite surface.

5.3.10 Multiplexes oxidation of A, G, C and T using Au–ErGO/MWCNT/graphite nanocomposite electrode

From the pH evaluation study, pH 7 was selected as the optimum condition for the multiplex detection of DNA bases. This pH condition was ideal for biological sample analysis and study (Ferancová et al., 2010). Fig. 5.24 shows the voltammogram of multiplex detection of A, G, T and C using Au–ErGO/MWCNT/graphite electrode, with the order of oxidation potential (E_{pa}) as G (0.77 V) < A (1.05 V) < T (1.21 V) < C (1.40 V). To evaluate the performance of the Au–ErGO/MWCNT/graphite electrode in DNA bases detection, a comparison study of the MWCNT/graphite and bare graphite were performed; and the results of the SWV voltammogram are illustrated in Fig. 5.24.

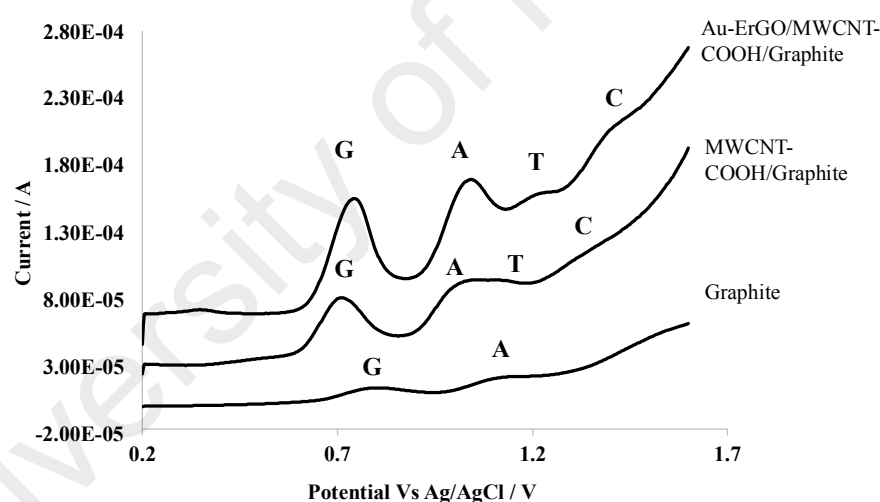


Figure 5.24: SWV of simultaneous detection of G, A, T and C that was performed using different surface modified graphite electrode compared to the bare graphite electrode.

C was not able to be detected using both electrode (MWCNT/graphite and bare graphite); for T, it can be detectable by MWCNT/graphite electrode but is fused to the adjacent adenine peak; while it remains undetectable by the bare graphite electrode. The detection of T and C by the Au–ErGO/MWCNT/graphite could be attributed by the much-improved electron transfer rate (k_s) and electrode overpotential. With an increase

in the heterogeneous electron transfer rate; the ratio of k_s/n is increasing, which is favourable to the diffusion controlled process of T and C that allows for a more reversible electrochemical reaction. Besides, the peak current (I_{pa}) of A and G were also improved significantly with Au–ErGO/MWCNT/graphite electrode. The anodic current response (I_{pa}) of the A (44.6 μ A) and G (71.4 μ A) were improved by 2 and 10 folds which corresponds to MWCNT/graphite and bare graphite electrode, respectively. This could be attributed by the Eff A of the Au–ErGO/MWCNT/graphite electrode.

5.3.11 Effect of supporting electrolyte in multiplexes analysis of A, G, T and C using Au–ErGO/MWCNT/graphite

The effect of supporting electrolyte to the multiplex detection of DNA bases was studied at pH 7.0, using the Britton Robinson buffer, phosphate buffer, potassium chloride, and also sodium nitrate solution that was prepared at a concentration of 0.1 mol L⁻¹. Fig. 5.25 illustrates the SWV of A, G, T and C using different supporting buffer. No peak was detected when potassium chloride was used as the electrolyte solution, this is because the baseline current (ampere) registered by blank analysis is much higher than the A, G, T and C standard; especially at the region of 0.6 to 1.4 V. This suggests a possible cut-off in the detection of the DNA bases. When sodium nitrate was used as the supporting electrolyte only G and A are detectable, with their anodic potential (E_{pa}) were shifted towards more positive potential (A shifted from 1.00 V to 1.35 V and G shifted from 0.75 V to 0.92 V). This indicates that the sodium nitrate supporting electrolyte could increase the Au–ErGO/MWCNT/graphite overpotential. The reason, both A and G are still detectable is because its oxidation potential still falls within the potential window of the Au–ErGO/MWCNT/graphite. Both T and C were affected in the analysis, as the oxidation potential of T and C were shifted out from the applied potential window of Au–ErGO/MWCNT/graphite sensor. Whereby, over this potential window will cause the electrode surface to be oxidised.

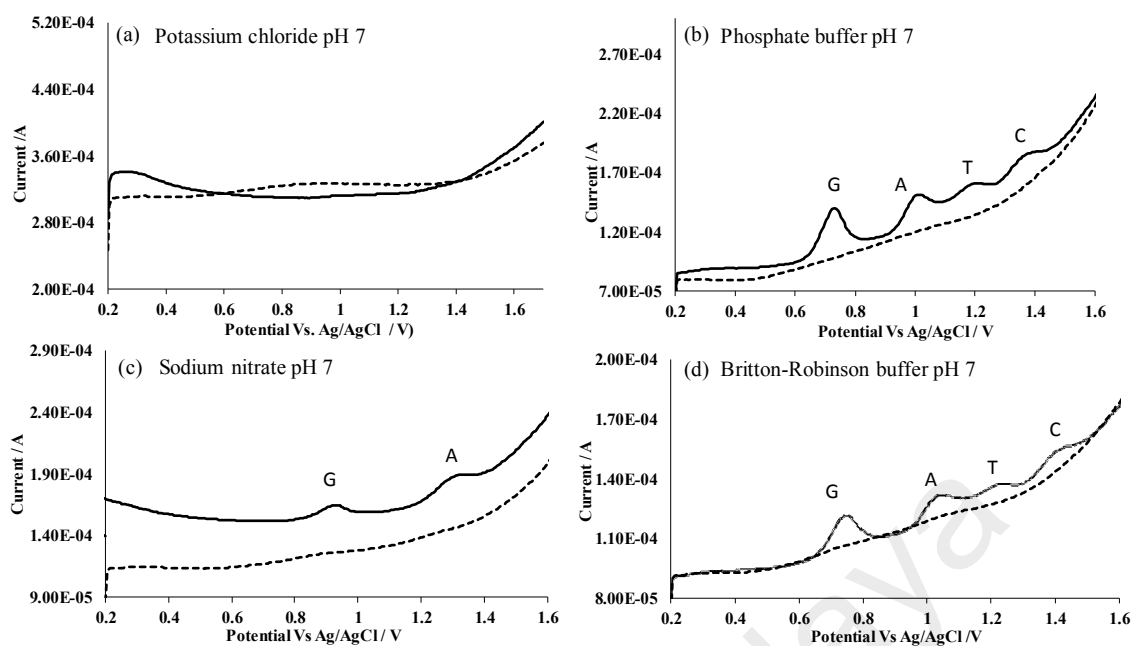


Figure 5.25: SWV of simultaneous detection of G, A, T and C using Au-ErGO/MWCNT/graphite in (a) 0.1 mol L⁻¹ potassium chloride; (b) 0.1 mol L⁻¹ phosphate buffer (c) 0.1 mol L⁻¹ sodium nitrate; and (d) 0.1 mol L⁻¹ Britton Robinson buffer. The standard A, G, T and C is represented by solid lines, and blank as dotted line.

A, C, T and G can be successfully detected simultaneously in both the Britton Robinson buffer and the phosphate buffer. A comparison on the result quality, suggests that the phosphate buffer gives a better peak separation than the Britton Robinson buffer, with A and T peaks separated by 17 mV; in contrast to Britton-Robinson buffer, which was separated by 12 mV apart. On the other hand, the peak potential of G, A, T and C that was performed in phosphate buffer corresponded with 0.71 V, 0.99 V, 1.18 V and 1.35 V, which also showed a more improved overpotential than the Britton Robinson buffer (G = 0.75 V, A = 1.04 V, T = 1.22 V and C = 1.41 V). This could be postulated by the lower ohmic resistance of the phosphate buffer, hence, it was selected for further study. Moreover, phosphate buffer was recommended as the supporting electrolyte in some of the DNA bases study due to its compatibility in the biological bases samples (H. Liu et al., 2008; Niu et al., 2012; Thangaraj et al., 2014).

5.3.12 Analytical performance of Au–ErGO/MWCNT/graphite electrode in multiplex analysis of DNA bases

The SWV of A, C, T and G at different concentration level is illustrated in Fig. 5.26 which shows a consistent peak current increment of A, C, T and G proportionally to its concentration. Successively, the correlation graph of the individual peak current versus concentration was plotted as illustrated in Fig. 5.27 (a) and (b).

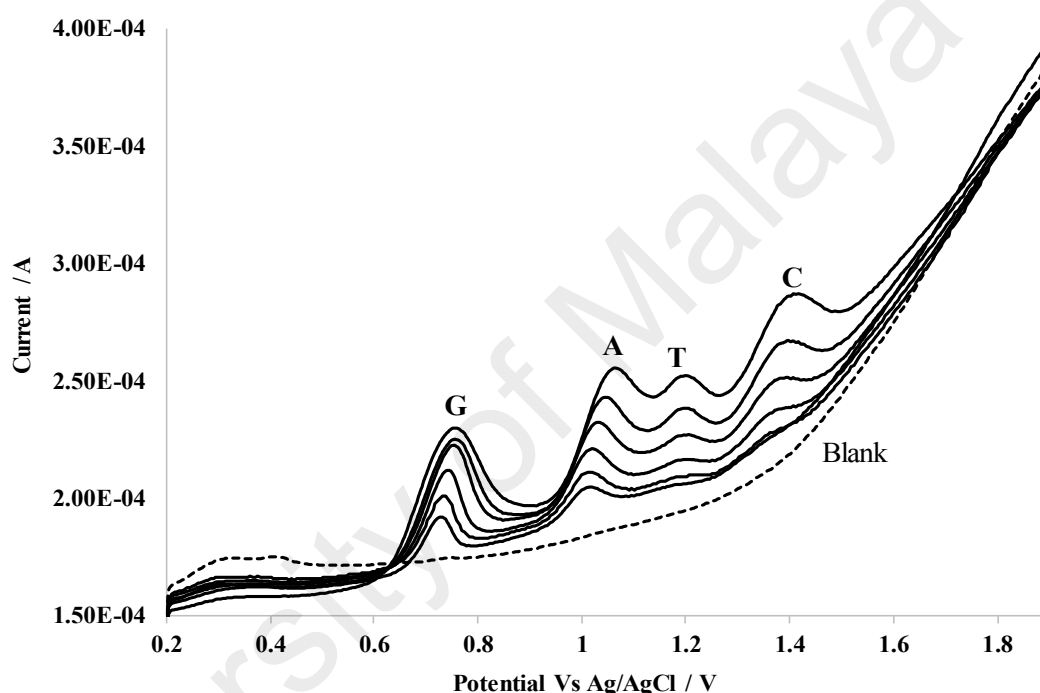


Figure 5.26: SWV of simultaneous detection of G, A, T and C with a concentration ranging from 2 to 20 $\mu\text{g mL}^{-1}$ for G, A; and 6 to 60 $\mu\text{g mL}^{-1}$ for T and C analyte.

The correlation coefficient (Fig. 5.27) of the individual A, G, T and C calibration curve was greater than 0.99; and the dynamic range for both G and A showed a linearity range from 0.5 to 25 $\mu\text{g mL}^{-1}$; as for T and C, the range is wider from 1 to 100 $\mu\text{g mL}^{-1}$. The order of sensitivity can be determined at the following sequence $G (171 \text{ nA}/\mu\text{g mL}^{-1}) > A (87.8 \text{ nA}/\mu\text{g mL}^{-1}) > C (14.0 \text{ nA}/\mu\text{g mL}^{-1}) > T (1.30 \text{ nA}/\mu\text{g mL}^{-1})$; which suggests that the sensor is more sensitive to G detection with a higher anodic current response. In contrast, T shows the least sensitivity. The reason to the low sensitivity of T and C are

proportionated to two factors, which are governed by the electron transfer rate and also by the ease of oxidation. Pyrimidine (C and T) are generally less oxidative than purines (A and G) (Oberacher et al., 2015), As a result, both T and C generate less electron from the oxidation and, therefore, the current response from the Au–ErGO/MWCNT/graphite are less; given the less sensitivity to the detection of T and C.

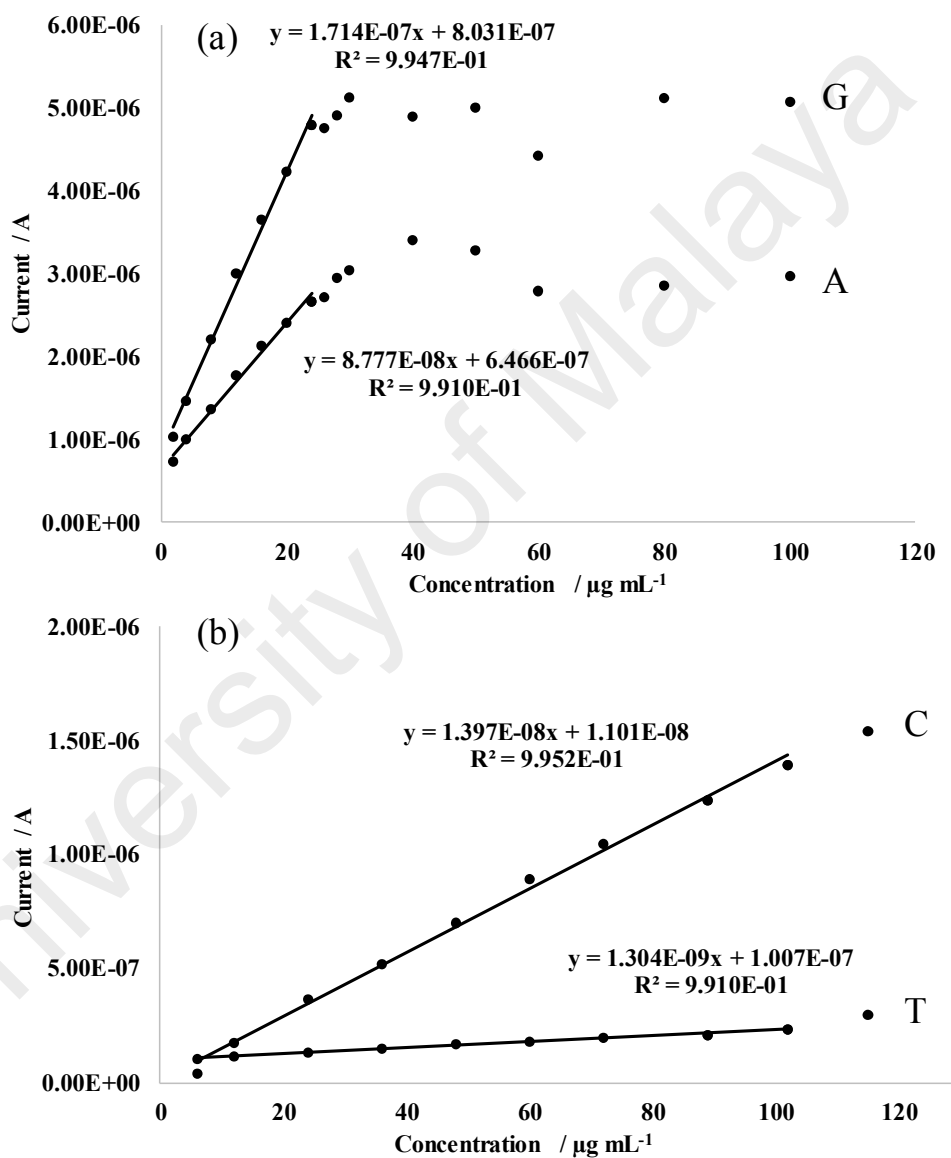


Figure 5.27: Correlation graph of peak current versus concentration for (a) G and A. (b) C and T.

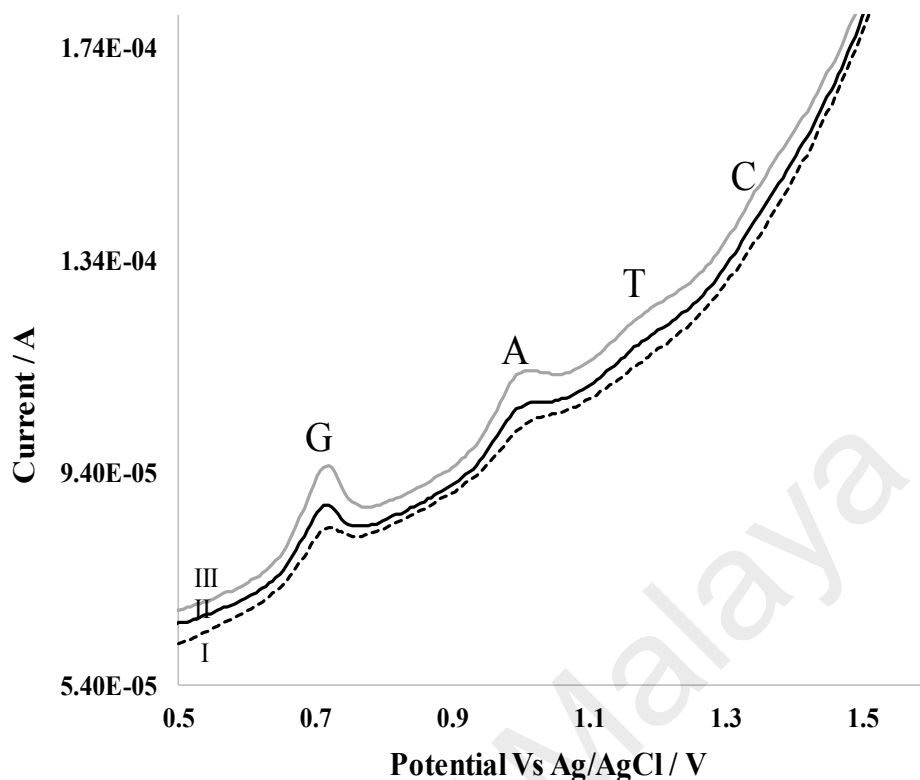


Figure 5.28: SWV of G, A, C and T tested at concentration (I) $0.25 \mu\text{g mL}^{-1}$; (II) $0.5 \mu\text{g mL}^{-1}$; and (III) $1.0 \mu\text{g mL}^{-1}$.

The limit of detection (LOD) in the analysis of G, A, T and C was performed by a serial dilution of a stock standard solution ($1 \mu\text{g mL}^{-1}$), and the resulted SWV voltammograms obtained are shown in Fig. 5.28. From the graph, the LOD of G, A, T and C are corresponding to $0.5 \mu\text{g mL}^{-1}$, $0.5 \mu\text{g mL}^{-1}$, $1 \mu\text{g mL}^{-1}$, and $1 \mu\text{g mL}^{-1}$, respectively. The LOQ was calculated at 5 times the standard deviation of the LOD, which the values corresponded to $0.8 \mu\text{g mL}^{-1}$, $1.2 \mu\text{g mL}^{-1}$, $1.4 \mu\text{g mL}^{-1}$, and $1.3 \mu\text{g mL}^{-1}$, respectively. The LOD and LOQ of A, G T and C detection using Au–ErGO/MWCNT/graphite electrode are summarised in Table 5.3 for clearer comparison.

Table 5.3: Comparison of the analytical performance of UPLC–PDA and SWV Au–ErGO/ MWCNT /graphite methods for the simultaneous analysis of G, A, C and T.

Analyte	Method	¹ LOD	² LOQ	Dynamic Range	Correlation coefficient	³ Sensitivity
		$\mu\text{g mL}^{-1}$	$\mu\text{g mL}^{-1}$	$\mu\text{g mL}^{-1}$		unit signal / $\mu\text{g mL}^{-1}$
G	SWV	0.5	0.8	0.5–25.0	0.9963	0.078
	UPLC	0.4	0.5	0.4–50.0	0.9996	0.066
A	SWV	0.5	1.2	0.5–25.0	0.9943	0.057
	UPLC	0.1	0.2	0.1–50.0	0.9999	0.079
C	SWV	1.0	1.3	1.0–100.0	0.9971	0.153
	UPLC	0.1	0.2	0.1–50.0	0.9998	0.081
T	SWV	1.0	1.4	1.0–100.0	0.9940	0.023
	UPLC	0.1	0.2	0.4–50.0	0.9999	0.080

¹ Limit of detection

² Limit of quantitation

³ Normalize response factor that relative to 10 $\mu\text{g mL}^{-1}$ standard (calibration slope divided by signal response of known standard)

5.3.13 Hydrolysis of DNA samples by acid digestion

DNA comprises of 3 components including the nucleic acid, ribose sugar and phosphate; to ensure the liberation of the A, G, T and C. A complete hydrolysis of DNA sample is important, which depends on the type of acid, concentration and hydrolysis time used. In this present study, 3 different concentrations of sulfuric acid corresponding to 1 mol L⁻¹, 4 mol L⁻¹ and 8 mol L⁻¹ were evaluated. At a lower acid concentration (1 and 4 mol L⁻¹), the C and T was undetectable by the UPLC and SWV (Au–ErGO/MWCNT/Graphite) method. This could be explained by the incomplete hydrolysis of the DNA sample to liberate C and T from the DNA backbone, and therefore may require a stronger concentration of acid. When using acid at a concentration of 8 mol L⁻¹, all the DNA bases was detectable by SWV and UPLC. The hydrolysis time used in the analysis was studied across 4 different time points (4, 5, 6 and 7 h), the recovery percentage (%) of A, G, T and C from its actual content in Calf thymus DNA (Note: actual content A = 28.0%, T = 28.0%, G = 22.0% and C = 22.0% in calf thymus DNA) was plotted against the hydrolysis time and the result is illustrated in Fig. 5.29. At 5-h

hydrolysis time the recovery of A, C, T and G were the most optimised, with a recovery sum of 99.6%. In which below this hydrolysis time (at 4 h) it showed a lower recovery of the DNA bases, with the recovery sum of 86.1%. Hydrolysis at more than 6 h showed the C recovery was lower at 20.4 % (at 6 h) and 21.3 % (at 7 h), which the value deviates from the expected content of 22.5%, whereas A, T and G remain stable after 6 h of hydrolysis. From this evaluation, it is proposed 5 h of hydrolysis time is optimum for the A, G, T and C analysis; with concentration of acid use at 8 mol L⁻¹.

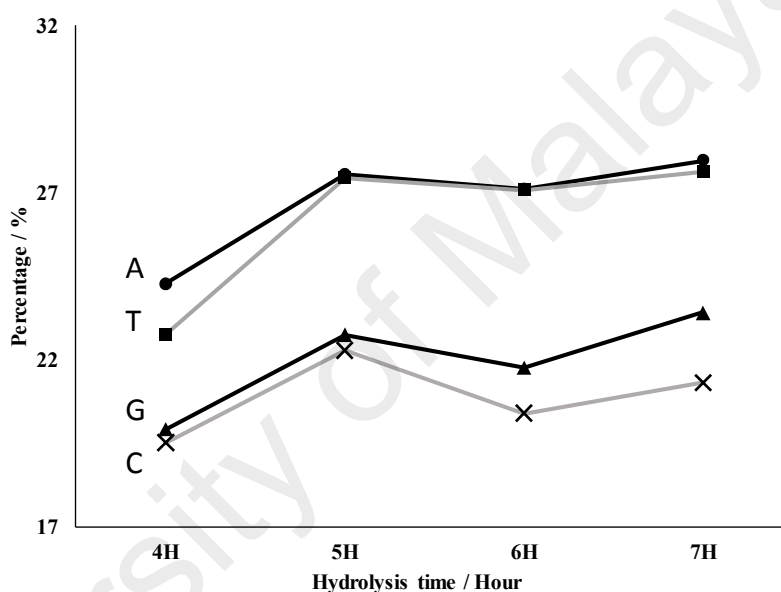


Figure 5.29: Percentage recovery of A, T, G and C in calf thymus DNA that was prepared at different hydrolysis time using 8 mol L⁻¹ sulfuric acid (Note: actual content A = 28.0 %, T = 28.0 %, G = 22.0 % and C = 22.0 % in calf thymus DNA).

The type of acid used in the hydrolysis was also studied, in which 8 mol L⁻¹ of hydrochloric and sulfuric acid were evaluated and the hydrolysis duration was fixed at 5 h. From the SWV results shown in Fig. 5.30, all the DNA bases were detected when hydrolysis was performed using sulfuric acid but for hydrochloric acid only A and G is detectable. It is postulated that the chloride ion from HCl acid could possibly interfere the applied potential range of Au–ErGO/MWCNT/graphite at higher value (> 1.3 V), causing tremendous increase in the baseline current (Fig. 5.30), which has impeded the detection

of T and C, as a result, sulfuric acid was recommended for the hydrolysis work of DNA sample.

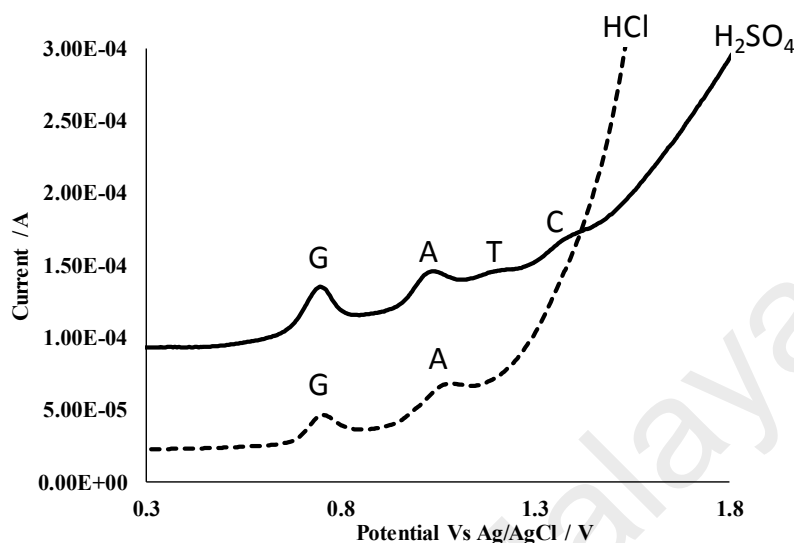


Figure 5.30: SWV of calf thymus DNA composition of hydrolyse using 8 mol L⁻¹ of sulfuric acid (H₂SO₄, solid line) versus hydrochloric acid (HCl, dotted line).

5.3.14 Analysis of DNA bases in real samples

The developed SWV (Au–ErGO/MWCNT/graphite sensor) method was tested in two real DNA samples, which are the calf thymus and extracted onion DNA. Both samples were selected for this study due to the difference in the DNA sources, which the calf thymus DNA was extracted from animal source and the onion DNA from plant source. This could provide a more comprehensive range in the real sample analysis, as the matrix or composition between the animal and plant cell can be different. Table 5.4 summarises the composition of DNA bases in the onion and calf thymus samples using the SWV Au–ErGO/MWCNT/graphite sensor. The mole percentage (mol/100 g) of G, A, T and C in the calf thymus DNA corresponds to 21.5 ± 0.5 , 27.9 ± 0.4 , 28.5 ± 0.4 and 22.0 ± 0.3 mol %, respectively; and for onion DNA the results corresponds to 29.1 ± 0.2 , 20.9 ± 0.2 , 21.2 ± 0.3 and 28.8 ± 0.1 mol %. According to Chargaff's rules, the mol percentage of G is equal to C and A is equal to T. The damaged DNA could have a mismatch in base

pairing or in the missing of DNA bases; therefore it could deviate from the Chargaff's rules. Based on the results obtained in both calf thymus and onion DNA, the ratio of C to G (onion = 0.99, calf thymus = 1.02) and T to A (onion = 1.01, calf thymus = 1.02) were close to unity, suggesting an intact DNA bases.

Table 5.4: Simultaneous determination of G, A, T and C contents in calf thymus and extracted onion DNA using SWV Au–ErGO/MWCNT/graphite and UPLC.

Analyte	Calf Thymus DNA		Extracted Onion DNA	
	² SWV	³ UPLC–PDA	² SWV	³ UPLC–PDA
	Result ¹ (mol %)	Result ¹ (mol %)	Result ¹ (mol %)	Result ¹ (mol %)
G	21.5 ± 0.5	21.2 ± 0.3	29.1 ± 0.2	29.4 ± 0.2
A	27.9 ± 1.1	28.1 ± 0.2	20.9 ± 0.2	20.7 ± 0.2
T	28.5 ± 0.8	28.5 ± 0.5	21.2 ± 0.3	20.6 ± 0.1
C	22.0 ± 0.3	22.1 ± 0.2	28.8 ± 0.1	29.2 ± 0.6

¹ 3 replicate (n=3) analyses with standard error at 95% confidence limit

² Square wave voltammetry

³ Ultra performance liquid chromatography photodiode array detector

The ratio of purines (C and A) to pyrimidine (G and T) were calculated using the formula $(C+G)/(A+T)$ (Gao et al., 2014; Liu et al., 2008; Švorc & Kalcher, 2014). According to Chargaff's rules, this value is specific for different organism. The ratio obtained for onion and calf thymus DNA in this study was 1.38 and 0.77 respectively. The DNA ratio of calf thymus obtained was close to the expected value of 0.78, and the result was also found to be in agreement to the reported value of 0.77 by Gao et al. (2014) and Liu et al. (2008) that was performed using polypyrrole/graphene (Gao et al., 2014) and polythionine/gold–nanoparticles/multi–walled carbon nanotubes (Liu et al., 2008), respectively. This ratio value is specific for calf thymus suggesting the DNA is intact. The limitation in both reported results were calculated based upon the G and A ratio only that excluded C and T. In this present study, the DNA bases ratio was calculated based on the simultaneous detection of A, G, T and C results set.

5.3.15 Accuracy and precision study of Au–ErGO/MWCNT/graphite sensor

In this study, the accuracy and precision of the method was evaluated based on the calf thymus DNA analysis. The samples purchased is a known standard with expected mol percentage values for G or C which corresponded to 22.0 mol % and for A or T is 28.0 mol %. The results were obtained using SWV with Au–ErGO/MWCNT/graphite sensor which was summarised in Table 5.4. The accuracy of the sensor can be assessed by calculating the percentage of recovery from the expected value. Based on the results, it showed the recovery of A, G, C, and T corresponded to 97.4%, 97.7%, 100.0% and 101.8%, respectively. According to Codex Alimentarius, the acceptable recovery range for accuracy is between 80 to 120%, suggesting that the accuracy of Au–ErGO/MWCNT/graphite sensor was acceptable.

The precision of the Au–ErGO/MWCNT/graphite sensor in A, G T and C measurement was calculated using a relative standard deviation (RSD). The RSD of A (3.5%), G (2.1%), T (2.6%) and C (2.9%) were determined at less than 5%. According to Horwitz's trumpet equation the acceptable RSD for the analysis of concentration above 1 g/100g is acceptable below RSD 5%; and for concentration measurement that is below this value will allow for a higher tolerance of RSD. In this study, the concentration of the DNA bases was measured at 0.05 g /100 g samples, and the RSD of the result obtained was calculated at less than 5%; therefore, suggesting an acceptable precision.

5.3.16 Method validation with UPLC-PDA

A liquid chromatography method was used to assess the result reliability of Au–ErGO/MWCNT/graphite sensor in the real samples analysis. Fig. 5.31 illustrates the chromatogram of C, G, T and A which was successfully separated in a C18 column by employing an ion pairing technique using phosphate buffer. The retention time of C, G, T and A corresponded to 0.7, 1.3, 2.1 and 2.6 min, respectively. The UPLC method was

used to analyse the mol percentage of G, A, T and C in real sample (onion and calf thymus DNA) and the results was summarised in Table 5.4. The mole percentage of G, A, T and C in calf thymus sample using UPLC corresponds to 21.2 ± 0.3 , 28.1 ± 0.2 , 28.5 ± 0.5 and 22.1 ± 0.2 %; and in the onion sample the mole percentage corresponds to 29.4 ± 0.2 , 20.7 ± 0.2 , 20.6 ± 0.1 and 29.2 ± 0.6 , respectively. Student T-test showed that both the results of SWV and UPLC were insignificantly different at 95% confidence limit ($p = 0.05$), suggesting the Au-ErGO/MWCNT/graphite SWV method was reliable, and can be used for the multiplex study of DNA bases composition (A, C, T and G).

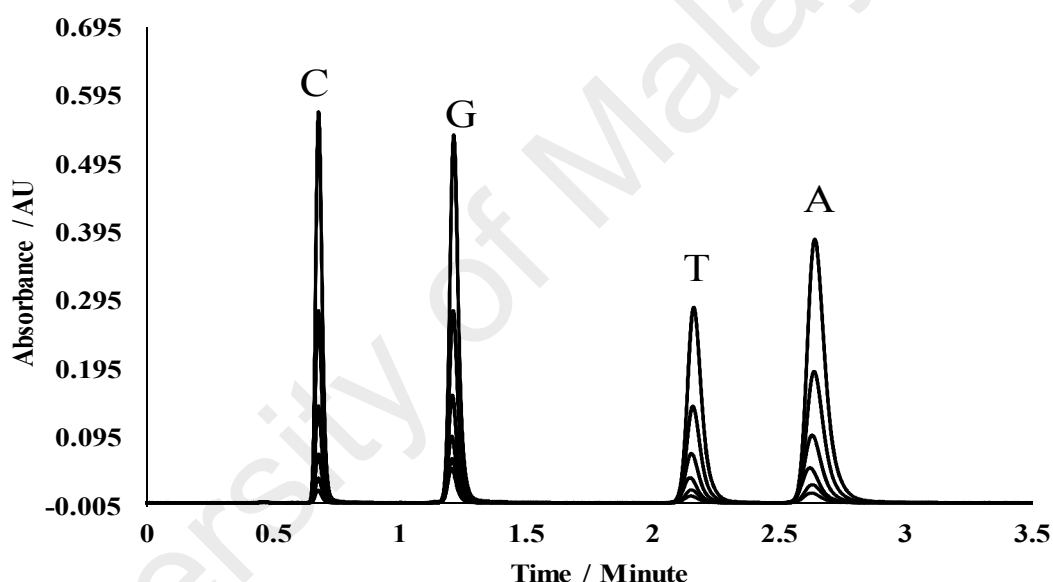


Figure 5.31: Liquid chromatogram of C, G, T and A peaks that was performed using UPLC with concentration ranging from 1 to 50 $\mu\text{g mL}^{-1}$.

The analytical performance of the liquid chromatography was also studied for comparison purpose with the SWV method (Au-ErGO/MWCNT/graphite). Fig. 5.32 illustrates the calibration plot of A, G, T and C using UPLC; a good correlation linearity of above 0.999 was obtained in each DNA bases.

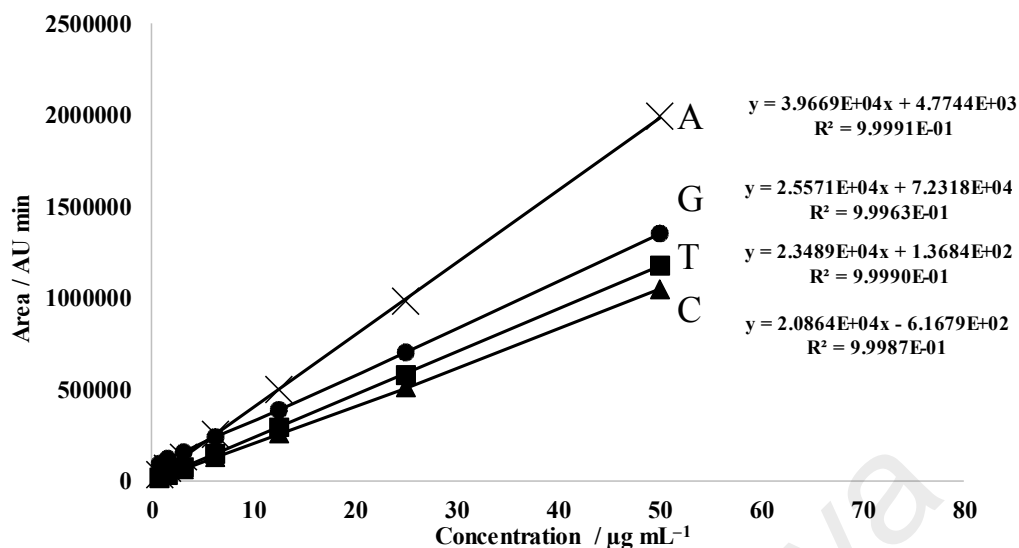


Figure 5.32: Calibration graph of A, G, T and C that was performed using UPLC.

The limit detection (LOD) of G, A, C and T using UPLC method was corresponded to 0.4, 0.1, 0.1 and 0.1 $\mu\text{g mL}^{-1}$, respectively; and the limit of quantification (LOQ) was determined at 5 times the LOD standard deviation, which corresponds to 0.5, 0.2, 0.2, and 0.2 $\mu\text{g mL}^{-1}$. The method dynamic range was linear from 0.4 $\mu\text{g mL}^{-1}$ to 50.0 $\mu\text{g mL}^{-1}$. Table 5.3 summarises the analytical performance of both SWV and UPLC methods, a comparison of the analytical performance between the two methods suggesting SWV are more sensitive in terms of G and C detection and vice versa for A and T by using UPLC. The sensitivity factor was calculated based on the normalised response of a 10 $\mu\text{g mL}^{-1}$ standard. From the dynamic range attribute, the SWV method had a wider linearity range in C and T analysis from 1 to 100 $\mu\text{g mL}^{-1}$; and a narrower range for G and A from 0.5 to 25 $\mu\text{g mL}^{-1}$. On the other hand, the UPLC method had a better detection limit, while the former could be explained by the advantages of the sample clean up procedure that by separating in the column and with less interference baseline, whereby the SWV is a direct sample analysis. However, the SWV method is more rapid in terms of the analysis time; which requires less than 30 s per analysis in contrast to 8 min by the UPLC method.

Table 5.5: Simultaneous determination of G, A, T and C contents in calf thymus DNA that was spiked with a known standard using SWV Au–ErGO/MWCNT/graphite and UPLC.

Analyte	Spiked ($\mu\text{g mL}^{-1}$)	² SWV		³ UPLC–PDA	
		Result ¹ ($\mu\text{g mL}^{-1}$)	Recovery (%)	Result ¹ ($\mu\text{g mL}^{-1}$)	Recovery (%)
G	25	25.9 \pm 0.5	103.7 \pm 1.9	24.1 \pm 0.6	96.2 \pm 2.4
	50	51.6 \pm 0.6	103.3 \pm 1.2	49.1 \pm 0.2	98.3 \pm 0.4
	75	75.3 \pm 1.3	100.4 \pm 1.7	77.6 \pm 0.2	103.4 \pm 0.2
A	25	24.6 \pm 0.7	98.5 \pm 2.6	24.1 \pm 0.3	96.3 \pm 1.0
	50	48.3 \pm 1.0	96.7 \pm 2.0	48.7 \pm 0.5	97.4 \pm 1.1
	75	74.6 \pm 2.1	99.4 \pm 2.8	76.4 \pm 0.4	101.9 \pm 0.5
T	25	25.1 \pm 0.5	100.4 \pm 2.0	25.5 \pm 1.1	102.1 \pm 4.6
	50	50.7 \pm 2.3	101.3 \pm 4.5	49.4 \pm 0.5	98.8 \pm 1.0
	75	75.1 \pm 1.0	100.1 \pm 1.3	77.3 \pm 0.3	103.0 \pm 0.4
C	25	25.2 \pm 0.5	100.6 \pm 2.1	25.7 \pm 0.2	102.8 \pm 0.6
	50	50.4 \pm 1.0	100.8 \pm 2.0	50.8 \pm 0.5	101.6 \pm 1.0
	75	75.8 \pm 2.6	101.0 \pm 3.0	76.2 \pm 2.1	101.6 \pm 2.8

¹ 3 replicate (n=3) analyses and with standard error at 95% confidence limit

² Square wave voltammetry

³ Ultra performance liquid chromatography-photodiode array detector

To further ensure the reliability of the SWV method, a spike recovery study was performed on the sample matrix at 3 different concentrations (25, 50 and 75 $\mu\text{g mL}^{-1}$). Table 5.5 summarises the percentage recovery of the spiked A, G, T and C that was performed using UPLC and SWV method. On average the SWV method had a recovery percentage for all DNA bases at 100.5 \pm 0.5 %, which is very close to the UPLC method at 100.3 \pm 0.8 %. Fig. 5.33 illustrates a graph of the SWV analysis result versus UPLC, a linear correlation was obtained with the linear coefficient of 0.9968; the slope value was equal to 1.0391 which showed that both method was correlated by a factor of 103.9%, suggesting the proposed SWV method (with Au–ErGO/MWCNT/graphite sensor) was reliable and comparable to the more established UPLC technique.

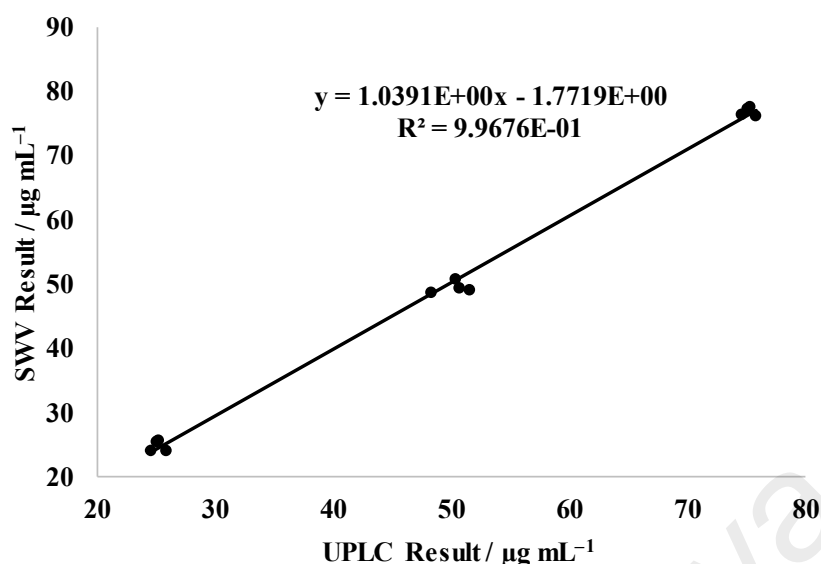


Figure 5.33: Correlation graph of SWV result (Au–ErGO/MWCNT/graphite sensor) versus UPLC result.

Table 5.6: Comparison of the analytical performance shown by different reported electrochemical sensors used for multiplex DNA base analysis.

Electrodes and DNA bases	Method	Detection limit, (mol L ⁻¹)	Linear range (mol L ⁻¹)	Notes	Reference	
CILE ^a	A	CV	2.5 x 10 ⁻⁷	7.0 x 10 ⁻⁵ – 1.5 x 10 ⁻⁶	Only A and G can be detected	Sun et al., 2008
	G		7.9 x 10 ⁻⁸	5.0 x 10 ⁻⁵ – 3.0 x 10 ⁻⁷		
CdS–CHIT/GC E ^b	A	DPV	4.0 x 10 ⁻⁸	5.0 x 10 ⁻⁶ – 2.0 x 10 ⁻⁸	Only A and G can be detected	Ferancová, 2010
	G		2.0 x 10 ⁻⁹	1.6 x 10 ⁻⁶ – 1.0 x 10 ⁻⁹		
ZnS–PEDOT–r GO/GC ^c	A	LSV	1.4 x 10 ⁻⁷	1.5 x 10 ⁻⁴ – 5.0 x 10 ⁻⁷	Only A, G and T can be detected	Ye et al., 2014
	G		1.2 x 10 ⁻⁷	1.5 x 10 ⁻⁴ – 5.0 x 10 ⁻⁷		
	T		2.6 x 10 ⁻⁶	6.0 x 10 ⁻⁴ – 5.0 x 10 ⁻⁶		
MWCNT–Fe ₃ O ₄ @PDA–Ag ^d	A	DPV	5.7 x 10 ⁻⁶	1.2 x 10 ⁻⁴ – 1.0 x 10 ⁻⁷	Only A and G can be detected	Yari et al., 2016
	G		1.5 x 10 ⁻⁶	1.3 x 10 ⁻⁴ – 8.0 x 10 ⁻⁶		
ECR Nanocarbon film	A	-	Not available	Not available	Only A, G and C can be detected. T detection by substration	Kato et. al., 2008
	G					
	T					
	C					
ER–GO/GCE	A	DPV	Not available	Not available	Only A and G can be detected. C and T not able to be integrated	Pumera et al., 2012
	G					
	T					
	C					
Au–ErGO / MWCNT / graphite ^e	A	SWV	3.7 x 10 ⁻⁶	1.9 x 10 ⁻⁴ – 3.0 x 10 ⁻⁶	All A, G, T, and C can be detected simultaneously within a single analysis	This study, 2017
	G		3.3 x 10 ⁻⁶	1.7 x 10 ⁻⁴ – 3.0 x 10 ⁻⁶		
	T		7.9 x 10 ⁻⁶	8.0 x 10 ⁻⁴ – 7.5 x 10 ⁻⁶		
	C		9.0 x 10 ⁻⁶	9.0 x 10 ⁻⁴ – 9.0 x 10 ⁻⁶		

CV: cyclic voltammetry; DPV: differential pulse voltammetry; LSV: linear sweep voltammetry; SWV: square-wave voltammetry

^a Carbon ionic liquid electrode

^b Cadmium sulfur–chitosan glassy carbon electrode

^c Zinc sulfur coated poly (3,4-ethylenedioxythiophene) reduce the graphene oxide hybrid film

^d Multi walled carbon nanotubes–Fe₃O₄ incorporated polydopamine silver nanoparticles

^e Intercalation gold nanoparticles–reduced graphene oxide/multiwall carbon nanotubes/graphite electrode

The analytical performance of the Au–ErGO/MWCNT/graphite in analysis of DNA bases was also compared with other reported sensors. Table 5.6 summarises the analytical performance of these sensors. Most of the reported sensors showed their limitation in multiplex detection of the 4 DNA bases, except for the ECR nanocarbon film and ER–GO/GCE sensors; which both were capable to detect the 4 DNA bases simultaneously; however it still facing the problem especially on the ER–GO/GCE sensor in integrating C and T due to low signal. For ECR nanocarbon film, subtraction of the voltammogram was required to obtain the T oxidation peak. The dynamic range and detection limit of the Au–ErGO/MWCNT/graphite as developed in this study for DNA bases analysis is comparable to other reported sensors.

5.3.17 Selectivity and stability study of Au–ErGO/MWCNT–COOH/Graphite in DNA bases analysis

The selectivity of the Au–ErGO/MWCNT/graphite sensor in the analysis of A, G, T and C was studied by evaluating the percentage recovery of DNA bases in the presence of common interferences. Various interferences including uracil, vitamin (niacinamide, panthothenic acid) amino acid (cysteine, serine, glutamine, and tyrosine), glucose and salt were studied. These interferences were commonly present in the animal or plant physiology samples. Table 5.7 shows the percentage recovery of the 20 $\mu\text{g mL}^{-1}$ A, G, T and C spiked in the present of these interferences (individual interferent study). From Table 5.7, it shows that all the DNA bases detection was recovered above 92%, even in the presence of the mentioned interferences. Uracil is a RNA base that is known to interact with adenine; nevertheless, the A, G, T and C were still recovered above 99%. This could infer that the proposed Au–ErGO/MWCNT/graphite sensor is selective towards the simultaneous detection of the A, C, T and G in real DNA samples.

Table 5.7: Percentage recovery of 20 $\mu\text{g mL}^{-1}$ G, A, T and C mix standard in the presence of individual interference compounds using SWV Au–ErGO/MWCNT/graphite.

NO	Interferences	G recovery, %	A recovery, %	T recovery, %	C recovery, %
1	Uracil	104.3 \pm 0.9	99.6 \pm 1.1	97.3 \pm 2.0	100.9 \pm 2.0
2	Niacinamide	95.9 \pm 4.3	95.4 \pm 2.8	96.9 \pm 1.0	99.3 \pm 0.5
3	Pantothenic acid	99.0 \pm 4.8	93.3 \pm 2.5	99.0 \pm 0.2	99.2 \pm 1.4
4	L–cysteine	99.0 \pm 1.3	99.0 \pm 1.1	99.9 \pm 5.5	96.9 \pm 0.7
5	L–serine	100.7 \pm 4.4	100.3 \pm 3.9	103.0 \pm 4.4	100.3 \pm 1.7
6	L–glutamine	103.5 \pm 3.9	104.0 \pm 1.9	103.8 \pm 6.1	97.8 \pm 3.1
7	D–glucose	101.3 \pm 1.8	99.9 \pm 1.4	98.1 \pm 2.4	99.8 \pm 1.0
8	Sodium	101.4 \pm 3.4	96.5 \pm 2.3	100.0 \pm 2.9	99.0 \pm 2.8
9	Chloride	101.4 \pm 3.4	96.5 \pm 2.3	100.0 \pm 2.9	99.0 \pm 2.8
10	L–tyrosine	92.3 \pm 4.2	93.1 \pm 2.0	98.9 \pm 2.6	97.4 \pm 1.6
11	Acetate	99.0 \pm 2.8	98.5 \pm 3.0	99.8 \pm 2.1	99.8 \pm 1.6
12	Magnesium	99.0 \pm 2.8	98.5 \pm 3.0	99.8 \pm 2.1	99.8 \pm 1.6

¹ 3 replicate (n=3) analyses

² Standard error at 95% confidence limit

The stability of the Au–ErGO/MWCNT/graphite was also evaluated for its storage stability purpose especially for laboratory or commercial use. Two stability conditions were performed at room temperature (25°C) and at accelerated condition of 45°C. Fig. 5.34 (a) and (b) illustrated the percentage response (anodic peak current response obtained during interval storage relative to the day 1 current response) of A, C, T and G obtained using the fabricated electrode that was measured throughout the 28 days at 25°C and 45°C, respectively. A higher temperature (45°C) condition was selected, in order to study the stability of Au–ErGO/MWCNT/graphite under accelerated conditions.

Fig. 5.34 shows the Au–ErGO/MWCNT/graphite sensor was stable under room temperature storage up to a month. Under 45°C storage condition, the sensor response towards C and T were degraded by 10% after 7 days and after which it remains stable throughout the 28 days; although the recovery was not 100% but at the level of 90% response the electrode is sufficient for the detection of T and C. According to Arrhenius equation of the reaction rate to temperature relation, the chemical stability is predicted to decrease exponentially with a temperature increment. Under the accelerated temperature

condition of 45°C, the fabricated Au–ErGO/MWCNT/graphite electrode was found to be still stable; which implies that the sensor could be stored for a longer storage time of approximate 6 months under room temperature (25°C) condition.

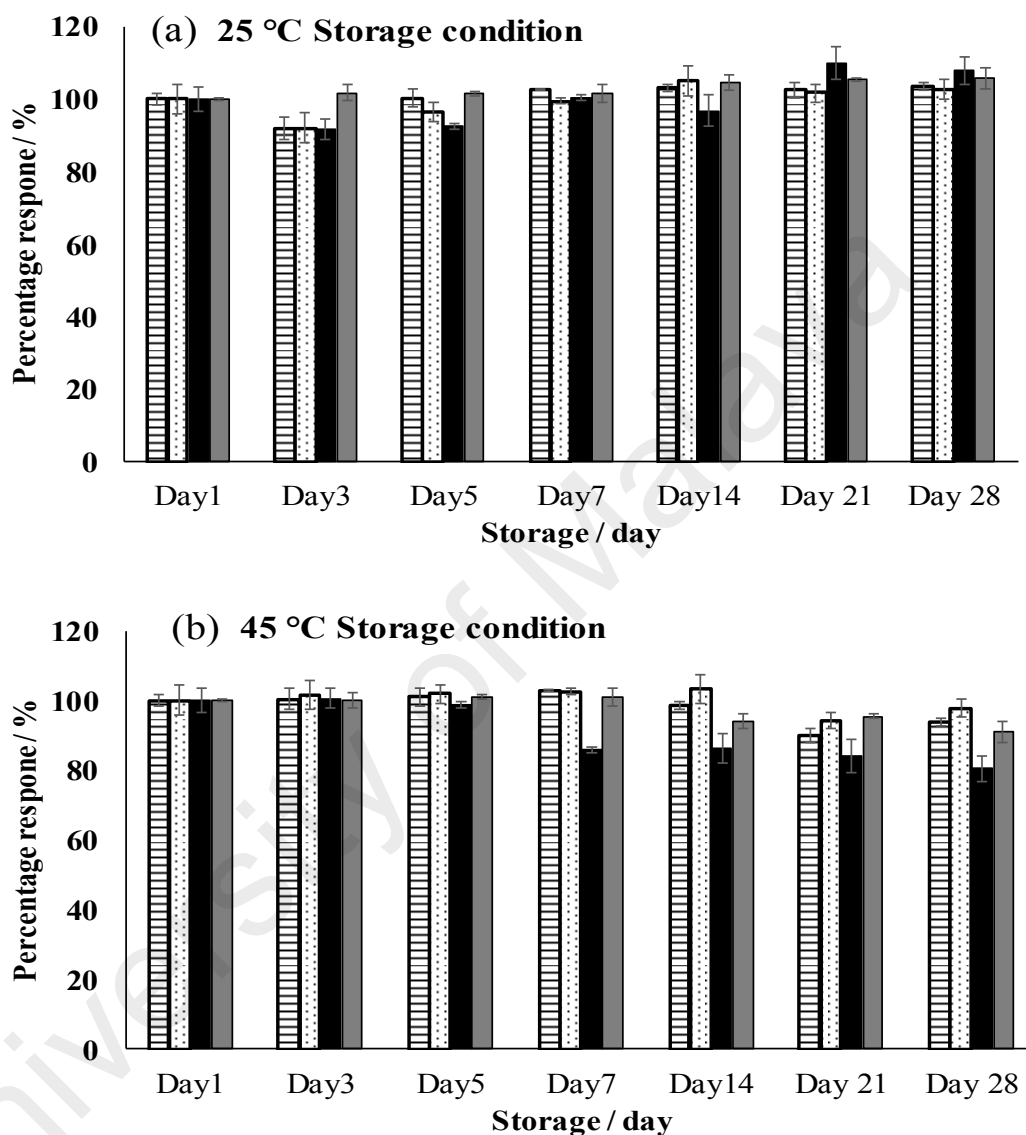


Figure 5.34: Percentage response of Au–ErGO/MWCNT/graphite electrode to A (line), G(dot), C(black) and T(grey) under storage condition of (a) 25°C room temperature and (b) 45°C accelerated temperature condition; throughout 28 days.

5.4 Conclusion

A carbon nanocomposite sensor of Au–ErGO/MWCNT/graphite was successfully developed using a two simple steps procedure employing a heat casting at 105°C and co-electrodeposition method. An evaluation on the particle size distribution and zeta potential charge of the MWCNT suggested that the heat casting method is most optimised at pH 7. Subsequently, from the co-electrodeposition method, cyclic voltammogram has evidenced the successful deposition of gold nanoparticles and reduced graphene oxide. It has also inferred that the optimum deposition condition of the nanocomposite material is at 16th deposition cycles. Modified graphite surface morphology analysis using FE–SEM has further confirmed the presence of MWCNT, gold nanoparticle and reduced graphene oxide on the bare graphite that was obtained from a used battery. The electrochemical impedance spectroscopy analysis has evidenced the deposited MWCNT layer function as an electron mediator network to the Au–ErGO layer; that was fitted to a modified Randles circuit.

The electrochemical characterisation of the Au–ErGO/MWCNT/graphite has shown tremendous improvement in the electrochemical properties particularly the heterogeneous electron transfer rate (k_s) and Eff A. With the surface modification using nanocomposite material (combination of two or more nanomaterials), it also shows an additional attribute including lower overpotential and better electrocatalysis. These attributes are important especially for the application of multiplex analyte detection. Coupled with the improved sensor sensitivity, the developed Au–ErGO/MWCNT/graphite sensor has successfully been used for the simultaneous detection of A, G, C and T using the SWV technique, which has not been managed using GCE or silica based nanocomposite sensor. The developed electrochemical sensor was reliable and can practically be used for the simultaneous analysis of A, G, T and C in real samples either of plant or animal DNA source; and the result obtained was correlated well to the liquid chromatography method

at 103.9%. Besides, the newly developed sensor also exhibited a high sensitivity, low LOD and LOQ that are comparable to the UPLC method. An accuracy assessment of the electrochemical sensor using a known standard of calf thymus DNA bases has shown the recovery of the DNA bases of above 96%; and pre-spiked recovery of DNA bases in the sample matrix was above 92% suggesting the hydrolysis and analysis procedure were at an optimum condition. C and T hydrolysis are found possible at only 8 mol L⁻¹ H₂SO₄, when this finding has not been reported before. The developed sensor was also very selective to A, G, T and C even in the presence of common biological interferents.

University of Malaya

CHAPTER 6: GENERAL CONCLUSION AND FUTURE WORK

Graphite from used battery has proven to be a potential material used for sensor development. In this Ph.D. work, a simple, rapid and green preparation procedure for the development of electrochemical sensor that utilises graphite from a used battery was successfully achieved. To improve the electro-properties of the graphite sensor, a few surface modification procedures have also been developed, which give a different performance outcome as compared to the bare graphite electrode depending on the attributes required for the intended applications. Modification with gold nanoparticles on graphite (Au-NPs/graphite) shows a greater Eff A that provides more active sites for redox reaction to take place. Hence, this improved the sensitivity of the sensor and can accommodate a wider concentration range of analyte either of single or multiplex detection before the electrode surface becomes saturated. Besides, electrode surface modified with nanomaterials also improved the heterogeneous electron transfer rate that contributes to the sensor sensitivity. On the other hand, a surface modification with electrochemically reduced graphene oxide and gold nanoparticles together have given considerable improvement to the electrocatalytic properties, which have an influence on the electrode overpotential. This characteristic is important especially for multiplex analysis; which involves difficulty to oxidise (detect) substances such as C and T. Besides, such nanomaterial combination also gives a 2-fold improvement to the heterogeneous electron transfer rate of the Au-ErGO/MWCNT/graphite.

The practical use of the proposed Au-NPs/graphite and Au-ErGO/MWCNT/graphite sensor was successfully used for the multiplex analysis of anti-oxidants (BHA, BHT and TBHQ) and DNA bases (A, G, T and C), respectively. This achievement has showcased the advantages of graphite based material in the chemical sensor development, which remained a challenge by other electrode platforms such as silica, indium titanium oxide

and glassy carbon in multiplex analysis. The analysis of BHA, BHT and TBHQ have been a concern especially in food regulatory control, which the Au-NPs/graphite sensor could fit for such application especially when in-situ or on field analysis is required by the regulatory enforcer. Similarly, in DNA bases analysis using Au-ErGO/MWCNT/graphite has shown the suitability for the detection of DNA damage especially in clinical laboratory. The reliability of both Au-NPs/graphite and Au-ErGO/MWCNT/graphite in anti-oxidants and DNA bases analyses have correlated excellently to the established liquid chromatography method. Moreover, method validation, spiked analysis and selectivity studies have confirmed the applicability of both methods in real samples analysis.

With the potential of nanocomposite graphite sensor in multiplex analysis, one of the future perspectives of this technology is its applications in the food industry as an online process analyser which could revolutionise the way to control the quality. Instead of the conventional instrumental method, using man-power; a probe or Au-NPs/graphite based sensor can be built in the production line for online monitoring of BHA, BHT and TBHQ, which gives live result on the concentration of preservatives in the food; where it could mitigate any production issue fast before mass rejection. Besides, the proposed sensor can also be incorporated into a chip device such as screen printed electrode (SPE), which can be connected or used with a mobile device and work as a sensor that can be used for analysing anti-oxidant (myricetin) in our daily consumption of food such as fruit juice or beverages. One of the remarkable applications of DNA bases using Au-ErGO/MWCNT/graphite sensor; is the possibility of using it as a probe for the detection of any DNA bases in outer space or distanced planet for evidence of DNA; besides it can also be used as a sensor in clinical laboratories for the study of DNA damage.

REFERENCES

- Abdel-Hamid, R., & Newair, E. F. (2011). Electrochemical behavior of antioxidants: I. Mechanistic study on electrochemical oxidation of gallic acid in aqueous solutions at glassy-carbon electrode. *Journal of Electroanalytical Chemistry*, 657(1–2), 107–112.
- Abou Samra, M., Chedea, V. S., Economou, A., Calokerinos, A., & Kefalas, P. (2011). Antioxidant/prooxidant properties of model phenolic compounds: Part I. Studies on equimolar mixtures by chemiluminescence and cyclic voltammetry. *Food Chemistry*, 125(2), 622–629.
- Aladedunye, F., Przybylski, R., Niehaus, K., Bednarz, H., & Matthäus, B. (2014). Phenolic extracts from *Crataegus × mordenensis* and *Prunus virginiana*: Composition, antioxidant activity and performance in sunflower oil. *LWT - Food Science and Technology*, 59(1), 308–319.
- Alipour, E., Reza, M., & Saadatirad, A. (2013). Electrochimica Acta Simultaneous determination of dopamine and uric acid in biological samples on the pretreated pencil graphite electrode. *Electrochimica Acta*, 91, 36–42.
- Alvarez-Rivera, G., Vila, M., Lores, M., Garcia-Jares, C., & Llompарт, M. (2014). Development of a multi-preservative method based on solid-phase microextraction-gas chromatography-tandem mass spectrometry for cosmetic analysis. *Journal of Chromatography. A*, 1339, 13–25.
- Amlashi, N. E., Hadjmohammadi, M. R., & Nazari, S. S. S. J. (2014). Water-contained surfactant-based vortex-assisted microextraction method combined with liquid chromatography for determination of synthetic antioxidants from edible oil. *Journal of Chromatography. A*, 1361, 9–15.
- Ananingsih, V. K., Sharma, A., & Zhou, W. (2013). Green tea catechins during food processing and storage: A review on stability and detection. *Food Research International*, 50(2), 469–479.
- Appy, D., Lei, H., Wang, C.-Z., Tringides, M. C., Liu, D.-J., Evans, J. W., & Thiel, P. a. (2014). Transition metals on the (0001) surface of graphite: Fundamental aspects of adsorption, diffusion, and morphology. *Progress in Surface Science*, 89(3–4), 219–238.
- Arvand, M., & Hemmati, S. (2017). Magnetic nanoparticles embedded with graphene quantum dots and multiwalled carbon nanotubes as a sensing platform for electrochemical detection of progesterone. *Sensors and Actuators, B: Chemical*, 238, 346–356.
- Asensi-Fabado, M. A., & Munné-Bosch, S. (2010). Vitamins in plants: Occurrence, biosynthesis and antioxidant function. *Trends in Plant Science*, 15(10), 582–592.
- Athar, N., Hardacre, A., Taylor, G., Clark, S., Harding, R., & McLaughlin, J. (2006). Vitamin retention in extruded food products. *Journal of Food Composition and Analysis*, 19(4), 379–383.

- Baena, J. R., Gallego, M., & Valcárcel, M. (2002). Fullerenes in the analytical sciences. *TrAC - Trends in Analytical Chemistry*, 21(3), 187–198.
- Bakhouché, A., Lozano-Sanchez, J., Ballus, C. A., Martínez-García, M., Velasco, M. G., Govantes, Alvaro Olavarria, & Segura-Carretero, A. (2014). Monitoring the moisture reduction and status of bioactive compounds in extra-virgin olive oil over the industrial filtration process. *Food Control*, 40(1), 292–299.
- Bakker, E., & Qin, Y. (2006). Electrochemical Sensors. *Analytical Chemistry*, 78(12), 3965–3984.
- Barnaba, C., Dellacassa, E., Nicolini, G., Nardin, T., Malacarne, M., & Larcher, R. (2015). Identification and quantification of 56 targeted phenols in wines, spirits, and vinegars by online solid-phase extraction - ultrahigh-performance liquid chromatography - quadrupole-orbitrap mass spectrometry. *Journal of Chromatography A*, 1423, 124–135.
- Barsan, M. M., Ghica, M. E., & Brett, C. M. a. (2015). Electrochemical sensors and biosensors based on redox polymer/carbon nanotube modified electrodes: A review. *Analytica Chimica Acta*, 881, 1–23.
- Bélanger, D., & Pinson, J. (2011). Electrografting: a powerful method for surface modification. *Chemical Society Reviews*, 40(7), 3995–4048.
- Belardi, G., Ballirano, P., Ferrini, M., Lavecchia, R., Medici, F., Piga, L., & Scoppettuolo, a. (2011). Characterization of spent zinc-carbon and alkaline batteries by SEM-EDS, TGA/DTA and XRPD analysis. *Thermochimica Acta*, 526(1–2), 169–177.
- Brahman, P. K., Suresh, L., Lokesh, V., & Nizamuddin, S. (2016). Fabrication of highly sensitive and selective nanocomposite film based on CuNPs/fullerene-C60/MWCNTs: An electrochemical nanosensor for trace recognition of paracetamol. *Analytica Chimica Acta*, 917, 107–116.
- Brennan, C., Brennan, M., Derbyshire, E., & Tiwari, B. K. (2011). Effects of extrusion on the polyphenols, vitamins and antioxidant activity of foods. *Trends in Food Science and Technology*, 22(10), 570–575.
- Brewer, M. S. (2011). Natural Antioxidants: Sources, Compounds, Mechanisms of Action, and Potential Applications. *Comprehensive Reviews in Food Science and Food Safety*, 10(4), 221–247.
- Cadet, J., & Poulsen, H. (2010). Measurement of oxidatively generated base damage in cellular DNA and urine. *Free Radical Biology and Medicine*, 48(11), 1457–1459.
- Campbell, F. W., & Compton, R. G. (2010). The use of nanoparticles in electroanalysis: an updated review. *Analytical and Bioanalytical Chemistry*, 396(1), 241–59.
- Caramit, R. P., De Freitas Andrade, A. G., Gomes De Souza, J. B., De Araujo, T. A., Viana, L. H., Trindade, M. A. G., & Ferreira, V. S. (2013). A new voltammetric method for the simultaneous determination of the antioxidants TBHQ and BHA in biodiesel using multi-walled carbon nanotube screen-printed electrodes. *Fuel*, 105, 306–313.

- Carocho, M., Morales, P., & Ferreira, I. C. F. R. (2015). Natural food additives: Quo vadis? *Trends in Food Science & Technology*, *45*(2), 284–295.
- Castro, C., Mura, F., Valenzuela, G., Figueroa, C., Salinas, R., Zuñiga, M. C., & Delporte, C. (2014). Identification of phenolic compounds by HPLC-ESI-MS/MS and antioxidant activity from Chilean propolis. *Food Research International*, *64*, 873–879.
- Chammem, H., Hafaïd, I., Bohli, N., Garcia, A., Meilhac, O., Abdelghani, A., & Mora, L. (2015). A disposable electrochemical sensor based on protein G for High-Density Lipoprotein (HDL) detection. *Talanta*, *144*, 466–473.
- Chen, L., Tang, Y., Wang, K., Liu, C., & Luo, S. (2011). Direct electrodeposition of reduced graphene oxide on glassy carbon electrode and its electrochemical application. *Electrochemistry Communications*, *13*(2), 133–137.
- Chen, L., Yu, G., Chu, Y., Zhang, J., Hu, B., & Zhang, X. (2013). Effect of three types of surfactants on fabrication of Cu-coated graphite powders. *Advanced Powder Technology*, *24*(1), 281–287.
- Chu, Y. F., Wise, M. L., Gulvady, A. a., Chang, T., Kendra, D. F., Jan-Willem Van Klinken, B., & O'Shea, M. (2013). In vitro antioxidant capacity and anti-inflammatory activity of seven common oats. *Food Chemistry*, *139*(1–4), 426–431.
- Ciric-Marjanovic, G. (2013). Recent advances in polyaniline research: Polymerization mechanisms, structural aspects, properties and applications. *Synthetic Metals*, *177*(3), 1–47.
- Conte, G., Benelli, G., Serra, A., Signorini, F., Bientinesi, M., Nicoletta, C., & Canale, A. (2017). Journal of Food Composition and Analysis Lipid characterization of chestnut and willow honeybee-collected pollen: Impact of freeze-drying and microwave-assisted drying. *Journal of Food Composition and Analysis*, *55*, 12–19.
- Cretu, R. C., Gligor, D. M., Muresan, L., Popescu, I. C., & Muresan, L. M. (2006). Kinetic characterization of Prussian Blue-modified graphite electrodes for amperometric detection of hydrogen peroxide. *Journal of Applied Electrochemistry*, *36*, 1327–1332.
- Daikhin L.I, A. A. Kornyshe. and M. Urbak. (1997). Double layer capacitance on a rough metal surface: surface roughness measured by debyce ruler. *Electrochimica Acta*, *42*(19), 2853–2860.
- de Carvalho, A. M., Carioca, A. A. F., Fisberg, R. M., Qi, L., & Marchioni, D. M. (2016). Joint association of fruit, vegetable, and heterocyclic amine intake with DNA damage levels in a general population. *Nutrition (Burbank, Los Angeles County, Calif.)*, *32*(2), 260–264.
- del Moral, P. G., Arín, M. J., Resines, J. A., & Díez, M. T. (2005). Simultaneous determination of adenine and guanine in ruminant bacterial pellets by ion-pair HPLC. *Journal of Chromatography B: Analytical Technologies in the Biomedical and Life Sciences*, *826*(1–2), 257–260.

- Delfanian, M., Esmailzadeh Kenari, R., & Sahari, M. A. (2015). Frying stability of sunflower oil blended with jujube (*Ziziphus mauritiana* Lam.) leaf extract. *Food Science & Nutrition*.
- Delpino-Rius, A., Eras, J., Marsol-Vall, A., Vilaró, F., Balcells, M., & Canela-Garayoa, R. (2014). Ultra performance liquid chromatography analysis to study the changes in the carotenoid profile of commercial monovarietal fruit juices. *Journal of Chromatography A*, *1331*, 90–99.
- Dhiman, S. B., Kamat, J. P., & Naik, D. B. (2009). Antioxidant activity and free radical scavenging reactions of hydroxybenzyl alcohols. Biochemical and pulse radiolysis studies. *Chemico-Biological Interactions*, *182*(2–3), 119–27.
- Dilgin, Y., Kızılkaya, B., Dilgin, D. G., Gökçel, H. İ., & Gorton, L. (2013). Electrocatalytic oxidation of NADH using a pencil graphite electrode modified with quercetin. *Colloids and Surfaces. B, Biointerfaces*, *102*, 816–21.
- Ding, M., Peng, J., Ma, S., & Zhang, Y. (2015). An environment-friendly procedure for the high performance liquid chromatography determination of benzoic acid and sorbic acid in soy sauce. *Food Chemistry*, *183*, 26–29.
- Dumur, F., Guerlin, A., Dumas, E., Bertin, D., Gimes, D., & Mayer, C. R. (2011). Controlled spontaneous generation of gold nanoparticles assisted by dual reducing and capping agents. *Gold Bulletin*, *44*(2), 119–137.
- Eckermann, A. L., Feld, D. J., Shaw, J. a, & Meade, T. J. (2010). Electrochemistry of redox-active self-assembled monolayers. *Coordination Chemistry Reviews*, *254*(15–16), 1769–1802.
- El-Yazbi, A. F., & Loppnow, G. R. (2014). Detecting UV-induced nucleic-acid damage. *TrAC - Trends in Analytical Chemistry*, *61*, 83–91.
- Estevão, M. S., Carvalho, L. C., Ferreira, L. M., Fernandes, E., & Marques, M. M. B. (2011). Analysis of the antioxidant activity of an indole library: cyclic voltammetry versus ROS scavenging activity. *Tetrahedron Letters*, *52*(1), 101–106.
- Esteves da Silva, J. C. G., & Gonçalves, H. M. R. (2011). Analytical and bioanalytical applications of carbon dots. *TrAC - Trends in Analytical Chemistry*, *30*(8), 1327–1336.
- Felix, F. S., Daniel, D., Matos, J. R., Lucio do Lago, C., & Angnes, L. (2016). Fast analysis of terbutaline in pharmaceuticals using multi-walled nanotubes modified electrodes from recordable compact disc. *Analytica Chimica Acta*, *928*, 32–38.
- Ferancová, A., Rengaraj, S., Kim, Y., Labuda, J., & Sillanpää, M. (2010). Electrochemical determination of guanine and adenine by CdS microspheres modified electrode and evaluation of damage to DNA purine bases by UV radiation. *Biosensors and Bioelectronics*, *26*(2), 314–320.
- Flores, G., & Luisa, M. (2015). Journal of Food Composition and Analysis Variations in ellagic acid , quercetin and myricetin in berry cultivars after preharvest methyl jasmonate treatments. *Journal of Food Composition and Analysis*, *39*, 55–61.

- Fotouhi, L., Fatollahzadeh, M., & Heravi, M. M. (2012). Electrochemical Behavior and Voltammetric Determination of Sulfaguanidine at a Glassy Carbon Electrode Modified With a Multi-Walled Carbon Nanotube. *International Journal of Electrochemical science*, 7, 3919–3928.
- Fratoddi, I., Venditti, I., Cametti, C., & Russo, M. V. (2015). Chemiresistive polyaniline-based gas sensors: A mini review. *Sensors and Actuators B: Chemical*, 220, 534–548.
- Freitas, K. H. G., & Fatibello-Filho, O. (2010). Simultaneous determination of butylated hydroxyanisole (BHA) and butylated hydroxytoluene (BHT) in food samples using a carbon composite electrode modified with Cu(3)(PO(4))(2) immobilized in polyester resin. *Talanta*, 81(3), 1102–8.
- Gabriela, I., Bizgan, A. C., Elena, D., Buleandra, M., Basaga, H., Ciucu, A. A., & Adriana, I. (2015). Rapid determination of total polyphenolic content in tea samples based on caffeic acid voltammetric behaviour on a disposable graphite electrode. *Food Chemistry*, 173, 1059–1065.
- Gao, Y. S., Xu, J. K., Lu, L. M., Wu, L. P., Zhang, K. X., Nie, T., & Wu, Y. (2014). Overoxidized polypyrrole/graphene nanocomposite with good electrochemical performance as novel electrode material for the detection of adenine and guanine. *Biosensors and Bioelectronics*, 62, 261–267.
- German, N., Ramanavicius, A., & Ramanaviciene, A. (2014). Electrochemical deposition of gold nanoparticles on graphite rod for glucose biosensing. *Sensors and Actuators B: Chemical*, 203, 25–34.
- German, N., Ramanavicius, A., Voronovic, J., & Ramanaviciene, A. (2012). Glucose biosensor based on glucose oxidase and gold nanoparticles of different sizes covered by polypyrrole layer. *Colloids and Surfaces A: Physicochemical and Engineering Aspects*, 413, 224–230.
- Ghazani, S. M., García-Llatas, G., & Marangoni, A. G. (2013). Minor constituents in canola oil processed by traditional and minimal refining methods. *JAOCs, Journal of the American Oil Chemists' Society*, 90(5), 743–756.
- Ghoreishi, S. M., Behpour, M., Hajisadeghian, E., & Golestaneh, M. (2012). Voltammetric determination of resorcinol on the surface of a glassy carbon electrode modified with multi-walled carbon nanotube. *Arabian Journal of Chemistry*.
- Gil, E. S., & Couto, R. O. (2013). Flavonoid electrochemistry: a review on the electroanalytical applications. *Revista Brasileira de Farmacognosia*, 23(3), 542–558.
- Girard-Lalancette, K., Pichette, A., & Legault, J. (2009). Sensitive cell-based assay using DCFH oxidation for the determination of pro- and antioxidant properties of compounds and mixtures: Analysis of fruit and vegetable juices. *Food Chemistry*, 115(2), 720–726.
- Glavin, D. P., Cleaves, H. J., Buch, A., Schubert, M., Aubrey, A., Bada, J. L., & Mahaffy, P. R. (2006). Sublimation extraction coupled with gas chromatography-mass

spectrometry: A new technique for future in situ analyses of purines and pyrimidines on Mars. *Planetary and Space Science*, 54(15), 1584–1591.

Gotti, G., Fajerweg, K., Evrard, D., & Gros, P. (2014). Electrodeposited gold nanoparticles on glassy carbon: Correlation between nanoparticles characteristics and oxygen reduction kinetics in neutral media. *Electrochimica Acta*, 128, 412–419.

Goulart, L. A., Teixeira, A. R. L., Ramalho, D. A., Terezo, A. J., & Castilho, M. (2014). Development of an analytical method for the determination of tert-butylhydroquinone in soybean biodiesel. *Fuel*, 115, 126–131.

Graven, P., Tambalo, M., Scapozza, L., & Perozzo, R. (2014). Purine metabolite and energy charge analysis of *Trypanosoma brucei* cells in different growth phases using an optimized ion-pair RP-HPLC/UV for the quantification of adenine and guanine pools. *Experimental Parasitology*, 141(1), 28–38.

Guo, S., & Wang, E. (2007). Synthesis and electrochemical applications of gold nanoparticles. *Analytica Chimica Acta*, 598(2), 181–92.

Hasanzadeh, M., Shadjou, N., Eskandani, M., Soleymani, J., Jafari, F., & de la Guardia, M. (2014). Dendrimer-encapsulated and cored metal nanoparticles for electrochemical nanobiosensing. *TrAC - Trends in Analytical Chemistry*, 53, 137–149.

Hashemzadeh, N., Hasanzadeh, M., Shadjou, N., Eivazi-Ziaei, J., Khoubnasabjafari, M., & Jouyban, A. (2016). Graphene quantum dot modified glassy carbon electrode for the determination of doxorubicin hydrochloride in human plasma. *Journal of Pharmaceutical Analysis*, 6(4), 235–241.

He, J.-B., Wang, Y., Deng, N., & Lin, X.-Q. (2007). Study of the adsorption and oxidation of antioxidant rutin by cyclic voltammetry-voltabsorptometry. *Bioelectrochemistry (Amsterdam, Netherlands)*, 71(2), 157–63.

Helden, P. D. Van, Victor, T. C., Warren, R. M., & Helden, E. G. Van. (2001). Isolation of DNA from *Mycobacterium tuberculosis*. *Methods in Molecular Medicine*, 54(15), 19–29.

Hezard, T., Fajerweg, K., Evrard, D., Collière, V., Behra, P., & Gros, P. (2012). Gold nanoparticles electrodeposited on glassy carbon using cyclic voltammetry: Application to Hg(II) trace analysis. *Journal of Electroanalytical Chemistry*, 664, 46–52.

Hossain, M. Z., Gilbert, S. F., Patel, K., Ghosh, S., Bhunia, A. K., & Kern, S. E. (2013). Biological clues to potent DNA-damaging activities in food and flavoring. *Food and Chemical Toxicology*, 55, 557–567.

Hu, S., Wang, Y., Wang, X., Xu, L., Xiang, J., & Sun, W. (2012). Electrochemical detection of hydroquinone with a gold nanoparticle and graphene modified carbon ionic liquid electrode. *Sensors and Actuators, B: Chemical*, 168, 27–33.

Hu, W., Guo, T., Jiang, W. J., Dong, G. L., Chen, D. W., Yang, S. L., & Li, H. R. (2015). Effects of ultrahigh pressure extraction on yield and antioxidant activity of

chlorogenic acid and cynaroside extracted from flower buds of *Lonicera japonica*. *Chinese Journal of Natural Medicines*, 13(6), 445–453.

- Hu, X., Dou, W., & Zhao, G. (2015). Electrochemical Immunosensor for *Enterobacter sakazakii* detection based on electrochemically reduced graphene oxide -Gold nanoparticles/ionic liquid modified electrode. *Journal of Electroanalytical Chemistry*, 756, 43–48.
- Huang, J. H., Huang, C. C., Fang, J. Y., Yang, C., Chan, C. M., Wu, N. L., & Hung, C. F. (2010). Protective effects of myricetin against ultraviolet-B-induced damage in human keratinocytes. *Toxicology in Vitro*, 24(1), 21–28.
- Inagaki, S., Esaka, Y., Deyashiki, Y., Sako, M., & Goto, M. (2003). A nalysis of DNA adducts of acetaldehyde by liquid chromatography – mass spectrometry. *Journal of Chromatography A*, 987, 341–347.
- Ioannou, I., Hafsa, I., Hamdi, S., Charbonnel, C., & Ghoul, M. (2012). Review of the effects of food processing and formulation on flavonol and anthocyanin behaviour. *Journal of Food Engineering*, 111(2), 208–217.
- Iverson, F. (1995). Phenolic antioxidants: Health protection branch studies on butylated hydroxyanisole. *Cancer Letters*, 93, 49–54.
- Jayasri, D., & Narayanan, S. S. (2006). Electrocatalytic oxidation and amperometric determination of BHA at graphite-wax composite electrode with silver hexacyanoferrate as electrocatalyst. *Sensors and Actuators, B: Chemical*, 119(1), 135–142.
- Jayasri, D., & Narayanan, S. S. (2007). Manganese(II) hexacyanoferrate based renewable amperometric sensor for the determination of butylated hydroxyanisole in food products. *Food Chemistry*, 101(2), 607–614.
- Jia, H., Chang, G., Lei, M., He, H., Liu, X., Shu, H., & He, Y. (2016). Platinum nanoparticles decorated dendrite-like gold nanostructure on glassy carbon electrodes for enhancing electrocatalysis performance to glucose oxidation. *Applied Surface Science*, 384, 58–64.
- Jiao, J., Gai, Q., Fu, Y., Zu, Y., Luo, M., Wang, W., & Zhao, C. (2013). Microwave-assisted ionic liquids pretreatment followed by hydro-distillation for the efficient extraction of essential oil from *Dryopteris fragrans* and evaluation of its antioxidant efficacy in sunflower oil storage. *Journal of Food Engineering*, 117(4), 477–485.
- José Jara-Palacios, M., Hernanz, D., Luisa Escudero-Gilete, M., & Heredia, F. J. (2014). Antioxidant potential of white grape pomaces: Phenolic composition and antioxidant capacity measured by spectrophotometric and cyclic voltammetry methods. *Food Research International*, 66, 150–157.
- Joshi, P. C., Gray, T. A., & Keane, T. C. (2012). Protection of riboflavin and UVB sensitized degradation of DNA and RNA bases by natural antioxidants. *Ecotoxicology and Environmental Safety*, 78, 86–90.
- Kalambate, P. K., & Srivastava, A. K. (2016). Simultaneous voltammetric determination

of paracetamol, cetirizine and phenylephrine using a multiwalled carbon nanotube-platinum nanoparticles nanocomposite modified carbon paste electrode. *Sensors and Actuators, B: Chemical*, 233, 237–248.

- Kameya, H., Watanabe, J., Takano-Ishikawa, Y., & Todoriki, S. (2014). Comparison of scavenging capacities of vegetables by ORAC and EPR. *Food Chemistry*, 145, 866–873.
- Kashyap, S., Mishra, S., Behera, S. K., Kashyap, S., Mishra, S., & Behera, S. K. (2014). Aqueous Colloidal Stability of Graphene Oxide and Chemically Converted Graphene, Aqueous Colloidal Stability of Graphene Oxide and Chemically Converted Graphene. *Journal of Nanoparticles, Journal of Nanoparticles*, 2014, 2014, e640281.
- Kerner, Z., & Pajkossy, T. (2000). On the origin of capacitance dispersion of rough electrodes. *Electrochimica Acta*, 46(2–3), 207–211.
- Kilmartin, P. A., & Hsu, C. F. (2003). Characterisation of polyphenols in green, oolong, and black teas, and in coffee, using cyclic voltammetry. *Food Chemistry*, 82(4), 501–512.
- Kiss, L., David, V., David, I. G., Lazar, P., Mihailciuc, C., Stamatina, I., & Ciucu, A. A. (2016). Electropolymerized molecular imprinting on glassy carbon electrode for voltammetric detection of dopamine in biological samples. *Talanta*, 160, 489–498.
- Kita, A., Bakowska-Barczak, A., Lisińska, G., Hamouz, K., & Kułakowska, K. (2014). Antioxidant activity and quality of red and purple flesh potato chips. *LWT - Food Science and Technology*, 62, 525–531.
- Kochana, J., Wapiennik, K., Kozak, J., Knihnicki, P., Pollap, A., Woźniakiewicz, M., ... Kościelniak, P. (2015). Tyrosinase-based biosensor for determination of bisphenol A in a flow-batch system. *Talanta*, 144, 163–170.
- Komorsky-Lovrić, Š., & Novak, I. (2013). Abrasive stripping voltammetry of myricetin and dihydromyricetin. *Electrochimica Acta*, 98, 153–156.
- Kumar, A., Malik, A. K., & Tewary, D. K. (2009). A new method for determination of myricetin and quercetin using solid phase microextraction-high performance liquid chromatography-ultra violet/visible system in grapes, vegetables and red wine samples. *Analytica Chimica Acta*, 631(2), 177–81.
- Kumar, S. A., Cheng, H. W., Chen, S. M., & Wang, S. F. (2010). Preparation and characterization of copper nanoparticles/zinc oxide composite modified electrode and its application to glucose sensing. *Materials Science and Engineering C*, 30(1), 86–91.
- Larangeira, P. M., Rosso, V. V. De, Hugo, V., Foot, C., Moura, G. De, & Ribeiro, D. A. (2016). Experimental and Toxicologic Pathology Genotoxicity, mutagenicity and cytotoxicity of carotenoids extracted from ionic liquid in multiples organs of Wistar rats. *Experimental and Toxicologic Pathology*, 68(10), 571–578.
- Lawal, A. T. (2016). Synthesis and utilization of carbon nanotubes for fabrication of

electrochemical biosensors. *Materials Research Bulletin*, 73, 308–350.

- Li, N., Lei, T., Liu, Y., He, Y., & Zhang, Y. (2010). Electrochemical preparation and characterization of gold-polyaniline core-shell nanocomposites on highly oriented pyrolytic graphite. *Transactions of Nonferrous Metals Society of China*, 20(12), 2314–2319.
- Li, X., Chen, F., Li, S., Jia, J., Gu, H., & Yang, L. (2016). An efficient homogenate-microwave-assisted extraction of flavonols and anthocyanins from blackcurrant marc: Optimization using combination of Plackett-Burman design and Box-Behnken design. *Industrial Crops & Products*, 94, 834–847.
- Li, X.-L., Meng, D.-L., Zhao, J., & Yang, Y.-L. (2014). Determination of synthetic phenolic antioxidants in essence perfume by high performance liquid chromatography with vortex-assisted, cloud-point extraction using AEO-9. *Chinese Chemical Letters*, 25(8), 1198–1202.
- Li, Y., & Ding, Y. (2012). Minireview: Therapeutic Potential of Myricetin in Diabetes Mellitus. *Food Science and Human Wellness*, 1(1), 19–25.
- Lin, X., Ni, Y., & Kokot, S. (2014). Electrochemical mechanism of eugenol at a Cu doped gold nanoparticles modified glassy carbon electrode and its analytical application in food samples. *Electrochimica Acta*, 133, 484–491.
- Liu, C., Wang, K., Luo, S., Tang, Y., & Chen, L. (2011). Direct electrodeposition of graphene enabling the one-step synthesis of graphene-metal nanocomposite films. *Small*, 7(9), 1203–1206.
- Liu, H., Wang, G., Chen, D., Zhang, W., Li, C., & Fang, B. (2008). Fabrication of polythionine/NPAu/MWNTs modified electrode for simultaneous determination of adenine and guanine in DNA. *Sensors and Actuators, B: Chemical*, 128(2), 414–421.
- Liu, J., Liu, Z., Barrow, C. J., & Yang, W. (2014). Molecularly engineered graphene surfaces for sensing applications: A review. *Analytica Chimica Acta*, 859, 1–19.
- Liu, J., Poh, C. K., Zhan, D., Lai, L., Lim, S. H., Wang, L., & Lin, J. (2013). Improved synthesis of graphene flakes from the multiple electrochemical exfoliation of graphite rod. *Nano Energy*, 2(3), 377–386.
- Liu, L., Ma, Z., Zhu, X., Zeng, R., Tie, S., & Nan, J. (2016). Electrochemical behavior and simultaneous determination of catechol, resorcinol, and hydroquinone using thermally reduced carbon nano-fragment modified glassy carbon electrode. *Analytical Methods*, 8(3), 605–613.
- Lu, G., & Zangari, G. (2006). Electrodeposition of platinum nanoparticles on highly oriented pyrolytic graphite. *Electrochimica Acta*, 51(12), 2531–2538.
- Lu, Q., Hu, H., Wu, Y., Chen, S., Yuan, D., & Yuan, R. (2014). An electrogenerated chemiluminescence sensor based on gold nanoparticles@C60 hybrid for the determination of phenolic compounds. *Biosensors & Bioelectronics*, 60, 325–31.

- Lucarini, M., & Pedulli, G. F. (2010). Free radical intermediates in the inhibition of the autoxidation reaction. *Chemical Society Reviews*, 39, 2106–2119.
- Ma, H., Zhang, X., Li, X., Li, R., Du, B., & Wei, Q. (2015). Electrochemical immunosensor for detecting typical bladder cancer biomarker based on reduced graphene oxide-tetraethylene pentamine and trimetallic AuPdPt nanoparticles. *Talanta*, 143, 77–82.
- Makhotkina, O., & Kilmartin, P. A. (2009). Uncovering the influence of antioxidants on polyphenol oxidation in wines using an electrochemical method: Cyclic voltammetry. *Journal of Electroanalytical Chemistry*, 633(1), 165–174.
- Makhotkina, O., & Kilmartin, P. a. (2012). The phenolic composition of Sauvignon blanc juice profiled by cyclic voltammetry. *Electrochimica Acta*, 83, 188–195.
- Maringa, A., Antunes, E., & Nyokong, T. (2014). Electrochemical behaviour of gold nanoparticles and Co tetraaminophthalocyanine on glassy carbon electrode. *Electrochimica Acta*, 121, 93–101.
- Martín, A., & Escarpa, A. (2014). Graphene: The cutting-edge interaction between chemistry and electrochemistry. *TrAC - Trends in Analytical Chemistry*, 56, 13–26.
- Martinez, S., Valek, L., Petrović, Ž., Metikoš-Huković, M., & Piljac, J. (2005). Catechin antioxidant action at various pH studied by cyclic voltammetry and PM3 semi-empirical calculations. *Journal of Electroanalytical Chemistry*, 584(2), 92–99.
- Masek, A., Chrzescijanska, E., Kosmalka, A., & Zaborski, M. (2014). Characteristics of compounds in hops using cyclic voltammetry, UV-VIS, FTIR and GC-MS analysis. *Food Chemistry*, 156, 353–61.
- Masek, A., Chrzescijanska, E., & Zaborski, M. (2014). Electrooxidation of morin hydrate at a Pt electrode studied by cyclic voltammetry. *Food Chemistry*, 148, 18–23.
- Mazloun-Ardakani, M., Ahmadi, R., Heidari, M. M., & Sheikh-Mohseni, M. A. (2014). Electrochemical detection of the MT-ND6 gene and its enzymatic digestion: Application in human genomic sample. *Analytical Biochemistry*, 455(1), 60–64.
- Medeiros, R. A., Rocha-Filho, R. C., & Fatibello-Filho, O. (2010). Simultaneous voltammetric determination of phenolic antioxidants in food using a boron-doped diamond electrode. *Food Chemistry*, 123(3), 886–891.
- Mehta, S. K., Salaria, K., & Umar, A. (2012). Electrochimica Acta Highly sensitive and selective cyanide ion sensor based on modified ZnS nanoparticles. *Electrochimica Acta*, 81, 308–312.
- Mehta, S. K., & Umar, A. (2011). Talanta Highly sensitive hydrazine chemical sensor based on mono-dispersed rapidly synthesized PEG-coated ZnS nanoparticles. *Talanta*, 85(5), 2411–2416.
- Mello, L. D., Hernandez, S., Marrazza, G., Mascini, M., & Kubota, L. T. (2006). Investigations of the antioxidant properties of plant extracts using a DNA-electrochemical biosensor. *Biosensors & Bioelectronics*, 21(7), 1374–82.

- Mendil, D., Uluözlü, Ö. D., Tüzen, M., & Soylak, M. (2009). Investigation of the levels of some element in edible oil samples produced in Turkey by atomic absorption spectrometry. *Journal of Hazardous Materials*, 165(1–3), 724–728.
- Moreno-Baron, L., Merkoçi, a., & Alegret, S. (2003). Graphite-epoxy composite as an alternative material to design mercury free working electrodes for stripping voltammetry. *Electrochimica Acta*, 48(18), 2599–2605.
- Nagy, E., Johansson, C., Zeisig, M., & Möller, L. (2005). Oxidative stress and DNA damage caused by the urban air pollutant 3-NBA and its isomer 2-NBA in human lung cells analyzed with three independent methods. *Journal of Chromatography B: Analytical Technologies in the Biomedical and Life Sciences*, 827(1), 94–103.
- Nia, P. M., Meng, W. P., & Alias, Y. (2015). Hydrogen peroxide sensor: Uniformly decorated silver nanoparticles on polypyrrole for wide detection range. *Applied Surface Science*, 357, 1565–1572.
- Niedziałkowski, P., Ossowski, T., Zięba, P., Cirocka, a., Rochowski, P., Pogorzelski, S. J., & Bogdanowicz, R. (2015). Poly-l-lysine-modified boron-doped diamond electrodes for the amperometric detection of nucleic acid bases. *Journal of Electroanalytical Chemistry*, 756, 84–93.
- Nijveldt, R. . (2001). Flavonoids : a review of probable mechanism of action and potential applications. *American Journal Clinical Nutrition*, 74, 418–425.
- Niu, X., Yang, W., Ren, J., Guo, H., Long, S., Chen, J., & Gao, J. (2012). Electrochemical behaviors and simultaneous determination of guanine and adenine based on graphene-ionic liquid-chitosan composite film modified glassy carbon electrode. *Electrochimica Acta*, 80, 346–353.
- Noor, A. M., Rameshkumar, P., Yusoff, N., Ming, H. N., & Sajab, M. S. (2016). Microwave synthesis of reduced graphene oxide decorated with silver nanoparticles for electrochemical determination of 4-nitrophenol. *Ceramics International*, 42(16), 18813–18820.
- Oberacher, H., Erb, R., Plattner, S., & Chervet, J.-P. (2015). Mechanistic aspects of nucleic-acid oxidation studied with electrochemistry-mass spectrometry. *TrAC Trends in Analytical Chemistry*, 70, 100–111.
- Pajkossy, T. (2005). Impedance spectroscopy at interfaces of metals and aqueous solutions — Surface roughness, CPE and related issues. *Solid State Ionics*, 176(25–28), 1997–2003.
- Pandey, K. B., & Rizvi, S. I. (2009). Plant polyphenols as dietary antioxidants in human health and disease. *Oxidative Medicine and Cellular Longevity*, 2(5), 270–278.
- Pang, P., Liu, Y., Zhang, Y., Gao, Y., & Hu, Q. (2014). Electrochemical determination of luteolin in peanut hulls using graphene and hydroxyapatite nanocomposite modified electrode. *Sensors and Actuators B: Chemical*, 194, 397–403.
- Pang, S., Zhang, Y., Wu, C., & Feng, S. (2016). Fluorescent carbon dots sensor for highly sensitive detection of guanine. *Sensors and Actuators, B: Chemical*, 222, 857–863.

- Pillay, J., Ozoemena, K. I., Tshikhudo, R. T., & Moutloali, R. M. (2010). Monolayer-protected clusters of gold nanoparticles: impacts of stabilizing ligands on the heterogeneous electron transfer dynamics and voltammetric detection. *Langmuir: The ACS Journal of Surfaces and Colloids*, 26(11), 9061–8.
- Pinelo, M., Manzocco, L., Nuñez, M. J., & Nicoli, M. C. (2004). Solvent effect on quercetin antioxidant capacity. *Food Chemistry*, 88, 201–207.
- Pohanka, M., Band'ouchová, H., Vlčková, K., Žd'árová Karasová, J., Kuča, K., Damková, V., & Pikula, J. (2011). Square wave voltammetry on screen printed electrodes: comparison to ferric reducing antioxidant power in plasma from model laboratory animal (Grey Partridge) and comparison to standard antioxidants. *Journal of Applied Biomedicine*, 9(2), 103–109.
- Potkonjak, N. I., Veselinović, D. S., Novaković, M. M., Gorjanović, S. Ž., Pezo, L. L., & Sužnjević, D. Ž. (2012). Antioxidant activity of propolis extracts from Serbia: a polarographic approach. *Food and Chemical Toxicology: An International Journal Published for the British Industrial Biological Research Association*, 50(10), 3614–8.
- Prior, R. L. (2014). Oxygen radical absorbance capacity (ORAC): New horizons in relating dietary antioxidants/bioactives and health benefits. *Journal of Functional Foods*, 1–14.
- Pumera, M., Aldavert, M., Mills, C., Merkoçi, A., & Alegret, S. (2005). Direct voltammetric determination of gold nanoparticles using graphite-epoxy composite electrode. *Electrochimica Acta*, 50(18), 3702–3707.
- Radhakrishnan, S., Krishnamoorthy, K., Sekar, C., Wilson, J., & Kim, S. J. (2015). A promising electrochemical sensing platform based on ternary composite of polyaniline–Fe₂O₃–reduced graphene oxide for sensitive hydroquinone determination. *Chemical Engineering Journal*, 259, 594–602.
- Ragubeer, N., Beukes, D. R., & Limson, J. L. (2010). Critical assessment of voltammetry for rapid screening of antioxidants in marine algae. *Food Chemistry*, 121(1), 227–232.
- Ramesh, P., Sivakumar, P., & Sampath, S. (2002). Renewable surface electrodes based on dopamine functionalized exfoliated graphite: NADH oxidation and ethanol biosensing. *Journal of Electroanalytical Chemistry*, 528(1–2), 82–92.
- Rao, H., Chen, M., Ge, H., Lu, Z., Liu, X., Zou, P., & Wang, Y. (2017). A novel electrochemical sensor based on Au@PANI composites film modified glassy carbon electrode binding molecular imprinting technique for the determination of melamine. *Biosensors and Bioelectronics*, 87(July 2016), 1029–1035.
- Rather, J. A., & De Wael, K. (2013). Fullerene-C60 sensor for ultra-high sensitive detection of bisphenol-A and its treatment by green technology. *Sensors and Actuators, B: Chemical*, 176, 110–117.
- Rebelo, M. J., Rego, R., Ferreira, M., & Oliveira, M. C. (2013). Comparative study of the antioxidant capacity and polyphenol content of Douro wines by chemical and

electrochemical methods. *Food Chemistry*, 141(1), 566–573.

- Rezaei, B., Boroujeni, M. K., & Ensafi, A. a. (2014). A novel electrochemical nanocomposite imprinted sensor for the determination of lorazepam based on modified polypyrrole@sol-gel@gold nanoparticles/pencil graphite electrode. *Electrochimica Acta*, 123, 332–339.
- Saha, A., Jiang, C., & Martí, A. a. (2014). Carbon nanotube networks on different platforms. *Carbon*, 79, 1–18.
- Santos, C. M. M., Garcia, M. B. Q., Silva, A. M. S., Santus, R., Morlière, P., & Fernandes, E. (2013). Electrochemical characterization of bioactive hydroxyxanthenes by cyclic voltammetry. *Tetrahedron Letters*, 54(1), 85–90.
- Schaich, K. M., Tian, X., & Xie, J. (2015). Hurdles and pitfalls in measuring antioxidant efficacy: A critical evaluation of ABTS, DPPH, and ORAC assays. *Journal of Functional Foods*, 14, 111–125.
- Selbmann, L., Isola, D., Zucconi, L., & Onofri, S. (2011). Resistance to UV-B induced DNA damage in extreme-tolerant cryptoendolithic Antarctic fungi: Detection by PCR assays. *Fungal Biology*, 115(10), 937–944.
- Sengupta, R., Bhattacharya, M., Bandyopadhyay, S., & Bhowmick, A. K. (2011). A review on the mechanical and electrical properties of graphite and modified graphite reinforced polymer composites. *Progress in Polymer Science (Oxford)*, 36(5), 638–670.
- Senoo, T., Yamanaka, M., Nakamura, A., Terashita, T., Kawano, S., & Ikeda, S. (2016). Quantitative PCR for detection of DNA damage in mitochondrial DNA of the fission yeast *Schizosaccharomyces pombe*. *Journal of Microbiological Methods*, 127, 77–81.
- Shahidi, F., & Ambigaipalan, P. (2015). Phenolics and polyphenolics in foods, beverages and spices: Antioxidant activity and health effects - A review. *Journal of Functional Foods*, 18, 820–897.
- Shamsi, M. H., & Kraatz, H. B. (2013). Interactions of Metal Ions with DNA and Some Applications. *Journal of Inorganic and Organometallic Polymers and Materials*, 23(1), 4–23.
- Sharma, S., Kori, S., & Parmar, A. (2015). Surfactant mediated extraction of total phenolic contents (TPC) and antioxidants from fruits juices. *Food Chemistry*, 185, 284–288.
- Shi, F., Xi, J., Hou, F., Han, L., Li, G., Gong, S., & Sun, W. (2016). Application of three-dimensional reduced graphene oxide-gold composite modified electrode for direct electrochemistry and electrocatalysis of myoglobin. *Materials Science and Engineering: C*, 58, 450–457.
- Shimelis, O., & Giese, R. W. (2006). Nuclease P1 digestion/high-performance liquid chromatography, a practical method for DNA quantitation. *Journal of Chromatography A*, 1117(2), 132–136.

- Shiomi, K., Kuriyama, I., Yoshida, H., & Mizushima, Y. (2013). Inhibitory effects of myricetin on mammalian DNA polymerase, topoisomerase and human cancer cell proliferation. *Food Chemistry*, 139(1–4), 910–918.
- Siger, A., Nogala-Kalucka, M., & Lampart-Szczapa, E. (2008). The content and antioxidant activity of phenolic compounds in cold-pressed plant oils. *Journal of Food Lipids*, 15(2), 137–149.
- Singh, R., Kalra, R. S., Hasan, K., Kaul, Z., Cheung, C. T., Huschtscha, L., & Wadhwa, R. (2014). Molecular characterization of collaborator of ARF (CARF) as a DNA damage response and cell cycle checkpoint regulatory protein. *Experimental Cell Research*, 322(2), 324–334.
- Soares, J. P., Silva, A. M., Fonseca, S., Oliveira, M. M., Peixoto, F., Gaivão, I., & Mota, M. P. (2015). How can age and lifestyle variables affect DNA damage, repair capacity and endogenous biomarkers of oxidative stress? *Experimental Gerontology*, 62, 45–52.
- Sochor, J., Dobes, J., Krystofova, O., Ruttkay-nedecky, B., Babula, P., Pohanka, M., & Kizek, R. (2013). Electrochemistry as a Tool for Studying Antioxidant Properties. *International Journal of Electrochemical Science*, 8, 8464–8489.
- Song, Y., Ma, Y., Wang, Y., Di, J., & Tu, Y. (2010). Electrochemical deposition of gold–platinum alloy nanoparticles on an indium tin oxide electrode and their electrocatalytic applications. *Electrochimica Acta*, 55(17), 4909–4914.
- Sprung, C. N., Ivashkevich, A., Forrester, H. B., Redon, C. E., Georgakilas, A., & Martin, O. A. (2015). Oxidative DNA damage caused by inflammation may link to stress-induced non-targeted effects. *Cancer Letters*, 356(1), 72–81.
- Sreeramulu, D. (2011). Antioxidant and Phenolic Content of Nuts, Oil Seeds, Milk and Milk Products Commonly Consumed in India. *Food and Nutrition Sciences*, 2(5), 422–427.
- Stetter, J. R., Penrose, W. R., & Yao, S. (2003). Sensors, Chemical Sensors, Electrochemical Sensors, and ECS. *Journal of The Electrochemical Society*, 150(2), S11.
- Stojiljković, D., Arsić, I., & Tadić, V. (2016). Extracts of wild apple fruit (*Malus sylvestris* (L.) Mill., Rosaceae) as a source of antioxidant substances for use in production of nutraceuticals and cosmeceuticals. *Industrial Crops and Products*, 80, 165–176.
- Stradiotto, N. R., Yamanaka, H., & Zanoni, M. V. B. (2003). Review Electrochemical Sensors: A Powerful Tool in Analytical Chemistry. *Journal of The Brazilian Chemical Society*, 14(2), 159–173.
- Streeter, I., & Compton, R. G. (2007). Diffusion-Limited Currents to Nanoparticles of Various Shapes Supported on an Electrode; Spheres, Hemispheres, and Distorted Spheres and Hemispheres. *Journal of Physical Chemistry C*, 111(49), 18049–18054.
- Sultana, B., & Anwar, F. (2008). Flavonols (kaempferol, quercetin, myricetin) contents

- of selected fruits, vegetables and medicinal plants. *Food Chemistry*, *108*, 879–884.
- Sun, M., Yang, X., Huisingh, D., Wang, R., & Wang, Y. (2015). Consumer behavior and perspectives concerning spent household battery collection and recycling in China: a case study. *Journal of Cleaner Production*, 1–11.
- Sun, W., Li, L., Lei, B., Li, T., Ju, X., Wang, X., & Sun, Z. (2013). Fabrication of graphene-platinum nanocomposite for the direct electrochemistry and electrocatalysis of myoglobin. *Materials Science & Engineering. C, Materials for Biological Applications*, *33*(4), 1907–13.
- Sun, W., Li, Y., Duan, Y., & Jiao, K. (2008). Direct electrocatalytic oxidation of adenine and guanine on carbon ionic liquid electrode and the simultaneous determination. *Biosensors and Bioelectronics*, *24*(4), 988–993.
- Sun, W., Wang, Y., Gong, S., Cheng, Y., Shi, F., & Sun, Z. (2013). Application of poly(acridine orange) and graphene modified carbon/ionic liquid paste electrode for the sensitive electrochemical detection of rutin. *Electrochimica Acta*, *109*, 298–304.
- Sutradhar, S., & Patnaik, A. (2017). A new fullerene-C60 Nanogold composite for non-enzymatic glucose sensing. *Sensors and Actuators, B: Chemical*, *241*, 681–689.
- Švorc, L., & Kalcher, K. (2014). Modification-free electrochemical approach for sensitive monitoring of purine DNA bases: Simultaneous determination of guanine and adenine in biological samples using boron-doped diamond electrode. *Sensors and Actuators B: Chemical*, *194*, 332–342.
- Tan, H. W., Abdul Aziz, A. R., & Aroua, M. K. (2013). Glycerol production and its applications as a raw material: A review. *Renewable and Sustainable Energy Reviews*, *27*, 118–127.
- Tan, S. C., & Yiap, B. C. (2009). DNA, RNA, and protein extraction: The past and the present. *Journal of Biomedicine and Biotechnology*, 2009.
- Teepoo, S., Chumsaeng, P., Nethan, P., Prueprang, W., & Tumsae, P. (2012). Highly Sensitive Pencil-Based Renewable Biosensor for Hydrogen Peroxide Detection With a Novel Bionanomultilayer. *International Journal of Electrochemical Science*, *7*, 4645–4656.
- Thangaraj, R., Nellaiappan, S., Sudhakaran, R., & Kumar, A. S. (2014). A flow injection analysis coupled dual electrochemical detector for selective and simultaneous detection of guanine and adenine. *Electrochimica Acta*, *123*, 485–493.
- Thi, N. Do, & Hwang, E. S. (2016). Effects of drying methods on contents of bioactive compounds and antioxidant activities of black chokeberries (*Aronia melanocarpa*). *Food Science and Biotechnology*, *25*(1), 55–61.
- Tomášková, M., Chýlková, J., Jehlička, V., Navrátil, T., Švancara, I., & Šelešovská, R. (2014). Simultaneous determination of BHT and BHA in mineral and synthetic oils using linear scan voltammetry with a gold disc electrode. *Fuel*, *123*, 107–112.

- Tong, Y., Li, H., Guan, H., Zhao, J., Majeed, S., Anjum, S., & Xu, G. (2013). Electrochemical cholesterol sensor based on carbon nanotube@molecularly imprinted polymer modified ceramic carbon electrode. *Biosensors and Bioelectronics*, *47*, 553–558.
- Tran, L. D., Nguyen, D. T., Nguyen, B. H., Do, Q. P., & Le Nguyen, H. (2011). Development of interdigitated arrays coated with functional polyaniline/MWCNT for electrochemical biodetection: Application for human papilloma virus. *Talanta*, *85*(3), 1560–1565.
- Verdolino, V., Cammi, R., Munk, B. H., & Schlegel, H. B. (2008). Calculation of pKa values of nucleobases and the guanine oxidation products guanidinohydantoin and spiroiminodihydantoin using density functional theory and a polarizable continuum model. *The Journal of Physical Chemistry. B*, *112*(51), 16860–16873.
- Wang, J., Wang, L., Di, J., & Tu, Y. (2008). Disposable biosensor based on immobilization of glucose oxidase at gold nanoparticles electrodeposited on indium tin oxide electrode. *Sensors and Actuators B: Chemical*, *135*(1), 283–288.
- Wang, J.-Y., Wu, H.-L., Sun, Y.-M., Gu, H.-W., Liu, Z., Liu, Y.-J., & Yu, R.-Q. (2014). Simultaneous determination of phenolic antioxidants in edible vegetable oils by HPLC-FLD assisted with second-order calibration based on ATLD algorithm. *Journal of Chromatography. B, Analytical Technologies in the Biomedical and Life Sciences*, *947–948*, 32–40.
- Wang, L., Yang, R., Wang, H., Li, J., Qu, L., & Harrington, P. D. B. (2015). High-selective and sensitive voltammetric sensor for butylated hydroxyanisole based on AuNPs-PVP-graphene nanocomposites. *Talanta*, *138*, 169–175.
- Wang, Y., Li, Y., Tang, L., Lu, J., & Li, J. (2009). Application of graphene-modified electrode for selective detection of dopamine. *Electrochemistry Communications*, *11*(4), 889–892.
- Wang, Z., Li, F., Xia, J., Xia, L., Zhang, F., Bi, S., & Xia, L. (2014). An ionic liquid-modified graphene based molecular imprinting electrochemical sensor for sensitive detection of bovine hemoglobin. *Biosensors and Bioelectronics*, *61*, 391–396.
- Wei, C., Huang, Q., Hu, S., Zhang, H., Zhang, W., Wang, Z., & Huang, L. (2014a). Simultaneous electrochemical determination of hydroquinone, catechol and resorcinol at Nafion/multi-walled carbon nanotubes/carbon dots/multi-walled carbon nanotubes modified glassy carbon electrode. *Electrochimica Acta*, *149*, 237–244.
- Williams, G. M., Iatropoulos, M. J., & Whysner, J. (1999). Safety assessment of butylated hydroxyanisole and butylated hydroxytoluene as antioxidant food additives. *Food and Chemical Toxicology*, *37*, 1027–1038.
- Williams, R. T., Nalbandian, J. N., Tu, A., & Wang, Y. (2013). Nuclease digestion and mass spectrometric characterization of oligodeoxyribonucleotides containing 1,2-GpG, 1,2-ApG, and 1,3-GpXpG cisplatin intrastrand cross-links. *Clinica Chimica Acta*, *420*, 160–170.

- Wissler, M. (2006). Graphite and carbon powders for electrochemical applications. *Journal of Power Sources*, 156(2), 142–150.
- Wring, S. A., & Hart, J. P. (1992). Chemically modified, carbon-based electrodes and their application as electrochemical sensors for the analysis of biologically important compounds. A review. *The Analyst*, 117, 1215.
- Xiu-Qin, L., Chao, J., Yan-Yan, S., Min-Li, Y., & Xiao-Gang, C. (2009). Analysis of synthetic antioxidants and preservatives in edible vegetable oil by HPLC/TOF-MS. *Food Chemistry*, 113(2), 692–700.
- Xu, H., Cheng, X., Zhong, J., Meng, J., Yang, M., Jia, F., & Kong, H. (2011). Characterization of multiwalled carbon nanotubes dispersing in water and association with biological effects. *Journal of Nanomaterials*, 2011.
- Xu, Y., Wang, F., Wang, L., Zhao, F., Yang, B., & Ye, B. (2012). Sensitive voltammetric sensor of dihydromyricetin based on Nafion/SWNT-modified glassy carbon electrode. *Journal of Solid State Electrochemistry*, 16(4), 1473–1480.
- Yáñez-Sedeño, P., Pingarrón, J. M., Riu, J., & Rius, F. X. (2010). Electrochemical sensing based on carbon nanotubes. *TrAC - Trends in Analytical Chemistry*, 29(9), 939–953.
- Yang, C., Denno, M. E., Pyakurel, P., & Venton, B. J. (2015). Recent trends in carbon nanomaterial-based electrochemical sensors for biomolecules: A review. *Analytica Chimica Acta*, 887, 17–37.
- Yang, F. Q., Ge, L., Yong, J. W. H., Tan, S. N., & Li, S. P. (2009). Determination of nucleosides and nucleobases in different species of Cordyceps by capillary electrophoresis-mass spectrometry. *Journal of Pharmaceutical and Biomedical Analysis*, 50(3), 307–314.
- Yao, Y., Lin, G., Xie, Y., Ma, P., Li, G., Meng, Q., & Wu, T. (2014). Preformulation studies of myricetin: A natural antioxidant flavonoid. *Pharmazie*, 69(1), 19–26.
- Yari, A., & Derki, S. (2016). New MWCNT-Fe₃O₄@PDA-Ag nanocomposite as a novel sensing element of an electrochemical sensor for determination of guanine and adenine contents of DNA. *Sensors and Actuators B: Chemical*, 227, 456–466.
- Ye, X., Du, Y., Duan, K., Lu, D., Wang, C., & Shi, X. (2014). Fabrication of nano-ZnS coated PEDOT-reduced graphene oxide hybrids modified glassy carbon-rotating disk electrode and its application for simultaneous determination of adenine, guanine, and thymine. *Sensors and Actuators, B: Chemical*, 203, 271–281.
- Yin, H., Zhang, Q., Zhou, Y., Ma, Q., Liu, T., Zhu, L., & Ai, S. (2011). Electrochemical behavior of catechol, resorcinol and hydroquinone at graphene-chitosan composite film modified glassy carbon electrode and their simultaneous determination in water samples. *Electrochimica Acta*, 56(6), 2748–2753.
- Yin, T., & Qin, W. (2013). Applications of nanomaterials in potentiometric sensors. *TrAC - Trends in Analytical Chemistry*, 51, 79–86.

- Zhang, Y., Shen, Y., Zhu, Y., & Xu, Z. (2015). Assessment of the correlations between reducing power, scavenging DPPH activity and anti-lipid-oxidation capability of phenolic antioxidants. *LWT - Food Science and Technology*, 63(1), 569–574.
- Zhao, D., Zhang, X., Feng, L., Qi, Q., & Wang, S. (2011). Sensitive electrochemical determination of luteolin in peanut hulls using multi-walled carbon nanotubes modified electrode. *Food Chemistry*, 127(2), 694–8.
- Zhou, Y., Yan, H., Xie, Q., & Yao, S. (2015). Determination of guanine and adenine by high-performance liquid chromatography with a self-fabricated wall-jet/thin-layer electrochemical detector at a glassy carbon electrode. *Talanta*, 134, 354–9.
- Zhu, J., Cheng, Y., Sun, H., Wang, H., Li, Y., Liu, Y., & Deng, X. (2010). Incorporation and/or adduction of formic acid with DNA in vivo studied by HPLC-AMS. *Nuclear Instruments and Methods in Physics Research, Section B: Beam Interactions with Materials and Atoms*, 268(7–8), 1317–1320.
- Zhu, Q. G., Sujari, A. N. A., & Ab Ghani, S. (2013). Nafion-MWCNT composite modified graphite paste for the analysis of quercetin in fruits of *Acanthopanax sessiliflorus*. *Sensors and Actuators, B: Chemical*, 177, 103–110.
- Zieliński, H., Zielińska, D., & Kostyra, H. (2012). Antioxidant capacity of a new crispy type food products determined by updated analytical strategies. *Food Chemistry*, 130(4), 1098–1104.
- Ziyatdinova, G., Salikhova, I., & Budnikov, H. (2014). Chronoamperometric estimation of cognac and brandy antioxidant capacity using MWNT modified glassy carbon electrode. *Talanta*, 125, 378–84.

LIST OF PUBLICATIONS

Ng, K. L., & Khor, S. M. (2017). Graphite-Based Nanocomposite Electrochemical Sensor for Multiplex Detection of Adenine, Guanine, Thymine, and Cytosine: A biomedical prospect for studying DNA damage study. *Analytical Chemistry*, 89, 10004 – 10012.

Ng, K. L., Lee, S. M., Khor, S. M., & Tan, G. H. (2015). Electrochemical preparation and characterization of a gold nanoparticles graphite electrode: Application to myricetin antioxidant analysis. *Analytical Sciences*, 31, 1075-1081.

Ng, K. L., Tan, G. H., & Khor, S. M. (2017). Graphite nanocomposite sensor for multiplex detection of antioxidants in food. *Food Chemistry*, 237, 912 – 920.

University of Malaya

LIST OF PAPERS PRESENTED

Ng, K. L., See Mun Lee, Guan Huat Tan, & Sook Mei Khor. *Electrochemical preparation and characterization of a gold nanoparticles graphite electrode: Application to myricetin antioxidant analysis*. 28th Regional symposium of Malaysian Analytical Sciences (SKAM 28), 17-20th August 2015, Ipoh, Perak, Malaysia – Oral presentation.

Ng, K. L., & Sook Mei Khor. *From battery to anti-oxidant sensor*. Three Minute thesis competition 2016 (Faculty level). 23th March 2016, Faculty of science, University Malaya, Kuala Lumpur, Malaysia.

University of Malaya